UNIVERSIDAD COMPLUTENSE DE MADRID
FACULTAD DE CIENCIAS QUÍMICAS
DEPARTAMENTO DE QUÍMICA ORGÁNICA I

TESIS DOCTORAL

Chemical reactivity of carbon nanoforms:
arylation and 1,3-dipolar cycloaddition reactions

(Reactividad química de nanoformas de carbono:
reacciones de arilación y cicloadición 1,3-dipolar)

MEMORIA PARA OPTAR AL GRADO DE DOCTOR
PRESENTADA POR

Jaime Mateos Gil

Directores

María Ángeles Herranz Astudillo
Nazario Martín León

Madrid, 2015

UNIVERSIDAD COMPLUTENSE DE MADRID

FACULTAD DE CIENCIAS QUÍMICAS

Departamento de Química Orgánica I

CHEMICAL REACTIVITY OF CARBON NANOFORMS: ARYLATION AND 1,3-DIPOLAR CYCLOADDITION REACTIONS

(REACTIVIDAD QUÍMICA DE NANOFORMAS DE CARBONO: REACCIONES DE ARILACIÓN Y CICLOADICIÓN 1,3-DIPOLAR)

TESIS DOCTORAL

Jaime Mateos Gil

Madrid, 2015

CHEMICAL REACTIVITY OF CARBON NANOFORMS: ARYLATION AND 1,3-DIPOLAR CYCLOADDITION REACTIONS

(REACTIVIDAD QUÍMICA DE NANOFORMAS DE CARBONO: REACCIONES DE ARILACIÓN Y CICLOADICIÓN 1,3-DIPOLAR)

Directores:

Dra. Mª Ángeles Herranz Astudillo

Dr. Nazario Martín León

Memoria que para optar al grado de

DOCTOR EN CIENCIAS QUÍMICAS

presenta

Jaime Mateos Gil

Madrid, 2015

D. Mª Ángeles Herranz Astudillo, Profesora Titular del Departamento de Química Orgánica de la Universidad Complutense de Madrid y **D. Nazario Martín León**, Catedrático de Universidad del Departamento de Química Orgánica de la Universidad Complutense de Madrid,

CERTIFICAN:

Que la presente Memoria titulada: *Chemical Reactivity of Carbon Nanoforms: Arylation and 1,3-Dipolar Cycloaddition Reactions (Reactividad química de nanoformas de carbono: Reacciones de arilación y cicloadición 1,3-dipolar)* se ha realizado bajo su dirección en el Departamento de Química Orgánica de la Facultad de Ciencias Químicas de la Universidad Complutense de Madrid por el Licenciado en Ciencias Químicas D. Jaime Mateos Gil y autorizan su presentación para ser calificada como Tesis Doctoral.

Y para que conste firman el presente certificado en Madrid, a 16 de marzo de 2015

Fdo. Dra. Mª Ángeles Herranz Astudillo Fdo. Dr. Nazario Martín León

"Ninguna victoria es válida en otro sitio
que no sea en tu interior"

Kilian Jornet

"Se puede vivir sin hacer muchas cosas,
y se pueden hacer muchas cosas sin vivir"

José Luis Sampedro

Es difícil agradecer y dedicar este trabajo a todas las personas que me han apoyado y ayudado, no solo durante estos cuatro años de investigación, sino desde que decidí emprender este camino.

*En primer lugar, quisiera expresar todo mi agradecimiento a mis directores de tesis, Nazario Martín y Mª Ángeles Herranz, por la confianza depositada en mi para formar parte de este grupo, por su ayuda y por la oportunidad de dedicarme a lo que siempre había querido, sinceramente, muchas gracias. También quisiera agradecer a Laura Rodríguez, Enrique Maroto y Yuta Takano, responsables directos de gran parte de este trabajo, de los que he aprendido muchísimo y sin cuyo esfuerzo esto no habría sido posible. Y del mismo modo, a los profesores Enrique Ortí (Universidad de Valencia) y Miquel Solá (Universidad de Girona), por su contribución en los cálculos teóricos y al profesor D.M. Guldi (*Friedrich-Alexander-Universität Erlangen-Nürnberg) *por las medidas fotofísicas.*

I would like to express all my gratitude and kindness to Prof. Takeshi Akasaka and all the members of his group at the Tsukuba Life Science Center for Advanced Research (Tsukuba, Japan), and in particular to Wenting Cai, Midori Oinuma and Mitsuaki Suzuki, for making nicest and easiest my stay. Moreover, I would like to thank to the group of Prof. Yasujiro Murata for their invaluable support and hospitality during my stay at Kyoto University (Kyoto-shi, Japan). Thanks so much!!

A mis compañer@s del grupo de Materiales Moleculares Orgánicos, tanto a los que están (Alberto, María, Marina, Valentina, José, Sonia, Javi, Rosa, Silvia, Laura, Luis M., Sara, Marta, Agustín, Andrés) como a los que han ido marchando (Andrea, Antonio, Juan, Raúl, Juan Luis, Enrique). A Salvatore, Beti, Ángel, Andreas, David y Carmen. Y por supuesto, a Virginia, Helena y Ana, por hacer que todo esto funcione.

A los que desde que llegué a Madrid hace ya diez años sois mi segunda familia: Sara, Alberto, Gong, Alicia, Sergio, Ainhoa, Mario, Antonio, David, Alberto M., Diego y María Jesús. No solo habéis sido grandes compañeros sino los mejores amigos que pudiera encontrar, os debo mucho. A Eva y Pablo, por todos los buenos ratos que pasamos y por estar siempre ahí.

A mis compañeros de TRIMAD, por tantos kilómetros en las piernas, tantos retos, tantas carreras, tantas horas de esfuerzo, en definitiva, por poder compartir lo duro y lo gratificante de esta manera de vivir.

También me gustaría agradecer a Roberto Montealegre, J.L. Rodríguez, Joaquín Fernández y Arturo Jiménez, por hacer del IES San Isidro mi otra casa, por todo lo que me enseñasteis, vuestros ánimos y vuestra manera de motivarme, y porque probablemente sin vosotros no habría llegado hasta aquí.

Y por último, a mi familia, porque sois lo más importante que tengo. A mis abuelos, tanto los que están como los que ya no, por su cariño y su preocupación. Y sobre todo, a mis padres y mi hermano. Porque os lo debo todo, todo vuestro cariño, toda vuestra ayuda, vuestra confianza y vuestra inmensa paciencia. Por apoyarme en todo momento, en todo lo que he emprendido en la vida. A mi padre, Jaime, por enseñarme el valor del esfuerzo, de trabajar por lo que uno quiere y ser el mejor ejemplo que puedo seguir. A mi madre, Maribel, por tu constancia día a día en que lleguemos lejos, por todo ese trabajo que nadie ve y ser donde apoyarme en las malas y en las peores. A mi hermano, Daniel, por darme lo que me faltó durante muchos años, por ser como eres, por tu cariño y por tu alegría constante, porque siempre me sentiré orgulloso de ti, porque sé que llegarás muy lejos.

A todos y todas, gracias.

Abbreviations and acronyms

In addition to the standard abbreviations and acronyms in organic chemistry (as defined in the *Journal of Organic Chemistry* author guidelines, *pubs.acs.org/paragonplus/submission/joceah/joceah_abbreviations.pdf*) the following terms have been used in this manuscript:

1-Cl-Np	1-Chloronaphthalene
AFM	Atomic force microscopy
CNF	Carbon nanoforms
CNT	Carbon nanotubes
CuAAC	Copper catalyzed azide-alkyne cycloaddition
CVD	Chemical vapour deposition
DSSC	Dye sensitized solar cells
EMF	Endohedral metallofullerenes
ESR	Electronic spin resonance
FET	Field effect transistor
HRTEM	High resolution transmission electron microscopy
mCPBA	*meta*-Chloroperoxybenzoic acid
MWNT	Multi wall carbon nanotubes
o-DCB	*ortho*-Dichlorobenzene
OFET	Organic field effect transistor
P3AT	Poly(3-alkylthiophene)s
π-exTTF	π-extended tetrathiafulvalene
PFx	Poly(9,9-dialkylfluorene)s
PMMA	Poly(methyl methacrylate)
POAV	π-Orbital Axis Vector
POM	Polyoxymethylene
SED	Surface-conduction electron-emitter display
SEM	Scanning electron microscopy
SWNT	Single wall carbon nanotubes
TCAQ	Tetracyano-p-anthraquinodimethane
TDAE	Tetrakis(dimethylamino)ethylene
TEM	Transmission electron microscopy
TFT	Thin-film transistor
TGA	Thermogravimetric analysis
TTF	Tetrathiafulvalene
XPS	X-ray photoelectron spectroscopy

Table of contents

Introduction

INTRODUCTION

A bit of history...

The origin and evolution of the civilizations is strongly linked to the development of new tools and the knowledge of new materials. From the first prehistoric stone spears to the latest carbon fibber composites, people have not only tried to obtain lighter and more resistant materials, but also to search new applications to improve their living conditions. In this scenario, where civilizations have traveled across a million years journey from the *Stone Age* to reach a basically *Plastic Society*, now is the time when carbon is supposed to play a leading role. During the next decades, carbon is expected to be the responsible of a new revolution grounded in the latest discoveries of new structures, with amazing and remarkable properties.

Mankind's use of charcoal extends back as far as human history itself. However there was no evidence of the use of *graphite* until the Boian Culture (today's Romania) in the Neolithic period (4^{th} millennium BC) where this carbon allotrope was utilized for decorating pottery. During the 15^{th} century, a very important graphite deposit was found and exploited in Cumbria (United Kingdom), reaching such a military importance that became under the protection of the crown of Elizabeth I. At that time, graphite was thought to be a type of lead and consequently, it was called black lead or plumbago. Actually, the name of *graphite* ("writing stone") was coined one century later by the German geologist Abraham Gottlob Werner and the determination of the exact structure came with the first works on X-ray diffraction at the beginning of the 19^{th} century.[1] A similar way was followed by *diamond*, well known by Indians six thousand years ago and applied by Chinese to polish objects during the 5^{th} millennium BC. However, its real structure was not totally described until the fabrication of the first difractometers.

Graphite and *diamond* have been during centuries the only known carbon allotropes. In fact, the evidence that demonstrated these substances were made by the same element was not obtained until the late 18^{th} century, when the experiments accomplished by Lavoisier and Tennant showed that burning the same amount of both minerals released the same amount of gas, establishing the chemical equivalency between them.[2]

---

[1] [(a)]Bernal, J. D., *Proc. R. Soc. London, A* **1924**, *106*, 749; [(b)]Debye, P. and Scherrer, P., *Physik. Z.* **1916**, *17*, 277; [(c)]Bragg, W. H. and Bragg, W. L., *Proc. R. Soc. London, A* **1913**, *89*, 277.

[2] [(a)]Tennant, S., *Philos. Trans. R. Soc. London, A* **1797**, *87*, 123; [(b)]Lavoisier, A., *Hist. Acad. Roy. Sci. Mém. Math. Phys.* **1772**, *Part 2*.

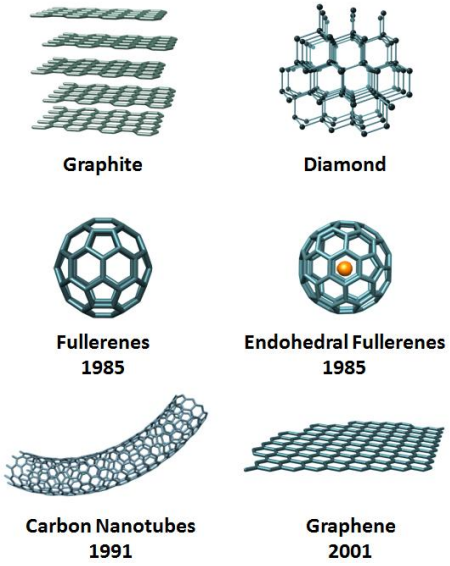

Figure 1. Structure and year of discovery of the main carbon allotropes.

During the last two decades of 20th century a new family of carbon structures emerged, exhibiting intriguing structures and properties. Firstly, the C_{60} molecule focused a huge attention because of its truncated icosahedral structure, the ability of accepting 6 electrons in solution and its size in the nanometre scale.[3] The importance of this discovery led to the recognition of Kroto, Smalley and Curl with the Nobel Prize in 1996 for the discovery of fullerenes. Different cage sizes have been discovered in the fullerene family, from the smallest conformed by 20 carbon atoms up to hundreds. Furthermore, interstellar *buckyonions* were found to exhibit outer shells up to 1500 carbon atoms.[4] Under the fullerene fabrication conditions, it was possible to find guest chemical species inside the cage inner space affording a novel family of fullerene relatives named as *endohedral fullerenes*.[5]

A few years later, in 1991, Iijima described carbon filamentous structures that were identified and characterized as c*arbon nanotubes*, that can be formed by one (Single Wall Carbon Nanotubes, SWNT) or several concentric tubes (Multi Wall Carbon Nanotubes, MWNT).[6] But the early 21th century

[3] Kroto, H. W., Heath, J. R., O'Brien, S. C., Curl, R. F. and Smalley, R. E., *Nature* **1985**, *318*, 162.
[4] Kroto, H. W., *Nature* **1992**, *359*, 670.
[5] [(a)]Li, Y., in *Endohedral Fullerenes*, World Scientific Publishing Co., **2014**, pp. 417; [(b)]Murata, M., Murata, Y. and Komatsu, K., in *Organic Nanomaterials*, John Wiley & Sons, Inc., **2013**, pp. 225.
[6] [(a)]Iijima, S. and Ichihashi, T., *Nature* **1993**, *363*, 603; [(b)]Iijima, S., *Nature* **1991**, *354*, 56.

brought a new nanostructure that focused even a larger attention than CNT. Geim and Novoselov described the mechanical exfoliation of isolated sheets from graphite to yield a new material named as *graphene* that overcome all the expectatives on any other material known to date (Figure 1).[7]

The attribution of these discoveries has aroused some controversy and discussion. For example, in 1980 Iijima described the observation of the tetrahedral bonding in graphitized carbon, conforming shell shape particles that were a clear evidence for the existence of fullerenes and buckyonions. Surprisingly, Iijima has been given all the credit in the CNT discovery when there are many previous works on this issue. In fact, Edison reported in 1889 a patent mentioning the formation of carbon filaments obtained from thermal decomposition of methane and its utilization in light bulbs. Nevertheless, there was a considerable amount of work between 1950-1970 decades on these filamentous carbon structures that used to obtain in nuclear reactors and brick walls of furnaces in metal industries that remained almost unknown during years.[8] In particular, there is a remarkable article by Radushkevich and Lukyanovich in the *Soviet Journal of Physical Chemistry* where MWNT are clearly observed by TEM.[9] Anyway, whoever was the first in reporting these novel carbon nanostructures, Iijima's work set the focus of the whole scientific community in CNT. In the case of graphene, in spite of several previous works on intercalated graphite derivatives and few layer graphite, the work of Geim and Novoselov is the first evidence of an atomic thin layer of carbon atoms.

Although there are many other carbon nanostructures, some obtained by extremely high temperature and pressure conditions and others found in small amounts among amorphous carbon, their classification may be a tough work. If we are strict with the allotrope definition, the classification of each kind of fullerene and their numerous isomers may be unaffordable, so the term *nanoform* (CNF) is more than suitable, and the most extended in the scientific community.[10] Nanohorns, nanofoams, nanobuds or nanodiamonds have been described during the last decades, but in spite of some interesting properties, their development cannot be compared to fullerenes, CNT or graphene (Figure 2). In contrast, the recently described graphyne, seems to be a tough competitor, although much work on it is still to do.[11]

---

[7] Novoselov, K. S., Geim, A. K., Morozov, S. V., D. Jiang, Zhang, Y., S. V. Dubonos, Grigorieva, I. V. and Firsov, A. A., *Science* **2004**, *306*, 666.

[8] [(a)]Bacon, R., *J. Appl. Phys.* **1960**, *31*, 283; [(b)]Sears, G. W., *J. Chem. Phys.* **1959**, *31*, 358; [(c)]Davis, W. R., Slawson, R. J. and Rigby, G. R., *Nature* **1953**, *171*, 756.

[9] Radushkevich, L. V. and Lukyanovich, V. M., *Zurn. Fisic. Chim.* **1952**, *26*, 88.

[10] Delgado, J. L., Herranz, M. A. and Martín, N., *J. Mater. Chem.* **2008**, *18*, 1417.

[11] Haley, M. M., *Pure Appl. Chem.* **2008**, *80*, 519.

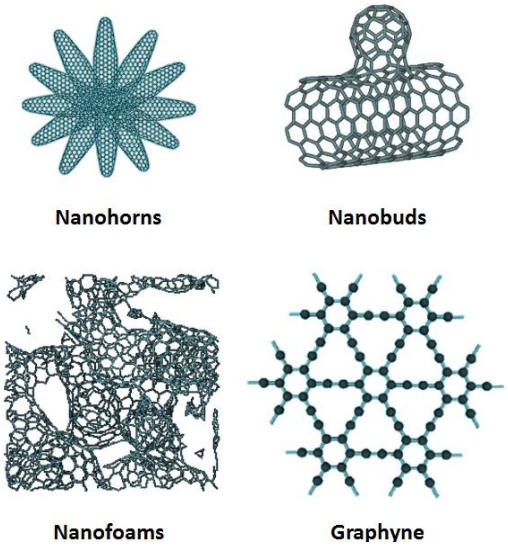

Figure 2. Related carbon nanostructures.

Why so much interest on CNF?

A clear signal of the importance of these structures is the enormous interest by many scientist from different fields (electronics, material sciences or biomedicine), that is evidenced by the large number of publications about these materials during the last decades (Figure 3).

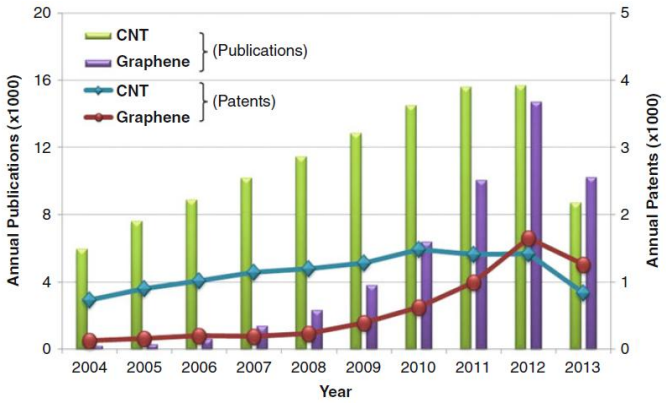

Figure 3. Trend in the number of publications and patents based on CNTs and graphene (Ref: Scifinder (http://scifinder.cas.org), US Patent & Trademark Office (http://patft.uspto.gov/), July 2013).

This huge interest on CNF, in particular CNT and graphene, is mainly due to their remarkable properties, for example, highest current density, ballistic transport, ultrahigh thermal conductivity, and extremely high mechanical strength, just to name a few (Table 1).

	Others	CNT [12]	Graphene [12]	Graphite [12]	Diamond [13]
Current dens. (J, A/cm^2)	Cu:10^6	10^9	10^7 to 10^{10}	15 to 2000	10
Resistivity (ρ, Ω·m)	Teflon:10^{22} Ag:$1.59\cdot10^{-8}$	1	10^{-8}	10^{-6}// plane $10^{-3}\perp$ plane	10^{11} to 10^{18}
Conductivity (σ, S/m)	Cu:10^7	10^8	10^8	10^5// plane $10^2\perp$ plane	10^{-13}
Electron mob. (μ, cm^2/V·s)	Si:1350 Polymers:10	10000	20000	20000	2000 to 5000
Young mod. (*E*, GPa)	Steel:200 Kevlar: 100	500 to 2000	500 to 1000	500 to 1000	1220
Therm. conduct. (*K*, W/m·K)	Ag:430	3000 to 7000	2000 to 5000	25 to 470	2200

Table 1. Comparative table with values for the main electrical, mechanical and thermal properties of carbon and related materials.

As it can be observed, CNT and graphene electrical properties are above typically utilized materials as copper or silicon, exhibiting higher values for current density, conductivity or electron mobility in several magnitude orders. Although there are no studies on the direct measurement of mechanical properties, different methodologies based on theoretical calculations or AFM and TEM revealed remarkable results, exhibiting larger strength and flexibility than other well known materials as kevlar or steel. A fact that corroborates this finding is the notable improvement on the tensile strength of different fibbers when small amounts of CNT or graphene (0.5-5 %) are inserted. Moreover, graphene and CNT are able to disperse heat better than many other materials and show a relatively high chemical stability, and in the case of graphene, it even resists ionizing radiation.

These physical parameters, together with their nanometre scale size, may result in many potential applications. Nowadays, several experimental devices and commercial products containing CNT and graphene are a reality, for example, organic field effect transistors (OFET), flexible thin film transistors (TFT), reinforcement in sport materials (shoes sole, baseball bats, bikes) and even a simple computer made of CNF based transistors able to perform the same operations that the first 80's computers. In fact, different companies and trademarks have recently developed different products and applications containing CNT and graphene (Table 2).

[12] Bhushan, B., Luo, D., Schricker, S. R., Sigmund, W. and Zauscher, S., *Handbook of Nanomaterials Properties*, Springer Berlin Heidelberg, **2014**.
[13] Yang, N., *Novel Aspects of Diamond: From Growth to Applications, Vol. 121*, Springer International Publishing, **2015**.

Company	Product
Adidas	Running shoe sole (CNT)
BASF	Conductive POM for fuel lines (with Audi) (CNT)
BMC	Composites Bicycles (CNT)
Canon	Field emission display; SED TV (Graphene and CNT)
Eagle Windpower	Wind turbine blades (CNT)
Fujitsu	Interconnect vias; thermal interfaces (CNT)
General Electric	Thermal sensing and imaging (CNT and graphene)
NEC	Printed electronics; FET (Graphene)
Nokia	Transparent conductor (Graphene)
Panasonic Boston	Transparent conductor and touch screen (CNT and Graphene)
Samsung	Transparent conductor (CNT and Graphene)

Table 2. Outstanding companies in different fields developing or selling CNT and graphene based products.

Figure 3. Some real applications of CNF. CNT-based body armour. High performance racing wheels for bikes developed by Vittoria Company. Chemical sensor based on CNT to detect TNT and sarin gas in water developed by Zhenan Bao group at Stanford University.

In contrast to graphene and CNT, that are studied from a materials point of view by considering them as polydisperse samples with different sizes and properties, fullerenes are discrete molecules with an homogeneous and a defined structure. The interest on fullerenes came from two different perspectives: i) its *spherical nanometre size* as scaffold for the attachment of different active motifs and constructions of supramolecular assemblies and

ii) the interesting *electronic properties* in order to obtain different organic active systems to be applied in organic electronics or photovoltaic devices.

To exploit and modulate fullerene properties, functionalization is almost mandatory so the *chemistry of fullerenes* has emerged as a relevant research field, leading to interesting new reactions and methodologies for its exohedral functionalization. In contrast to the well known C_{60} fullerene, the novel endohedral fullerenes have not been so deeply studied. Despite the possibility of modulating the fullerene properties by changing the encapsulated species, the hardness to get enough available amount of these materials makes the chemistry of endohedral fullerenes still a very challenging topic in science.

Challenges to be accomplished?

Considering the possibilities that CNT, graphene and endohedral fullerenes offer to the society, it may seem strange that we are not surrounded by many devices and products based on them. There are several reasons that justify this point and make thousands of scientists and companies to keep on searching on these topics. Firstly, as prepared CNT and graphene samples are polydisperse materials with different sizes and properties, in addition to the presence of fabrication impurities, that require separation procedures for most of the potential applications. Secondly, CNT and graphene exhibit a low solubility in water and common organic solvents what makes very tough to work with them. In the case of endohedral fullerenes, the low availability of these materials for extensive research is probably the most critical point that still hampers the development of these unprecedented systems.

In this sense, chemists must play a leading role and synthetic methodologies accompanied by the latest techniques in materials science are considered powerful tools. The aim of this work is to contribute to the development of these intriguing materials by means of their chemical modification. The novel carbon-based materials thus prepared should exhibit a variety of properties of interest in different scientific and technological fields.

Chapter 1:

Carbon nanotubes and graphene chemistry

1.1. Background

1.1. BACKGROUND

1.1.1. CHEMICAL REACTIVITY OF CARBON NANOTUBES

CNT are defined as rolled graphitic sheets conforming a cylinder. Considering the number of concentric tubes that the material can be composed of, CNT can be classified as Single Wall Carbon Nanotubes (SWNT) and Multi Wall Carbon Nanotubes (MWNT) (Figure 1.1-1).

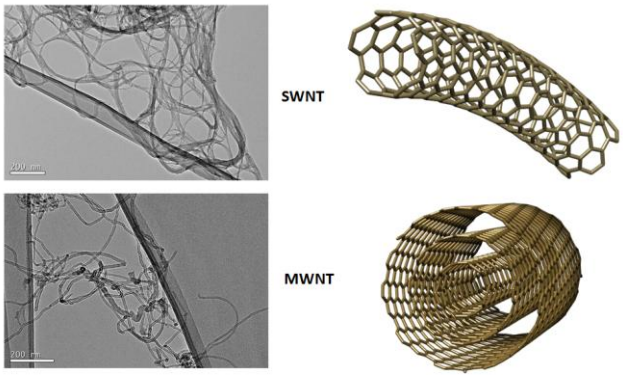

Figure 1.1-1. Images of SWNT and MWNT obtained by TEM (200 nm scale bar) and depictive models for their chemical structures.

A large variety of methodologies for the preparation of CNT have been reported to date,[14] although the most utilized are arc discharge, laser ablation, electrolysis and chemical vapour deposition (CVD). This latter has displaced other methods because of the lower necessary temperatures during the synthesis and the better control on product properties. Depending on the fabrication method, the CNT diameter varies between 0.6 to a few nanometres and they can reach several micrometres of length. Besides these differences in size, the way of ordering of the carbon atoms is not the same in all CNT. Taking SWNT as example, this fact can be easily explained as the different way of rolling an infinite graphene layer to afford the nanotube, described by an (*n,m*) vector, as depicted in Figure 1.1-2. Three types of SWNT could be formed: armchair (*n*,*n*), zig-zag (*n*,0) and chiral (*n*,*m*). Whereas armchair type are metallic, those chiral that obey the rule n-m=3q (where q is any natural number), exhibit semiconductor character with a small band gap. The other tubes are moderate semiconductors. Unfortunately, pristine CNT are a mixture of all types.

[14] Prasek, J., Drbohlavova, J., Chomoucka, J., Hubalek, J., Jasek, O., Adam, V. and Kizek, R., *J. Mater. Chem.* **2011**, *21*, 15872.

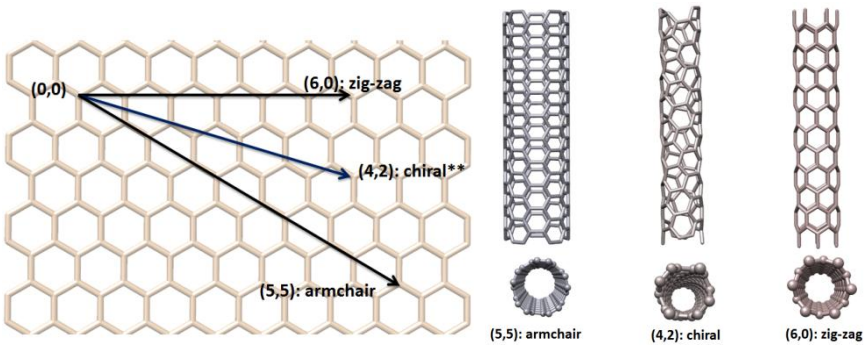

Figure 1.1-2. Different types of SWNT obtained upon rolling a graphene sheet.

CNT display very interesting properties and even some promising applications have been reported, what makes them one of the most relevant research fields in the last decade.[15] For example, considering their mechanical properties, MWNT exhibit a specific strength 300 times higher than high carbon steels, or a tensile strength 10 times higher than Kevlar.[16] As mentioned above, they can behave as electrical conductors or semiconductors with different band gaps and related to this electrical performance they present a huge thermal conductivity and very interesting optical properties.

Unfortunately, as CNT samples, these properties are not homogeneous and their separation is still a mandatory challenge to make real applications. The highly aromatic surface of CNT makes them to form aggregates or bundles very difficult to solubilise or disperse in water or common organic solvents and it is here where chemistry has many skills to work.

In this sense, chemistry has revealed to be crucial to overcome this problem.[17] Two main approaches have been tried in order to improve the solubility and, at the same time, modify or improve those mentioned properties of CNT (Figure 1.1-3). On the one hand, the *covalent modification* by different reactions on the walls, defects or end capes of CNT allows a notable improvement in solubility and dispersibility, at the time that different functional groups or active molecules can be attached in a stable manner conferring new or better properties to the material. Unfortunately, an uncontrolled excess of the functionalization degree could involve a

[15] De Volder, M. F. L., Tawfick, S. H., Baughman, R. H. and Hart, A. J., *Science* **2013**, *339*, 535.
[16] Coleman, J. N., Khan, U., Blau, W. J. and Gun'ko, Y. K., *Carbon* **2006**, *44*, 1624.
[17] [(a)]Langa, F. and Nierengarten, J. F., *Fullerenes: Principles and Applications* The Royal Society of Chemistry, **2012**; [(b)]Akasaka, T., Wudl, F. and Nagase, S., *Chemistry of Nanocarbons*, John Wiley & Sons, Ltd, **2010**; [(c)]Guldi, D. M. and Martín, N., *Carbon Nanotubes and Related Structures*, Wiley-VCH Verlag GmbH & Co. KGaA, **2010**.

substantial impairment of the π surface, hindering further applications. On the other hand, *non-covalent* or *supramolecular modification*s afford a dispersed material with no disruption in the sp^2 carbon framework. However, the interactions that stabilize these supramolecular complexes are usually weak and depending on temperature, pH or the utilized solvent. Deciding on which strategy is better is not still a clear issue and it relies on the material purpose.

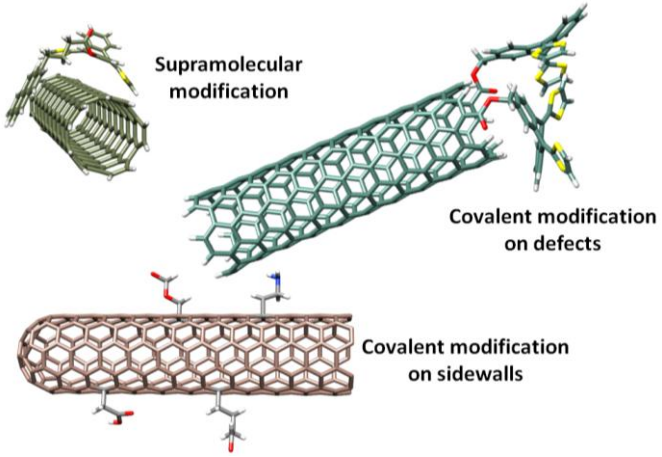

Figure 1.1-3. Different approaches for the modification of CNT.

Obviously, the different lengths, chiralities or diameters of the as produced CNT samples not only provide different properties, but also a different chemical reactivity. A comprehensive study of the reactivity dependence with the length, diameter and curvature of the nanotube was reported by Hirsch *et al.*[18] considering as principles some aspects about fullerene reactivity. Taking in mind the concave inner face and the convex outer face in C_{60}, when a double bound is taken out of planarity, carbon atoms tend to pyramidalize. The *pyramidalization*, defined by $\boldsymbol{\Theta_P}$, causes the exohedral lobes of the π orbitals to be larger than their endohedral counterparts. The reactivity of the convex surface is enhanced by the pronounced exposure of the hybrid π orbitals from the exterior which favours the orbital overlap with incoming addends (kinetic effect) and by the assistance of the σ system (thermodynamic effect) because of the formation of strain-free geometries in the region of the addend. Considering that the SWNT curvature happens only in one dimension (cyclic) whereas in fullerenes this curvature takes place bidimensionally (spherical), $\boldsymbol{\Theta_P}$ for C_{60} must be higher, what matches the observed reactivity (Figure 1.1-4). If we compare nanotubes with different diameters, those smaller will be more reactive.

[18] [(a)]Hirsch, A. and Vostrowsky, O., *Top. Curr. Chem.* **2005**, *245*, 193; [(b)]Chen, Z., Thiel, W. and Hirsch, A., *ChemPhysChem* **2003**, *4*, 93.

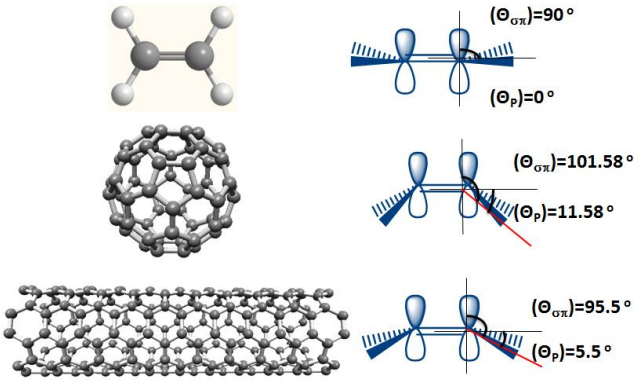

Figure 1.1-4. Depictive picture of the different pyramidalization degrees Θ_P in C_{60} and SWNT (*n,n*) compared to the standard C=C ethylene bond.

Another consideration for the analysis of the chemical reactivity in non-planar polyaromatic structures is the π-*orbital alignment* (Φ). If we consider those bonds that are not parallel to the tube curvature, there is a misalignment between adjacent carbon orbitals (Figure 1.1-5). This misalignment causes a strain in the bond that drives the extent of addition reactions.

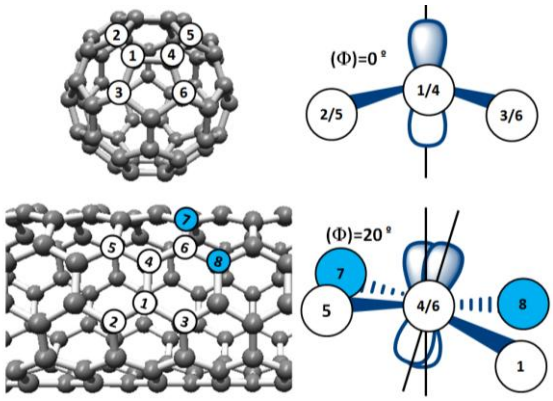

Figure 1.1-5. Depictive picture of the different π-*orbital alignment*(Φ) in C_{60} and SWNT (*n,n*).

This analysis corroborates the reactivity order for outer additions on carbon nanostructures: C_{60} > SWNT > MWNT > graphene, but unfortunately, the different reactivity observed for different chiral SWNT cannot be explained using the concepts described above. A new parameter, the bond curvature (*K*), was introduced to define the reactivity of any kind of bond in SWNT.[19]

[19] [(a)]Li, J., Jia, G., Zhang, Y. and Chen, Y., *Chem. Mater.* **2006**, *18*, 3579; [(b)]Li, I. L., Li, G. D., Liu, H. J., Chan, C. T. and Tang, Z. K., *Appl. Phys. Lett.* **2003**, *82*, 1467.

$$K = \frac{\sin^2(\theta)}{R}$$

The curvature bond depends on the nanotube radius and the bond angle θ respect to the SWNT axial vector. When θ takes value 0^0 (axial bond in zig-zag), the curvature bond *K* is null, while for 90^0 (armchair) *K* is equal to 1/R (maximum value) and it will take larger values for smaller diameter tubes, what means a higher reactivity. The non-equivalent atoms present in zig-zag, armchair and chiral nanotubes and the corresponding angle are depicted in Figure 1.1-6.

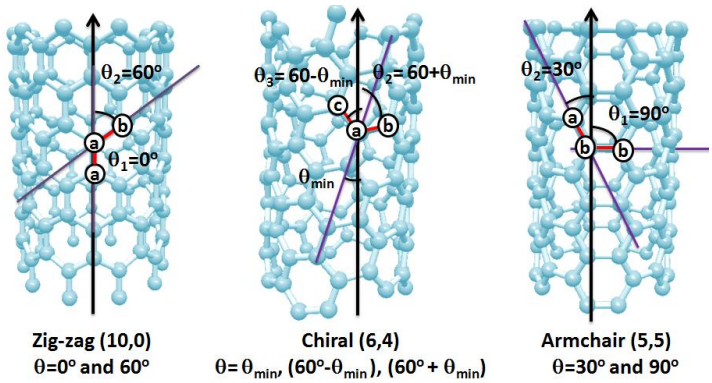

Figure 1.1-6. Depictive picture of the different C-C bonds present in each type of SWNT and their angles and geometrical relationship to the axial vector.

Different tubes of similar radius were compared by calculating the bond curvature *K* for each non equivalent bond. As the armchair or zig-zag types only present two non equivalent C-C bonds, chiral SWNT present three with a remarkable different reactivity. The *K* values predicted that, under mild conditions, zig-zag type SWNT hardly react allowing a selective removal from a non-homogenous sample (Table-1.1-1).

	R (nm)	θ_1	θ_2	θ_3	K_1	K_2	K_3
(10,0); ($C_{100}H_{20}$)	0.392	0	60	-	0	1.913	-
(5,5); ($C_{100}H_{20}$)	0.339	90	30	-	2.950	0.737	-
(6,4); ($C_{148}H_{20}$)	0.341	23.41	83.41	36.59	0.463	2.894	1.041

Table 1.1-1. Curvature bonds (*K*) values calculated for similar size nanotubes with different chiralities.

At a first sight, this fact opens the possibility of carrying out reactions selectively over only one kind of nanotubes or even to obtain a certain degree of selectivity. In practise, these proposals are much more complicated than expected because the general low reactivity of CNT, involving the use of highly reactive addends that do not distinguish among the different bonds or kind of SWNT. In the next pages, the different

chemical reactions and strategies developed for the CNT functionalization will be described. This background does not intend to be a comprehensive review of the reported methods, since only some selected representative examples related to the topics of this dissertation will be discussed.[20]

a) Covalent modification on defects

Although the *perfect* nanotube could be defined as a complete sp^2 carbon long cylinder framework with two hemifullerene units at the ends, the different production conditions provide a broad variety of defects and dislocated carbon atoms in the CNT surface. The defects areas use to be mainly located at the end of the nanotubes, where the catalyst particles were attached and the growth process was started, leading to disordered fullerene caps and dangling bonds. These defects may be also found at the sidewalls and, normally, shorter tubes feature a higher degree of point defects in order to relax and reduce the strain energy of the framework.[21] Some of the more typical structure disturbances are pentagon-heptagon defects, Stone-Wales defects (5-7-7-5 ring pattern), sp^3 saturated atoms, structural holes or vacancies and open tube ends terminated by carboxylic acid functionalities (Figure 1.1-7).

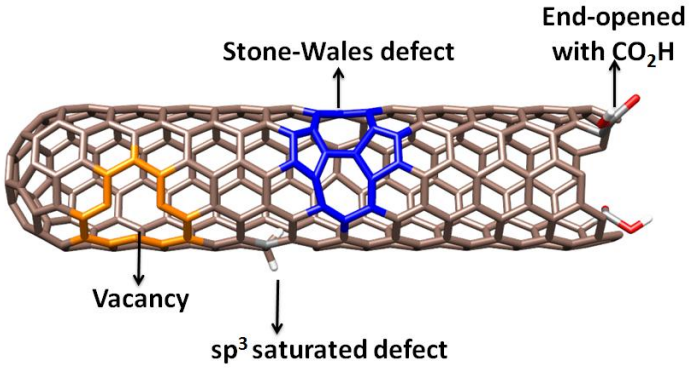

Figure 1.1-7. Some of the defects that can be found in CNT.

The present defects in the carbon nanotube sp^2 framework represent locations of higher reactivity toward aggressive chemicals such as oxidizing

[20] For reviews on the chemical functionalization of CNT see: [(a)]Vazquez, E., Giacalone, F. and Prato, M., *Chem. Soc. Rev.* **2014**, *43*, 58; [(b)]Hodge, S. A., Bayazit, M. K., Coleman, K. S. and Shaffer, M. S. P., *Chem. Soc. Rev.* **2012**, *41*, 4409; [(c)]Singh, P., Campidelli, S., Giordani, S., Bonifazi, D., Bianco, A. and Prato, M., *Chem. Soc. Rev.* **2009**, *38*, 2214; [(d)]Zhao, Y.-L. and Stoddart, J. F., *Acc. Chem. Res.* **2009**, *42*, 1161; [(e)]Tasis, D., Tagmatarchis, N., Bianco, A. and Prato, M., *Chem. Rev.* **2006**, *106*, 1105.

[21] [(a)]Carlsson, J. M., *Phys. Stat. Sol. (B),* **2006**, *243*, 3452; [(b)]Charlier, J. C., *Acc. Chem. Res.* **2002**, *35*, 1063; [(c)]Ebbesen, T. W. and Takada, T., *Carbon* **1995**, *33*, 973.

agents and, therefore, the opening of the CNT framework at defects is more probable.[22]

Besides the defects present by fabrication, remaining catalyst particles, and amorphous carbon, whose removal is critical for further reactions or applications, are usually found in as prepared CNT. The most efficient purification procedures are based in the use of very aggressive oxidative conditions, such as, boiling in concentrated acid mixtures, piranha solution or ozone.[23] As a consequence of the conditions, the introduction of carboxylic acid functionalities and other oxygen bearing groups at the ends and defect sites of the carbon nanotube framework is produced, a fact that is exploited to increase the solubility of CNT and attach different functionalities. Moreover, when more aggressive conditions are utilized, tubes could be shorten. Taking advantage of these defects many functionalization methodologies have been reported to date and the most remarkable, depicted in Figure 1.1-8, will be explained in the next paragraphs.

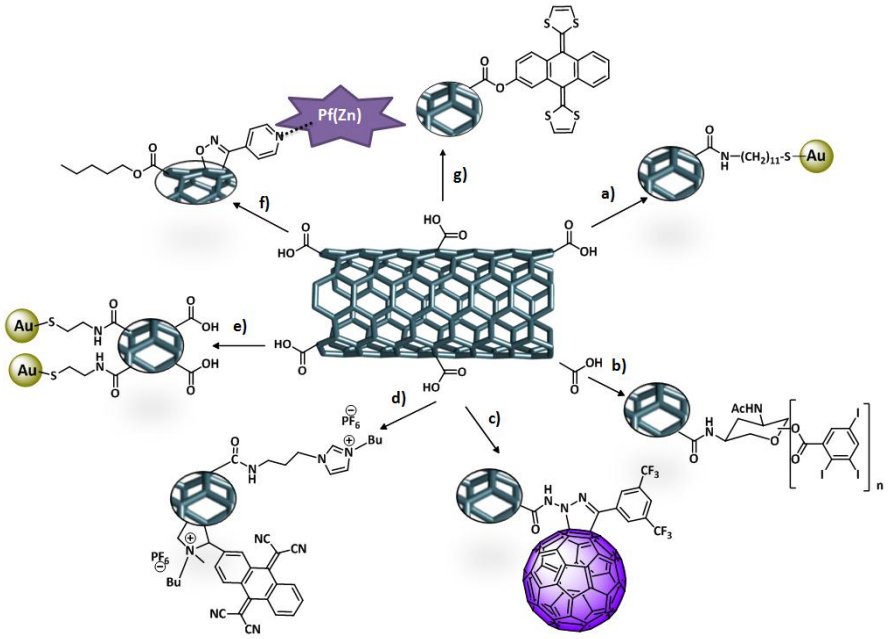

Figure 1.1-8. Some of the most remarkable reactions on the defects of CNT.

The first published *on defect* functionalization method described the amide formation of shorten SWNT after $SOCl_2$ treatment and reaction with an aliphatic aminothiol derivative. (Figure 1.1-8, a). This soluble functionalized

[22] Wang, C., Zhou, G., Liu, H., Wu, J., Qiu, Y., Gu, B.-L. and Duan, W., *J. Phys. Chem. B* **2006**, *110*, 10266.

[23] Mahalingam, P., Parasuram, B., Maiyalagan, T. and Sundaram, S., *J. Environ. Nanotechnol.* **2012**, *1*, 53.

SWNT (*f*-SWNT) were finally attached to gold nanoparticles and studied by AFM.[24] In a similar approach, the amidation of oxidized SWNT with carbohydrates tagged with PhI_3 allowed its visualization by using HRTEM (Figure 1.1-8, b).[25] An important challenge in the defect reactions is the co-functionalization, allowing the selective insertion of different addends. Langa *et al.* accomplished a double modification by using an etherification with penthanol and a cycloaddition with a nitrile oxide derivative bearing a pyridine (Figure 1.1-8, f). This pyridine was then able to interact with a zinc porphirine, leading to the first example of a donor-acceptor supramolecular complex with SWNT.[26]

Another related strategy is the asymmetric end-functionalization of CNT. Chopra *et al.* described a singular methodology based on the protection of MWNT sidewalls by a polystyrene layer.[27] Both tips were then oxidized, followed by on top floating in a reactive solution of 2-aminoethanethiol with EDC coupling reagent, allowing the selective reaction of only one end, leaving non reacted the carboxylic acid groups on the other end. The interaction with gold nanoparticles led TEM images showing the decoration of only one end (Figure 1.1-8, e). Besides gold nanoparticles, CdSe, CdTe and Fe_3O_4 quantum dots have been attached to *f*-CNT enhancing their photoluminescence.[28] Many other applications using terminal functionalized CNT have been reported: reinforced polymers,[16] bioapplications,[29] molecular electronic devices (nanowires, electrodes)[30] or donor-acceptor assemblies[31] (photovoltaic cells, capacitors). In our group we were able to synthesize and study an π-exTTF/SWCNT conjugate, identifying the reduced SWCNT and oxidized π-exTTF units as metastable states in a series of donor–acceptor nanoconjugates with remarkable lifetimes in the range of hundreds of

[24] Liu, J., Rinzler, A. G., Dai, H., Hafner, J. H., Bradley, R. K., Boul, P. J., Lu, A., Iverson, T., Shelimov, K., Huffman, C. B., Rodriguez-Macias, F., Shon, Y.-S., Lee, T. R., Colbert, D. T. and Smalley, R. E., *Science* **1998**, *280*, 1253.

[25] Hong, S. Y., Tobias, G., Ballesteros, B., El Oualid, F., Errey, J. C., Doores, K. J., Kirkland, A. I., Nellist, P. D., Green, M. L. H. and Davis, B. G., *J. Am. Chem. Soc.* **2007**, *129*, 10966.

[26] Alvaro, M., Atienzar, P., de la Cruz, P., Delgado, J. L., Troiani, V., Garcia, H., Langa, F., Palkar, A. and Echegoyen, L., *J. Am. Chem. Soc.* **2006**, *128*, 6626.

[27] [27] Chopra, N., Majumder, M. and Hinds, B. J., *Adv. Funct. Mater.* **2005**, *15*, 858.

[28] [(a)]Ahmad, R., Soni, U., Srivastava, R., Singh, V. N., Chand, S. and Sapra, S., *J. Phys. Chem. C* **2014**, *118*, 11409; [(b)]Li, W., Gao, C., Qian, H., Ren, J. and Yan, D., *J. Mater. Chem.* **2006**, *16*, 1852; [(c)]Pan, B., Cui, D., He, R., Gao, F. and Zhang, Y., *Chem. Phys. Lett.* **2006**, *417*, 419.

[29] Lu, F., Gu, L., Meziani, M. J., Wang, X., Luo, P. G., Veca, L. M., Cao, L. and Sun, Y.-P., *Adv. Mater.* **2009**, *21*, 139.

[30] [(a)]Dirian, K., Herranz, M. A., Katsukis, G., Malig, J., Rodriguez-Perez, L., Romero-Nieto, C., Strauss, V., Martín, N. and Guldi, D. M., *Chemical Science* **2013**, *4*, 4335; [(b)]Feldman, A. K., Steigerwald, M. L., Guo, X. and Nuckolls, C., *Acc. Chem. Res.* **2008**, *41*, 1731.

[31] Guldi, D. M., Rahman, G. M. A., Zerbetto, F. and Prato, M., *Acc. Chem. Res.* **2005**, *38*, 871.

nanoseconds (Figure 1.1-8, g).[32] Another family of organic molecules broadly studied are porphyrins, remarkable chromophores able to quench their fluorescence by efficient light-induced electron transfer to the carbon nanotube.[33] Fullerene has also been attached to SWNT through the defect modification approach, yielding conjugates of two different CNF. (Figure 1.1-8, c).[34] An interesting way of modulating the solubility of *f*-SWNT is the utilization of ionic liquids and it can be combined with the attachment of electroactive molecules. In these sense, we have recently reported the preparation of SWNT endowed with ionic liquids and the electron-acceptor tetracyanoanthaquinodimethane (TCAQ) motif (Figure 1.1-8, d).[35]

b) Covalent modification on sidewalls

A large variety of CNT materials have been synthesized by sidewall covalent modification.[20e] Some relevant approaches are discussed below.

i) Cycloadditions:

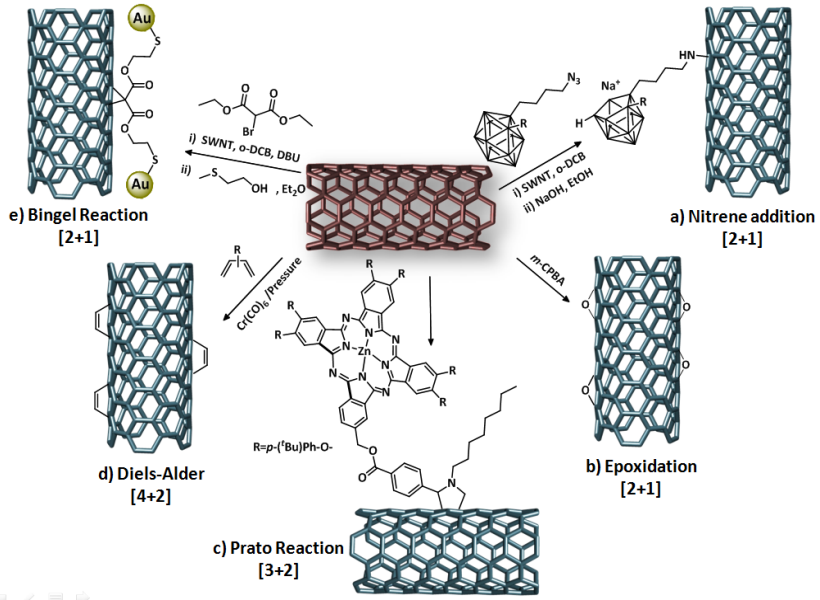

Figure 1.1-9. Cycloadditions performed on the sidewalls of CNT.

[32] Herranz, M. Á., Martín, N., Campidelli, S., Prato, M., Brehm, G. and Guldi, D. M., *Angew. Chem., Int. Ed.* **2006**, *45*, 4478.
[33] Baskaran, D., Mays, J. W., Zhang, X. P. and Bratcher, M. S., *J. Am. Chem. Soc.* **2005**, *127*, 6916.
[34] Delgado, J. L., de la Cruz, P., Urbina, A., López Navarrete, J. T., Casado, J. and Langa, F., *Carbon* **2007**, *45*, 2250.
[35] Rodríguez-Pérez, L., García, R., Herranz, M. Á. and Martín, N., *Chem. Eur. J.* **2014**, *20*, 7278.

Many different cycloaddition reactions have been tried on CNT during the last decade. In particular [2+1] nitrene addition has been studied, foregrounding the work of Takagaki *et al.*, where substituted C_2B_{10} carborane cages were successfully attached to SWCNT.[36] Carborane cages were then head opened under the presence of NaOH in EtOH while the three-membered ring formed by the nitrene and SWCNT was opened to produce water soluble *f*-SWNT by both substituted nido-C_2B_9 carborane units and ethoxide moieties (Figure 1.1-9, a). Moreover, this derivative revealed to show a high affinity for tumoral cells, making it an attractive nanovehicle for the delivery of boron to tumour cells for an effective boron neutron capture therapy in the treatment of cancer.

Another widely utilized [2+1] cycloaddition is the Bingel reaction. Green *et al.,* described the synthesis of SWNT-cycloadducts by a standard procedure followed by a transesterification with 2-(methylthio)ethanol able to bind to gold nanoparticles (Figure 1.1-9, e).[37] Concerning the epoxidation reaction onto CNT sidewalls, Barron *et al.* studied the reaction with either trifluorodimethyldioxirane, formed *in situ* from trifluoroacetone and oxone (potassium peroxymonosulphate, $KHSO_5$), or 3-chloroperoxybenzoic acid.[38] The authors developed a chemical approach for the quantitative determination of the oxygen content in the epoxide-modified CNT by the use of triphenylphosphine as deoxygenating agent (Figure 1.1-9, b).

As in the case of fullerene, the well-known 1,3-cycloaddition of azomethine ylides on the sidewalls of CNT (Prato reaction) still attracts the interest of a great number of scientists. The surface of CNT has been modified with pyrrolidine rings, which can carry a great number of functional groups including, for example, tetraphenylporphyrins,[39] phthalocyanines,[40] or poly-3-hexylthiophene polymers (P3HT) (Figure 1.1-9, c).[41] Furthermore, bioactive molecules have been attached too by the 1,3-dipolar cycloaddition of azomethine ylides to CNT, opening a door to the biomolecule delivery to cells and organs. Promising results were reported by Bianco *et al.,* being able to

[36] Yinghuai, Z., Peng, A. T., Carpenter, K., Maguire, J. A., Hosmane, N. S. and Takagaki, M., *J. Am. Chem. Soc.* **2005**, *127*, 9875.

[37] Coleman, K. S., Bailey, S. R., Fogden, S. and Green, M. L. H., *J. Am. Chem. Soc.* **2003**, *125*, 8722.

[38] Ogrin, D., Chattopadhyay, J., Sadana, A. K., Billups, W. E. and Barron, A. R., *J. Am. Chem. Soc.* **2006**, *128*, 11322.

[39] [(a)]Arai, T., Nobukuni, S., Sandanayaka, A. S. D. and Ito, O., *J. Phys. Chem. C* **2009**, *113*, 14493; [(b)]Campidelli, S., Sooambar, C., Lozano Diz, E., Ehli, C., Guldi, D. M. and Prato, M., *J. Am. Chem. Soc.* **2006**, *128*, 12544.

[40] Ballesteros, B., De la Torre, G., Ehli, C., Rahman, G. M. A., Agullo-Rueda, F., Guldi, D. M. and Torres, T., *J. Am. Chem. Soc.* **2007**, *129*, 5061.

[41] de Freitas, J. N., Maubane, M. S., Bepete, G., van Otterlo, W. A. L., Coville, N. J. and Nogueira, A. F., *Synth. Met.* **2013**, *176*, 55.

attach amphotericin B (antibiotic) and ethotrexate (drug) to MWNT and tested their delivery by labelling the functionalized CNT with fluorescein.[42]

The Diels-Alder cycloaddition can also take place on the sidewalls of CNT. An original method based on the double activation of the nanotube surface by combining high pressure and $Cr(CO)_6$ was reported allowing the efficient functionalization of SWNT by electron-rich dienes (Figure 1.1-9, d).[43] Moreover, Chang *et al.* demonstrated that MWNT can serve as either a dienophile or a diene in Diels-Alder reactions.[44] Briefly, they managed to employ a furan derivative, carrying electron-withdrawing substituents, as a diene reagent, to modify MWNT through a Diels-Alder cycloaddition, and in a similar approach they utilized a maleimide compound as a dienophile for the covalent functionalization of MWNT.

ii) Radical additions:

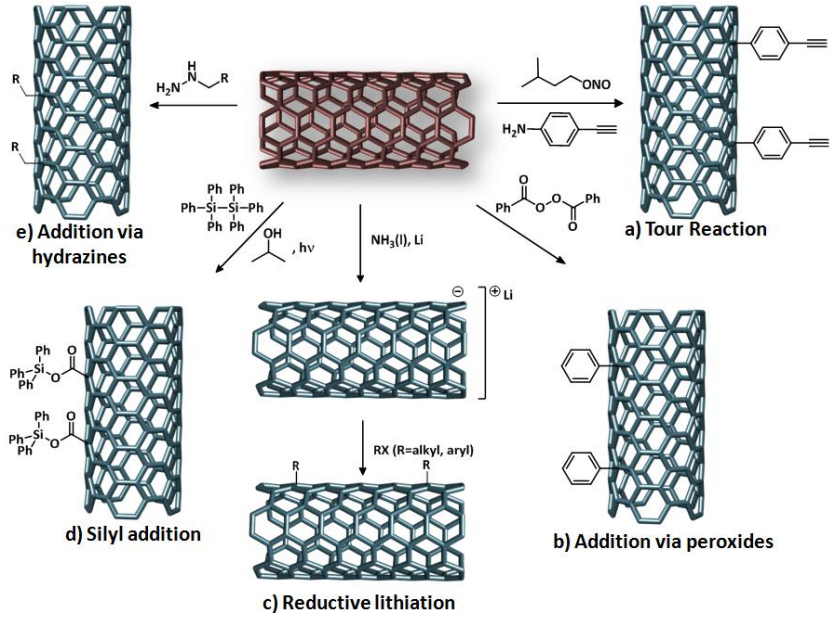

Figure 1.1-10. Radical additions performed on the sidewalls of CNT.

Probably the most utilized reaction on the covalent modification of CNT is the aryl addition via *in situ* generation of diazonium salts, the so called Tour

[42] [(a)]Pastorin, G., Wu, W., Wieckowski, S., Briand, J. P., Kostarelos, K., Prato, M. and Bianco, A., *Chem. Commun.* **2006**, 1182; [(b)]Lacerda, L., Bianco, A., Prato, M. and Kostarelos, K., *Adv. Drug Delivery Rev.* **2006**, *58*, 1460; [(c)]Wu, W., Wieckowski, S., Pastorin, G., Benincasa, M., Klumpp, C., Briand, J. P., Gennaro, R., Prato, M. and Bianco, A., *Angew. Chem., Int. Ed.* **2005**, *44*, 6358.

[43] Menard-Moyon, C., Dumas, F., Doris, E. and Mioskowski, C., *J. Am. Chem. Soc.* **2006**, *128*, 14764.

[44] Chang, C.-M. and Liu, Y.-L., *Carbon* **2009**, *47*, 3041.

reaction (Figure 1.1-10, a). The possibility to attach phenyl groups without interrupting the conjugation in the nanotube and bearing many different organic functional groups, made this procedure a very powerful tool. From the first protocols, involving the use of oleum[45] or ionic liquids,[46] to the latest solvent free methodologies, a considerable amount of reports on this reaction have been published. For example, as occurred with the Prato addition, porphyrins, subphtalocyanines, DNA, and a large collection of functional molecules have been attached to the nanotubes surface. The revolution brought by the organometallic catalysis has not been immune to this methodology and Suzuki couplings,[47] Heck's reactions[48] or Huysgen[49] cycloadditions have been utilized on SWNT decorated with phenyl rings containing an alkyne group.

An easy way to obtain directly alkylated CNT was reported by Murata *et al.*[50] by using hydrazine in a surfactant media (Figure 1.1-10, e). Wei *et al*. reported the electron transfer from potassium to benzophenone to produced a radical intermediate able to react rapidly with the SWNT surface, affording diphenylcarbinol functionalized SWNT.[51] In the same line, different peroxides were tried by Billups *et al.,*[52] who observed the thermal decomposition of four diacyl peroxides (benzoyl, 4-methoxybenzoyl, phthaloyl, and trifluoroacetyl) in the presence of SWNT (Figure 1.1-10, b).[53] Sylil groups have also been anchored to CNT sidewalls by using silane derivatives under irradiation (Figure 1.1-10, d).[54]

Another useful methodology developed by Billups *et al.* is the reductive lithiation of SWNT in liquid ammonia, which affords a CNT^{-}-Li^{+} suspension able to react with a large variety of electrophiles, improving the solubility of

[45] Hudson, J. L., Casavant, M. J. and Tour, J. M., *J. Am. Chem. Soc.* **2004**, *126*, 11158.
[46] Price, B. K., Hudson, J. L. and Tour, J. M., *J. Am. Chem. Soc.* **2005**, *127*, 14867.
[47] Cheng, F. and Adronov, A., *Chem. Mater.* **2006**, *18*, 5389.
[48] Gomez-Escalonilla, M. J., Atienzar, P., Garcia Fierro, J. L., Garcia, H. and Langa, F., *J. Mater. Chem.* **2008**, *18*, 1592.
[49] Campidelli, S., Ballesteros, B., Filoramo, A., Diaz Diaz, D., de la Torre, G., Torres, T., Rahman, G. M. A., Ehli, C., Kiessling, D., Werner, F., Sgobba, V., Guldi, D. M., Cioffi, C., Prato, M. and Bourgoin, J.-P., *J. Am. Chem. Soc.* **2008**, *130*, 11503.
[50] Yokoi, T., Iwamatsu, S.-i., Komai, S.-i., Hattori, T. and Murata, S., *Carbon* **2005**, *43*, 2869.
[51] Wei, L. and Zhang, Y., *Chem. Phys. Lett.* **2007**, *446*, 142.
[52] Liang, F., Beach, J. M., Rai, P. K., Guo, W., Hauge, R. H., Pasquali, M., Smalley, R. E. and Billups, W. E., *Chem. Mater.* **2006**, *18*, 1520.
[53] Engel, P. S., Billups, W. E., Abmayr, D. W., Tsvaygboym, K. and Wang, R., *J. Phys. Chem. C* **2008**, *112*, 695.
[54] Hemraj-Benny, T. and Wong, S. S., *Chem. Mater.* **2006**, *18*, 4827.

the starting material.[55] One advantage of this methodology is the preferred reaction on metallic tubes rather than semiconductors (Figure 1.1-10, c).[56]

iii) Nucleophilic and electrophilic additions:

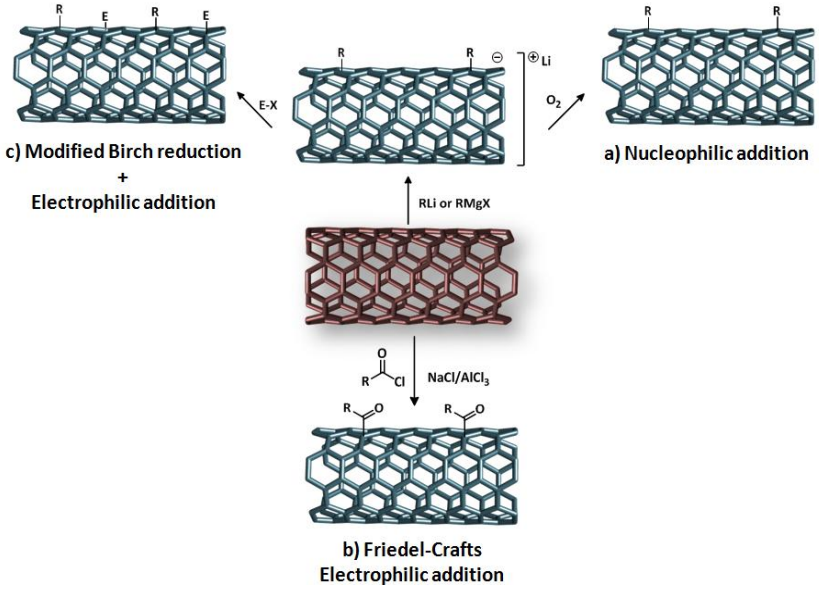

Figure 1.1-11. Nucleophilic and electrophilic additions performed on the sidewalls of CNT.

Hirsch *et al.* reported the nucleophilic addition of organolithium and organomagnesium derivatives to SWNT, affording highly unbundled charged intermediates that after oxygen bubbling resulted in neutral highly exfoliated SWNT derivatives (Figure 1.1-11, a). Furthermore, the reaction seems to take place selectively on metallic SWNT.[57] Another classical organic reaction applied to nanotubes is the Friedel-Crafts acylation (Figure 1.1-11, b).[58] An interesting combination of both additions was accomplished by Hirsch *et al.* affording a double functionalization utilizing in a first step organolithium reagents and, afterwards, ketones, esters or halides as electrophiles (Figure 1.1-11, c).[59]

---

[55] Mukherjee, A., Combs, R., Chattopadhyay, J., Abmayr, D. W., Engel, P. S. and Billups, W. E., *Chem. Mater.* **2008**, *20*, 7339.

[56] Wunderlich, D., Hauke, F. and Hirsch, A., *J. Mater. Chem.* **2008**, *18*, 1493.

[57] [(a)]Wunderlich, D., Hauke, F. and Hirsch, A., *Chem. Eur. J.* **2008**, *14*, 1607; [(b)]Graupner, R., Abraham, J., Wunderlich, D., Vencelová, A., Lauffer, P., Röhrl, J., Hundhausen, M., Ley, L. and Hirsch, A., *J. Am. Chem. Soc.* **2006**, *128*, 6683.

[58] Lee, H.-J., Han, S.-W., Kwon, Y.-D., Tan, L.-S. and Baek, J.-B., *Carbon* **2008**, *46*, 1850.

[59] Gebhardt, B., Syrgiannis, Z., Backes, C., Graupner, R., Hauke, F. and Hirsch, A., *J. Am. Chem. Soc.* **2011**, *133*, 7985.

c) Supramolecular functionalization of CNT

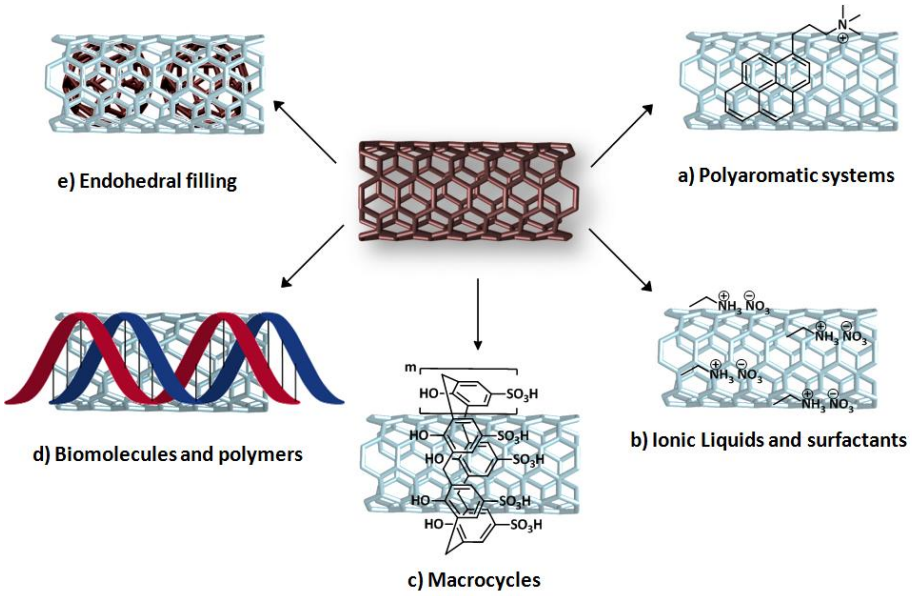

Figure 1.1-12. Different strategies for the supramolecular modification of CNT.

Polyaromatic compounds have been broadly tested on the non-covalent modification of CNT because of the strong interaction with the huge π surface of CNT. Condensed aromatic derivatives carrying a hydrophilic or hydrophobic moiety can disperse CNT in aqueous and organic media, respectively. In particular, pyrene derivatives have demonstrated to be very efficient solubilizers as compared to benzene, phenanthrene or anthracene. When pyrene is tailored with an alkyl ammonium chain is able to solubilise SWNT in aqueous media and even make them interact with other anionic units, such as porphyrins, by electrostatic interactions, affording supramolecular donor-acceptor systems (Figure 1.1-12, a). Moreover, pyrene revealed a specific diameter range of interactions (0.9-1.0 nm).[60] Pyrene was linked to other electroactive functionalities including fullerene[61] or tetrathiafulvalene,[62] revealing an electronic communication between donor and acceptor units. Considering porphyrins, Diederich *et al.* utilized fused porphyrin oligomers to improve the solubility of SWNT and trimers revealed

[60] Ehli, C., Rahman, G. M. A., Jux, N., Balbinot, D., Guldi, D. M., Paolucci, F., Marcaccio, M., Paolucci, D., Melle-Franco, M., Zerbetto, F., Campidelli, S. and Prato, M., *J. Am. Chem. Soc.* **2006**, *128*, 11222.

[61] Guldi, D. M., Menna, E., Maggini, M., Marcaccio, M., Paolucci, D., Paolucci, F., Campidelli, S., Prato, M., Rahman, G. M. and Schergna, S., *Chem. Eur. J.* **2006**, *12*, 3975.

[62] Ehli, C., Guldi, D. M., Herranz, M. Á., Martin, N., Campidelli, S. and Prato, M., *J. Mater. Chem.* **2008**, *18*, 1498.

to be better solubilizer than dimers.[63] Porphyrin dendrimers were also utilized with remarkable results in solubility.[64]

Amphipilic substances like surfactants or ionic liquids have been widely utilized for solubilizing CNT. Typical examples include sodium dodecyl sulphate (SDS), tetrabutylammonium bromide (TBAB) or alkyl-substituted imidazolium salts. The main advantage of using ionic liquids is the possibility of modulating the solubility in a range from aqueous to polar or non-polar organic solvents (Figure 1.1-12, b).[65]

Taking in mind the advances in the supramolecular chemistry of fullerenes and in particular in the search of suitable hosts for them, preorganized structures as macrocycles have shown to complex with CNT (Figure 1.1-12, c). Cucurbiturils or calixarenes were able to solubilise SWNT in aqueous media in a reversible process after the addition of a second guest, precipitating the released SWNT.[66]

Another interesting approach is the use of biomolecules, such as proteins, DNA or polysaccharides, opening new horizons in the development of bionanotechnology (Figure 1.1-12, d).[67] Proteins can be considered a poly amphiphilic system able to host the aromatic surface of the CNT into their non-polar pockets. This ability shown to be very dependent on the pH conditions and the aminoacidic residues. In the case of polysaccharides, chitosan has demonstrated diameter selectivity for the wrapping of small diameter CNT.[68] DNA/SWNT systems have been utilized as sensors for different biomolecules as proteins, odours or other ligands, using the SWNT structure to enhance the electric current based response.[69]

The utilization of conjugated polymers for the non-covalent modification of CNT have allowed the selective separation of the different CNT present in as prepared samples. The use of poly(9,9-dialkylfluorene)s (PFx) or regioregular poly(3-alkylthiophene)s (P3AT) around the SWNT improve the dispersibility

[63] Cheng, F., Zhang, S., Adronov, A., Echegoyen, L. and Diederich, F., *Chem. Eur. J.* **2006**, *12*, 6062.
[64] Cheng, F. and Adronov, A., *Chem. Eur. J.* **2006**, *12*, 5053.
[65] Jiang, W., Yu, B., Liu, W. and Hao, J., *Langmuir* **2007**, *23*, 8549.
[66] Ogoshi, T., Inagaki, A., Yamagishi, T.-a. and Nakamoto, Y., *Chem. Commun.* **2008**, 2245.
[67] Yang, W., Thordarson, P., Gooding, J. J., Ringer, S. P. and Braet, F., *Nanotechnol.* **2007**, *18*, 412001.
[68] Wang, S.-F., Shen, L., Zhang, W.-D. and Tong, Y.-J., *Biomacromolecules* **2005**, *6*, 3067.
[69] Wind, S. J., Penzo, E., Palma, M., Wang, R., Fazio, T., Porath, D., Rotem, D., Livshits, G. and Stern, A., *J. Self-Assem. Mol. Electron.* **2013**, *1*, 177.

of CNT and allows a discrimination by diameter and chirality, a crucial step for further applications.[70]

The endohedral filling of CNT can be also consider a supramolecular modification. In this sense, remarkable results have been obtained in the insertion of fullerenes and EMFs into SWNTs (Figure 1.1-12, e). Moreover, when submitting the material to high pressures, inner fullerenes are able to polymerize.[71]

[70] Samanta, S. K., Fritsch, M., Scherf, U., Gomulya, W., Bisri, S. Z. and Loi, M. A., *Acc. Chem. Res.* **2014**, *47*, 2446.
[71] Britz, D. A. and Khlobystov, A. N., *Chem. Soc. Rev.* **2006**, *35*, 637.

1.1.2. CHEMICAL REACTIVITY OF GRAPHENE

Graphene is the latest discovered CNF and it can be defined as a planar hexagonal arrangement of sp^2 carbons comprising an atomic thin layer.[7]As initially occurred with its relatives CNT, a great expectative arose for this amazing material because of its remarkable properties. Only for naming a few characteristics: extraordinary mechanical properties (huge elastic constant and strength), thermal properties (high thermal conductivity, negative thermal expansion coefficient) and opto-electronic properties (zero band-gap and high conductivity). In addition, a whole range of potential applications make this material the promising revolution in the different material sciences.[72]

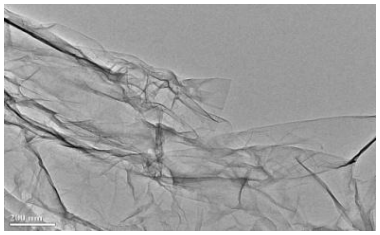

Figure 1.1-13. TEM micrograph of a few layer graphene sample (200 nm scale bar).

Several production methodologies of graphene have been developed during the last decade: micromechanical cleavage, anodic bonding, photo exfoliation, liquid phase exfoliation, growth on SiC, segregation/precipitation from carbon containing metal substrates, chemical vapour deposition (CVD) and molecular epitaxial beam or chemical synthesis using benzene as building block.[73] The different conditions for its production determine diverse graphene qualities with different sizes, defects, impurities or aggregation degrees of the graphene layers, which make the different kinds of graphene more or less appropriated for certain applications.

Regardless the fabrication methodology, the low solubility and the formation of a multilayer material is a hardness to overcome and, in this sense, chemical modification may be a powerful tool. Analogously to CNT, the different approaches to the chemical modification of graphene (covalent and supramolecular) allow not only an improvement in the solubility, but the opportunity of conferring new and better properties to the material. Several

[72] [(a)]Lau, C. N., Bao, W. and Velasco Jr, J., *Mater. Today* **2012**, *15*, 238; [(b)]Castro Neto, A. H., Guinea, F., Peres, N. M. R., Novoselov, K. S. and Geim, A. K., *Rev. Mod. Phys.* **2009**, *81*, 109.

[73] Bonaccorso, F., Lombardo, A., Hasan, T., Sun, Z., Colombo, L. and Ferrari, A. C., *Mater. Today* **2012**, *15*, 564.

recent interesting review articles and books deal with this topic,[74] and in the next pages only a selection of examples are commented.

a) Covalent modification of graphene

Despite the geometrical differences between graphene and CNT, from a chemical viewpoint they are polyenes with different bond strength. This fact has driven graphene chemistry in a parallel way to that of CNT and, therefore, similar reactions have been reported in the bibliography.

Although an excess in the generated defects on the graphene lattice could dramatically change the properties, the controlled modification could be mandatory for certain applications, such as obtaining semiconductors by inducing holes in graphene electronic structure.[75] Considering the electronic and geometrical disturbance in the π system induced by any chemical reaction, carbon atoms at the edges are supposed to be more reactive. Moreover, the inner honeycomb presents defects that activate chemically the sp^2 atoms surrounding them. Since both sides of the graphene layer are accessible to reagents, the chemistry of graphene affords species that would be unthinkable on graphite.

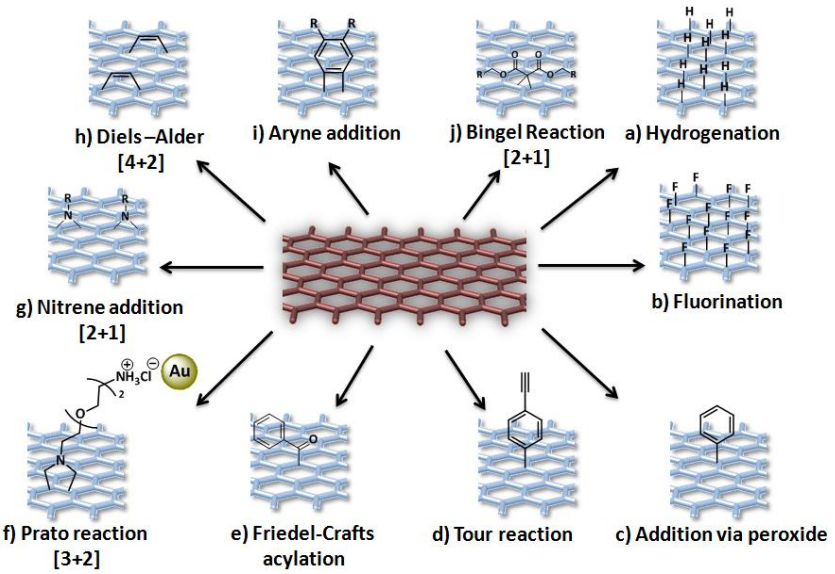

Figure 1.1-14. Different strategies for the covalent modification of graphene.

[74] [(a)]Georgakilas, V., *Functionalization of Graphene*, Wiley-VCH Verlag GmbH & Co. KGaA, **2014**; [(b)]Eigler, S. and Hirsch, A., *Angew. Chem., Int. Ed.* **2014**, *53*, 7720; [(c)]Rodriguez-Perez, L., Herranz, M. A. and Martin, N., *Chem. Commun.* **2013**, *49*, 3721; [(d)]*Special Issue in Graphene (part I and II), Vol. 46*, Accounts of Chemical Research, American Chemical Society, **2012**.

[75] Luo, G., Liu, L., Zhang, J., Li, G., Wang, B. and Zhao, J., *ACS Appl. Mater. Interfaces* **2013**, *5*, 11184.

The first reaction tested on pristine graphene was its reduction to graphane converting a semimetal into an insulator (Figure 1.1-14, a). Under annealing conditions, the reverse process was achieved.[76] Totally fluorinated graphene was also synthesized, affording an insulator whose mechanical properties are quite similar to graphene but with an improved solubility and stability (Figure 1.1-14, b).[77]

The low reactivity of graphene requires the use of highly reactive species such as radicals. The reaction with peroxides was described observing a remarkable increase in the D mode of the Raman spectrum in the obtained material because of the sp^3 generated atoms (Figure 1.1-14, c).[78] Following the well established methodology by Tour *et. al.* different functional materials have been prepared using aryl diazonium salts (Figure 1.1-14, d).[79] The introduction of sp^3 atoms results in a band gap opening affording a semiconductor material with different conductor and insulator domains into the structure.

The use of a Na/K alloy on bulk graphite followed by the addition of diazonium salts was reported by Hirsch *et. al.*, resulting in an interesting strategy to obtained functionalized graphene directly from a cheap commercially available material as graphite.[80] Moreover, the ionic intermediate can be utilized for electrophile additions. The most important fact from this kind of additions is the later reactions that can be accomplished on the pendant functional groups of the attached phenyl rings. As in the related CNT, the Cu(I)-catalyzed Huisgen [3+2] cycloaddition reaction or the Heck reaction[81] have been studied. Different active molecules have been attached to graphene using this strategy, for example, Zn-porphyrins, Ru-phenantroline[82] or phthalocyanines.[83]

---

[76] Savchenko, A., *Science* **2009**, *323*, 589.

[77] Nair, R. R., Ren, W., Jalil, R., Riaz, I., Kravets, V. G., Britnell, L., Blake, P., Schedin, F., Mayorov, A. S., Yuan, S., Katsnelson, M. I., Cheng, H.-M., Strupinski, W., Bulusheva, L. G., Okotrub, A. V., Grigorieva, I. V., Grigorenko, A. N., Novoselov, K. S. and Geim, A. K., *Small* **2010**, *6*, 2877.

[78] Liu, H., Ryu, S., Chen, Z., Steigerwald, M. L., Nuckolls, C. and Brus, L. E., *J. Am. Chem. Soc.* **2009**, *131*, 17099.

[79] Jin, Z., Lomeda, J. R., Price, B. K., Lu, W., Zhu, Y. and Tour, J. M., *Chem. Mater.* **2009**, *21*, 3045.

[80] Englert, J. M., Dotzer, C., Yang, G., Schmid, M., Papp, C., Gottfried, J. M., Steinrück, H.-P., Spiecker, E., Hauke, F. and Hirsch, A., *Nat. Chem.* **2011**, *3*, 279.

[81] Bao, Q., Zhang, H., Yang, J.-x., Wang, S., Tang, D. Y., Jose, R., Ramakrishna, S., Lim, C. T. and Loh, K. P., *Adv. Funct. Mater.* **2010**, *20*, 782.

[82] Wang, H.-X., Zhou, K.-G., Xie, Y.-L., Zeng, J., Chai, N.-N., Li, J. and Zhang, H.-L., *Chem. Commun.* **2011**, *47*, 5747.

[83] Ragoussi, M.-E., Malig, J., Katsukis, G., Butz, B., Spiecker, E., de la Torre, G., Torres, T. and Guldi, D. M., *Angew. Chem., Int. Ed.* **2012**, *51*, 6421.

The Friedel–Crafts acylation was reported as previous step for an improved chemical exfoliation of graphite, reacting at the edges of graphite and facilitating through this way the wettability with the exfoliating solvent (Figure 1.1-14, e).[84] The so called Prato reaction that was broadly studied for fullerenes and CNT has also been applied to graphene. The pyrrolidine modified graphene is able to bind gold nanorods in its pendant groups, that were utilized as contrast markers (Figure 1.1-14, f).[85]

Nitrene additions were performed forming aziridine rings on the graphene lattice bearing different substituents able to modulate the material solubility (Figure 1.1-14, g).[86] The Bingel reaction was tested on graphene by using a tetrathiafulvalene based bromomalonate derivative assisted by microwave irradiation (Figure 1.1-14, j).[87] Arynes have been utilized in [2+2] cycloaddition on graphene by using 2-(trimethylsilyl)aryl triflates as active benzyne precursors (Figure 1.1-14, i).[88] Graphene has also been investigated in Diels-Alder reaction. Interestingly, Haddon *et al.* have demonstrated the graphene ability to act both as diene or dienophile (Figure 1.1-14, h).[89]

b) Supramolecular modification of graphene

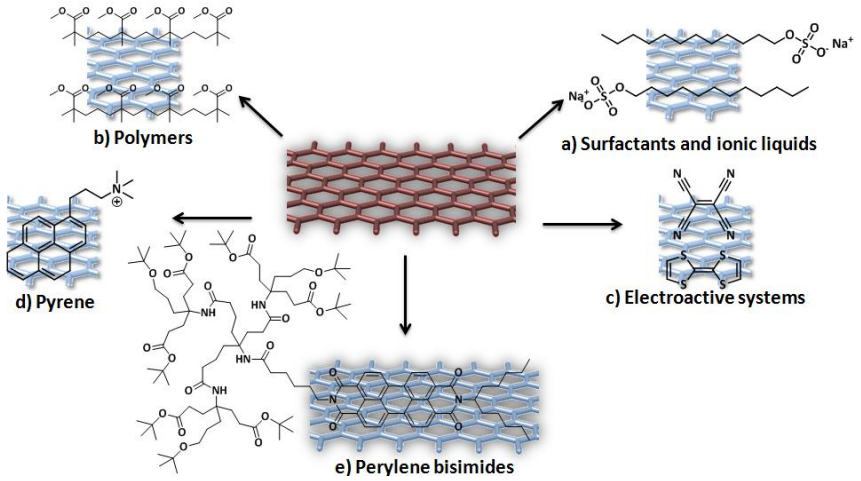

Figure 1.1-15. Different strategies for the supramolecular modification of graphene.

[84] Choi, E.-K., Jeon, I.-Y., Bae, S.-Y., Lee, H.-J., Shin, H. S., Dai, L. and Baek, J.-B., *Chem. Commun.* **2010**, *46*, 6320.
[85] Quintana, M., Spyrou, K., Grzelczak, M., Browne, W. R., Rudolf, P. and Prato, M., *ACS Nano* **2010**, *4*, 3527.
[86] Choi, J., Kim, K.-j., Kim, B., Lee, H. and Kim, S., *J. Phys. Chem. C* **2009**, *113*, 9433.
[87] Economopoulos, S. P., Rotas, G., Miyata, Y., Shinohara, H. and Tagmatarchis, N., *ACS Nano* **2010**, *4*, 7499.
[88] Zhong, X., Jin, J., Li, S., Niu, Z., Hu, W., Li, R. and Ma, J., *Chem. Commun.* **2010**, *46*, 7340.
[89] Sarkar, S., Bekyarova, E. and Haddon, R. C., *Acc. Chem. Res.* **2012**, *45*, 673.

In order to obtain stable supramolecular complexes with graphene flakes it is necessary to find species able to establish stable strong interactions within the thin layers, disrupting the huge tendency to stack of the pristine material. Successful solvents in graphite exfoliation use to be those whose surface energy matches that of graphene, for example DMF (dimethylformamide), NMP (N-methylpyrrolidone), *o*-DCB (*o*-dichlorobenzene) or 1-Cl-Np (1-chloronaphtalene)[90], but most of the times their high boiling points or chemical incompatibility with other functionlaities on the graphene surface are a drawback in the later steps or applications. In order to overcome this problem, water soluble graphene has been obtained with surfactants such as SDS or sodium cholate (Figure 1.1-15, a).[91] Ionic liquids have been tested in a similar approach, allowing the dispersion of graphene in a variety of organic solvents.[92]

The utilization of polymers reinforced with carbon nanostructures is probably the field which, to the date, has been most commercially exploited. The use of polymers not only leads exfoliated layers, moreover results in an amazing improvement of the composite mechanical properties. For example, a nanocomposite containing poly(methyl methacrylate) (PMMA)/graphene (1% graphene) increases in an 80% the elastic modulus and about a 20% the tensile strength reported to PMMA (Figure 1.1-15, b).[93]

As aforementioned, the formation of holes is necessary to induce a band gap suitable for the fabrication of capacitors. In this sense, the supramolecular interaction with donor or acceptor molecules induces important changes in the graphene Raman G-mode as consequence of the electronic interaction. Charge transfer bands were observed in the visible region when TTF or TCNE are utilized (Figure 1.1-15, c).[94]

As reported for CNT, polyaromatic systems are ideal candidates for establishing strong $\pi-\pi$ interactions and exfoliate graphene layers. Pyrene derivatives have been reported to afford graphene suspension in aqueous solutions (Figure 1.1-15, d).[95] Abruña *et al.*, reported the strong interaction

[90] Lotya, M., Hernandez, Y., King, P. J., Smith, R. J., Nicolosi, V., Karlsson, L. S., Blighe, F. M., De, S., Wang, Z., McGovern, I. T., Duesberg, G. S. and Coleman, J. N., *J. Am. Chem. Soc.* **2009**, *131*, 3611.

[91] Lin, S., Shih, C.-J., Strano, M. S. and Blankschtein, D., *J. Am. Chem. Soc.* **2011**, *133*, 12810.

[92] Liu, N., Luo, F., Wu, H., Liu, Y., Zhang, C. and Chen, J., *Adv. Funct. Mater.* **2008**, *18*, 1518.

[93] Barun, D., Prasad, K. E., Ramamurty, U. and Rao, C. N. R., *Nanotechnol.* **2009**, *20*, 125705.

[94] Rakesh, V., Barun, D., Chandra Sekhar, R. and Rao, C. N. R., *J. Phys.: Condens. Matter* **2008**, *20*, 472204.

[95] Xu, Y., Bai, H., Lu, G., Li, C. and Shi, G., *J. Am. Chem. Soc.* **2008**, *130*, 5856.

of a tripodal pyrene derivative with graphene allowing the formation of monolayer suspensions.[96] Another polyaromatic systems with remarkable properties are perylene bisimides (PBI) (Figure 1.1-15, e). These kind of systems have proved to carry out the exfoliation of graphene at the time that set electronic communication between both units even in water.[97]

[96] Mann, J. A., Rodríguez-López, J., Abruña, H. D. and Dichtel, W. R., *J. Am. Chem. Soc.* **2011**, *133*, 17614.
[97] Kozhemyakina, N. V., Englert, J. M., Yang, G., Spiecker, E., Schmidt, C. D., Hauke, F. and Hirsch, A., *Adv. Mater.* **2010**, *22*, 5483.

1.1.3. π-exTTF AS ELECTRON DONOR AND RECOGNITION MOTIF

After the synthesis of tetrathiafulvalene (TTF) by Wudl in 1970,[98] the remarkable electronic properties found on this compound spur on researchers to exploit its structure and obtain new and better derivatives able to improve its characteristics, leading a new family of substances known as *organic synthetic metals*.[99] One of these strategies was the separation of the 1,3-dithiole rings through a *p*-quinoid system, yielding the 9,10-bis-(1,3-dithiol-2-ylidene)-9,10-dihydroanthracene (π-exTTF or simply exTTF).

While TTF analogues exhibit two well separated one-electron oxidation processes at relatively low oxidation potential values (E_{ox}^{1} = 0.37 V and E_{ox}^{2} = 0.67 V vs. SCE, in dichloromethane), π-exTTF exhibits a two-electron oxidation process to form a dication species (E_{ox}^{1} = 0.44 V vs. SCE, in dichloromethane). Moreover, the two-electron oxidation process to form the dication aromatic species in π-exTTF is accompanied by a geometrical change from a "butterfly" shape structure to a planar di-cationic structure where the 1,3-dithiolium rings are located orthogonal to the anthracene skeleton (Figure. 1.1-16).

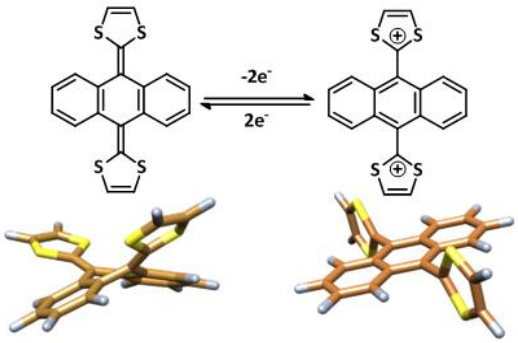

Figure 1.1-16. Changes in the π-exTTF geometry promoted by the oxidation process.

The change to planarity and gain in aromaticity to afford a very stable structure is the driving force in the oxidation process, what made π-exTTF to hold a great promise in the organic electronics field. Furthermore, its geometry and self-assembly ability has afforded several studies revealing the formation of macromolecular architectures and the selective recognition of fullerenes (Figure 1.1.-17).[100]

[98] Wudl, F., Smith, G. M. and Hufnagel, E. J., *J. Chem. Soc. D.: Chem, Commun.* **1970**, 1453.
[99] [(a)]Martin, N., *Chem. Commun.* **2013**, *49*, 7025; [(b)]Fabre, J. M., *J. Solid State Chem.* **2002**, *168*, 367.
[100] Brunetti, F. G., Lopez, J. L., Atienza, C. and Martin, N., *J. Mater. Chem.* **2012**, *22*, 4188.

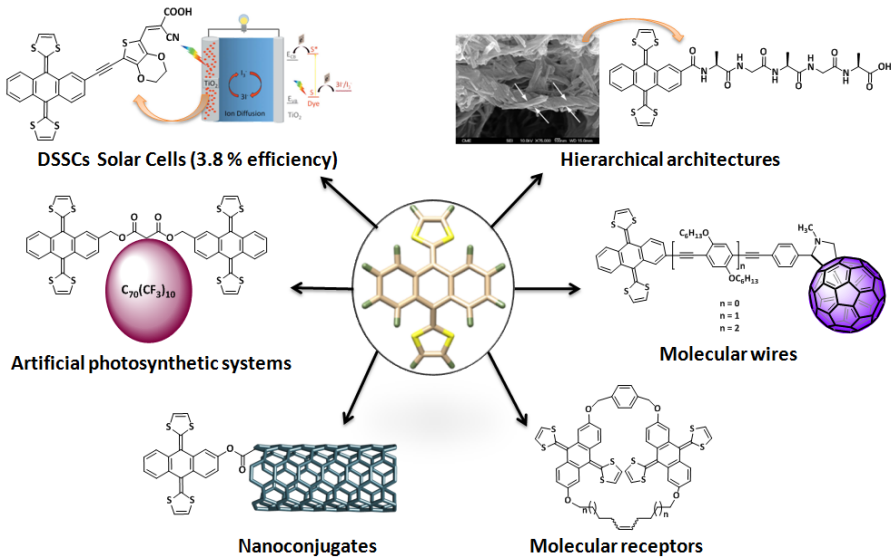

Figure 1.1-17. Some of the applications of π-exTTF in organic molecular electronics and supramolecular chemistry.

a) π-exTTF in organic molecular electronics

The π-exTTF ability to get oxidized granting a pair of electrons, gaining planarity and aromaticity has made π-exTTF more than a suitable candidate to the design and synthesis of donor-acceptor systems that could be applied in different electronic devices. For example, several diads (C_{60}-bridge-π-exTTF) have been studied as molecular wires employing different π-conjugated systems as bridges (oligo *p*-phenylenevinylenes, *p*- and *m*-oligo(phenylene)ethynylene, oligofluorenes or [2,2]-paracyclophanes), (Figure 1.1-17, right centre). The small attenuation factor (β) values and the strong electronic donor-acceptor coupling found in these systems are responsible for the nanowire behaviour.[101]

In order to mimic the photosynthesis process, several diads and triads were investigated upon photoinduced electron-transfer conditions. The combination of π-exTTF with C_{60} provides long lived radical ion pairs with lifetimes ranging from nanoseconds to hundreds of microseconds (Figure 1.1-18).[102]

---

[101] [(a)]Wielopolski, M., Molina-Ontoria, A., Schubert, C., Margraf, J. T., Krokos, E., Kirschner, J., Gouloumis, A., Clark, T., Guldi, D. M. and Martín, N., *J. Am. Chem. Soc.* **2013**, *135*, 10372; [(b)]Molina-Ontoria, A., Wielopolski, M., Gebhardt, J., Gouloumis, A., Clark, T., Guldi, D. M. and Martín, N., *J. Am. Chem. Soc.* **2011**, *133*, 2370; [(c)]Guldi, D. M., Illescas, B. M., Atienza, C. M., Wielopolski, M. and Martín, N., *Chem. Soc. Rev.* **2009**, *38*, 1587.

[102] [(a)]Castellanos, S., Vieira, A. A., Illescas, B. M., Sacchetti, V., Schubert, C., Moreno, J., Guldi, D. M., Hecht, S. and Martin, N., *Angew. Chem., Int. Ed.* **2013**, *52*, 13985; [(b)]Martín,

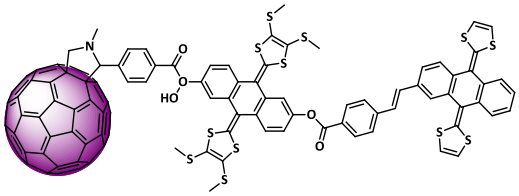

Figure 1.1-18. Structure of C_{60}-π-exTTF $_1$-π-exTTF $_2$ with 111 μs of charge separated state lifetime.

Taking advantage of the remarkable properties of endohedral metallofullerenes (EMF), our group reported different diads containing π-exTTF and these novel higher fullerenes, revealing the influence of the electronic structure of La@C_{82} and La_2@C_{80} in stabilizing the radical ion pair state of the diads when compared with the related C_{60} system (Figure 1.1-19).[103] The use of EMFs instead of C_{60} harness the possibility of modulating the electronic properties of the carbon cage by changing the inner encapsulated metal or the size of the cage and even afford the possibility of preparing diamagnetic or paramagnetic systems.

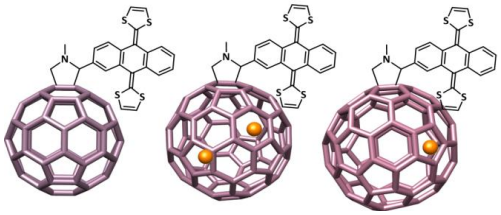

Figure 1.1-19. C_{60}, La_2@C_{80} and La@C_{82} systems investigated in photoinduced electron transfer processes.

As previously mentioned, π-exTTF has been attached to carboxylic acid groups in SWNT with different spacers. The nanoconjugates were investigated upon photoinduced electron transfer, yielding radical ion pair species with a charge recombination dynamics function of the spacer linking the π-exTTF moiety to the SWNT.[32] In order to avoid disturbing the electronic properties of SWNT, π–π interaction between SWNT and π-exTTF via pyrene derivatives has been utilized, affording supramolecular donor–acceptor nanohybrids with an improved solubility compared to the starting pristine material. We recently achieved the SWNT solubilisation in water considering dendronized or oligomeric molecules endowed with π-exTTF moieties.[104]

N., Sánchez, L., Herranz, M. Á., Illescas, B. and Guldi, D. M., *Acc. Chem. Res.* **2007**, *40*, 1015; [(c)]Sánchez, L., Pérez, I., Martín, N. and Guldi, D. M., *Chem. Eur. J.* **2003**, *9*, 2457.

[103] Schubert, C., Rudolf, M., Guldi, D. M., Takano, Y., Mizorogi, N., Herranz, M. Á., Martín, N., Nagase, S. and Akasaka, T., *Philos. Trans. R. Soc. London, A* **2013**, *371*.

[104] [(a)]Brunetti, F. G., Romero-Nieto, C., López-Andarias, J., Atienza, C., López, J. L., Guldi, D. M. and Martín, N., *Angew. Chem., Int. Ed.* **2013**, *52*, 2180; [(b)]Romero-Nieto, C., Garcia, R.,

The combination of π-exTTF with graphene has been considered in a couple of reports to date. In our group we have accomplished the supramolecular modification of graphene with π-exTTF. Results revealed that π–π and CH–π interactions are fundamental, and a negligible contribution from charge transfer was observed too. Moreover, these weak forces were amplified through multivalent gold nanoparticles, demonstrating that planarity is not a prerequisite in recognition motifs for graphene (Figure 1.1-20).[105] The other related work reported the graphene covalent modification by a Bingel reaction with an π-exTTF-malonate derivative. Although preliminary electrochemical measurements were carried out, the photophysical properties have not been reported for these donor-acceptor nanoconjugates.[87]

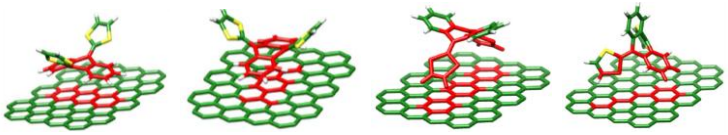

Figure 1.1-20. Different orientations in the π-exTTF-graphene interaction.

Within the field of organic electronics, it is interesting to remark the presence of π-exTTF in dye sensitized solar cells (DSSC or "Gratzel Cells"). The special π-exTTF shape reduces the possibilities of aggregation when is deposited onto TiO_2 and is notable how the dye is easily regenerated in spite of the expected low tendency to lose the aromaticity gained during the oxidation step, reaching efficiencies up to 3.8 %.[106]

b) π-exTTF as fullerene receptors

From the point of view of molecular recognition, fullerenes are interesting guests that interact with different tweezers or macrocyclic hosts.[107] Considering the large π-surface and the ability to yield charge, the particular geometry of π-exTTF has demonstrated to fit notably to the spherical shape of fullerenes, recognizing efficiently the convex surface of C_{60}. Systems based

---

Herranz, M. A., Ehli, C., Ruppert, M., Hirsch, A., Guldi, D. M. and Martin, N., *J. Am. Chem. Soc.* **2012**, *134*, 9183; [(c)]Herranz, M. Á., Ehli, C., Campidelli, S., Gutiérrez, M., Hug, G. L., Ohkubo, K., Fukuzumi, S., Prato, M., Martín, N. and Guldi, D. M., *J. Am. Chem. Soc.* **2007**, *130*, 66.

[105] Brunetti, F. G., Isla, H., Aragó, J., Ortí, E., Pérez, E. M. and Martín, N., *Chem. Eur. J.* **2013**, *19*, 9843.

[106] Wenger, S., Bouit, P.-A., Chen, Q., Teuscher, J., Censo, D. D., Humphry-Baker, R., Moser, J.-E., Delgado, J. L., Martín, N., Zakeeruddin, S. M. and Grätzel, M., *J. Am. Chem. Soc.* **2010**, *132*, 5164.

[107] [(a)]Canevet, D., Pérez, E. M. and Martín, N., in *Organic Nanomaterials*, John Wiley & Sons, Inc., **2013**, pp. 147; [(b)]Canevet, D., Pérez, E. M. and Martín, N., *Angew. Chem., Int. Ed.* **2011**, *50*, 9248; [(c)]Diederich, F. and Gomez-Lopez, M., *Chem. Soc. Rev.* **1999**, *28*, 263.

on π-exTTF/C_{60} have been able to interact affording many different arrangements, from discrete 1:1 complexes to oligomers, polymers, dendrimers and even supramolecular structures as helix or fibres. Limiting to the simply recognition of C_{60}, the first reported π-exTTF based receptors were connected through isophthalic and terephthalic ester spacers respectively (Figure 1.1-21). A dramatic solvent dependence was observed, even resulting in 1:1 stoichiometries for aromatic solvents while a polar mixture $CHCl_3/CS_2$ yielded complex stoichiometries with cooperative effects.[108]

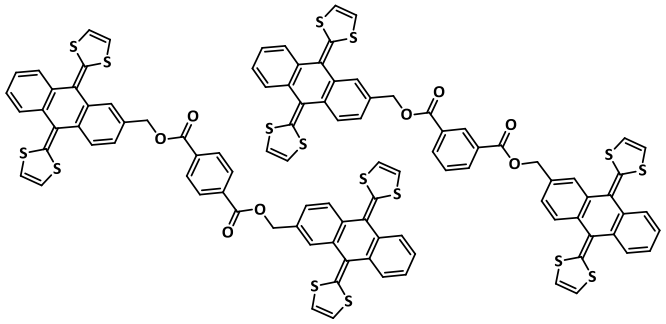

Figure 1.1-21. First reported π-exTTF based molecular tweezer receptors.

The typical UV-Vis titrations for π-exTTF based receptors, performed by addition of C_{60} to a host solution, show always very similar features. By increasing the amount of C_{60} in the solution, a decrease in intensity of the lowest-energy π-exTTF absorption band at 434 nm is observed. Simultaneously, the appearance of a charge-transfer band at 483 nm is detected. The mathematical treatment of these spectral changes resulted in binding constants about log K_a = 4.5. Calculations by DFT clearly confirmed the donor-acceptor interaction between π-exTTF and C_{60}.

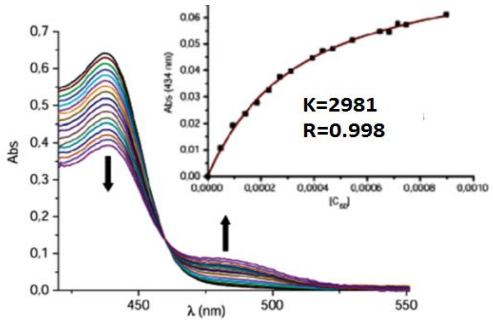

Figure 1.1-22. Absorption spectral changes of receptors in Figure 1.1-21 in chlorobenzene upon addition of fullerene. Binding isotherm is shown in the inset.

[108] Pérez, E. M., Sánchez, L., Fernández, G. and Martín, N., *J. Am. Chem. Soc.* **2006**, *128*, 7172.

The next step to improve the interaction was the introduction of some pre-organization elements. An alkyl linker was introduced and results on the titration experiments demonstrated the formation of the 1:1 complex, affording association constant values of log K_a = 6.5.[109] This promising result drove our group to study the changes in the degree of preorganization and the relative position of the recognition motif (Figure 1.1-23). The values obtained for log K_a revealed how very small changes in the spacer length or the position respect to the phenyl ring (*meta*- or *para*-) trigger dramatic changes in the global interaction, even reducing the binding constant in three orders of magnitude.[110]

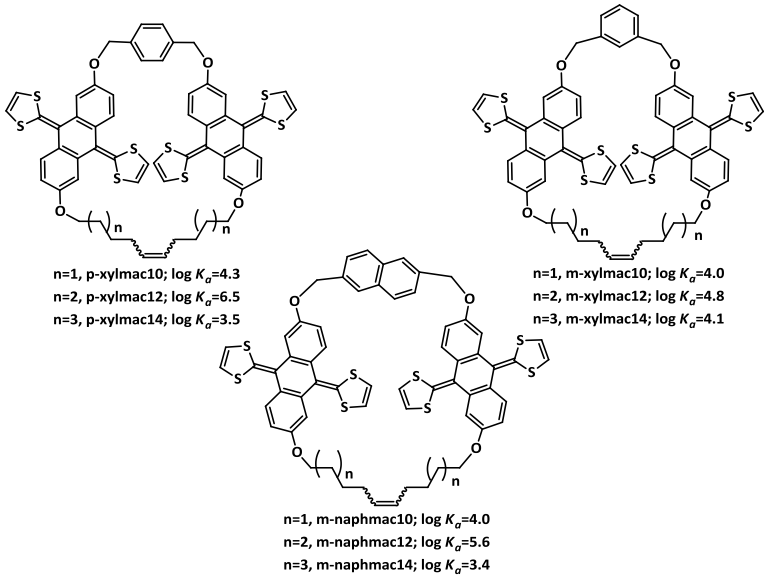

Figure 1.1-23. Preorganized π-exTTF based macrocyclic receptors.

To know the real relevance of the non-planarity and the charge transfer in the recognition of fullerene, four benchmark analogous receptors were synthesized and their binding constants calculated (Figure 1.1-24). Results revealed a clear influence of the π–π interactions, being the major driving force for the supramolecular complex formation, whereas geometry plays an important role. Finally, it is revealed that the charge transfer contribution is involved in the formation of the complex.[111]

[109] Isla, H., Gallego, M., Pérez, E. M., Viruela, R., Ortí, E. and Martín, N., *J. Am. Chem. Soc.* **2010**, *132*, 1772.
[110] Canevet, D., Gallego, M., Isla, H., de Juan, A., Pérez, E. M. and Martín, N., *J. Am. Chem. Soc.* **2011**, *133*, 3184.
[111] Perez, E. M., Capodilupo, A. L., Fernandez, G., Sanchez, L., Viruela, P. M., Viruela, R., Orti, E., Bietti, M. and Martin, N., *Chem. Commun.* **2008**, 4567.

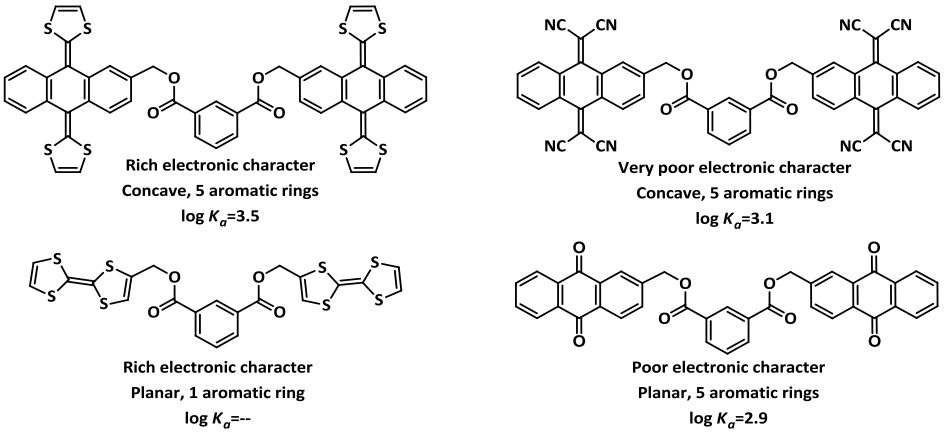

Figure 1.1-24. Comparison of the binding constants when an π-exTTF based receptor changes the electron donor recognition motif by others with different geometry or electronic character.

Very recently, several π-exTTF receptors containing triazole rings have been reported comparing the influence of different linkers in this kind of receptors.[112] From the six receptors reported in this work, only the ones shown in Figure 1.1-25 display notable interactions with C_{60}. Those bearing three π-exTTF units or a more extended conjugation on the 1,3-dithiole rings did not reveal any remarkable interaction, probably because of steric hindrance. Moreover, the authors reported the formation of two complexation stoichiometries, 1:1 and 1:2, when certain solvent conditions are utilized.

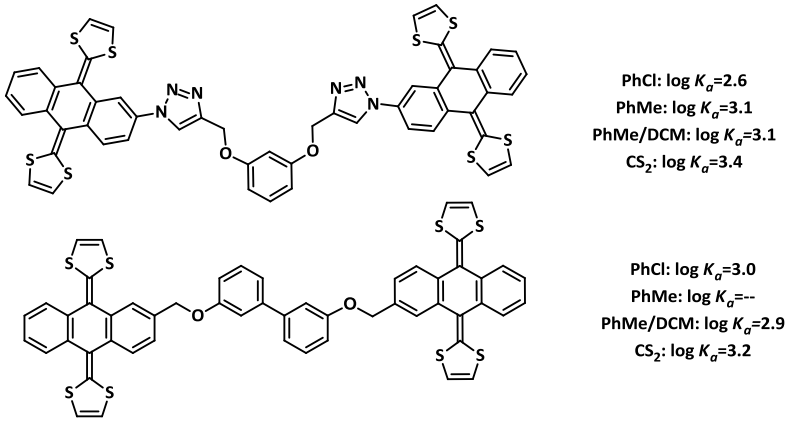

Figure 1.1-25. Reported π-exTTF based receptors by Morin *et al.* that showed affinity for C_{60}

[112] Iden, H., Fontaine, F. G. and Morin, J. F., *Org. Biomol. Chem.* **2014**, *12*, 4117.

1.2. Objectives

1.2. OBJECTIVES

Considering the aforementioned precedents as well as the expertise of our research group in fullerene chemistry, our aim in this chapter is the extension of our knowledge to other novel carbon nanomaterials such as SWNT, MWNT and graphene. The following specific goals are considered in Chapter 1:

i) Development of the first comparative study on the chemical reactivity of SWNT, MWNT and Graphene

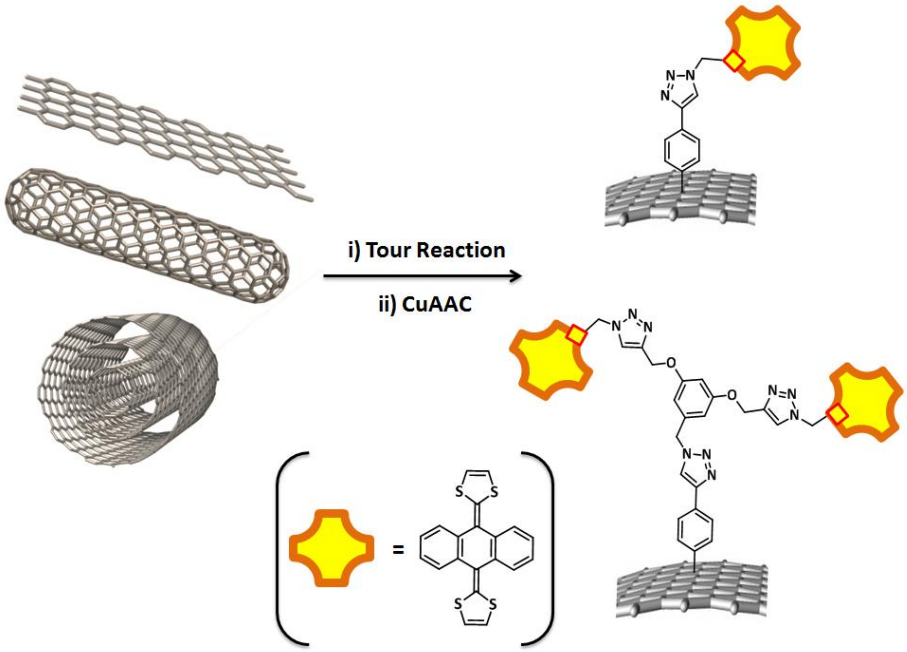

- Synthesis of a set of analogous nanoconjugates of SWNT, MWNT and graphene utilizing arylation reactions by *in situ* formation of arenediazonium salts of aromatic compounds, bearing an alkyne functional group, and subsequent Cu(I)-catalyzed 1,3-dipolar cycloaddition reaction (CuAAC) with π-exTTF derivatives.
- Full characterization of the nanoconjugates obtained by a thorough set of analytical, spectroscopic, electrochemical and microscopic techniques (TGA, FTIR, Raman, UV-Vis-NIR, cyclic voltammetry, TEM and XPS).
- The Tour reaction as benchmark process will allow carrying out the first comparative study on the different reactivity of each carbon nanoform.

ii) Photophysical study of the synthesized nanoconjugates

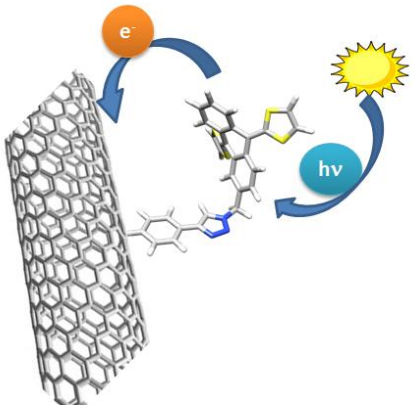

- Study of the electronic communication between the π-exTTF motifs and the carbon nanoforms by a series of steady-state and time resolved spectroscopy experiments.

iii) Preparation of SWNT, MWNT and graphene based receptors for fullerenes

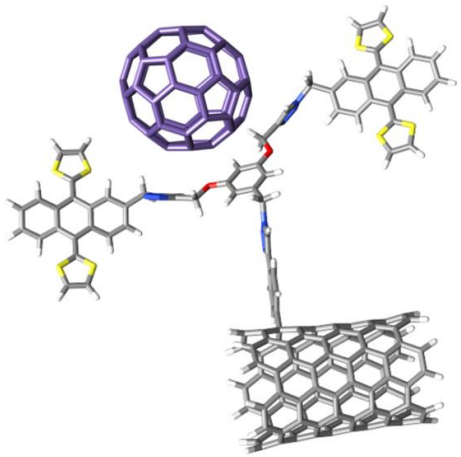

- Extension of the methodology in i) to the synthesis and characterization of a π-exTTF based "tweezer" system attached on CNF able to recognize C_{60} fullerene. Study of the supramolecular interaction between the receptor and C_{60} by UV-vis spectroscopy.
- Comprehensive study of the supramolecular interaction of the π-exTTF based "tweezer" system by comparison with other related receptors containing tetracyano-*p*-anthraquinodimethane (TCAQ) and benzene rings as recognition motifs by using UV-Vis spectroscopy, ^{1}H-NMR and theoretical calculations.

1.3. Results and discussion

1.3. RESULTS AND DISCUSSION

A set of nanoconjugates containing π-exTTF motifs were synthesized following the pathway represented in Scheme 1.3.1. Carbon nanoforms (SWNT, MWNT and graphene) were covalently modified using the previously established procedure by Tour *et al.,*[45,46] followed by a Cu(I)-catalyzed 1,3-dipolar cycloaddition reaction previously utilized on carbon nanostructures,[49,113] with different π-exTTF azide derivatives.

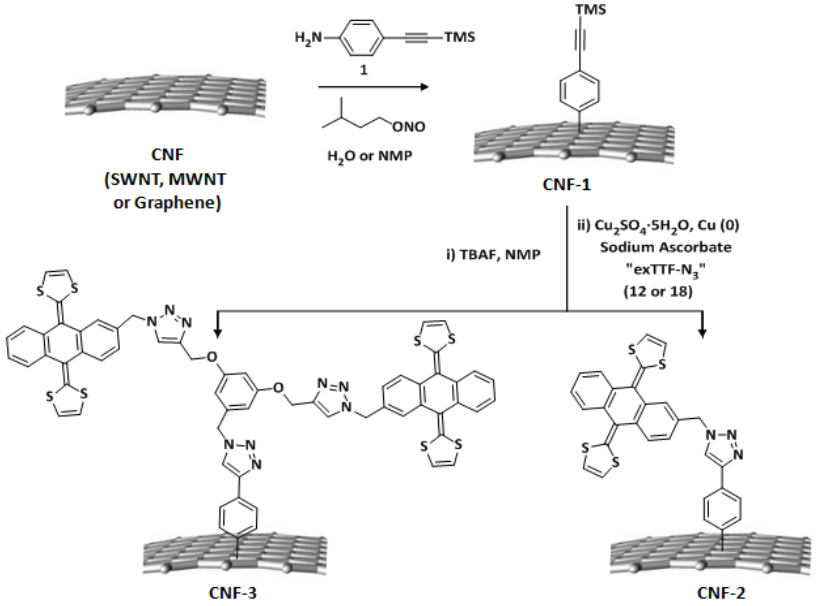

Scheme 1.3-1. Synthetic procedure for the covalent modification of CNF.

1.3.1. SYNTHESIS OF π-exTTF DERIVATIVES

Previous to the covalent modification of CNF, the synthesis of π-exTTF azide derivatives **12** and **18** was accomplished (Chart 1.3-1).

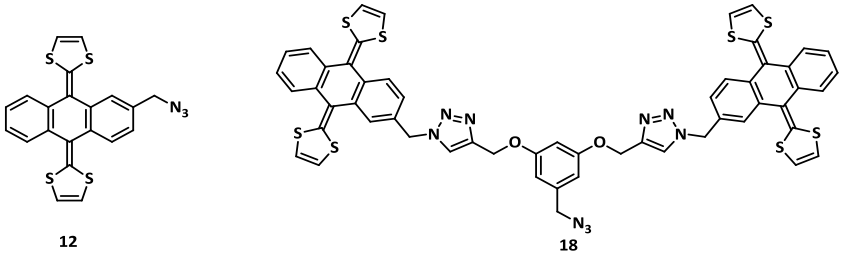

Chart 1.3-1. Structure of the π-exTTF azide derivatives used for the Cu(I)-catalyzed 1,3-dipolar cycloaddition reaction.

[113] Yenchalwar, S. G., Reddy Devarapalli, R., Deshmukh, A. B. and Shelke, M. V., *Chem. Eur. J.* **2014**, *20*, 7402.

The key step for the synthesis of π-exTTF derivatives **12** and **18** is the Horner-Wadsworth-Emmons reaction between an anthraquinone derivative and the dimethyl (1,3-dithiol-2-yl)phosphonate **6**. The synthesis of this necessary phosphonate was achieved following an established methodology well known in our group (Scheme 1.3.2.).[114] Commercially available vinylene trithiocarbonate **2** was methylated with Me_2SO_4, reduced with $NaBH_4$ and treated with HBF_4 to produce the respective intermediates **3**, **4** and **5**. Final treatment of **5** with $P(OMe)_3$ yielded phosphonate **6**.[115]

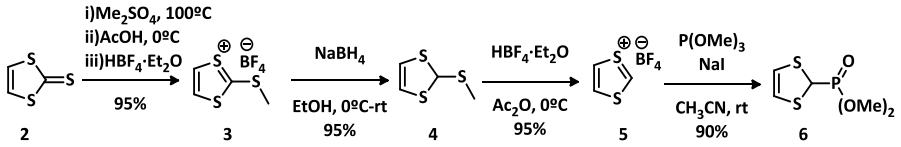

Scheme 1.3-2. Synthetic pathway for the preparation of phosphonate **6**.

The addition of *n*BuLi over the phosphonate **6** produced a very reactive carbanion that rapidly reacted with the protected 2-hydroxymethylanthraquinone **8** to yield the corresponding π-exTTF **9**. After the cleavage of the protective group, the addition of $MeSO_2Cl$ results in the formation of mesylate **11** that was heated under the presence of NaN_3 to provide the desired 2-azidomethyl-π-exTTF **12** (Scheme 1.3-3).[116]

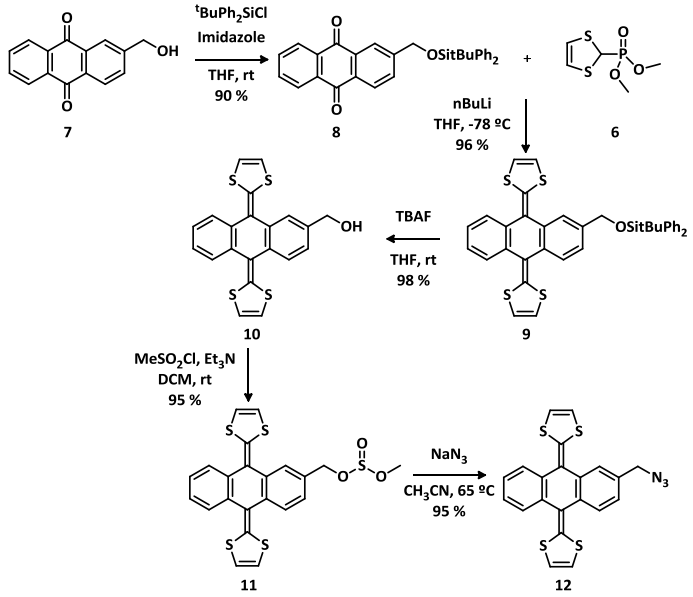

[114] González, S., Martín, N. and Guldi, D. M., *J. Org. Chem.* **2003**, *68*, 779.
[115] Moore, A. J. and Bryce, M. R., *Synthesis* **1991**, *1991*, 26.
[116] González, S., Martín, N., Swartz, A. and Guldi, D. M., *Org. Lett.* **2003**, *5*, 557.

Scheme 1.3-3. Synthetic pathway for the preparation of 2-azidomethyl π-exTTF **12**.

Once obtained **12**, the preparation of the 3,5-bis(propargyloxy)benzyl chloride **16** necessary for the central core preparation of *molecular tweezer* **18**, was performed by a three step synthesis (Scheme 1.3-4).[117] The starting methyl 3,5-dihydroxybenzoate **13** was treated with propargyl bromide, then reduced with $LiAlH_4$ and finally chlorinated with $SOCl_2$ to yield the desired product.

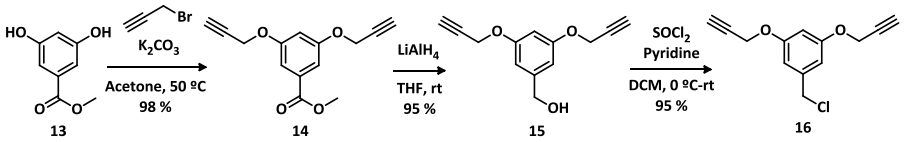

Scheme 1.3-4. Synthetic pathway for the preparation of 3,5-bis(propargyloxy)benzyl chloride **16**.

The synthesis of the molecular twezer **18** was eventually achieved by Cu(I)-catalyzed 1,3-dipolar cycloaddition reaction under microwave irradiation, followed by the conversion from the chloride **17** to the final azide **18** (Scheme 1.3-5). Different conditions were used for the cycloaddition to yield **17**, involving a broad range of solvent mixtures, catalytic systems and temperatures. Serious problems were found because of the precipitation of the monoaddition intermediate resulting in very low yields. The use of DMSO under microwave irradiation allowed to keep the intermediates solubilised during the reaction, and a faster purification was accomplished by precipitating the final product **17** in other organic solvents such as ethyl acetate, ethanol or chloroform.

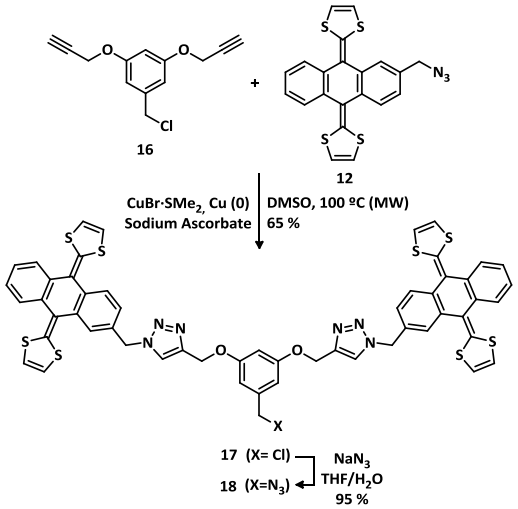

[117] Wu, P., Feldman, A. K., Nugent, A. K., Hawker, C. J., Scheel, A., Voit, B., Pyun, J., Fréchet, J. M. J., Sharpless, K. B. and Fokin, V. V., *Angew. Chem., Int. Ed.* **2004**, *43*, 3928.

Scheme 1.3-5. Synthetic pathway for the preparation of molecular tweezer **18**.

These products were fully characterized by ^{1}H-NMR, ^{13}C-NMR, FTIR, Mass Spectrometry and UV-Vis spectroscopy. The detailed description of the synthesis can be found in the Experimental section and spectra are collected in *Annexe 1: Molecular materials spectra gallery and related data*.

1.3.2. COMPARATIVE STUDY ON THE COVALENT MODIFICATION OF SWNT, MWNT AND GRAPHENE WITH π-exTF DERIVATIVES

Once compounds **12** and **18** were synthesized, the covalent modification of SWNT, MWNT and graphene (CNF to refer to all three) was studied. As stated in the background, Tour reactions involve the use of aniline derivatives in the presence of isoamyle nitrite to yield a material with phenyl units directly attached to the different CNF surfaces.[118]

For preparing **SWNT-1**, (Scheme 1.3-6) commercial HiPco **SWNT** were utilized as starting material. This pristine material was utilized as received, with no further purification. The starting **MWNT** were prepared by CVD.[119] Under Tour conditions, using deoxygenated and deionized water as solvent, a suspension of these starting materials was reacted with isoamyle nitrite and 4-[(trimethylsilyl)ethynyl]aniline **1** to yield **SWNT-1** and **MWNT-1**, respectively. In the case of the **GR-1** preparation, a few layer graphene flakes suspension in NMP[120] (named as graphene here on for simplification) was utilized as starting material, so the reaction conditions were slightly modified, choosing NMP instead of water as solvent. Because of the low reactivity of graphene, in order to increase the functionalization degree, another reaction cycle was repeated on the obtained material during the first cycle (Scheme 1.3-6).

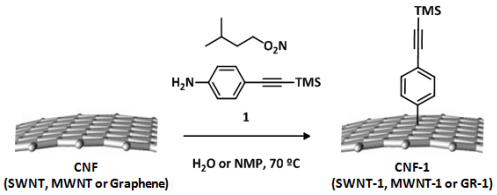

Scheme 1.3-6. Arylation on the different **CNF** affording **CNF-1**.

[118] Bahr, J. L., Yang, J., Kosynkin, D. V., Bronikowski, M. J., Smalley, R. E. and Tour, J. M., *J. Am. Chem. Soc.* **2001**, *123*, 6536.
[119] Corrias, M., Caussat, B., Ayral, A., Durand, J., Kihn, Y., Kalck, P. and Serp, P., *Chem. Eng. Sci.* **2003**, *58*, 4475.
[120] Hernandez, Y., Nicolosi, V., Lotya, M., Blighe, F. M., Sun, Z., De, S., McGovern, I. T., Holland, B., Byrne, M., Gun'Ko, Y. K., Boland, J. J., Niraj, P., Duesberg, G., Krishnamurthy, S., Goodhue, R., Hutchison, J., Scardaci, V., Ferrari, A. C. and Coleman, J. N., *Nat. Nanotechnol.* **2008**, *3*, 563.

TMS protective groups in **CNF-1** were cleaved by addition of TBAF previous to CuAAC reaction. The cycloaddition was performed *in situ* under thermal conditions affording **CNF-2** and **CNF-3**, respectively, for azides **12** and **18** (Scheme1.3-7).

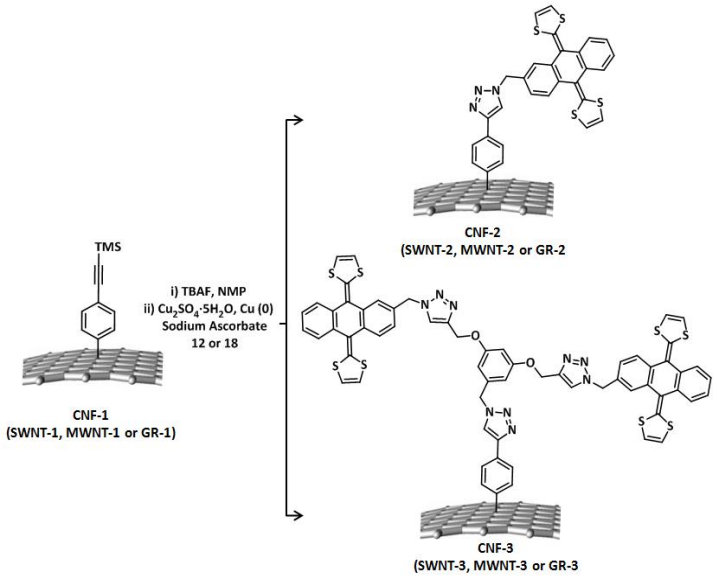

Scheme 1.3-7. Cleavage and subsequent CuAAC reaction of azides **12** and **18** to obtain **CNF-2** and **CNF-3**.

All the obtained nanoconjugates were fully characterized by different analytical, spectroscopic and microscopic techniques (FTIR, Raman, TGA, XPS, UV-Vis-NIR, TEM and electrochemistry). A brief description of the fundamentals and main features of some of these techniques can be found in *Annexe 2*, supported on some selected figures from the obtained results. In the case of nanoconjugates bearing π-exTTF, a series of steady state and time resolved spectroscopy measurements were performed to study the electronic communication between the donor and acceptor units.

a) FTIR spectroscopy

The alkyne group, that presents a sharp band in a very clear zone in FTIR (C≡C, 2000-2200 cm^{-1}), was unequivocally identified in **CNF-1**, and its disappearance served us as indicative signal of the CuAAC evolution. This signal appears at 2159 cm^{-1}, 2156 cm^{-1} and 2165 cm^{-1} for **SWNT-1**, **MWNT-1** and **GR-1**, respectively (Figure 1.3-1). Moreover, the carbon network exhibits characteristic bands of the skeletal in-plane vibrations that are observed at 1599 cm^{-1} for SWNT, 1580 cm^{-1} for MWNT and 1583 cm^{-1} for graphene derivatives, respectively.

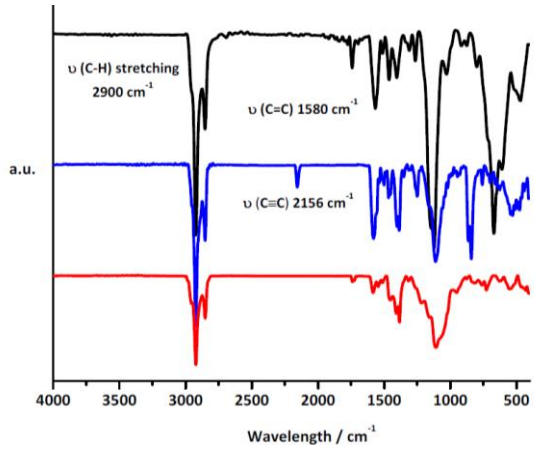

Figure 1.3-1. FTIR spectra of **MWCNT-2** (red), **MWCNT-1** (blue), and pristine MWCNT (black).

b) Raman spectroscopy

As FTIR provides important chemical information about the funtional groups present on the nanoconjugates, the information about how the material is modified is extracted from Raman spectroscopy. SWNT, **SWNT-1**, **SWNT-2** and **SWNT-3** were analyzed upon excitation at 785 nm, studying the most important features.[121] The RBM bands, between 186 and 270 cm^{-1}, suggest the presence of metallic and semiconducting SWNT, with a range of diameters between 0.8 and 1.4 nm. The D mode, assigned to the presence of sp^3 hybridized carbon atoms in the material, is observed about 1290 cm^{-1}, and its ratio respect to the G mode intensity, about 1595 cm^{-1}, provides semiquantitative information on the amount of covalently attached moieties. The I_D/I_G value is increased from 0.064 to 0.283 when the arylation is performed to obtain **SWNT-1**. When the CuACC is performed to yield **SWNT-2** and **SWNT-3** the I_D/I_G value remained almost unaltered demonstrating that the azide addition takes place preferably on the attached alkyne groups. Moreover, the G mode band is slightly up-shifted when the **SWNT-1** is modified with π-exTTF, as reported previously in other π-exTTF containing systems (Figure 1.3-2).[122] On the other hand, the I_D/ I_G relationship is practically not modified when MWNT are functionalized, although the broad G band includes contributions from the induced disorder in the material.

[121] Dresselhaus, M. S., Dresselhaus, G., Saito, R. and Jorio, A., *Phys. Rep.* **2005**, *409*, 47.
[122] de Juan, A., Pouillon, Y., Ruiz-Gonzalez, L., Torres-Pardo, A., Casado, S., Martín, N., Rubio, A. and Perez, E. M., *Angew. Chem., Int. Ed.* **2014**, *53*, 5394.

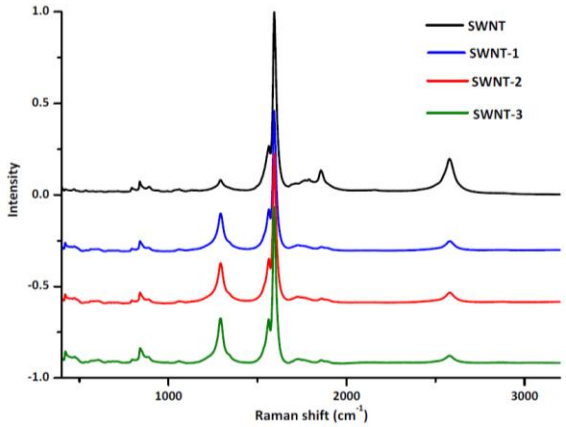

Figure 1.3-2. Raman spectra of **SWNT-3** (green), **SWNT-2** (red), **SWNT-1** (blue), and pristine SWCNT (black).

Raman analysis on graphene samples was performed by irradiation at 532 nm, observing the characteristic modes: D at 1340 cm^{-1}, G at 1565 cm^{-1} and 2D at 2678 cm^{-1} (Figure A2-6 in *Annexe 2*). When graphite is submitted to ultrasonication to be exfoliated, some defects are generated, observing a slight increase in the D mode of graphene samples. There is a notable change in the 2D mode band shape and intensity from bulk graphite to exfoliated graphene. This band presented a full width at half maximum (FWHM) value of 76 cm^{-1} and after fitting with 6 different Lorentzian functions results in a 24 cm^{-1} FWHM, corresponding to a few layer graphene sample.[123]

When Tour reactions are carried out to obtain **GR-1**, the D band intensity was increased, and directly the I_D/ I_G ratio, as a consequence of the carbon atoms conversion from sp^2 to sp^3. This relationship remained constant when CuAAC took place to yield **GR-2** and **GR-3**, but it is important to remark that this lower increase in I_D/ I_G, comparing graphene and SWNT samples, is a clear evidence of the higher reactivity of SWNT against graphene under the same conditions. A statistical distribution analysis of the I_{2D}/I_G ratio was performed for **GR-2**, fitting to a Gaussian distribution with maximum peaks at 0.4, lower than 0.7, which are usually attributed to few and multi-layer graphene samples (Figure 1.3-3).[124]

[123] Malard, L. M., Pimenta, M. A., Dresselhaus, G. and Dresselhaus, M. S., *Phys. Rep.* **2009**, *473*, 51.
[124] Ferrari, A., Meyer, J., Scardaci, V., Casiraghi, C., Lazzeri, M., Mauri, F., Piscanec, S., Jiang, D., Novoselov, K., Roth, S. and Geim, A., *Phys. Rev. Lett.* **2006**, *97*, 187401.

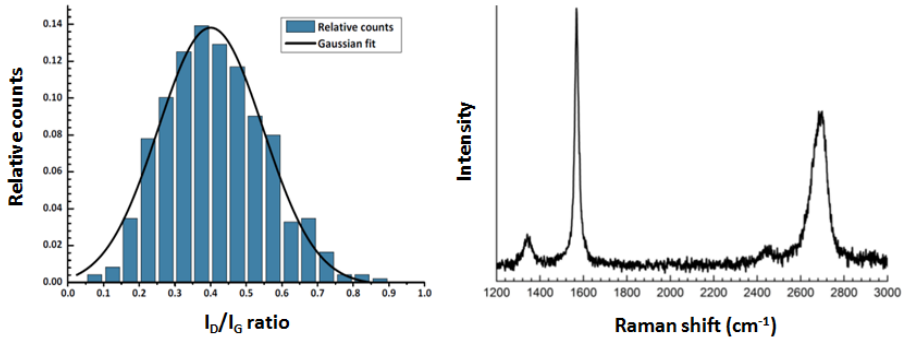

Figure 1.3-3. Histogram for relative counts vs. I_{2D}/ I_G ratio and its corresponding Gaussian with maximum peaks at 0.4.

c) Thermogravimetric analysis (TGA)

In order to evaluate in a quantitative manner the functionalization degree and compare the different CNF reactivity, thermogravimetric analyses (TGA) were performed on the obtained nanoconjugates. The analyses results are obtained in curves as shown in Figure 1.3-4 for SWNT. It can be observed in black how the starting pristine material doesn't decompose up to 800 ºC. In green, the analysis revealed a 26 % weight loss (% W.L.) for **SWNT-1**. This value is increased when the CuAAC reaction is performed, observing a 38 % W.L. for **SWNT-2**. The thermal decomposition analysis for compound **12** is represented in blue, observing a maximum in the % W.L. at 300 ºC that matches the first desorption in **SWNT-2**.

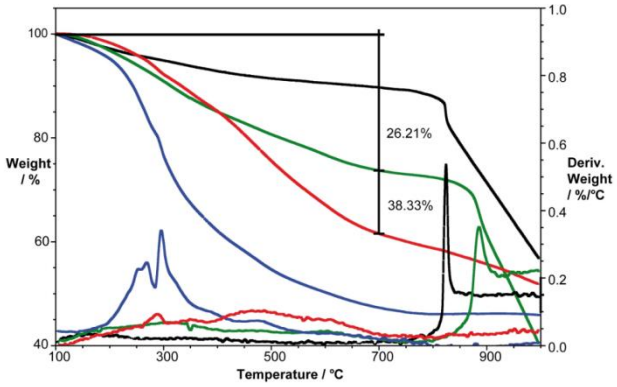

Figure 1.3-4. TGA results for SWNT samples under inert conditions: SWCNT (black) **SWCNT-1** (green) and **SWCNT-2** (red). The thermal decomposition of π-exTTF azide **12** is shown in blue.

Considering the weight loss at the desorption temperature (% W.L.) and the molecular weight of the anchored organic motifs, the number of carbon atoms surrounding each functionality can be calculated. Thereby, this value calculated after the first reaction (C. at. per Ph-C≡C-TMS), which is the only

one that directly happens on the CNF surface, furnish a real parameter to evaluate how altered is the structure of the CNF. In other words, a higher number of carbon atoms surrounding each organic motif means a lower degree of functionalization. On the other hand, the calculation of this value after the CuAAC reaction (C. at. per π-exTTF) provides information about the extension of the CuAAC.

	% W.L. [CNF-1]	C. at. per Ph-C≡C-TMS (CNF-1)	% W. L. (CNF-2)	C. at. per π-exTTF (CNF-2)
SWNT	26 %	41	38 %	72
MWNT	8 %	105	29 %	106
Graphene	14 %	89	21 %	168

Table 1.3-1. Results extracted from TGA analysis: weight loss after each step, number of carbon atoms per functionality and CuAAC reaction yield for **CNF-2**.

In view of the results shown in Table 1.3-1, and considering the % W.L [**CNF-1**] and the number of C atoms per Ph-C≡C-TMS group, it is easy to remark the higher reactivity of SWNT against MWNT and graphene under similar conditions for the arylation reaction. This different reactivity could be justified by the different geometry of each CNF, since the higher curvature of SWNT makes their C=C bonds more reactive. Nevertheless, the same reasoning between MWNT and graphene is not in accordance with the obtained results that apparently revealed a higher reactivity of graphene. However we must consider that MWNT are a multilayer material with a major proportion of carbon in the sample compared with the organic addends and only the outer wall is functionalized.

Another fact to remark is the different increases in the %W.L. when the CuAAC reaction is performed, observing a higher increase in the case of **MWNT-2** (from 8 % to 29 %) compared to **SWNT-2** (from 26 % to 38 %). Several reasons may justify this finding. On the one hand MWNT exhibit a better solubility than SWNT increasing the efficiency of any reaction. On the other hand, the lower curvature in MWNT decreases the reactivity against arylation reaction, inducing a smaller distance between Ph-C≡C-TMS addends on **SWNT-1** compared to those in **MWNT-1**. This smaller distance in **SWNT-1** makes that once some π-exTTF azide **12** are added, the addition of more units may be hampered by the high π-exTTF surface (Figure 1.3-6). Both reasoning can justify the different efficiencies in the CuAAC cycloaddition reaction. In the case of graphene, the lower efficiency in the CuAAC reaction probably comes from the flakes high tendency to stack.

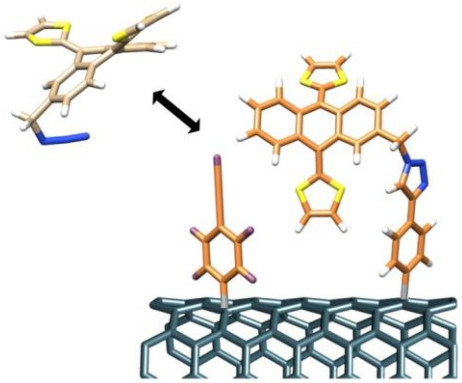

Figure 1.3-5. Representative image of the hindrance in the CuAAC reaction when various functionalities are close in the surface of CNT.

The same reasoning extracted from **CNT-1** and **CNT-2** TGA results was extended to **CNF-3**, revealing similar conclusions (Table 1.3-2). The CuAAC reaction on **CNF-1** to afford **CNF-3** took place in a similar extension to that in **CNF-2**. In the case of **MWNT-3**, the increase in the % W.L. after the CuAAC cycladdition reaction was higher (from 8 % to 46 %) than that found on **SWNT-3** (from 26 % to 50 %), as occurs when **MWNT-2** and **SWNT-2** were compared. The same reasoning based on the higher solubility of MWNT and the closest distance of Ph-C≡C-TMS addends in SWNT that decrease the efficiency can also be applied in this case. As found in **GR-2** the high tendency of the graphene flakes to stack may be the main reason for the lower efficiency in the CuAAC reaction to afford **GR-3**.

	% W.L. [CNF-1]	C. at. per Ph-C≡C-TMS (CNF-1)	% W. L. (CNF-3)	C. at. per π-exTTF (CNF-3)
SWNT	26 %	41	50 %	**72**
MWNT	8 %	105	46%	**135**
Graphene	14 %	89	23 %	**348**

Table 1.3-2. Results extracted from TGA analysis: weight loss after each step, number of carbon atoms per functionality and CuAAC reaction yield for **CNF-3**.

d) X-ray photoelectron spectroscopy (XPS)

XPS analyses were performed to complete and corroborate the covalent modification and the presence of the new functional groups (Figure 1.3-6, Figures A2-10 and A2- 11 in *Annexe 2*). All **CNF-1** analyses afforded silicon peaks (Si 2p, 100-103 eV) due to the trimethylsilyl protective groups. No nitrogen presence was observed, implying no starting reagents (isoamyl nitrite or **1**) in the samples. The **CNF-2** and **CNF-3** analyses revealed the presence of sulphur (170 eV) and nitrogen (N 1s, 400 eV). In fact, the nitrogen peak deconvolution revealed the contribution of two kinds of N in

the triazole ring, corresponding to the N atom in 1-position and those forming the double bond. The absence of remaining azide from **12** or **18** was confirmed since the peak of N corresponding to this functional group at 405 eV was not observed either in **CNF-2** or **CNF-3**.[125] The carbon signal (C 1s, 285 eV) was submitted to deconvolution too, revealing the presence of different kinds of carbon atoms in the nanoconjugates (C sp^2 at 284.5 eV, C sp^3 at 284.9 eV, C=O at 285.7 eV and C-O at 285.4 eV). Moreover, the typical aromatic π-π* shake-up transitions at 290 eV are observed.[126] A small silicon peak was still observed in the analyses of **CNF-2** and **CNF-3** whose contribution probably comes from some impurities (glass, filters, etc) and still remaining protective groups from **CNF-1**.

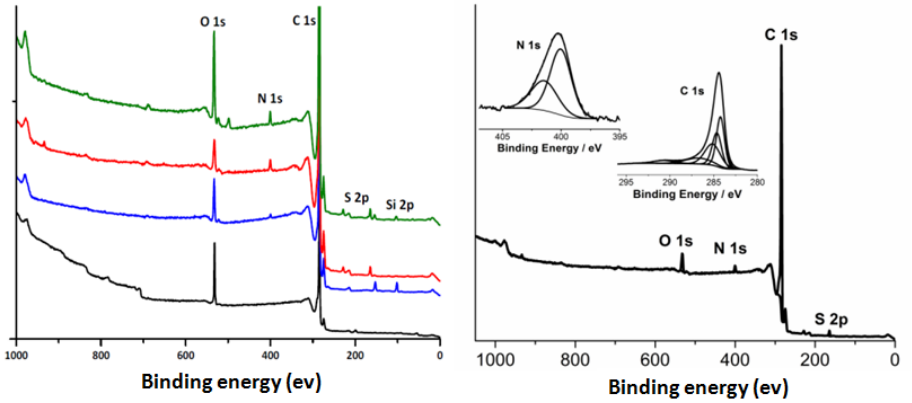

Figure 1.3-6. Comparative XPS analyses for MWNT (black), **MWNT-1** (blue), **MWNT-2** (red) and **MWNT-3** (green). Right: Deconvolution at core level for C 1s and N 1s peaks in **MWNT-2**.

e) Transmission Electron Microscopy (TEM)

The nanoconjugates morphology study was accomplished by TEM. The images obtained for pristine SWNT revealed the presence of bundles. Meanwhile, for **SWNT-1** and **SWNT-2,** these bundles are formed by nanotubes with larger diameters coexisting with individual units, as effect of the covalent modification performed (Figure 1.3-7 and Figure A2-12 in *Annexe 2*).

[125] Collman, J. P., Devaraj, N. K., Eberspacher, T. P. A. and Chidsey, C. E. D., *Langmuir* **2006**, *22*, 2457.
[126] Lipińska, M. E., Rebelo, S. L. H., Pereira, M. F. R., Gomes, J. A. N. F., Freire, C. and Figueiredo, J. L., *Carbon* **2012**, *50*, 3280.

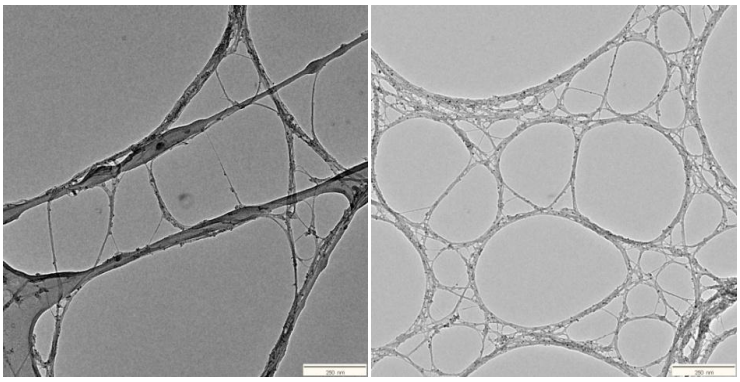

Figure 1.3-7. Images obtained by TEM on holey carbon copper grids (scale bar 250 nm) for pristine **SWNT** and **SWNT-1**.

The same analysis performed on **MWNT** and **MWNT-2** did not reveal any difference in morphology between the starting material and the nanoconjugates (Figure A2-13 in *Annexe 2*). In the case of graphene, the TEM analysis corroborates the information extracted from Raman, demonstrating the presence of bi/tri-layer graphene obtained upon the exfoliation of graphite. A significative reagregation of the flakes was partially avoided by keeping the exfoliated graphene in a NMP suspension, observing few-layer graphene sheets in **GR-2** (Figure 1.3-8).

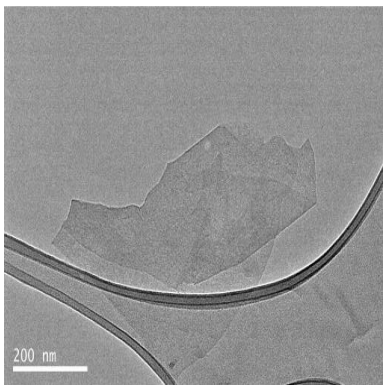

Figure 1.3-8. TEM image of pristine graphene obtained after the exfoliation procedure.

f) Electrochemical measurement

The electrochemical properties of **SWNT-2**, **MWNT-2** and **GR-2** samples were analyzed by cyclic voltammetry (CV) and compared with **12** as a reference. In all samples, the single two-electron and chemically quasi-reversible oxidation waves of the π-exTTF unit to form the dication species is clearly discernible.[100] The oxidations waves are noticeably broader and positively shifted by 220-270 mV relative to the reference system **12** (Figure 1.3-9),

which is likely to be a result of the intramolecular electronic interaction between the electroactive units (CNF and π-exTTF) in the nanoconjugates, as previously observed in related samples.[32, 87]

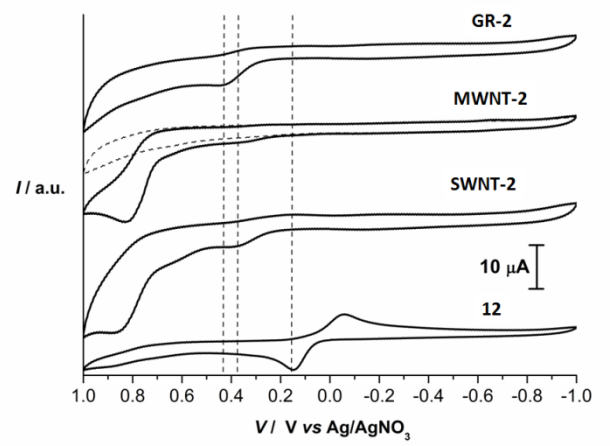

Figure 1.3-9. Cyclic voltammograms of **SWNT-2**, **MWNT-2**, **GR-2** and reference π-exTTF **12**, obtained in DMF solutions containing 0.1 M $TBAPF_6$ and using $Ag/AgNO_3$ as reference electrode, glassy carbon as working electrode and a Pt wire counter electrode. Scan rate is 100 mV/s. The dashed line corresponds to the background signal.

g) Photophysical study

Several photophysical measurements (absorption, emission and transient absorption) were performed to evaluate the nanoconjugates electronic properties, and how these are altered upon covalent modification. These measurements were carried out by the group of Prof. D. M. Guldi, Erlangen University.

When different **SWNT**, **SWNT-1** and **SWNT-2** suspensions in DMF were analyzed by absorption spectroscopy, the absorption features of covalently functionalized SWNT were notably blue shifted when compared to the pristine sample (Figure 1.3-10). In particular, SWNT reveals absorption maxima at 560, 661, 741, 814, 1006, 1072, 1172, and 1313 nm. After SWNT functionalization, the transitions at higher energies in, for example, **SWNT-1** undergo slight hypsochromic shifts to 558, 652, 733, and 812 nm, while those at lower energies are shifted appreciably stronger, that is, to 989, 1051, 1145, and 1279 nm. The absorption spectrum of **SWNT-2** reveals only a minor shift to 557, 655, 734, 810, 998, 1054, 1154, and 1287 nm. This is likely due to a redistribution of charge density within the covalently functionalized SWCNT.

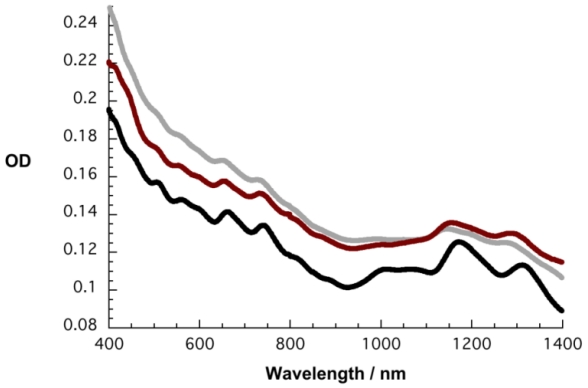

Figure 1.3-10. Absorption spectra of **SWNT** (black), **SWNT-1** (grey), and **SWNT-2** (red) in DMF.

Fluorescence measurements in DMF were performed on pristine SWNTs revealing maxima at 1057, 1128, 1211, 1305, and 1419 nm, which correspond to (10,2), (7,6), (11,3), (13,2), and (9,8) SWNT, respectively (Figure 1.3-10).[127] It is important to note that the fluorescence features mirror image those seen in the absorption measurements. For **SWNT-1** and **SWNT-2**, a similar fluorescence pattern was found with just minor hypsochromic shifts relative to pristine SWNT (Figure 1.3-11). Moreover, the comparison between the fluorescence of the functionalized SWNT with that of pristine SWNT at equal absorbance at the excitation wavelength unravels quenching of the SWNT fluorescent features (Figure 1.3-11, right bottom). As a matter of fact, the fluorescence intensities of **SWNT-1** and **SWNT-2** are quenched with values of 82 and 63 %, respectively, relative to pristine SWNT. Especially the latter is remarkable, since it prompts to a fast deactivation pathway in the form of either energy or electron transfer.

[127] Bachilo, S. M., Strano, M. S., Kittrell, C., Hauge, R. H., Smalley, R. E. and Weisman, R. B., *Science* **2002**, *298*, 2361.

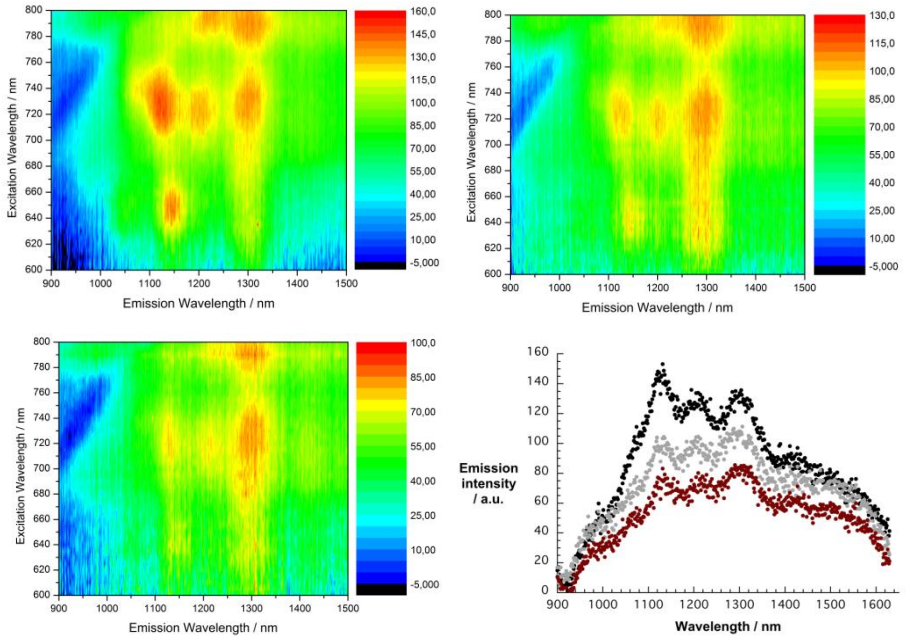

Figure 1.3-11. 3D steady-state fluorescence spectra of pristine SWNT (left top), **SWNT-1** (right top), and **SWNT-2** (left bottom) in DMF with increasing intensity from blue to green to yellow and to red. Comparison of the NIR fluorescence spectra of pristine SWNT (black), **SWNT-1** (grey) and **SWNT-2** (red) in DMF upon 720 nm excitation (right bottom).

Femtosecond transient absorption measurements were performed to support the electronic communication between the donor unit (π-exTTF) and the acceptor unit (SWNT). Looking at SWNT, which were simply suspended in DMF, a set of transient minima were observed at 455, 515, 565, 570, 665, 1195, 1315, and 1375 nm (Figure A2-15 in *Annexe 2*). All features decay similarly during the recovery of the ground state with two major lifetime components (i.e., 1.5 and 80 ps). Overall, no particular shifts of the transitions were observable during the decay. Notably, this behaviour resembles that seen numerously for pristine SWNT suspended in various solvents.

When turning to **SWNT-1**, minima at 455, 510, 560, 570, 660, 1190, 1310, and 1360 nm were noted upon 387 nm excitation (Figure A2-16 in *Annexe 2*). The features are hypsochromically shifted when compared to pristine SWNT as in the ground state absorption. From a multiwavelength analysis we derive major lifetime components for the excited state decay with values of 1.5 and 65 ps. The overall difference in terms of lifetimes relative to pristine SWNT relates to the impact that the functionalization exerts on the electron properties of SWNT.

Finally, for **SWNT-2** we note the same minima at 455, 510, 560, 570, 660, 1185, 1310, and 1360 nm at the conclusion of the excitation (Figure 1.3-13).

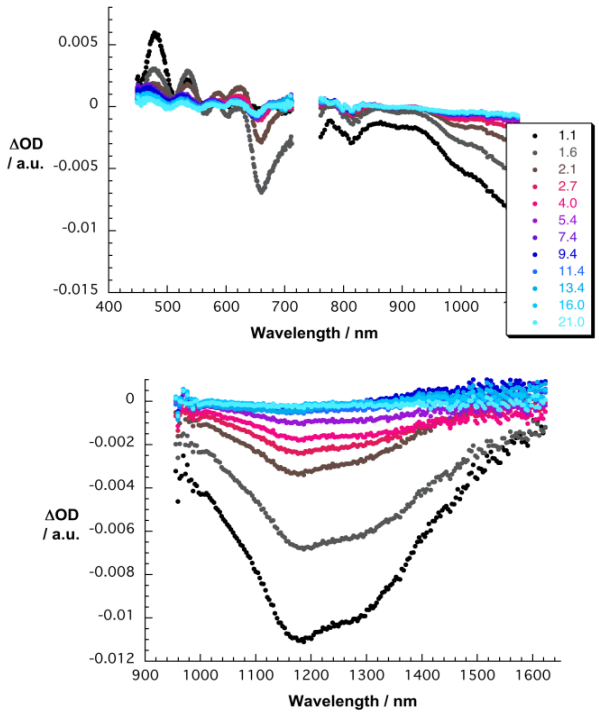

Figure 1.3-12. Differential absorption spectra (visible and near infrared) obtained upon femtosecond pump probe experiments (387 nm) of **SWNT-2** with several time delays between 1.1 and 21.0 ps at room temperature (Upper part). Differential absorption spectra (extended near infrared) obtained upon femtosecond pump probe experiments (387 nm) 55 of **SWNT-2** with several time delays between 1.1 and 21.0 ps at room temperature (Lower part).

Unlike what it is seen for **SWNT-1**, in which minima decay with 1.5 and 65 ps, in **SWNT-2** a major decay takes place with a lifetime of 15 ps (Figure 1.3-13). Overall, appreciable blue shifts of the transient bleaching with minima at 500, 554, 650, 1175 and 1360 nm evolve in this deactivation. Implicit are new conduction bands, in which electrons are injected from π-exTTF shifting the transitions to lower energies. Important is also the 600 to 800 nm range, where a new transition correlates well with the one-electron oxidized π-exTTF. In other words, the lifetime of 15 ps in **SWNT-2** correlates with a charge separation. A global analysis resulted in a lifetime of this newly generated radical ion pair state of about 250 ps.

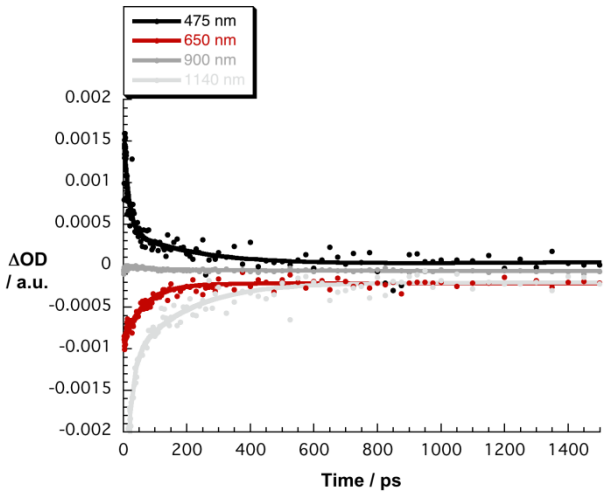

Figure 1.3-13. Time absorption profiles of the spectra shown in 1.3-12 at 475, 650, 900, and 1140 nm monitoring the charge separation and charge recombination.

Unfortunately, the lower degree of functionalization achieved in MWNT and graphene samples do not allowed a proper photophysical characterization of the aggregates formed.

1.3.3. STUDY OF SUPRAMOLECULAR INTERACTIONS

a) Titrations by UV-vis-NIR spectroscopy

Considering the background of our group in the design, synthesis and study of π-exTTF-based systems for the recognition of fullerenes,[100] the nanoconjugates **SWNT-3** and **MWNT-3** were considered suitable host candidates to recognize fullerenes since they bear π-exTTF-based molecular tweezer receptors. Prior to this study, it was necessary to evaluate the behaviour of the isolated host **18** by determining the interaction strength, defined by the binding constant K_a (Figure 1.3-15)

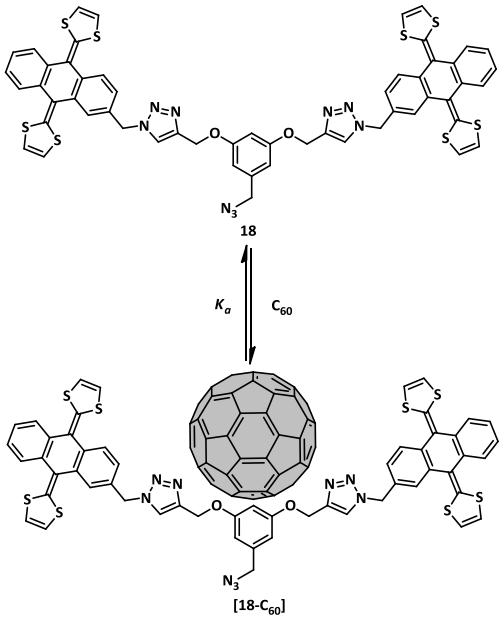

Scheme 1.3-8. Titration experiment for host **18** to form the supramolecular complex **[18·C_{60}]** by addition of C_{60}.

The way of determining the value of K_a by titrations depends on several parameters such as its magnitude order, solubility, harshness on synthesis and other inner properties of the host and guest (*Annexe 3*). The well defined and separated absorption bands in UV-Vis of **18** and C_{60} and the previous obtained results for similar systems,[108] led us to choose this technique as first approach to evaluate the interaction between both molecular motifs.

The titration experiment was repeated twice using a solution of **18** in PhCl ($1.75 \cdot 10^{-5}$ M) and a stock C_{60} solution ($1.34 \cdot 10^{-3}$ M) where the solution of **18** acts as solvent, in order to keep the concentration of **18** constant during all the measurements. The spectra were recorded for each addition in the UV-Vis-NIR from 0 to 14 equivalents of fullerene. The intensity of the π-exTTF band at 438 nm is reduced upon the addition of fullerene, while a new band

at 490 nm appears and increases its intensity (Figure 1.3-14). This behaviour matched to the observed evolution in other related π-exTTF-C_{60} systems.[108,109]

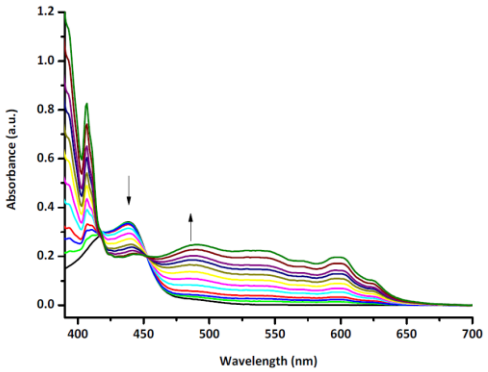

Figure 1.3-14. UV-Vis titration by addition of C_{60} to a **18** solution.

After a mathematical treatment to subtract the C_{60} absorption, the data were fitted to the Hill equation for different *n* values (*Origin Microcal 8.0*), obtaining the better result for n=1.4 and log K_a= 3.51. These results indicate a very low or even the absence of cooperativity and are in line with the Job's plot experiment performed, that revealed a 1:1 stoichiometry in the interaction (Figure 1.3-15).[108] To support these results the same calculations were performed utilizing *Specfit* as software, affording a value of log K_a = 3.96 (Figure A3-2 in *Annexe 3*).

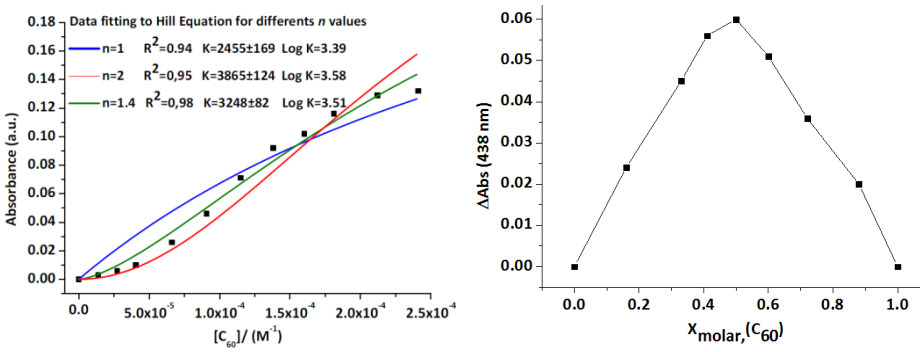

$$\Delta Abs = \frac{Abs_{max} \cdot [C_{60}]^n \cdot K_n}{1 + [C_{60}]^n \cdot K_n}$$

Figure 1.3-15. Data fitting to Hill's equation for different *n* values (left) and Job's plot (right).

Once obtained the preliminary information about the receptor behaviour in a free state, the titrations were performed utilizing **SWNT-3** and **MWNT-3** as hosts (Figure 1.3-16). The hosts were suspended in o-DCB and sonicated

during 30 minutes to improve the nanoconjugates disaggregation and a C_{60} (1.10^{-5} M) stock solution in the same solvent was utilized for carrying out the additions.

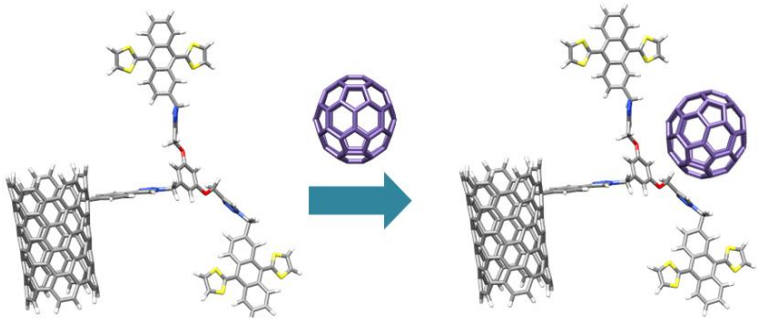

Figure 1.3-16. Depictive picture of the [**SWNT-3·C_{60}**] complex formation.

The spectra for each addition of fullerene to **SWNT-3** were recorded in the UV-Vis-NIR region observing a cross point at 630 nm. As in the free state receptor the well defined and separated absorption regions allow to observe a clear decrease in the band at 438 nm and the increase of a new charge transfer band at 490 nm, in the case of **SWNT-3**, the own nanotube absorption precluded the same observation. However, at the right of the cross point, a decrease in the SWNT absorption upon the addition of fullerene C_{60} was observed, what may involve the formation of the supramolecular complex between **SWNT-3** and fullerene (Figure 1.3-17). To check if this finding may be caused by effect of the dilution or the precipitation during the experiment, a blank titration utilizing pristine SWNT instead of **SWNT-3** was performed and no similar behaviour was observed.

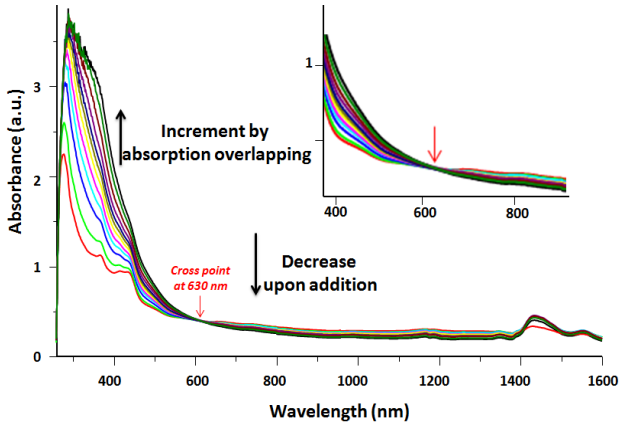

Figure 1.3-17. UV-Vis titration by addition of C_{60} to a **SWNT-3** suspension.

Going further, the same experiment was performed on **MWNT-3** and new cross points were found during the titration (Figure 1.3-18). In line with the result observed in the **SWNT-3** titration experiment, a decrease in the MWNT

absorptions over 650 nm was also found, with a first cross point at 630 nm. A new absorption band was found between the first and the second cross point (468 nm) which match to the charge transfer from π-exTTF to C_{60} observed in the **18** vs. C_{60} titration (Figure 1.3-14). Moreover, after this second cross point, the small π-exTTF absorption band decreased its intensity upon the addition of C_{60} in line with the results obtained for the free receptor.

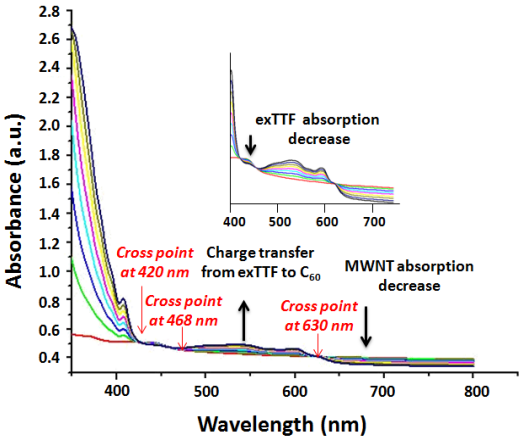

Figure 1.3-18. UV-Vis titration by addition of C_{60} to a **MWNT-3** suspension.

As it can be observed, the MWNT lower absorption compared to SWNT allowed an easier observation of the charge transfer from π-exTTF to C_{60} as a consequence of the complex formation. These results show how the formation of the complex not only affects to the absorption features of C_{60} and π-exTTF, but also to MWNT resulting in a decrease of its absorbance upon the addition and the formation of a new cross point. This finding corroborates the observation in the titration on **SWNT-3** where the change in the C_{60} and the π-exTTF features was not possible to be observed but, the decrease on the SWNT absorption suggest the supramolecular interaction between the π-exTTF acting as molecular receptor for the guest fullerene.

b) Titrations by NMR spectroscopy

In order to complete the study of the interaction between the tweezer-like hosts and C_{60} and obtain a value for the binding constant for the free state receptor by using a different technique, several ^{1}H-NMR titrations were carried out. Two different analogous to the host **18** were synthesized changing the nature of the recognition motif (Chart 1.3-2). The same central scaffold utilized for the synthesis of the π-exTTF-based receptor **18** was utilized for the synthesis of **22** and **24**, where the π-exTTF motifs were replaced by TCAQ,[128] an electron-acceptor system, and a simple phenyl ring, respectively. These three systems allowed to test out the possible contributions of the concave-convex interaction of π-exTTF /fullerene and the charge transfer to the binding constant.

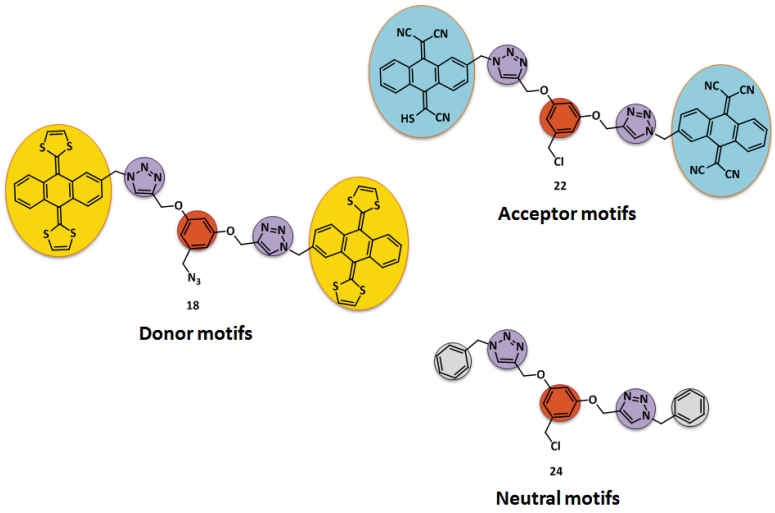

Chart 1.3-2. Three different hosts studied by ^{1}H-NMR titration experiments.

Following the procedure depicted in Scheme 1.3-9, the TCAQ tweezer precursor **21** was synthesized. The azide derivative **20** was reacted with the Lehnert's reagent[129] to afford the corresponding 2-azidomethyl-TCAQ **21**.

[128] [(a)]Ortí, E., Viruela, R. and Viruela, P. M., *J. Phys. Chem.* **1996**, *100*, 6138; [(b)]Martin, N., Behnisch, R. and Hanack, M., *J. Org. Chem.* **1989**, *54*, 2563.
[129] Lehnert, W., *Tetrahedron Lett.* **1970**, *11*, 4723.

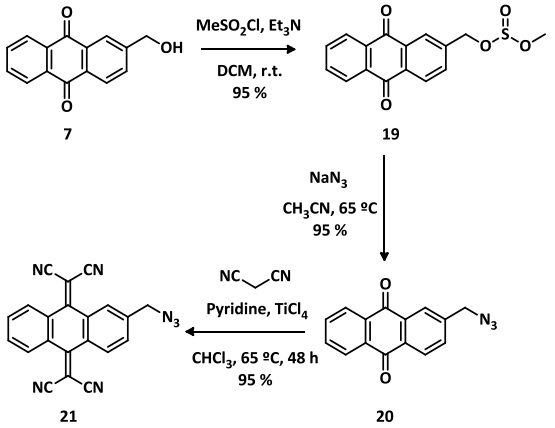

Scheme 1.3-9. Synthetic pathway for the preparation of 2-azidomethyl-TCAQ.

Once **21** was synthesized, a CuAAC reaction with **16** was performed under microwave irradiation to yield the TCAQ tweezer **22** (Scheme 1.3-10). The supramolecular interaction of TCAQ nanotweezers with C_{60} and SWNT was previously investigated.[111]

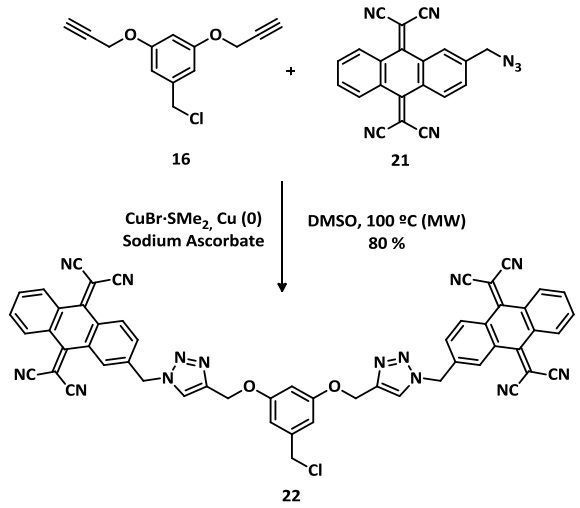

Scheme 1.3-10. Synthetic pathway for the preparation of **22**.

In a similar way, the phenyl tweezer **24** was synthesized from commercially available benzyl azide **23** utilizing a modified procedure from the bibliography (Scheme 1.3-11).[117]

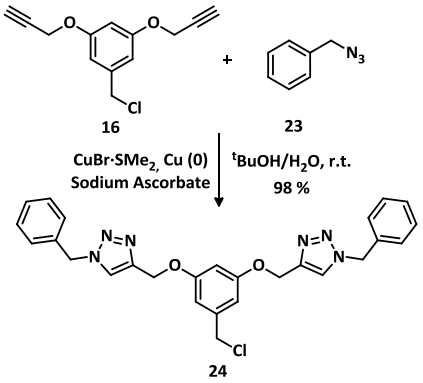

Scheme 1.3-11. Synthetic pathway for the preparation of **24**.

First, the titration experiments were accomplished by using a **18** solution ($4.0 \cdot 10^{-4}$ M) in a $CDCl_3/CS_2$ mixture utilizing this solution as solvent for C_{60} ($3.4 \cdot 10^{-3}$ M) in order to keep a constant concentration of **18**. During the experiment, ^{1}H-NMR spectra were recorded after each addition, reaching 6.3 equivalents of fullerene. For an easier understanding of the complete study, a general view of the ^{1}H-NMR spectrum is shown in Figure 1.3-19, indicating the signals or set of them with different coloured symbols.

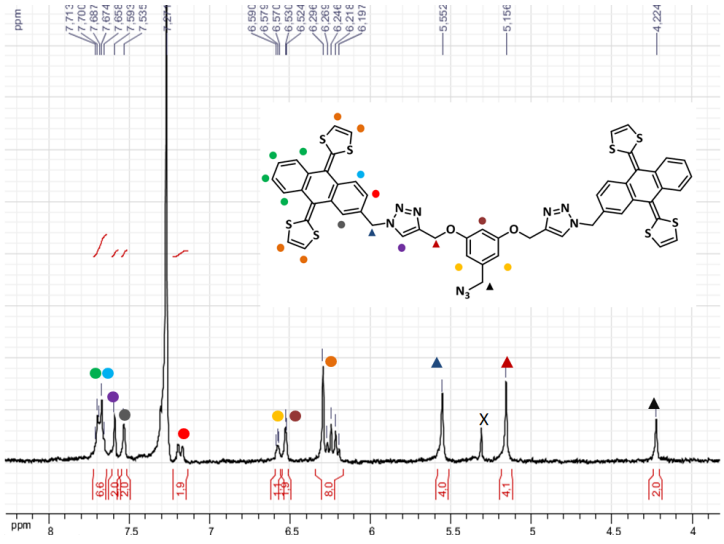

Figure 1.3-19. General view for ^{1}H-NMR spectrum for **18** π-exTTF based receptor ($CS_2/CDCl_3$, 300 MHz).

The most remarkable feature that was modified upon the addition of C_{60} is the change in the signal at 7.18 ppm (*dd*, Ar-**H** in position 3 of anthracene skeleton), that decreased at the time that a new singlet appears (Figure 1.3-20). The other anthracene signals and central phenyl ring were notably shifted (up to 0.025 ppm), whereas those owing to the dithiole rings were

unaltered. The triazole signal was slightly shifted as well as the methylene close to the azide (C**H**$_2$N$_3$) (Figures A3-4 to A3.8 in *Annexe 3*).

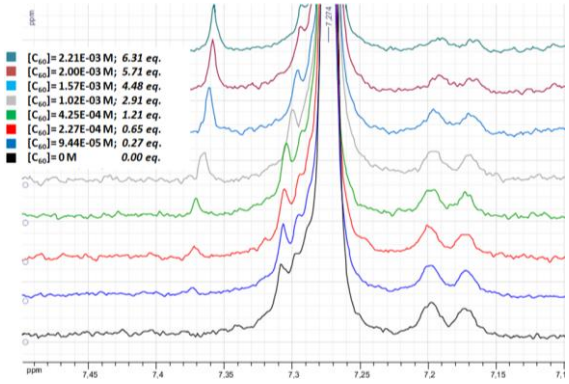

Figure 1.3-20. ^{1}H-NMR spectrum enhancing the change in the position 3 in the **18** anthracene skeleton.

These results were fitted to the equation:[130]

$$\frac{\Delta\delta}{\Delta\delta_{max}} = \frac{K\cdot[C_{60}]-K\cdot[H]-1+\sqrt{((K\cdot[C_{60}]+K\cdot[H]+1)-4\cdot K^2\cdot[H]\cdot[C_{60}])}}{1+K\cdot[C_{60}]-K\cdot[H]+\sqrt{((K\cdot[C_{60}]+K\cdot[H]+1)-4\cdot K^2\cdot[H]\cdot[C_{60}])}}$$

using *Origin Microcal 8.0* and affording values for log K 3.1, in the same magnitude range that those obtained by UV-Vis spectroscopy (Figure 1.3-21 and Table 1.3-2). In the case of anthracene signals, because of the complexity of the multiplet, only the most feasible signals to be identified and followed by NMR were fitted to the equation.

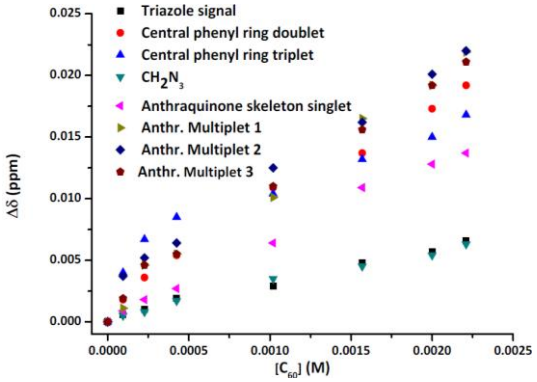

Figure 1.3-21. Data fitting for signals change in the ^{1}H-NMR spectrum upon the addition of C_{60} to **18**.

[130] Thordarson, P., in *Supramolecular Chemistry: From Molecules to Nanomaterials*, John Wiley & Sons, Ltd, **2012**.

[18·C_{60}]	K value	Fitting error	log K	R^2
triazole signal	1113	32	3.05	0.986
central ring doublet	1158	24	3.06	0.992
central ring triplet	1321	94	3.12	0.855
CH_2-N_3	1123	22	3.05	0.993
Anthr. skeleton singlet	1130	24	3.05	0.993
Anthr. mult 1	931	50	2.97	0.948
Anthr. mult 2	1203	37	3.08	0.981
Anthr. mult 3	1115	28	3.05	0.988

Table 1.3-2. Binding constant values obtained for each followed signal during the ^{1}H-NMR-titration of system [**18**·C_{60}].

All the obtained values for log K are in the same order of magnitude than those resulting from the UV-Vis spectroscopy titrations. If we focus on the most altered signals upon the C_{60} additions, the central ring and some of the anthracene skeleton signals seem to be mostly involved in the global interaction, while the triazole ring does not seem to play an important role (Figures A3-4 to A3-8 in *Annexe 3*).[111]

The same analysis was performed on **22** and **24** under the same conditions, using a **22** ($4.0\cdot10^{-3}$ M) and **24** ($5.0\cdot10^{-4}$ M) solutions in a $CDCl_3/CS_2$ mixture, respectively. Each solution was utilized as solvent too for the C_{60} ($3.4\cdot10^{-3}$ M) guest solution.

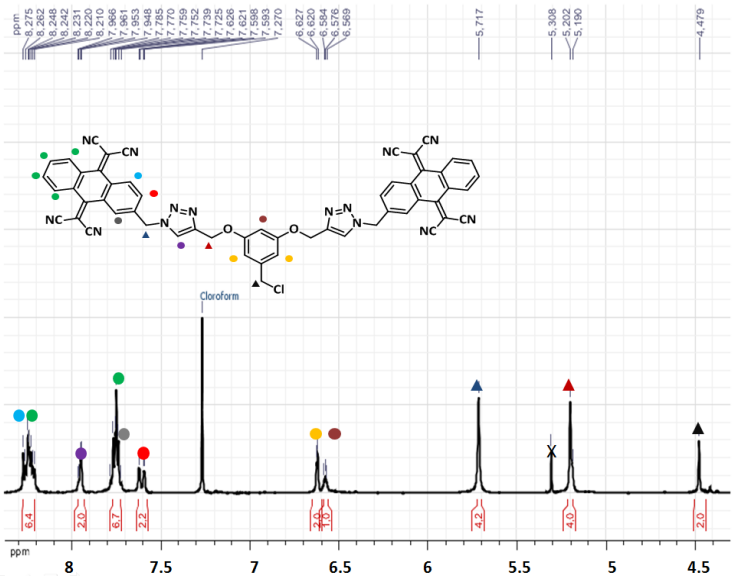

Figure 1.3-22. ^{1}H-NMR spectrum of host molecular tweezer **22**.

On the one hand, the detailed follow up of the spectra signals for the system **[22·C_{60}]** revealed notable shifts in the triazole (7.95 ppm), central phenyl ring (6.62 and 6.58 ppm, Figure 1.3-23) and CH_2Cl (4.48 ppm) signals. On the other hand, very small changes were observed in the signals assigned to the anthracene skeleton of TCAQ, so they were not considered for the calculations. The singlet corresponding to the methylene group between the TCAQ unit and the triazole remained almost unaltered, but the other one close to the central ring showed a very small shift.

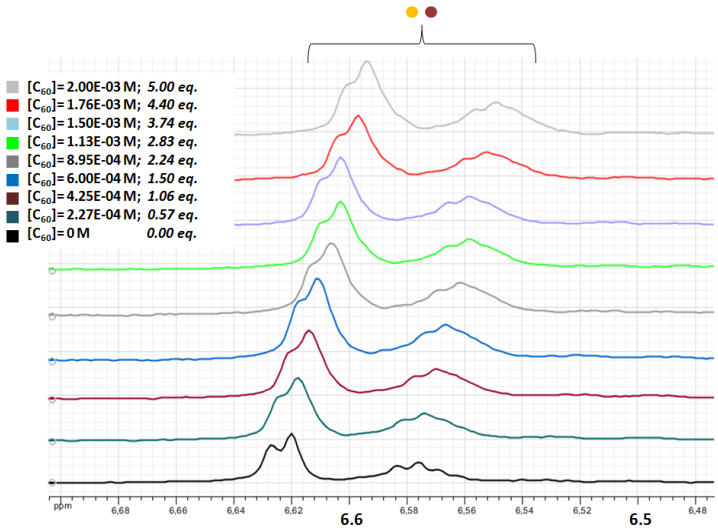

Figure 1.3-23. ^{1}H-NMR titration experiment for system **[22·C_{60}]** enhancing the change in the doublet and triplet of the central phenyl ring.

The data fitting to the equation shown above revealed very similar values for the binding constant to those obtained for **[18·C_{60}]** (Table 1.3-3 and Figures A3-9 to A3-14 in *Annexe 3*).

[22·C_{60}]	K value	Fitting error	Log K	R^2
triazole signal	1320	37	3.12	0.981
central ring doublet	1282	20	3.11	0.995
central ring triplet	1284	26	3.11	0.991
CH_2-Cl	1243	30	3.09	0.988

Table 1.3-3. Binding constant values obtained for each followed signal during the ^{1}H-NMR titration of system **22·C_{60}**.

The analysis on the system **[24·C_{60}]** revealed the same tendency, demonstrating notable shifts in the triazole (7.55 ppm), central phenyl ring (6.60 and 6.54 ppm) and CH_2Cl (4.46 ppm) signals as the side phenyl rings signals were almost unaltered. As in the case of the **[22·C_{60}]**, the absence of a

strong electron donor motif as π-exTTF makes the triazole motif to play a more important role in the global interaction with C_{60}. The data fitting yield results in the same line that the other studied systems (Table 1.3-4 and Figures A3-16 to A3-18 in *Annexe 3*).

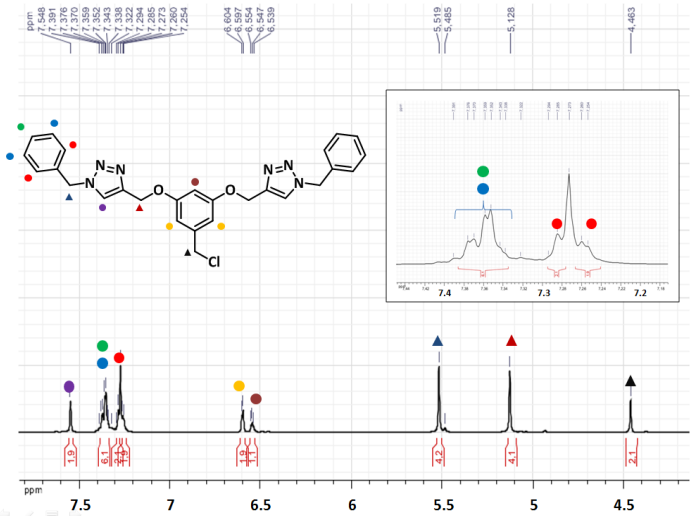

Figure 1.3-24. ^{1}H-NMR spectrum of host molecular tweezer **24**.

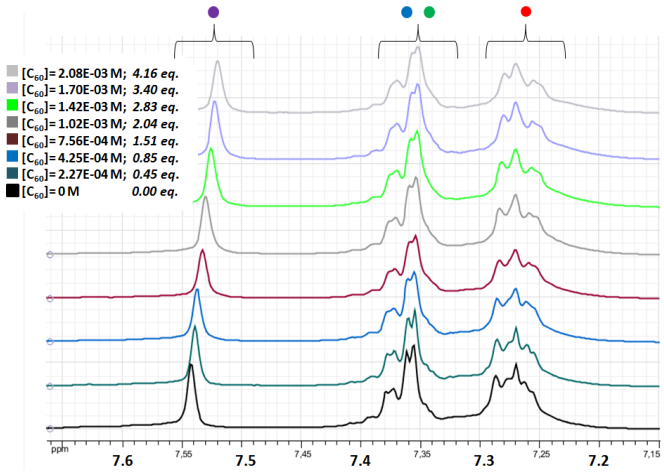

Figure 1.3-25. ^{1}H-NMR titration experiment for system **[24·C_{60}]** enhancing the change in the triazole signal (purple) whereas the side phenyl rings signals (blue, green and red) remain almost unaltered.

[24·C_{60}]	K value	Fitting error	Log K	R^2
triazole signal	1262	78	3,10	0.948
central ring doublet	1205	58	3,08	0.967
central ring triplet	1287	62	3,11	0.963
CH_2-Cl	1207	60	3,08	0.965

Table 1.3-4. Binding constant values obtained for each followed signal during the ^{1}H-NMR-titration of system **24·C_{60}**.

In view of the obtained results, it is clear the leading role that the triazole and the central phenyl ring play in the interaction with fullerene C_{60} in the three different systems studied. According to the experimental findings, the benzene ring closer to the triazole ring in π-exTTF and TCAQ also participate in the complexation with the C_{60} unit, although in a considerable lesser extent. These observations are in agreement with that found for the complex **[24·C_{60}]** endowed with phenyl rings at terminal positions. Furthermore, these complexations would account for the similar binding constants determined for all complexes.

c) Theoretical calculations

Because of the similar binding constant values calculated for hosts **18**, **22** and **24** in the recognition of C_{60}, a theoretical study has been carried out by the group of Prof. Enrique Ortí at the Institut de Ciència Molecular, Universitat de València. In order to shed light on the obtained results, the calculations have been performed by means of the Density Functional Theory (DFT) using the dispersion-corrected exchange-correlation B97D functional with the 6-31G** basis set.

We first focused on the spatial arrangement of the receptor **24** in the free state. Several conformations can be modelled due to the high rotational flexibility along the single bonds in the host, resulting in five minimum-energy conformations. Four of these conformations are almost isoenergetic except the folded conformation 5, which stands more than 4 kcal/mol lower in energy with respect to the others (Figure 1.3-26). This stabilization stems from dispersion interactions originated by intramolecular short contacts between the arms and the core of the pincer.

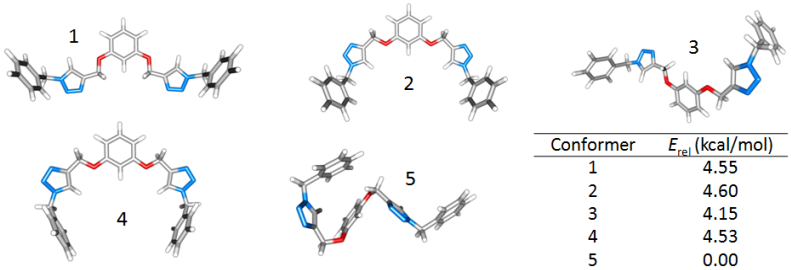

Conformer	E_{rel} (kcal/mol)
1	4.55
2	4.60
3	4.15
4	4.53
5	0.00

Figure 1.3-26. Conformations of several minimum-energy geometries optimized for **24**. The relative stabilities between them are summarized in the adjacent table.

The **[24·C_{60}]** dimmer structure was also modelled resulting in five minimum-energy conformations with similar association energies (Figure 1.3-27). Among them, the most stable structure corresponds to the conformer 3, where the tweezer arms wrapped themselves around the central benzene ring in a concave shape. However, conformers 1 and 4, in which the benzene arms stand extended to embrace the fullerene guest are also computed with similar association energies of -26.11 and -26.22 kcal/mol, respectively. The energy of the most stable structure (conformer 5 in Figure 1.3-27) was used to compute the binding energy.

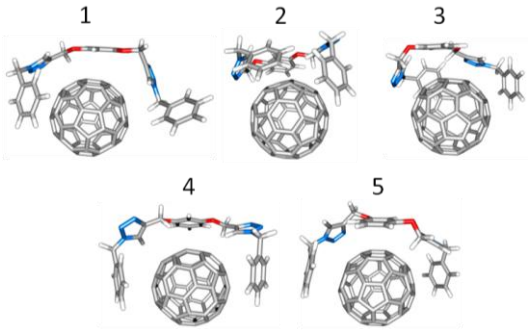

Conformer	E_{bind} (kcal/mol)
1	-26.11
2	-26.03
3	-27.13
4	-26.22
5	-19.39

Figure 1.3-27. Minimum-energy geometry computed for several dispositions of **24** around C_{60}. Association energies computed for the different conformations are summarized in the inset table.

In order to reduce the conformational possibilities and analyze structures directly comparable between the different dimers, symmetry-restricted C_s optimizations were performed. Interaction energies were computed using the geometries for the monomers **24** in the dimer species. Several types of host-guest arrangements where optimized for **[24·C_{60}]** even in a C_s point

group (Figure 1.3-28). The most stable conformer **[24·C_{60}]**, which accounts for an interaction energy of -31.18 kcal/mol, arranges their benzene arms in an open-like shape combining both π-π and C-H···π interactions (central benzene, triazole and lateral benzenes, interacting with C_{60}).

Conformers **[24·C_{60}]**-1 and **[24·C_{60}]**-2 provide similar interaction energies and their arms are arranged in an embraced and crown shape around C_{60} (Figure 1.3-28). Similar conformers were obtained for **[18·C_{60}]** and **[22·C_{60}]**, but now the interaction energy notably increases to -51.45 and -49.69 kcal/mol, respectively.

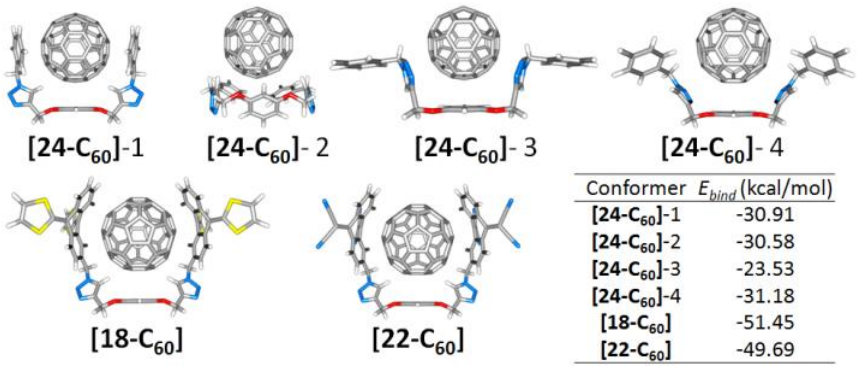

Conformer	E_{bind} (kcal/mol)
[24-C_{60}]-1	-30.91
[24-C_{60}]-2	-30.58
[24-C_{60}]-3	-23.53
[24-C_{60}]-4	-31.18
[18-C_{60}]	-51.45
[22-C_{60}]	-49.69

Figure 1.3-28. Minimum-energy geometries for the diametric species of tweezers **a**, **b** and **c** hosting the fullerene C_{60}. Association energies for the different conformers are collected in the inset table.

Intermolecular contacts between the triazole-based tweezers and the guest C_{60} are computed in the range of typical dispersion interactions (Table 1.3-5). Short distances between the central benzene ring of the tweezer and the closest double bond of C_{60} are computed at 3.31 Å for **[24·C_{60}]**. In the π-exTTF and TCAQ-based dimers (**[18·C_{60}]** and **[22·C_{60}]**), this distance is reduced to 3.23 and 3.22 Å, respectively, due to the embracing effect of the efficient π-exTTF and TCAQ arms to host C_{60}. The hydrogen atom of the triazole group plays also a significant role in the dimeric association, pointing toward the fullerene guest. The distance computed between this H atom and the closest 6-atom ring of C_{60} is 2.47 Å, and shortens to 2.39 and 2.40 Å in **[18·C_{60}]** and **[22·C_{60}]**, respectively, due to the aforementioned embracing enhancement of π-exTTF and TCAQ. In **[24·C_{60}]**, a short distance of 3.19 Å is computed between the lateral benzene rings and the closest C atom of C_{60}. The substitution of those benzenes by π-exTTF or TCAQ introduces additional π-π interactions between the anthracene skeleton and the fullerene guest with closest distances computed at 3.00 and 3.02 Å, respectively (Table 1.3-5).

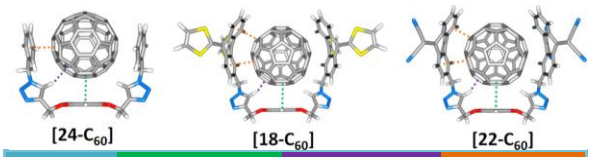

	Bz···C=C(C_{60})	NH···Bz(C_{60})	Bz···C(C_{60})
[24·C_{60}]	3.31	2.47	3.19
[18·C_{60}]	3.23	2.39	3.00 / 3.18
[22·C_{60}]	3.22	2.40	3.02 / 3.16

Table 1.3-5. Characteristic intermolecular distances governing the intermolecular stabilizing interactions between the triazole-based pincers and the fullerene C_{60}.

Interaction energies for the three compounds therefore show that dimer **[24·C_{60}]** should present a lower binding constant in comparison with **[18·C_{60}]** and **[22·C_{60}]**, whereas the latter two would present similar values. This trend is understood by the increased number of dispersion interactions present between the host and the guest C_{60} in **[18·C_{60}]** and **[22·C_{60}]**.

However, a large inner reorganization in the free state host optimization produces a considerable reduction of the interaction energy in the dimer complex, especially in **[18·C_{60}]** and **[22·C_{60}]**, when the energy difference between dimer and monomers is calculated. Figure 1.3-29 displays the difference in structure and energy obtained between the frozen geometries of the hosts at the optimized dimer and the reoptimized isolated host. The stabilization that suffers upon reoptimization amounts 8.44 kcal/mol whereas it reaches 19.07 and 22.04 kcal/mol for **[18·C_{60}]** and **[22·C_{60}]**, respectively. The larger arms of **[18·C_{60}]** and **[22·C_{60}]** permit an increased number of intramolecular interactions in the optimized monomer with respect to **[24·C_{60}]** which is translated into a larger reorganization energy when compared to the frozen structures at the dimer geometry.

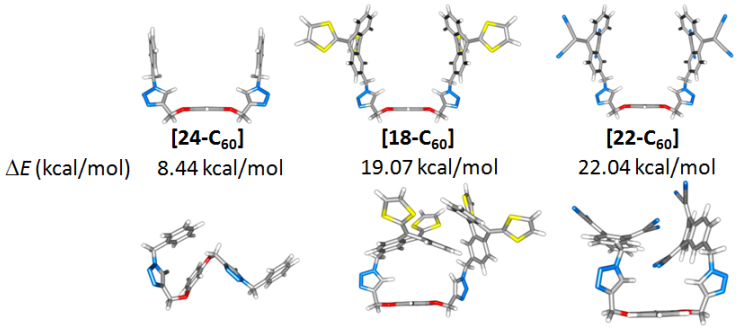

Figure 1.3-29. Comparison between the frozen monomer structures at the optimized supramolecular dimers (top) and after optimization (bottom). The energy difference between the frozen and the optimized monomer structures are collected between the computed structures.

Interaction energies at the frozen pincer geometries in the dimer therefore show that dimers **[18·C_{60}]** and **[22·C_{60}]** present larger interaction energies in comparison to **[24·C_{60}]** due to the increased number of dispersion interactions. Reorganization energy of the large monomeric tweezers of **[18·C_{60}]** and **[22·C_{60}]** provoke a bigger destabilization in the dimeric association compared to **[24·C_{60}]** and, as a consequence, the final binding energy is computed similar in the three compounds.

Conformer	E_{bind} (kcal/mol) Geom dimer	E_{bind} (kcal/mol) Geom reopt
24-1	-30.91	-22.47
24-2	-30.58	-28.67
24-3	-23.53	-13.33
24-4	-31.18	-25.68
18	-51.45	-32.01
22	-49.69	-26.85

Table 1.3-6. Summary of the interaction energies for the different conformers computed at the C_s point group of symmetry using both the pincer energy at the geometry of the dimer and at the minimum-energy geometry after reoptimization of the isolated monomer.

These results are in good agreement with the aforementioned experimental findings, corroborating the importance of the central benzene and the triazole rings in the supramolecular interaction. Moreover, in spite of the very similar binding constant values, the calculations revealed the important role of the anthracene skeleton wrapping around the fullerene. The larger number of interactions is not, however, reflected in the *K* value because of the reorganization energy determined between the free state and the dimer geometry.

1.4. Experimental section

1.4. EXPERIMENTAL SECTION

General Methods

Materials

Organic solvents and reagents used in this work were purchased from commercial suppliers and used as received, unless stated otherwise.

HiPco SWNT were purchased from Carbon nanotechnologies (lot: P0261, purity >82 %, <18 % remaining iron particles, length = 100-1000 nm, diameter = 0.8-1.4 nm) and used without any further purification treatment.

MWCNT were synthesized by CVD using Fe/Al_2O_3 as catalyst at 650 °C.[119] The starting MWNTs can attain 10 μm in length and most of them exhibit closed ends. The internal diameter varies between 4 and 12 nm, while the external goes from 8 to 21 nm.

The **graphite** from TIMCAL (TIMREX SFG15, ρ = 2.26 g/cc, particle size = 8.80 μm, specific surface = 9.50 m^2/g, ashes ≤ 0.100%, interlamelar distance = 3354-3358 nm) was used to obtain graphene. For the exfoliation of **graphene**, graphite flakes (200 mg) were dispersed in NMP (100 mL) and sonicated at a low-power sonication bath for 150 minutes. The dispersion was centrifuged at 500 rpm for 45 minutes; the supernatant was decanted and stored in solution.

Instruments

TLC was performed using aluminum coated Merck Kieselgel 60 F254 to check the evolution of the reactions. Visualization was made by UV-light (λ = 254 or 365nm).

Flash column chromatography were performed using silica gel (230-400 mesh).

Microwave reactions were performed in an Anton Paar Monowave 300, using vessels previously dry at 150 ºC during two hours and sealed with Ar gas. Maximum power (850 W) was utilized at the indicated reaction temperatures.

Melting points were determined on a Gallenkamp apparatus.

NMR spectra were recorded on a Bruker DPX-300 at 298K using partially deuterated solvents as internal standards.

UV-vis spectra were recorded with a Shimadzu Spectrophotometer UV-3600 at 298K.

Mass spectra were realized by the mass spectra services at the Universidad Complutense de Madrid. Electronic Impact measurements (EI) were recorded

utilizing a HP 5989A aparatus (70 eV, 200º C). MALDI-TOF measurements were recorded utilizing a BRUKER-REFLEX III apparatus (matrix: ditranol, N_2 laser at 337 nm).

FTIR spectra were carried out using pellets of dispersed samples of the corresponding compounds in dried KBr for solid products. The instrument used was a Bruker TENSOR FTIR. The spectral range was 4000-400 cm^{-1}.

TGA analyses were carried out under air and nitrogen in a TA-TGA-Q500 apparatus. The sample (~ 0.5 mg) was introduced inside a platinum crucible and equilibrated at 90 ºC followed by a 10 °C min^{-1} ramp between 90 and 1000 °C.

XPS analyses were carried out using a SPECS GmbH (PHOIBOS 150 9MCD) spectrometer operating in the constant analyzer energy mode. A non monochromatic aluminium X-ray source (1486.61 eV) was used with a power of 200 W and voltage of 12 kV. Pass energies of 75 and 25 eV were used for acquiring both survey and high resolution spectra, respectively. Survey data were acquired from kinetic energies of 1487-400 eV with an energy step of 1 eV and 100 ms dwell time per point. The high resolution scans were taken around the emission lines of interest with 0.1 eV steps and 100 ms dwell time per point. *SpecsLab Version 2.48* software was used for spectrometer control and data handling. The semi-quantitative analyses were performed from the C 1s (284.3 eV) signal. The samples were introduced as pellets of 8 mm diameter.

Raman spectra were recorded on Renishaw in Via Microscope at room temperature using two different exciting laser sources (785 and 532 nm).

TEM micrographs were obtained using a JEOL 2100 microscope operating at 200 kV. The samples were dispersed in organic solvents as DMF or NMP, sonicated for 5 minutes and the resulting suspension dropped onto a holey carbon copper grid (200 mesh), the solvent was allowed to evaporate before analysis.

Cyclic Voltammetry experiments were carried out on a potentiostat/galvanostat AUTOLAB with PGSTAT30 equipped with a software GPES for windows version 4.8 in a conventional three compartment cell. Measurements were carried out using a GCE (glassy carbon) as working electrode, a $Ag/AgNO_3$ reference electrode, and a Pt wire as counter electrode. $TBAPF_6$ was used as supporting electrolyte and DMF as solvent.

Steady-state absorption spectra were recorded with a Varian Cary 50 spectrophotometer and a Varian Cary 5000 spectrometer.

Steady-state fluorescence spectra were taken with a FluoroLog3 spectrometer (Horiba) with an IGA Symphony (5121 1 μm) detector in the NIR detection range.

Transient absorption measurements based on femtosecond laser photolysis were performed with 387 nm laser pulses (1 kHz, 150 fs pulse width) from an amplified Ti:sapphire laser system (Model CPA-2110 from Clark-MXR Inc.) the laser energy was 200 nJ.

1.4.1. SYNTHESIS OF ORGANIC COMPOUNDS

2-(Methylthio)-1,3-dithiolium tetrafluoroborate (3)[115]

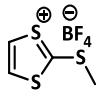

1,3-Dithiole-2-thione **2** (5.29 g, 39.39 mmol) was suspended in Me_2SO_4 (39.4 mL, 416.40 mmol), heated at 95 ºC during 30 minutes and then left to cool to 0 ºC. At this temperature, glacial acetic acid (8 mL) was added and kept stirring during 10 minutes. HBF_4-Et_2O (5.4 mL, 39.39 mmol) was added and the solution was stirred during 20 minutes extra, followed by the addition of diethyl ether (125 mL) to yield a precipitate that was filtered and washed with diethyl ether (95 %).

^{1}H-NMR (DMSO-d_6, 300 MHz), δ: 8.73 (s, 2H), 3.17 (s, 3H).

2-(Methylthio)-1,3-dithiole (4)[115]

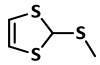

$NaBH_4$ (0.28 g, 7.41 mmol) was slowly added to a 0 ºC cooled solution of 2-(methylthio)-1,3-dithiolium tetrafluoroborate **3** (1.72 g, 7.29 mmol) in absolute ethanol under Ar atmosphere, and the mixture was kept stirring during 2 hours. The solvent was removed under reduced pressure, washed with water and extracted with DCM. The organic layer was dried over $MgSO_4$, filtered and taken to dryness to yield the desired product as a dark oil (95 %).

^{1}H-NMR ($CDCl_3$, 300 MHz), δ: 6.12 (s, 1H), 6.07 (s, 2H), 2.20 (s, 3H).

1,3-Dithiolium tetrafluoroborate (5)[115]

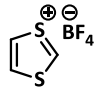

To a solution of 2-(methylthio)-1,3-dithiole **4** (0.77 g, 5.12 mmol) in acetic anhydride (12.5 mL) at 0 ºC, HBF_4·Et_2O (0.7mL, 5.22 mmol) was added dropwise. The solution was stirred during 15 minutes, when diethyl ether (125 mL) was added. The mixture was stirred again during 30 minutes to yield a white solid that was filtered and washed with ether (95 %).

^{1}H-NMR (DMSO-d_6, 300 MHz), δ: 6.79 (s, 1H), 9.37 (s, 2H).

Dimethyl-(1,3-dithiol-2-yl)-phosphonate (6)[115]

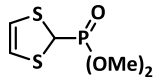

To a solution of 1,3-dithiolium tetrafluoroborate **5** (0.63 g, 3.31 mmol) in acetonitrile, $P(OMe)_3$ (0.4 mL, 3.31 mmol) and NaI (0.48 g, 3.31 mmol) was added successively, stirring the resultant mixture at r.t. during 2 hours. The crude reaction solvent was then removed under reduced pressure, washed with water and extracted with DCM. The organic layer is dried over $MgSO_4$, filtered and the solvent is removed to yield the desired product as a dark oil (90 %).

^{1}H NMR ($CDCl_3$, 300 MHz), δ: 5.98 (2H, s), 4.73 (d, 1 H, *J* = 4.5 Hz), 3.75 (d, 6H, *J* = 10.5 Hz).

2-(((*Tert*-butyldiphenylsilyl)oxy)methyl)anthraquinone (8)[131]

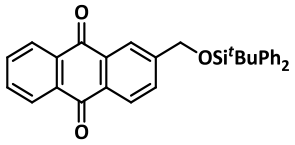

2-Hydroxymethylanthraquinone **7** (1.00 g, 4.20 mmol) was dissolved in 50 mL of anhydrous THF and, under argon atmosphere, imidazole (1.43 g, 21.00 mmol) and *tert*-butyldiphenylsilane chloride (1.3 mL, 5.03 mmol) were added. The reaction mixture was kept stirring overnight. Then, the solvent was removed under reduced pressure and the residue was dissolved in DCM and washed with water. The organic layer was dried with $MgSO_4$ and filtered, the solvent was then evaporated to yield a crude that is purified by silica gel column chromatography, using a hexane/DCM (2:1) mixture as eluent. The final product was obtained as a pale yellow solid (90 %).

^{1}H-NMR ($CDCl_3$, 300 MHz), δ: 8.33-8.25 (m, 4H), 7.83-7.79 (m, 3H), 7.73- 7.70 (m, 4H), 7.47-7.38 (m, 6H), 4.92 (s, 2H), 1.16 (s, 9H).

[131] Marshallsay, G. J. and Bryce, M. R., *J. Org. Chem.* **1994**, *59*, 6847.

2-(((*Tert*-butyldiphenylsilyl)oxy)methyl)-9,10-bis(1,3-dithiol-2-ylidene)-9,10-dihydroanthracene (9)[114]

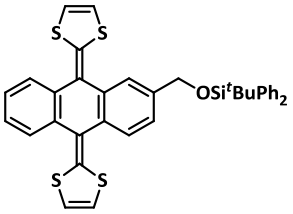

A volume of 2.0 mL of *n*BuLi (1.6 M in hexane, 3.20 mmol) was added to a solution of dimethyl (1,3-dithiol-2-yl)phosphonate **6** (0.58 g, 2.75 mmol) in anhydrous THF (100 mL) at -78 ºC under argon atmosphere and the mixture was kept stirring during 45 minutes at the same temperature. Then, 2-(((*tert*-butyldiphenylsilyl)oxy)methyl)anthraquinone **8** (0.22 g, 0.47 mmol) was dissolved in anhydrous THF (100 mL) and added dropwise. The mixture was kept at -78 ºC during 1 hour and then was left to reach r.t. overnight. The solvent was removed under reduced pressure and the crude was washed with water (100 mL) and extracted with DCM (3 x 100 mL). The combined organic layers are washed with water (2 x 100 mL) and a saturated NaCl aqueous solution (2 x 100 mL), dried over $MgSO_4$ and filtered. The solvent was removed and the residue was purified by silica gel column chromatography using an hexane/DCM (2:1) mixture as eluent. The final product was obtained as a yellow solid (96 %).

^{1}H-NMR ($CDCl_3$, 300 MHz), δ: 8.25-8.14 (m, 7H), 8.03-7.72 (m, 10H), 6.79 (s, 4H), 4.83 (m, 2H), 1.16 (s, 9H).

2-(hydroxymethyl)-9,10-bis(1,3-dithiol-2-ylidene)-9,10-dihydroanthracene (10)[114]

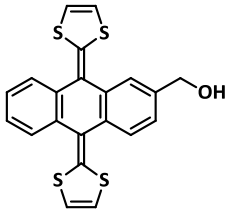

To a solution of 2-(((*tert*-butyldiphenylsilyl)oxy)methyl)-π-exTTF **9** (0.29 g, 0.50 mmol) in anhydrous THF, a volume of 0.16 mL of TBAF (0.54 mmol, 1.0 M in THF) was added under argon atmosphere. The mixture was kept stirring during 2 hours at r.t. After this time, the reaction mixture was washed with water and extracted with DCM. The organic layer was dried over $MgSO_4$, filtered and the solvent was removed. The residue was purified by silica gel column chromatography, using DCM as eluent, to yield a yellow solid (98 %).

^{1}H-NMR (DMSO-d_6, 300 MHz), δ: 7.66-7.57 (m, 4H), 7.36-7.23 (m, 3H), 6.74-6.73 (m, 4H), 5.29 (t, 1H, *J* = 5.6 Hz), 4.54 (d, 2H, *J* = 5.6 Hz).

[9,10-Bis(1,3-dithiol-2-ylidene)-9,10-dihydroanthracen-2-yl]methyl methanesulfonate (11)[116]

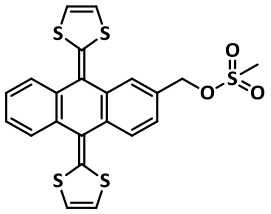

A solution of 2-hydroxymethyl-π-exTTF **10** (0.17 g, 0.42 mmol), triethylamine (0.06 mL, 0.4 mmol) and methanosulfonyl chloride (0.04 mL, 0.55 mmol) in anhydrous DCM (50 mL) was stirred during 2 hours. The reaction mixture was then washed with water (2 x 100 mL) and extracted with (2 x 75 mL) DCM. The organic layer was washed again with water (2 x 100 mL), dried over $MgSO_4$ and filtered. After removing the solvent, the crude was quickly percolated over silica gel using DCM as eluent, to yield a yellow solid (95 %).

^{1}H-NMR ($CDCl_3$, 200 MHz), δ: 7.71-7.67 (4H, m), 7.45-7.29 (3H, m), 6.32 (4H, s) 4.65 (2H, s), 3.07 (3H,s).

9,10-Bis(1,3-dithiol-2-yliden)-2-azidomethyl-9,10-dihidroanthracene (12)[116]

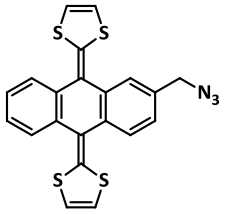

A 2-π-exTTF-methyl mesylate **11** (0.21 g, 0.24 mmol) suspension in acetonitrile (100 mL) was heated at 60 ºC under argon atmosphere. Previously activated sodium azide (0.82 g, 12.60 mmol) was added in small portions and the mixture was stirred overnight. The reaction was left to get r.t. and water was added (100 mL). The crude was extracted with DCM (2 x 100 mL) and the organic layer was dried over $MgSO_4$, filtered and taken to dryness. The residue was purified by silica gel column chromatography using a hexane/DCM (1:1) mixture as eluent to yield a yellow solid (95 %).

^{1}H-NMR ($CDCl_3$, 200 MHz), δ: 7.70-7.67 (4H, m), 7.43-7.21 (3H, m), 6.31 (4H, s), 4.40 (2H, s).

Methyl 3,5-bis(propargyloxy)benzoate (14)[117]

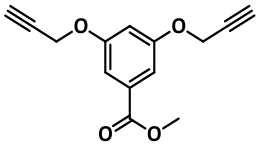

Methyl 3,5-dihydroxybenzoate **13** (6.00 g, 35.70 mmol) was dissolved in a K_2CO_3 (12.33 g, 89.20 mmol) suspension in acetone. The mixture was heated at 50 ºC and propargyl bromide was then added, keeping stirring overnight. The mixture was filtered and the solvent was removed to yield the desired product as pale brown crystals (98 %)

^{1}H-NMR ($CDCl_3$, 300 MHz), δ: 7.31 (d, 2H, *J* = 2.3 Hz), 6.83 (t, 1H, *J* = 2.3 Hz), 4.73 (d, 4H, *J* = 2.4 Hz), 3.92 (s, 3H), 2.55 (t, 2H, *J* = 2.4 Hz).

3,5-Bis(propargyloxy)benzyl alcohol (15)[117]

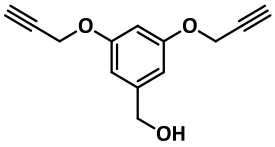

To a stirred solution of methyl 3,5-bis(propargyloxy)benzoate **14** (2.05 g, 8.40 mmol) in anhydrous THF (75 ml), lithium aluminum hydride (0.49 g, 12.6 mmol) in small portions was added. A few minutes later, a white solid appears suspended into the reaction mixture. The remaining lithium aluminum hydride was then quenched with AcOEt and EtOH consecutively, and the mixture was filtered under vacuum, rinsing the solid with DCM. The filtrate was dried with $MgSO_4$ filtered and taken to dryness, yielding the desired product as white crystals (90 %).

^{1}H-NMR ($CDCl_3$, 300 MHz), δ: 6.56 (d, 2H, *J* = 2.2 Hz), 6.46 (t, 1H, *J* = 2.2 Hz), 4.61 (d, 4H, *J* = 2.4 Hz), 4.45 (s, 2H), 2.46 (t, 2H, *J* = 2.4 Hz), 1.67 (bs, 1H).

3,5-Bis(propargyloxy)benzyl chloride (16)[117]

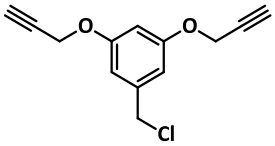

3,5-Bis(propargyloxy)benzyl alcohol **15** (0.500 g, 2.31 mmol) was dissolved in anhydrous DCM (25 mL) and pyridine (0.37mL, 4.62 mmol). Thionyl chloride (0.25 mL, 3.47 mmol) was then added dropwise and the mixture was kept stirring under Ar atmosphere overnight. The reaction was quenched with water and the organic layer separated and washed again with water (3 x 50 mL). The organic layer was dried over $MgSO_4$, filtered and the solvent was

removed. The crude was purified by silica gel column chromatography using a DCM/Hexane (2:1) mixture as eluent to yield the desired product as a white solid (95 %).

^{1}H-NMR ($CDCl_3$, 300 MHz), δ: 6.80 (d, 1H, *J* = 2.2 Hz), 6.59 (t, 2H, *J* = 2.2 Hz), 4.73 (d, 4H, *J* = 2.4 Hz), 4.55 (s, 2H), 2.57 (t, 2H, *J* = 2.4 Hz).

5-(Chloromethyl)-1,3-bis(((9,10-di(1,3-dithiol-2-ylidene)-9,10-dihydroanthracen-2-yl)methyl)-1*H*-4-(1,2,3-triazolyl)methyloxy) benzene (17)

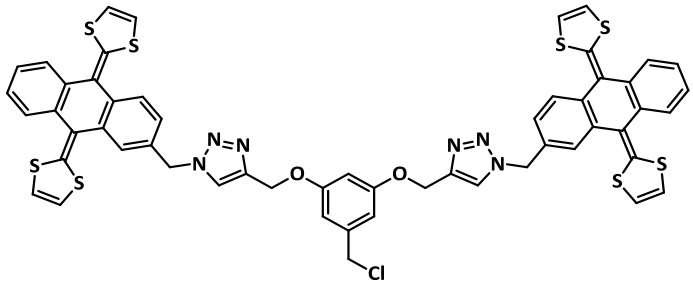

A DMSO suspension of azidomethyl-π-exTTF **12** (0.150 g, 0.345 mmol), 3,5-bis(propargyloxy)benzyl chloride **16** (0.041 g, 0.173 mmol), $CuBr{\cdot}SMe_2$ (0.014 g, 0.07 mmol), sodium ascorbate (0.009 g, 0.07 mmol) and copper wires were sealed under Ar atmosphere and irradiated under microwave conditions (110 ºC, 850 W) during 2 hours. The resulting dark solution was percolated through a small column containing Quadrasyl-MT to remove the remaining copper. Ethanol was then added to precipitate the desired product that after several cycles of centrifugation/EtOH washing was isolated as a dark yellow solid (65 %).

^{1}H-NMR ($CDCl_3$, 300 MHz), δ: 7.71-7.63 (Ar-**H**, m, 6H), 7.58 (N-C**H**, s, 2H), 7.51 (Ar-**H**, d, 2H, *J* = 1.3 Hz), 7.31-7.25 (Ar-**H**, m, 4H), 7.16 (Ar-**H**, d, 2H, *J* = 8.1 Hz), 6.59 (Ar-**H**, s, 2H), 6.55 (Ar-**H**, s, 1H), 6.27 (S-C**H**, s, 4H), 6.23 (S-C**H**, d, 2H, *J* = 6.7 Hz), 6.18 (S-C**H**, d, 2H, *J* = 6.7 Hz), 5.53 (C**H$_2$**N, s, 4H), 5.13 (C**H$_2$**O, s, 4H), 4.45 (C**H$_2$**Cl, s, 2H).

^{13}C-NMR ($CDCl_3$, 75 MHz), δ: 159.6 (Ar**C**-O), 144.4 (**C**-N), 139.7 (Ar**C**-CH_2Cl), 137.0 (Ar**C**), 136.8 (Ar**C**), 136.3 (Ar**C**), 135.8 (Ar**C**), 135.2 (Ar**C**), 135.1 (Ar**C**), 131.9 (Ar**C**), 126.2 (Ar**C**H), 126. 1(Ar**C**H), 125.6 (Ar**C**H), 125.5 (Ar**C**H), 125.0 (Ar**C**H), 124.9 (Ar**C**H), 124.5 (Ar**C**H), 122.9 (N-**C**H), 121.4 (Ar**C**-S), 121.1 (Ar**C**-S), 117.4 (S**C**H), 117.1 (S**C**H), 108.1 (Ar**C**H), 101.8 (Ar**C**H), 62.3 (**C**H_2N), 54.2 (**C**H_2OAr), 46.1 (**C**H_2Cl).

FTIR ($CHCl_3$) cm^{-1}: 3068, 3009, 2926, 2859, 1666, 1599, 1548, 1510, 1457, 1342, 1290, 1157, 1050, 802, 755.

HRMS (MALDI): *m/z* calculated for $C_{55}H_{37}ClN_6O_2S_8Na$: 1127.0330, experimental: 1127.0365.

UV-Vis ($CHCl_3$), λmax: 367, 414, 425 nm.

m.p. (ºC):275-277.

5-(Azidomethyl)-1,3-bis(((9,10-di(1,3-dithiol-2-ylidene)-9,10-dihydroanthracen-2-yl)methyl)-1*H*-4-(1,2,3-triazolyl)methyloxy) benzene (18)

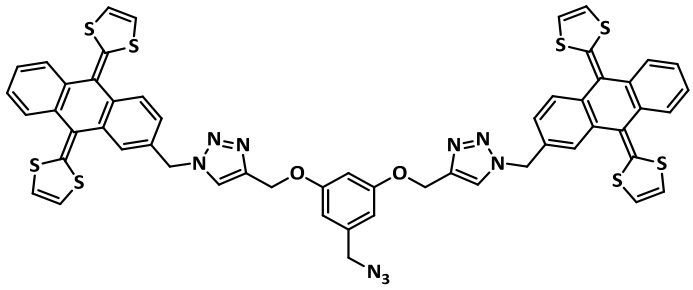

A solution of chloride **17** (0.050 g, 0.05 mmol) and NaN_3 (0.059 g, 0.90 mmol) in THF/water was heated under Ar atmosphere at 70 ºC overnight. The reaction was followed by ^{1}H-NMR observing the decrease in the methylene signal at 4.45 ppm and the increase in the signal at 4.22 ppm corresponding to the azidomethyl group. When the C**H$_2$**Cl signal disappeared totally, the reaction was allowed to reach r.t. The crude is extracted with $CHCl_3$, dry over $MgSO_4$, filtered and taken to dryness, yielding the desired product as a dark yellow product (98 %).

^{1}H-NMR ($CDCl_3$, 300 MHz), δ: 7.71-7.63 (Ar-**H**, m, 6H), 7.59 (N-C**H**, s, 2H), 7.53 (Ar-**H**, d, 2H, *J* = 1.3 Hz), 7.30-7.25 (Ar-**H**, m, 4H), 7.18 (Ar-**H**, d, 2H, *J* = 8.1 Hz), 6.57 (Ar-**H**, s, 1H), 6.52 (Ar-**H**, m, 2H), 6.29 (S-C**H**, s, 4H), 6.25 (S-C**H**, d, 2H, *J* = 6.7 Hz), 6.20 (S-C**H**, d, 2H, *J* = 6.7 Hz), 5.54 (C**H$_2$**N, s, 4H), 5.15 (C**H$_2$**O, s, 4H), 4,22 (C**H$_2$**N_3, s, 2H).

^{13}C-NMR ($CDCl_3$, 75 MHz), δ: 159.9 (Ar**C**-O), 144.4 (**C**-N), 140.8 (Ar**C**-CH_2Cl), 137.1 (Ar**C**), 136.9 (Ar**C**), 136.5 (Ar**C**), 136.0 (Ar**C**), 135.3 (Ar**C**), 135.2 (Ar**C**), 131.9 (Ar**C**), 126.3 (Ar**C**H), 126.2(Ar**C**H), 126.1 (Ar**C**H), 125.7 (Ar**C**H), 125.1 (Ar**C**H), 125.0 (Ar**C**H), 124.7 (Ar**C**H), 123.0 (N-**C**H), 121.8 (Ar**C**-S), 121.6 (Ar**C**-S), 117.5 (S**C**H), 117.2 (S**C**H), 107.8 (Ar**C**H), 101.9 (Ar**C**H), 62.3 (**C**H_2N), 54.2 (**C**H_2OAr), 29.9 (**C**H_2 N_3).

FTIR ($CHCl_3$) cm^{-1}: 2924, 2856, 2099, 1735, 1597, 1548, 1511, 1459, 1349, 1259, 1217, 1161, 1049, 801, 755.

HRMS (MALDI): *m/z* calculated for $C_{55}H_{37}N_9O_2S_8Na$: 1134.0734. Experimental: 1134.0647.

UV-Vis ($CHCl_3$), λmax (log ε): 369 , 416 , 423 nm.

m.p. (ºC):260-263.

2-((methylsulfonyloxy)methyl)anthraquinone (19)

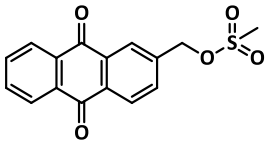

A solution of 2-hydroxymethylanthraquinone (0.25 g, 1.05 mmol), methanosulfonyl chloride (0.2 mL, 2.10 mmol) and triethylamine (0.3 mL, 2.10 mmol) in anhydrous DCM (50 mL) was stirred during 2 hours. The reaction mixture was then washed with water (2 x 50 mL) and extracted with DCM (2 x 75 mL). The organic layer was washed again with water (2 x 50 mL), dried over $MgSO_4$ and filtered. After removing the solvent, the crude was quickly percolated over silica gel using DCM as eluent, to yield a yellow solid (95 %). Because its low stability, only ^{1}H-NMR could be performed.

^{1}H-NMR ($CDCl_3$, 200 MHz), δ: 8.39 (d, 1H, *J* = 8.0 Hz), 8.38-8.31 (m, 3H), 7.86 (dd, 1H, *J* = 8.0 Hz, *J* = 2.0 Hz), 7.85 (d, 1H, *J* = 6.0 Hz), 7.84 (d, 1H, *J* = 6.0 Hz), 5.40 (s, 2H), 3.1 (s, 3H).

2-(Azidomethyl)anthraquinone (20)[132]

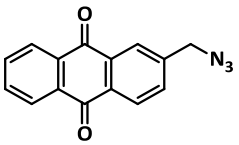

A modified procedure was utilized for the preparation of **20**. A 2-(methyl methanesulfonate)anthraquinone **19** (1.33 g, 0.24 mmol) suspension in acetonitrile (50 mL) was heated at 60 ºC under argon atmosphere. Previously activated sodium azide (8.20 g, 126.00 mmol) was added in little portions and the mixture was stirred overnight. The reaction was left to get r.t. and water was added (100 mL). The crude was extracted with DCM(2 x 100 mL) and the organic layer was dried over $MgSO_4$, filtered and taken to dryness. The residue was purified by silica gel column chromatography using a hexane/DCM (1:1) mixture as eluent to yield a yellow solid (95 %).

^{1}H-NMR ($CDCl_3$, 200 MHz), δ: 8.36 (d, 1H, *J* = 8.1 Hz), 8.35 (d, 1H, *J* = 5.7 Hz), 8.34 (d, 1H, *J* = 5.7 Hz), 8.27 (d, 1H, *J* = 1.7 Hz), 7.84 (d, 1H, *J* = 5.7 Hz), 7.84 (d, 1H, *J* = 5.7 Hz), 7.78 (dd, 1H, *J* = 8.0 Hz, *J* = 1.7 Hz), 4.58 (s, 2H).

[132] Myers, E. L. and Raines, R. T., *Angew. Chem., Int. Ed.* **2009**, *48*, 2359.

2-Azidomethyl-9,10-bis-(dicyamomethylen)anthracene (21)

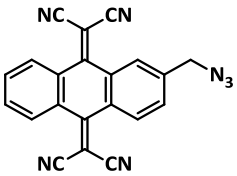

A solution of 2-(methyl azide)anthraquinone **20** (0.16 g, 0.61 mmol) and malonitrile (0.10 g, 1.52 mmol) in $CHCl_3$ (50 mL) was heated under Ar atmosphere at 65 ºC. Then, $TiCl_4$ and pyridine are added dropwise, keeping the solution stirring at this temperature 24 hours. The same amounts of malonitrile, $TiCl_4$ and pyridine are added again, stirring 24 hours more. The reaction mixture was left to reach r.t. and filtered over celite, washed with water, dry over Na_2SO_4, and filtered. The crude was taken to dryness and then purified by silica gel column chromatography using a hexane/DCM (2:1) mixture as eluent to yield a yellow solid (90 %).

^{1}H-NMR ($CDCl_3$, 300 MHz), δ: 8.22-8.16 (m, 3H), 8.14 (d, 1H, *J* = 1.4 Hz), 7.72-7.65 (m, 2H), 7.62 (dd, 1H, *J* = 8.1 Hz, *J* = 1.7 Hz), 4.52 (s, 2H).

^{13}C-NMR ($CDCl_3$, 75 MHz), δ: 160.2 (Ar**C**), 160.0 (Ar**C**), 141.5 (**C**-CH_2N_3), 133.0 (Ar**C**H), 131.9 (Ar**C**H), 131.2 (Ar**C**), 130.5 (Ar**C**), 130.4 (Ar**C**), 128.5 (Ar**C**H), 128.1 (Ar**C**H), 127.1 (Ar**C**H), 113.3 (**C**≡N), 84.0 (**C**-C≡N), 83.7 (**C**-C≡N), 54.1 (**C**H_2N_3).

FTIR ($CHCl_3$) cm^{-1}: 3005, 2970, 2228, 2105, 1589, 1560, 1337, 1282, 1221, 836, 767, 694.

HRMS (MALDI): *m/z* calculated for $C_{21}H_9N_7Na$: 382.0817. Experimental: 382.08205.

UV-vis ($CHCl_3$), λmax: 354 nm.

m.p. (ºC): 292-294.

5-(Chloromethyl)-1,3-bis(((9,10-bis(dicyanomethylidene)-9,10-dihydroanthracen-2-yl)methyl)-1*H*-4-(1,2,3-triazolyl)methyloxy) benzene (22)

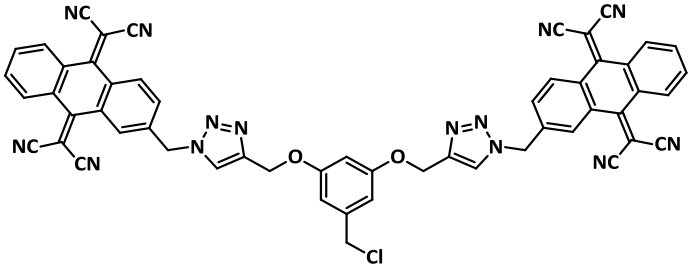

A DMSO suspension of azidomethyl-TCAQ **21** (0.306 g, 0.85 mmol), 3,5-bis(propargyloxy)benzyl chloride **16** (0.100 g, 0.42 mmol), $CuBr{\cdot}SMe_2$ (0.035 g, 0.17 mmol), sodium ascorbate (0.022 g, 0.17 mmol) and copper wires were sealed under Ar atmosphere and irradiated under microwave conditions (110 ºC, 850 W) during 2 hours. The resulting dark solution was percolated through a small column containing Quadrasyl-MT to remove the remaining copper. Ethanol was then added to precipitate the desired product that after several cycles of centrifugation/EtOH washing was isolated as dark yellow solid (85 %).

^{1}H-NMR ($CDCl_3$, 300 MHz), δ: 8.28-8.21 (Ar-**H**, m, 6H), 7.95 (N-C**H**, s, 2H), 7.77-7.74 (Ar-**H**, m, 6H), 7.61 (Ar-**H**, dd, 2H, *J* = 8.0 Hz, *J* = 1.5 Hz), 6.62 (Ar-**H**, d, 2H, *J* = 2.2 Hz), 6.58 (Ar-**H**, t, 1H, *J* = 2.2 Hz), 5.71 (C**H$_2$**N, s, 4H), 5.20 (C**H$_2$**O, s, 4H), 4.48 (C**H$_2$**Cl, s, 2H).

^{13}C-NMR ($CDCl_3$, 75 MHz), δ: 159.4 (Ar**C**), 159.3 (Ar**C**-O), 145.0 (**C**-N), 139.7 (Ar**C**-CH_2Cl), 132.7 (Ar**C**H), 131.3 (Ar**C**H), 131.2 (Ar**C**), 130.4 (Ar**C**), 129.9 (Ar**C**), 128.4 (Ar**C**H), 127.7 (Ar**C**H), 126.4 (Ar**C**H), 123.5 (N-**C**H), 113.1 (**C**≡N), 113.0 (**C**≡N), 112.9 (**C**≡N), 112.8 (**C**≡N), 108.3 (Ar**C**H), 102. (Ar**C**H), 83.6 (**C**-C≡N), 62.0 (**C**H_2N). 53.0 (**C**H_2OAr), 46.1 (**C**H_2Cl).

FTIR ($CHCl_3$) cm^{-1}: 3145, 3072, 2932, 2228, 1596, 1558, 1459, 1329, 1294, 1225, 1158, 1048, 825, 771, 733, 693.

HRMS (MALDI): *m/z* calculated for $C_{55}H_{29}ClN_{14}O_2Na$: 975.2184, experimental: 975.2197.

UV-Vis ($CHCl_3$), λmax (log ε): 353 (4.79) nm.

m.p. (ºC):276-280.

5-(Chloromethyl)-1,3-bis(((9,10-bis(dicyanomethylidene)-9,10-dihydroanthracen-2-yl)methyl)-1*H*-4-(1,2,3-triazolyl)methyloxy) benzene (24)[117]

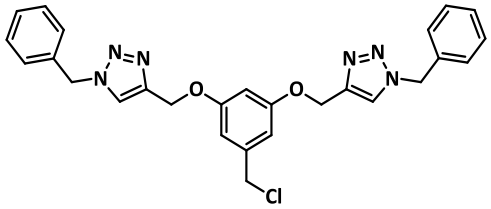

A suspension of benzylazide **23** (0.306 g, 0.85 mmol), 3,5-bis(propargyloxy)benzyl alcohol **16** (0.100 g, 0.42 mmol), $CuBr{\cdot}SMe_2$ (0.035 g, 0.17 mmol), sodium ascorbate (0.022 g, 0.17 mmol) and some copper wires in a $^tBuOH/H_2O$ (1:1) mixture was sealed under Ar atmosphere and kept stirring during 48 hours. The resulting dark solution was percolated through a small column containing Quadrasyl-MT to remove the remaining copper. The collected fraction was extracted with chloroform (2 x 25 mL) and the resulting organic layer was washed with water, dried over Na_2SO_4 and then filtered. The solvent was finally removed to afford a pale yellow oil (90 %).

^{1}H-NMR ($CDCl_3$, 300 MHz), δ: 7.55 (N-C**H**, s, 2H), 7.39-7.32 (Ar-**H**, m, 6H), 7.29-7.25 (Ar-**H**, m, 4H), 6.60 (Ar-**H**, d, 2H, *J* = 2.2 Hz), 6.54 (Ar-**H**, t, 1H, *J* = 2.2 Hz), 5.52 (C**H**$_2$N, s, 4H), 5.12 (C**H**$_2$O, s, 4H), 4.46 (C**H**$_2$Cl, s, 2H).

1.4.2. SYNTHESIS AND CHARACTERIZATION OF NANOCONJUGATES

General procedure for the synthesis of CNF-1

An amount of 25 mg of pristine SWNT or 100 mg of pristine MWNT were reacted in a deoxygenated solution of deionized water (25 mL) with of 4-[(trimethylsilyl)ethynyl]aniline (1 eq., 0.42 mmol) and isoamyl nitrite (2 eq., 0.84 mmol) for 24 hours at 70 °C under argon. The reaction mixture was filtered on a 0.2 µm pore size polycarbonate membrane and washed with deionized water. Afterwards, the solid was washed by filtration over a 0.2 µm poly(tetrafluoroethylene) (PTFE) membrane several times with NMP, CH_2Cl_2, and MeOH (sonicated, centrifuged and filtered) until the filtrated solution remained colourless affording the desired material.

The general procedure for the synthesis was slightly modified in the case of graphene, by using 50 mL of the as produced exfoliated graphene suspensions in NMP instead of the deionized water suspension. The suspension was reacted with 4-[trimethylsilyl)ethynyl]aniline (1.2 mmol) and isoamyle nitrite (2.5 mmol) under argon atmosphere at 70 °C for 24 hr and purified as aforementioned. The product obtained was redispersed on 50 mL of NMP and submitted to the same reaction conditions to complete a second reaction cycle in order to increase the amount of functional groups presented on the graphene surface, followed by the same filtration step.

General procedure for the synthesis of CNF-2 and CNF-3

The alkyne functionalized **CNF-1,** (20 mg) was suspended in NMP (20 mL) with 0.08 mL of tetra-*n*-butylammonium fluoride (TBAF) (1M in THF) (0.27 µmol) for two hours to cleavage the TMS protecting groups. Subsequently, the π-exTTF azide **12** (0.05 mmol), copper sulphate (31.3 µm), sodium ascorbate (31.3 µm) and some copper wires were added. After 24 hours at 70 °C, the reaction mixture was filtered and washed over a PTFE membrane several times with NMP, CH_2Cl_2, and MeOH (sonicated, centrifuged and filtered) until the filtrated solution remained colourless to remove the non reacted material. In a second washing step, the solid was washed with water to eliminate the copper catalysts affording **CNF-2.** The same procedure was utilized for preparing **CNF-3** but replacing **12** by the π-exTTF based tweezer **18** and the reaction time was extended to 4 days.

SWNT-1

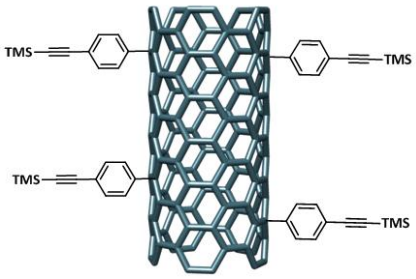

FTIR (KBr) cm^{-1}: 2900 (C-H stretching mode), 1599 (C-H in-plane stretching mode) and 2159 (C≡C stretching mode).

TGA: weight loss and temperature desorption (organic anchoring groups): 26.21 %, 700 °C.

Raman: I_D/I_G = 0.283.

XPS (% atomic): C (284.6 eV) = 90.89, O (531.6 eV) = 4.91, N (399.6 eV) = 0.64, Si (100.7 eV) = 3.55.

SWNT-2

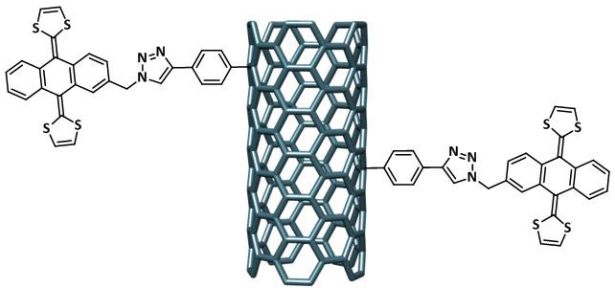

FTIR (KBr) cm^{-1}: 2900 (C-H stretching mode) and 1596 (C-H in-plane stretching mode).

TGA: weight loss and temperature desorption (organic anchoring groups): 38.33 %, 700 °C.

Raman: I_D/I_G = 0.284.

XPS (% atomic): C (284.6 eV) = 82.36, O (532.6 eV) = 13.52, N (399.6 eV) = 1.03, S (169.6 eV) = 1.04, Si (103.6 eV) = 2.0.

SWNT-3

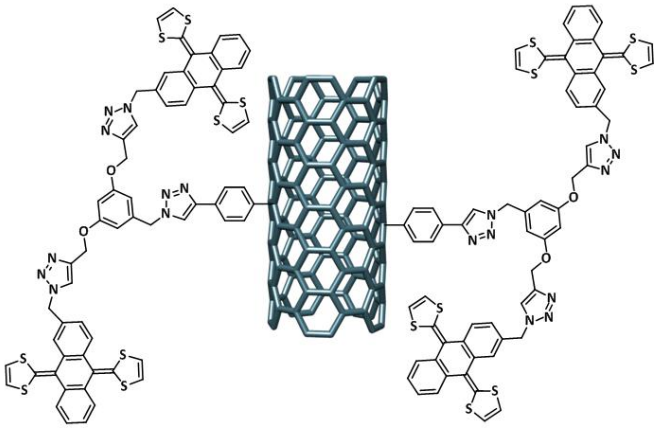

FTIR (KBr) cm^{-1}: 2900 (C-H stretching mode) and 1597 (C-H in-plane stretching mode).

TGA: weight loss and temperature desorption (organic anchoring groups): 49.89 %, 700 °C.

Raman: I_D/I_G = 0.284.

XPS (% atomic): C (284.6 eV) = 82.23, O (532.6 eV) = 10.38, N (399.6eV) = 2.91, S (169.6 eV) = 2.69, Si (103.6 eV) = 1.79.

MWNT-1

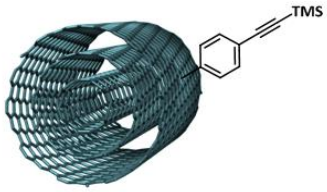

FTIR (KBr) cm^{-1}: 2900 (C-H stretching mode), 1580 (C-H in-plane stretching mode) and 2156 (C≡C stretching mode).

TGA: weight loss and temperature desorption (organic anchoring groups): 8.07 %, 600 °C.

XPS (% atomic): C (284.6 eV) = 91.33, O (532.6 eV) = 4.84, N (399.6 eV) = 0.46, Si (101.6 eV) = 3.36.

Raman: I_D/I_G =2.08.

MWNT-2

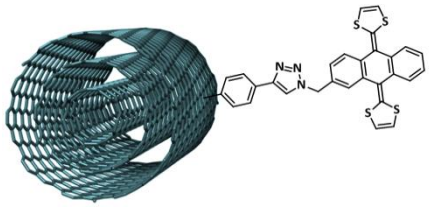

FTIR (KBr) cm^{-1}: 2900 (C-H stretching mode) and 1583 (C-H in-plane stretching mode).

TGA: weight loss and temperature desorption (organic anchoring groups): 29.59 %, 600 °C.

Raman: I_D/I_G =2.08.

XPS (% atomic): C (284.6 eV) = 94.57, O (532.6 eV) = 2.92, N (400.6 eV) = 1.36, S (164.6 eV) = 1.14.

MWNT-3

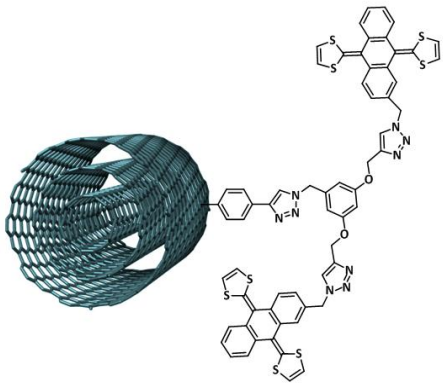

FTIR (KBr) cm^{-1}: 2900 (C-H stretching mode) and 1585 (C-H in-plane stretching mode).

TGA: weight loss and temperature desorption (organic anchoring groups): 45.57 %, 600 °C.

Raman: I_D/I_G =2.10.

XPS (% atomic): C (284.6 eV) = 88.71, O (532.6 eV) = 8.6, N (400.6 eV) = 1.47, S (164.6 eV) = 1.46.

GR-1

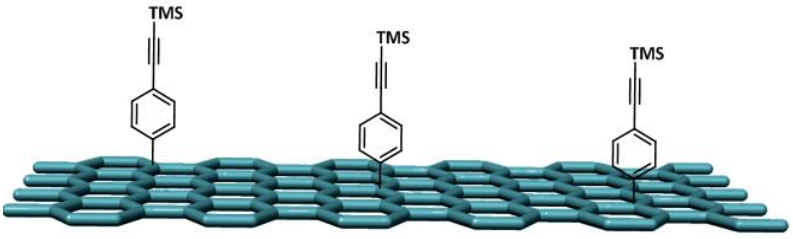

FTIR (KBr) cm^{-1}: 2900 (C-H stretching mode), 1583 (C-H in-plane stretching mode) and 2165 (C≡C stretching mode).

TGA: weight loss and temperature desorption (organic anchoring groups): 14.42 %, 700 °C.

Raman: I_D/I_G = 0.18.

XPS (% atomic): C (284.6 eV) = 79.26, O (532.6 eV) = 12.53, Si (102.6 eV) = 8.2.

GR-2

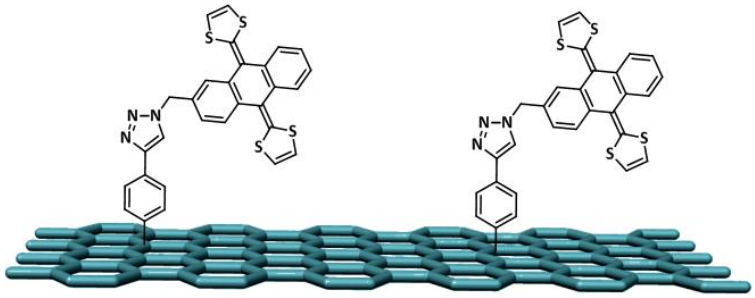

FTIR (KBr) cm^{-1}: 2900 (C-H stretching mode) and 1596 (C-H in-plane stretching mode).

TGA: weight loss and temperature desorption (organic anchoring groups): 21.30 %, 700 °C.

Raman: I_D/I_G = 0.18.

XPS: % atomic: C (284.6 eV) = 84.32, O (532.6 eV) = 9.02, N (400.6 eV) = 0.95, S (170.5 eV) = 1.4, Si (102.6 eV) = 4.3.

GR-3

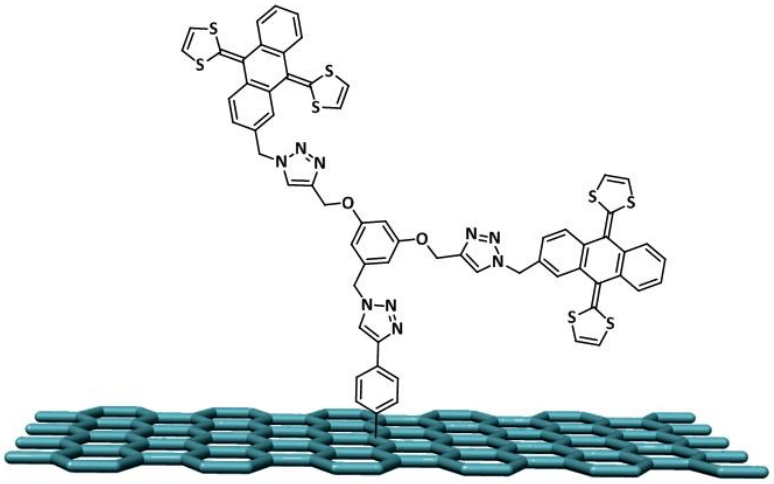

FTIR (KBr) cm^{-1}: (C-H stretching mode) and 1593 (C-H in-plane stretching mode).

TGA: weight loss and temperature desorption (organic anchoring groups): 22.70 %, 700 °C.

Raman: I_D/I_G = 0.18.

XPS: % atomic: C (284.6 eV) = 87.94, O (532.6 eV) = 5.51, N (400.6 eV) = 0.33, S (170.5 eV) = 0.36, Si (102.6 eV) = 1.84.

Chapter 2:

Chemical reactivity of endohedral fullerenes

2.1. Background

2.1. BACKGROUND

Endohedral fullerenes are defined as carbon cages encapsulating different atoms, clusters or small molecules in their inner space. These novel structures are notated as X@C_n, where X is the enclosed species and the @ symbol denotes that is contained inside the cage. Those that hold metals or clusters inside, known as Endohedral Metallofullerenes (EMF),[133] are usually obtained during the process of formation of the cage by arc discharge or laser evaporation, although the most utilized system is the Krätschmer–Huffman generator.[134] On the other hand, those that present small molecules or noble gases (i.e. He, H_2, N_2 or H_2O), known as Non-Metal Endohedral Fullerenes, are usually prepared by ion implanting or by molecular surgery (Figure 2.1-1).[5b]

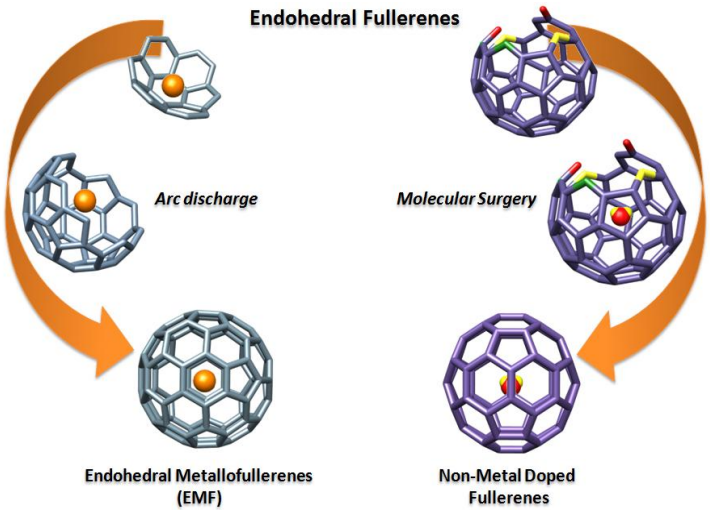

Figure 2.1-1. Depiction of the two main approaches to prepare endohedral fullerenes.

Far from being exotic species, endohedral fullerenes exhibit a broad range of properties that could be of interest for different fields such as materials science and medicine. For example, they can be utilized as a contrast agent for NMR image.[135] Moreover, the presence of metallic clusters allow the X-ray characterization, and the notable different chemical reactivity, particularly in EMF, compared to the well known C_{60}, open a window to new

[133] Feng, L., Akasaka, T. and Nagase, S., in *Carbon Nanotubes and Related Structures*, Wiley-VCH Verlag GmbH & Co. KGaA, **2010**, pp. 455.
[134] Liu, F., Guan, J., Wei, T., Wang, S. and Yang, S., in *Endohedral Fullerenes*, World Scientific Publishing Co., **2014**, pp. 19.
[135] Fatouros, P. P., Corwin, F. D., Chen, Z. J., Broaddus, W. C., Tatum, J. L., Kettenmann, B., Ge, Z., Gibson, H. W., Russ, J. L., Leonard, A. P., Duchamp, J. C. and Dorn, H. C., *Radiology* **2006**, *240*, 756.

fullerene derivatives. Furthermore, the encapsulation of metal clusters in EMF takes places in cages that not always satisfy the isolated pentagon rule (IPR). In contrast to previous proposals, the maximum aromaticity criterion determines the most suitable hosting cages.[136]

2.1.1. ENDOHEDRAL METALLOFULLERENES

a) Synthesis and main features

The first evidence on the existence of EMF came together the C_{60}, revealing the presence of a very stable La@C_{60}.[137] The development of new production methods and experiments on new conditions led to the discovery of new endohedral species hosting a large variety of metals in different cages sizes. Although the selective preparation of a determined species is still a challenge, the experience demonstrated a high correlation between the metal radius and the final cage size. The chance of encapsulating one or several metal atoms inside different size cages results in the possibility of transferring a different number of electrons and, thus, results in a large variety of species with unique properties and possible applications in photovoltaic, biomedicine or catalysis. [5a,138] Moreover, inner metals can play an important role in the control of the selective reactivity of the cage in certain reactions, at the time that reactions can control the location and movement of the metals inside.

The reported results to date, reveal that only group 2, 3 and 4 (including lanthanides and actinides) metals are able to be encapsulated. Although it is difficult to set general statements for EMF, several review articles have established a quite correct classification and description of properties and reactivity.[139] Depending on the number of encapsulated metals inside, EMF can be classified in the following different types:

- *Mono-EMF.* Among the cages that host only one metal, it is possible to distinguish between divalent or trivalent mono-EMF. When alkali-

[136] [(a)]Garcia-Borràs, M., Osuna, S., Swart, M., Luis, J. M. and Solà, M., *Angew. Chem., Int. Ed.* **2013**, *52*, 9275; [(b)]Rodríguez-Fortea, A., Alegret, N., Balch, A. L. and Poblet, J. M., *Nat. Chem.* **2010**, *2*, 955.

[137] Heath, J. R., O'Brien, S. C., Zhang, Q., Liu, Y., Curl, R. F., Tittel, F. K. and Smalley, R. E., *J. Am. Chem. Soc.* **1985**, *107*, 7779.

[138] Zhang, J., Kiselev, B. M., Ye, Y. and Dorn, H. C., in *Endohedral Fullerenes*, World Scientific Publishing Co., **2014**, pp. 401.

[139] [(a)]Lu, X., Bao, L., Akasaka, T. and Nagase, S., *Chem. Commun.* **2014**, *50*, 14701; [(b)]Wang, T. and Wang, C., *Acc. Chem. Res.* **2014**, *47*, 450; [(c)]Popov, A. A., Yang, S. and Dunsch, L., *Chem. Rev.* **2013**, *113*, 5989; [(d)]Lu, X., Akasaka, T. and Nagase, S., *Chem. Commun.* **2011**, *47*, 5942; [(e)]Chaur, M. N., Melin, F., Ortiz, A. L. and Echegoyen, L., *Angew. Chem., Int. Ed.* **2009**, *48*, 7514.

earth metals or either Sm, Eu, Tm or Yb are encapsulated, the cage can accept two electrons from the metal. Meanwhile, those that present other rare earth metals usually transfer three electrons from the metal to the cage. Both types exhibit different characteristics and properties. For example, divalent species use to be obtained in lower yields but they appear in a large variety of isomers for a determined cage whereas trivalent species are obtained in higher yields but appear in a minor number of isomeric forms.[140] A general tendency in mono-EMF is the off-centre location of the metal, making the charge density to be distributed anisotropically, a fact that allows a control in the reactivity.[141]

- *Di-EMF.* Di-EMF ($M_2@C_X$) contain only metal atoms inside and usually appear only with C_s and C_{3v} isomers for C_{82} cages, I_h and D_{5h} isomers for C_{80}, and D_{3h} for C_{78}. In contrast to mono-EMF, the pair of metals tend to move fast and closest to the regions consisting of hexagonal motifs, although for smaller cages this movement is more restricted.

- *Cluster EMF.* Metals can form clusters in form of carbides, nitrides and even oxides. More frequently found carbide clusters in EMF are those containing Sc, Y and Er. In fact, the first reported cluster was $Sc_2C_2@D_{2d}(23)$-C_{84}.[142] Metal nitrides are usually found in the high symmetric $I_h(7)C_{80}$ cage, and in the case of $ScN_3@C_{80}$ is obtained in very high yields, being the third fullerene species in abundance after C_{60} and C_{70}.[143] Larger size metals prefer larger cages as for example Nd or Ce that appear in C_{88} cages. These clusters exhibit a planar rotating conformation. Furthermore, $Sc_3CN@C_{80}$ has been reported as the first example of a cyanide cluster.[144] Moreover, when graphite rods are doped by metal oxides or sulphur containing compounds, cages containing oxide and sulphide clusters inside, respectively, can be found.[145]

---

[140] Lu, X., Slanina, Z., Akasaka, T., Tsuchiya, T., Mizorogi, N. and Nagase, S., *J. Am. Chem. Soc.* **2010**, *132*, 5896.

[141] Inakuma, M. and Shinohara, H., *J. Phys. Chem. B* **2000**, *104*, 7595.

[142] Lu, X., Akasaka, T. and Nagase, S., *Acc. Chem. Res.* **2013**, *46*, 1627.

[143] Stevenson, S., Rice, G., Glass, T., Harich, K., Cromer, F., Jordan, M. R., Craft, J., Hadju, E., Bible, R., Olmstead, M. M., Maitra, K., Fisher, A. J., Balch, A. L. and Dorn, H. C., *Nature* **1999**, *401*, 55.

[144] Wang, T.-S., Feng, L., Wu, J.-Y., Xu, W., Xiang, J.-F., Tan, K., Ma, Y.-H., Zheng, J.-P., Jiang, L., Lu, X., Shu, C.-Y. and Wang, C.-R., *J. Am. Chem. Soc.* **2010**, *132*, 16362.

[145] [(a)]Zhao, P., Yang, T., Guo, Y. J., Dang, J. S., Zhao, X. and Nagase, S., *J. Comput. Chem.* **2014**, *35*, 1657; [(b)]Stevenson, S., Mackey, M. A., Stuart, M. A., Phillips, J. P.,

b) Chemistry of EMF

Because of the large variety of EMF and hardness on the systematic study of EMF chemistry, in the next lines only some of the most relevant examples related to this work will be briefly described. For simplicity, the reactions have been classified in cycloadditions and radical additions. For further information some interesting review articles and book chapters have been reported to the date with extended data about this topic.[133]

i) Influence of the inner metal and cage geometry in the reactivity

Whereas there are some species whose chemistry has been widely explored (i.e. La@C_{82}, La_2@C_{80} or ScN_3@C_{80}), the low production yields of some other EMF made the reactivity still almost unknown. In particular, $C_{2v}C_{82}$ (for mono-EMF) and I_hC_{80} (for di-EMF or nitride clusters) cages are the most studied cases because of their major abundance compared to others. Their geometrical and electronic features need to be investigated in order to understand and control their chemical reactivity.

In the case of the $C_{2v}C_{82}$ cage, 24 non-equivalent C atoms can be identified, forming 16 [5,6] bonds and 19 [6,6] bonds (Figure 2.1-2) of different nature. This fact would suppose an impossible control over the regioselectivity of any reaction. However, the off-centre position of the inner metal under the hexagonal ring defined by C1 and C2 plays an outstanding role in these sense. The π-orbital axis vector (POAV) value in these carbons, a measure of the local strain of fullerene carbons, is higher because of the interaction with the metal, making them more reactive than others. Even more, the three electrons that are transferred from La to the cage are mainly located on the carbons close to the La atom, as corroborated by Mülliken charge density values.[146] Moreover, as result of this transfer, equatorial located C atoms show a major spin density leading to a major tendency to radical additions.[147]

Easterling, M. L., Chancellor, C. J., Olmstead, M. M. and Balch, A. L., *J. Am. Chem. Soc.* **2008**, *130*, 11844.

[146] Maeda, Y., Matsunaga, Y., Wakahara, T., Takahashi, S., Tsuchiya, T., Ishitsuka, M. O., Hasegawa, T., Akasaka, T., Liu, M. T. H., Kokura, K., Horn, E., Yoza, K., Kato, T., Okubo, S., Kobayashi, K., Nagase, S. and Yamamoto, K., *J. Am. Chem. Soc.* **2004**, *126*, 6858.

[147] Takano, Y., Ishitsuka, M. O., Tsuchiya, T., Akasaka, T., Kato, T. and Nagase, S., *Chem. Commun.* **2010**, *46*, 8035.

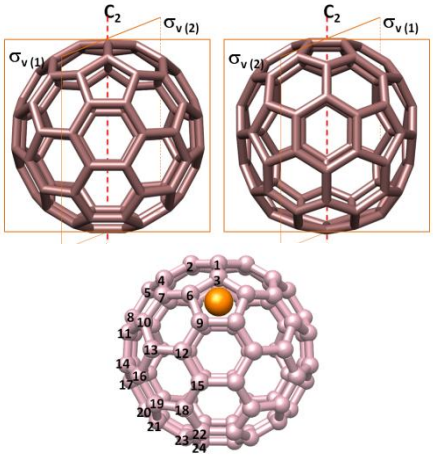

Figure 2.1-2. Different side views for the $C_{2v}C_{82}$ isomer cage indicating the three symmetry elements (upper) and La location in La@C_{2v}-C_{82} (lower). Note that the symmetry group is referred to the empty cage.

The geometrical features analysis on $I_h C_{80}$ reveals only two kinds of C atoms, resulting in only two kind of bonds corresponding to [5,6] and [6,6] junctions. Each La atom can transfer 3 electrons to reach a total of 6, however both are rotating with no preference location in $La_2@I_h$-C_{80} and charge is homogenously distributed along the cage. In this case, the high symmetry is the responsible of the high regioselectivity on this cage and make it ideal for chemical modifications. Other minor isomers as M@C_s-C_{82} (M=Y, La, Ce ,etc)[148] and M@D_{5h}-C_{82} have been reported,[149] but their properties and reactivity have not been investigated in a large extension due to their low production yield and lower stability.

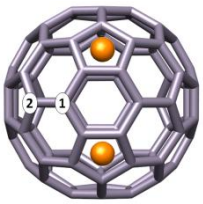

Figure 2.1-3. La@I_h-C_{80} isomer structure indicating the two different carbon atoms.

[148] [(a)]Akasaka, T., Kono, T., Matsunaga, Y., Wakahara, T., Nakahodo, T., Ishitsuka, M. O., Maeda, Y., Tsuchiya, T., Kato, T., Liu, M. T. H., Mizorogi, N., Slanina, Z. and Nagase, S., *J. Phys. Chem. A* **2008**, *112*, 1294; [(b)]Tagmatarchis, N., Taninaka, A. and Shinohara, H., *Chem. Phys. Lett.* **2002**, *355*, 226; [(c)]Akasaka, T., Wakahara, T., Nagase, S., Kobayashi, K., Waelchli, M., Yamamoto, K., Kondo, M., Shirakura, S., Maeda, Y., Kato, T., Kako, M., Nakadaira, Y., Gao, X., Van Caemelbecke, E. and Kadish, K. M., *J. Phys. Chem. B* **2001**, *105*, 2971.

[149] Cai, T., Xu, L., Anderson, M. R., Ge, Z., Zuo, T., Wang, X., Olmstead, M. M., Balch, A. L., Gibson, H. W. and Dorn, H. C., *J. Am. Chem. Soc.* **2006**, *128*, 8581.

ii) Cycloaddition reactions on EMF

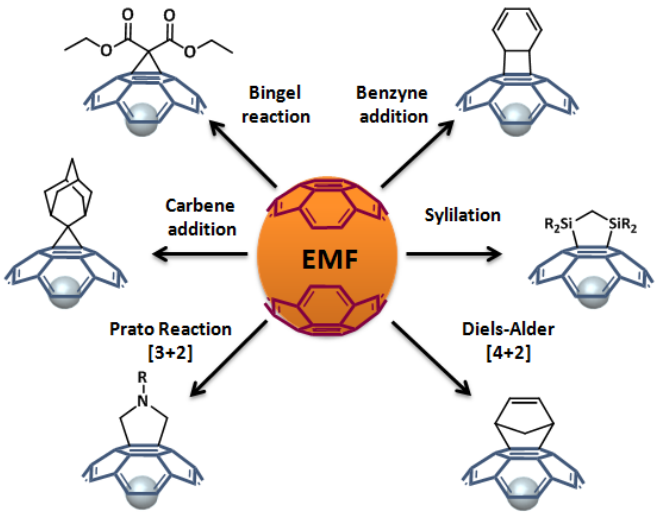

Figure 2.1-4. Some of the most relevant cycloadditions performed on EMF.

The first reaction performed on EMF, was disilylation on La@C_{82}.[150] This methodology has been utilized in mono and di-EMF (M@C_{82}, for M=Y, Ce, Pr, Gd; La_2@C_{80}) and clusters (Sc_3N@C_{80}). Results revealed that mono and di-EMF undergo the reaction thermally and photochemically and clusters only photochemically. Moreover, the anions and cations electrochemically generated of several EMF have been studied and demonstrated a very different behaviour upon disilylation, allowing the tuning of the reactivity. A more important fact is the interruption in the metal movement inside the cage when the adduct is formed, as in the case of La_2@C_{80} (only a little metal hop is allowed).[151]

Diels-Alder reactions on EMF only occur on [5,6] bonds while on empty cages, the reaction tend to occur on [6,6] bonds. When the reaction was performed on Sc_3N@C_{80} using 6,7-dimethoxyisochromon-3-one, the [5,6] adduct was only obtained and the metal cluster position was fixed.[152]Another

[150] Akasaka, T., Kato, T., Kobayashi, K., Nagase, S., Yamamoto, K., Funasaka, H. and Takahashi, T., *Nature* **1995**, *374*, 600.

[151] [(a)]Wakahara, T., Yamada, M., Takahashi, S., Nakahodo, T., Tsuchiya, T., Maeda, Y., Akasaka, T., Kako, M., Yoza, K., Horn, E., Mizorogi, N. and Nagase, S., *Chem. Commun.* **2007**, 2680; [(b)]Wakahara, T., Iiduka, Y., Ikenaga, O., Nakahodo, T., Sakuraba, A., Tsuchiya, T., Maeda, Y., Kako, M., Akasaka, T., Yoza, K., Horn, E., Mizorogi, N. and Nagase, S., *J. Am. Chem. Soc.* **2006**, *128*, 9919.

[152] Iezzi, E. B., Duchamp, J. C., Harich, K., Glass, T. E., Lee, H. M., Olmstead, M. M., Balch, A. L. and Dorn, H. C., *J. Am. Chem. Soc.* **2001**, *124*, 524.

notable example is the cycloaddition of pentamethylcyclopentadiene (Cp*) on La@C_{82}, where only a monoadduct is obtained.[153]

Another strategy extended from C_{60} was the Prato reaction. A remarkable example is the addition to La_2C_{80}, where both [5,6] and [6,6] adducts are obtained, although a different behaviour of the inner metal is appreciated. While La atoms are placed obliquely in the [6,6] adduct, in the [5,6] adduct they freely move.[154] As example of the influence of the metal, the same reaction on $Y_3N@C_{80}$ and $Sc_3N@C_{80}$ was carried out in a regioselectively manner affording only the [6,6] adduct for Y and the [5,6] adduct for Sc. This fact evidences the strong metal-cage interaction. In addition, when the kinetic [6,6]-$Y_3N@C_{80}$ adduct is heated it turns to the [5,6] one, involving a structural modification in the metal cluster, changing its geometry from planar to pyramidal. Further studies with different clusters and addends revealed how larger metal sizes lead to the major stability of [6,6] adducts.[155]

Additionally, carbene additions have been tested on different EMF. An adamantane-aziridine derivative demonstrated a high reactivity and selectivity on M@C_{82}, affording an open cage type derivative as major product.[156] This reaction showed to be very effective in the minor isomer C_s of La@C_{82}.[148] When the same reaction is performed on La_2C_{80}, the [6,6] adduct was observed to set the two La atoms colinear to the *spiro* carbons of the adamantane group.[157]

When bromoethylmalonate is treated with 1,8-diazabicyclo[5.4.0]-undec-7-ene (DBU) a carbanion is produced and added to EMF (Bingel-Hirsch reaction). An unexpected result was obtained when this reaction is tested on La@C_{82}, affording several singly bonded adducts and only one cycloadduct.[158] Calculations revealed that these singly bonded adducts exhibit a close-shell configuration, revealing the tendency of paramagnetic EMF to furnish a diamagnetic product when possible. In the case of metal clusters type EMF,

[153] Maeda, Y., Sato, S., Inada, K., Nikawa, H., Yamada, M., Mizorogi, N., Hasegawa, T., Tsuchiya, T., Akasaka, T., Kato, T., Slanina, Z. and Nagase, S., *Chem. Eur. J.* **2010**, *16*, 2193.

[154] Yamada, M., Wakahara, T., Nakahodo, T., Tsuchiya, T., Maeda, Y., Akasaka, T., Yoza, K., Horn, E., Mizorogi, N. and Nagase, S., *J. Am. Chem. Soc.* **2006**, *128*, 1402.

[155] Cardona, C. M., Kitaygorodskiy, A. and Echegoyen, L., *J. Am. Chem. Soc.* **2005**, *127*, 10448.

[156] Takano, Y., Aoyagi, M., Yamada, M., Nikawa, H., Slanina, Z., Mizorogi, N., Ishitsuka, M. O., Tsuchiya, T., Maeda, Y., Akasaka, T., Kato, T. and Nagase, S., *J. Am. Chem. Soc.* **2009**, *131*, 9340.

[157] Cao, B., Nikawa, H., Nakahodo, T., Tsuchiya, T., Maeda, Y., Akasaka, T., Sawa, H., Slanina, Z., Mizorogi, N. and Nagase, S., *J. Am. Chem. Soc.* **2007**, *130*, 983.

[158] Feng, L., Nakahodo, T., Wakahara, T., Tsuchiya, T., Maeda, Y., Akasaka, T., Kato, T., Horn, E., Yoza, K., Mizorogi, N. and Nagase, S., *J. Am. Chem. Soc.* **2005**, *127*, 17136.

while $Sc_3N@C_{80}$ did not provide any product in the reaction with DBU $Y_3N@C_{80}$ leads to a [6,6] open adduct where one Y atom is fixed at the time the two others are still rotating.[159]

The [2+2] addition of benzyne, generated from anthranilic acid and isoamyl nitrite, was performed on $La@C_{82}$ isolating a product with two benzene groups and NO_2 attached to the cage. The NO_2 group has not only the function of turning the $La@C_{82}$ cage into diamagnetic, but also to direct the addition of benzyne.[160] In a similar approach, the same reaction was applied to $Sc_3N@C_{80}$ obtaining both [5,6] and [6,6] stable products.[161]

iii) Radical additions on EMF

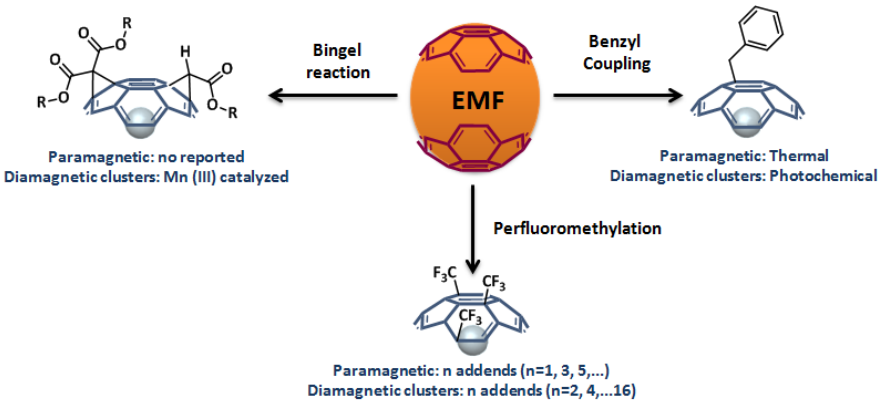

Figure 2.1-5. Some of most relevant radical additions performed on EMF.

The different diamagnetic or paramagnetic character that EMF exhibit strongly influences the nature of the obtained products when they are reacted with radical species. In most cases, paramagnetic EMF afford an odd number of single bonds in order to obtain a close shell configuration. On the other hand, diamagnetic EMF afford an even number of bonds.

The most representative examples of paramagnetic EMF are $M@C_{82}$ (M=La, Ce, Y). The trifluoromethylation by using CF_3 generated *in situ* has been extensively tested on them and, firstly accomplished on $Y@C_{82}$, where five

[159] Lukoyanova, O., Cardona, C. M., Rivera, J., Lugo-Morales, L. Z., Chancellor, C. J., Olmstead, M. M., Rodríguez-Fortea, A., Poblet, J. M., Balch, A. L. and Echegoyen, L., *J. Am. Chem. Soc.* **2007**, *129*, 10423.

[160] Lu, X., Nikawa, H., Tsuchiya, T., Akasaka, T., Toki, M., Sawa, H., Mizorogi, N. and Nagase, S., *Angew. Chem., Int. Ed.* **2010**, *49*, 594.

[161] Li, F.-F., Pinzón, J. R., Mercado, B. Q., Olmstead, M. M., Balch, A. L. and Echegoyen, L., *J. Am. Chem. Soc.* **2011**, *133*, 1563.

CF_3 were attached in order to form a close shell.[162] When Prato conditions were extended to photoirradiation, a benzyl coupling was found, obtaining La@C_s-$C_{82}(CH_2C_6H_5)$, La@C_{2v}-$C_{82}(CH_2C_6H_5)$ or Ce@$C_{2v}C_{82}(CH_2C_6H_5)$. In contrast, when diamagnetic species are submitted to the same conditions only the Prato cycloadducts were obtained.[154] The explanation to this fact is found on the generation of benzyl radicals from toluene, utilized as solvent. The strategy was studied utilizing *o*-DCB as solvent and, surprisingly, $La@C_{82}(CHClC_6H_3Cl_2)$ was obtained. It is interesting to remark that the utilization of radical trapping reagents afford the starting EMF, a methodology that can be utilized for the selective isolation of EMF.[163]

Whereas some diamagnetic cluster-EMF have been reported to undergo radical additions, diamagnetic mono-EMF or divalent mono-EMF are not able to afford it. Trifluoromethylation on $Sc_3N@D_{5h}$-C_{80} and $Sc_3N@I_h$-C_{80} results on derivatives with an even number of CF_3 motifs. The isolated bis-adducts show a 1,4 addition pattern with two Sc atoms oriented to the CF_3 motifs, decreasing the HOMO-LUMO bandgap and generating new redox processes in $Sc_3N@C_{80}(CF_3)_2$.[164] Even new derivatives with a major number of CF_3 anchored units (up to 16 units) have been described.[165]

A radical approach to Bingel-Hirsch reaction was accomplished on $Sc_3N@C_{80}$ and $Lu_3N@C_{80}$ by heating diethyl malonate in the presence of Mn(III).[166] Moreover, dibenzyl adducts on this EMF were synthesized by benzyl bromide irradiation and, again, a 1,4-addition pattern was found with metals oriented again to the radically modified carbons of the cage.[167]

A more appealing example based on a 1,3-dipolar cycloaddition reaction of a suitable functionalized azomethine ylide and Bingel-Hirsch type reactions on metal nitride cluster fullerene $M_3N@C_{80}$ (M=Y, Sc) was the preparation of the

---

[162] Kareev, I. E., Lebedkin, S. F., Bubnov, V. P., Yagubskii, E. B., Ioffe, I. N., Khavrel, P. A., Kuvychko, I. V., Strauss, S. H. and Boltalina, O. V., *Angew. Chem., Int. Ed.* **2005**, *44*, 1846.

[163] Takano, Y., Yomogida, A., Nikawa, H., Yamada, M., Wakahara, T., Tsuchiya, T., Ishitsuka, M. O., Maeda, Y., Akasaka, T., Kato, T., Slanina, Z., Mizorogi, N. and Nagase, S., *J. Am. Chem. Soc.* **2008**, *130*, 16224.

[164] Popov, A. A., Shustova, N. B., Svitova, A. L., Mackey, M. A., Coumbe, C. E., Phillips, J. P., Stevenson, S., Strauss, S. H., Boltalina, O. V. and Dunsch, L., *Chem. Eur. J.* **2010**, *16*, 4721.

[165] Shustova, N. B., Chen, Y.-S., Mackey, M. A., Coumbe, C. E., Phillips, J. P., Stevenson, S., Popov, A. A., Boltalina, O. V. and Strauss, S. H., *J. Am. Chem. Soc.* **2009**, *131*, 17630.

[166] Shu, C., Cai, T., Xu, L., Zuo, T., Reid, J., Harich, K., Dorn, H. C. and Gibson, H. W., *J. Am. Chem. Soc.* **2007**, *129*, 15710.

[167] Shu, C., Slebodnick, C., Xu, L., Champion, H., Fuhrer, T., Cai, T., Reid, J. E., Fu, W., Harich, K., Dorn, H. C. and Gibson, H. W., *J. Am. Chem. Soc.* **2008**, *130*, 17755.

first dyads.[168] Photophysical studies on a ferrocenyl-$Sc_3N@C_{80}$-fulleropyrrolidine dyad revealed the existence of a photoinduced electron transfer process yielding radical ion pairs whose life time resulted to be three times that observed for the analogous C_{60} dyad. Other related dyads involving endohedrals ($Y_3N@C_{80}$, $Sc_3N@C_{80}$, $Ce_2@I_h$-C_{80} or La_2-C_{80}) covalently linked to a variety of electron-donors[103,168,169] and acceptors[170] have also been reported. These experimental findings show the interest of EMF for the stabilization of radical ion species and, therefore, for their further applications in photovoltaic devices.[171]

Figure 2.1-6. Example of dyads containing donor and acceptor motifs combined with EMF.

168 [(a)]Pinzón, J. R., Cardona, C. M., Herranz, M. Á., Plonska-Brzezinska, M. E., Palkar, A., Athans, A. J., Martín, N., Rodríguez-Fortea, A., Poblet, J. M., Bottari, G., Torres, T., Gayathri, S. S., Guldi, D. M. and Echegoyen, L., *Chem. Eur. J.* **2009**, *15*, 864; [(b)]Pinzón, J. R., Plonska-Brzezinska, M. E., Cardona, C. M., Athans, A. J., Gayathri, S. S., Guldi, D. M., Herranz, M. Á., Martín, N., Torres, T. and Echegoyen, L., *Angew. Chem., Int. Ed.* **2008**, *47*, 4173.

169 [(a)]Takano, Y., Obuchi, S., Mizorogi, N., García, R., Herranz, M. Á., Rudolf, M., Wolfrum, S., Guldi, D. M., Martín, N., Nagase, S. and Akasaka, T., *J. Am. Chem. Soc.* **2012**, *134*, 16103; [(b)]Takano, Y., Herranz, M. Á., Martín, N., Radhakrishnan, S. G., Guldi, D. M., Tsuchiya, T., Nagase, S. and Akasaka, T., *J. Am. Chem. Soc.* **2010**, *132*, 8048.

170 Takano, Y., Obuchi, S., Mizorogi, N., García, R., Herranz, M. Á., Rudolf, M., Guldi, D. M., Martín, N., Nagase, S. and Akasaka, T., *J. Am. Chem. Soc.* **2012**, *134*, 19401.

171 Ross, R. B., Cardona, C. M., Guldi, D. M., Sankaranarayanan, S. G., Reese, M. O., Kopidakis, N., Peet, J., Walker, B., Bazan, G. C., Van Keuren, E., Holloway, B. C. and Drees, M., *Nat. Mater.* **2009**, *8*, 208.

2.1.2. NON-METAL ENDOHEDRAL FULLERENES

Molecular surgery: from open cages to the species encapsulation

Considering the limitations on typical production methodologies for endohedral fullerenes (low yields, difficult control on the cage size or the encapsulated metal form), Rubin proposed a different strategy for the preparation of endohedral fullerenes based in organic reactions. This method, coined as *molecular surgery*, consists of 4 steps (Figure 2.1-7): i) hole opening in the cage by organic reactions, ii) hole enlargement to a suitable size that allows the trapping or insertion of the desirable host, iii) insertion of the atom or molecule to encapsulate and iv) closure by different rearrangement reactions avoiding the loss of the encapsulated species. Although several atoms and small molecules have been trapped in C_{60} open cages (He, H_2, H_2O, CO , NH_3, N_2 and CH_4) in the early ages of this methodology, Komatsu and Murata were the first ones in succeeding in the devious closure last step.

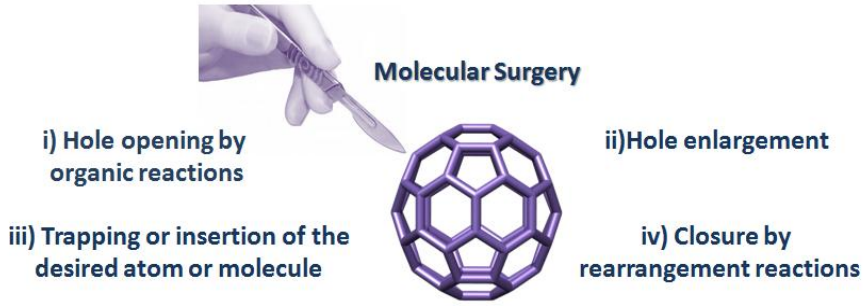

Figure 2.1-7. Steps in the molecular surgery procedure.

The first open cage fullerene was reported by Rubin, holding a 14 members ring built by the addition of a diazidobutadiene and hole expansion by singlet oxygen attack.[172] This 14-member open cage allowed the insertion of H_2 and He at low rates (5 % and 1.5 % respectively).[173] The opening of a wider hole in the cage allowed the encapsulation of bigger molecules. In fact, open cages holding 18, 19 and 20 member rings exhibited higher rates of encapsulations for H_2O (75-83 %),[174] CO (84%),[175] or even NH_3 (50%) (Figure

[172] Schick, G., Jarrosson, T. and Rubin, Y., *Angew. Chem., Int. Ed.* **1999**, *38*, 2360.

[173] Rubin, Y., Jarrosson, T., Wang, G.-W., Bartberger, M. D., Houk, K. N., Schick, G., Saunders, M. and Cross, R. J., *Angew. Chem., Int. Ed.* **2001**, *40*, 1543.

[174] [(a)]Xiao, Z., Yao, J., Yang, D., Wang, F., Huang, S., Gan, L., Jia, Z., Jiang, Z., Yang, X., Zheng, B., Yuan, G., Zhang, S. and Wang, Z., *J. Am. Chem. Soc.* **2007**, *129*, 16149; [(b)]Iwamatsu, S., Uozaki, T., Kobayashi, K., Re, S., Nagase, S. and Murata, S., *J. Am. Chem. Soc.* **2004**, *126*, 2668.

[175] Iwamatsu, S.-i., Stanisky, C. M., Cross, R. J., Saunders, M., Mizorogi, N., Nagase, S. and Murata, S., *Angew. Chem., Int. Ed.* **2006**, *45*, 5337.

2.1-8).[176] The main problem is that these kinds of open cage hosts are almost impossible to be restored to the starting cage by organic chemistry reactions.

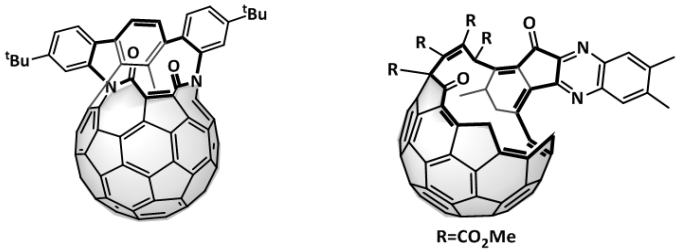

a) 14 members ring
[H_2 and He at low rates]

b) 20 members ring
[H_2O (75-83 %), CO (84%), or even NH_3 (50%)]

Figure 2.1-8. Some examples of open cages able to trap atoms and several small molecules.

The utilization of different aza-derivatives by Murata and Komatsu provided a new strategy for the easy opening and expansion of the cages hole.[177] An initial [4+2] addition followed by the extrusion of N_2 and an intramolecular [4+4] rearrangement to conclude with a final [2+2+2] reordering led an 8 member ring on the cage with a butadiene motif (Figure 2.1-9). This motif is a very important intermediate because the high HOMO coefficients of the molecule are mainly located there, so the reaction with $^1O_2$ mainly takes place in these bonds to yield a 12 members ring by forming different diketones.[178] Even the enlargement by introduction of S or Se was possible to obtain a 13 members ring. The H_2 encapsulation in both species (S and Se) was then accomplished under high pressure (800 atm, 200 ºC for S and 760 atm, 190 ºC for Se) in a 100 % rate. The H_2 ejection was studied revealing to be faster for the Se containing cage. The closure of the cage was observed during MALDI-TOF measurement, noticing a decrease in the signal at m/z= 1068 and an increase in the corresponding C_{60} (m/z =720) and $H_2@C_{60}$ (m/z =722) signals when the laser power is increased.

[176] Whitener, K. E., Frunzi, M., Iwamatsu, S., Murata, S., Cross, R. J. and Saunders, M., *J. Am. Chem. Soc.* **2008**, *130*, 13996.
[177] [(a)]Murata, Y., Kato, N. and Komatsu, K., *J. Org. Chem.* **2001**, *66*, 7235; [(b)]Murata, Y., Murata, M. and Komatsu, K., *J. Org. Chem.* **2001**, *66*, 8187.
[178] [(a)]Murata, Y., Murata, M. and Komatsu, K., *Chem. Eur. J.* **2003**, *9*, 1600; [(b)]Murata, Y. and Komatsu, K., *Chem. Lett.* **2001**, *30*, 896.

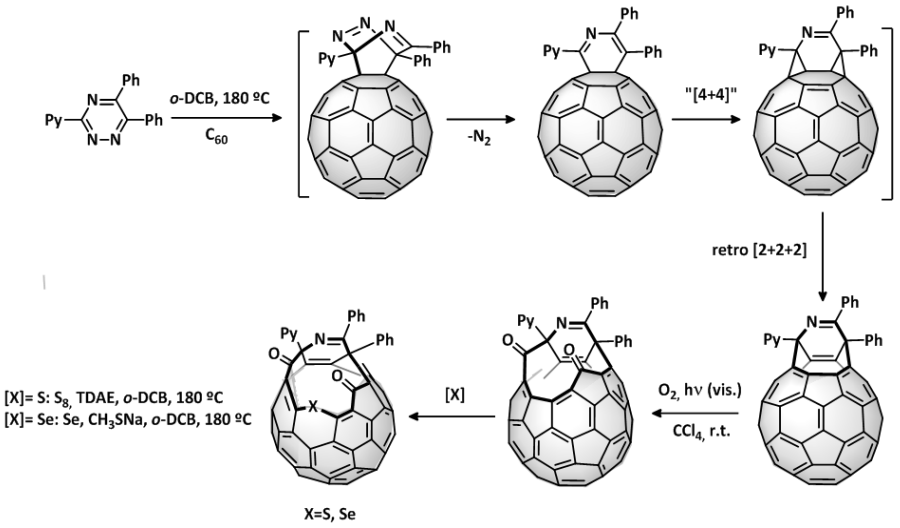

Figure 2.1-9. Molecular surgery reported by Komatsu and Murata.

The next challenge to the H_2 insertion and cage closure was the inclusion of other species. The smallest noble gas, He, was studied and a low encapsulation level was achieved at the time that higher ejection rates were observed on the sulphured form (Figure 2.1-9). That meant that He encapsulation required a smaller hole than that used for H_2. The followed strategy was the carbonyl reduction by using $NaBH_4$ just after submitting it to 650 atm. and 90 ºC during 24h. This reduction drove to the formation of an intramolecular ether that shrink the hole avoiding the He escaping (35 % encapsulation rate).[179]

To attempt the suture of the open cages required the prior S removal by the oxidation of S by MCPBA, yielding a sulfoxide that was withdrawn by irradiation. This 12 members ring intermediate presents a very close distance between carbonyl groups which allowed their coupling under McMurry conditions, restoring a pentagonal ring and conducting to a 8 members ring structure. Although the mechanism for the final closure step is far from being trivial, it was accomplished by simple heating under vacuum conditions, retaining the H_2 inside in a 90 %. (Figure 2.1-10). It could be described as a [2+2+2] cyclization followed by a [4+4] radical cleavage and a final [2+2+2] retrocyclization. The detection of 2-cyanopyridine, diphenylacetylene and an unknown 'Ph_2PyC_3N' may justify the proposed pathway.[180]

[179] Chuang, S.-C., Murata, Y., Murata, M. and Komatsu, K., *Chem. Commun.* **2007**, 1751.
[180] Komatsu, K., Murata, M. and Murata, Y., *Science* **2005**, *307*, 238.

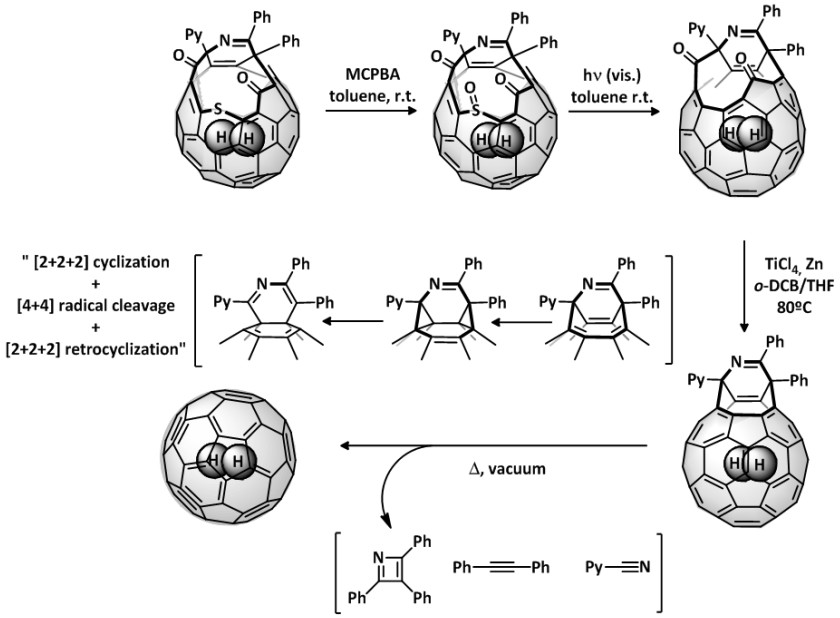

Figure 2.1-10. Closure pathway for the $H_2@C_{60}$ synthesis.

Because of the inert character of the encapsulated H_2, no remarkable influence in the outer cage chemical reactivity has been found[181], in contrast to findings on many EMF. However, it is necessary to remark some interesting modifications on $H_2@C_{60}$ (Bingel, Prato and benzyne additions)[182] as well as the extension of the methodology to the synthesis of $H_2@C_{70}$ and $(H_2)_2@C_{60}$.[183] It was expected that more polar molecules, such as H_2O may exhibit a different character. In this sense, the last reported challenge in molecular surgery, the synthesis of the $H_2O@C_{60}$,[184] open the door to the possibility of finding new clues about it. The synthesis of this singular molecule and its chemical behaviour will be discussed along this chapter.

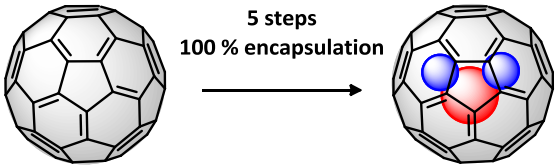

Figure 2.1-11. $H_2O@C_{60}$ synthesis.

[181] Maroto, E. E., Izquierdo, M., Murata, M., Filippone, S., Komatsu, K., Murata, Y. and Martín, N., *Chem. Commun.* **2014**, *50*, 740.
[182] Murata, M., Murata, Y. and Komatsu, K., *J. Am. Chem. Soc.* **2006**, *128*, 8024.
[183] Murata, M., Maeda, S., Morinaka, Y., Murata, Y. and Komatsu, K., *J. Am. Chem. Soc.* **2008**, *130*, 15800.
[184] Kurotobi, K. and Murata, Y., *Science* **2011**, *333*, 613.

2.2. Objectives

2.2. OBJECTIVES

Research on EMF has demonstrated that they constitute a family of novel compounds whose chemical reactivity depends on the encaged atoms or molecules and on the size and geometry of the cage. However, not many reports have tried to unveil the real role of the metal in the control of some reactions and its regioselectivity. In this sense, low symmetry cages are considered less stable and tend to afford complex mixtures of adducts when reactions are performed on them.

On the other hand, molecular surgery nowadays is the main way of preparing fullerenes containing small non-metallic atoms or molecules. Moreover, the few reactions performed on these kind of endohedral fullerenes have not evidenced any influence of the encapsulated specie on the cage reactivity.

In order to shed light in these two specific topics of the endohedral fullerene chemistry, we adress the next objectives during this thesis work:

i) Study on the chemical reactivity of the paramagnetic endohedral metallofullerene La@C_s-C_{82}

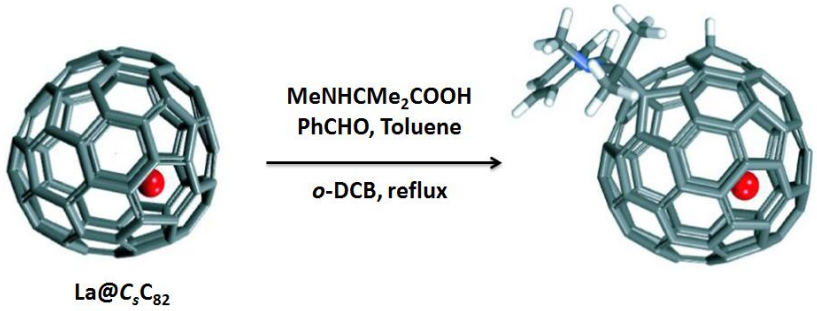

In contrast to the C_{2v} isomer, a much lower number of reports are available for the chemical derivatization of La@C_s-C_{82}, mainly owing to the relatively poor selectivity of La@C_s-C_{82} in addition reactions because of the presence of 44 non-equivalent carbon atoms. In this work we decided to test new reactions in this challenging cage with the following specific goals:

- Studying the scope of 1,3-dipolar cycloaddition reactions of La@C_s-C_{82} with azomethine ylides.
- Isolation and characterization of the obtained Prato adducts.
- With the aid of theoretical calculations, identify the more feasible positions for the cycloaddition reaction and study the unprecedented H addition observed.
- Investigate the electronic properties of the obtained adducts by a combination of UV-vis spectroscopy and electrochemical methods.

ii) Synthesis of enantiomerically enriched endohedral derivatives. Enantiospecific cis/trans isomerization

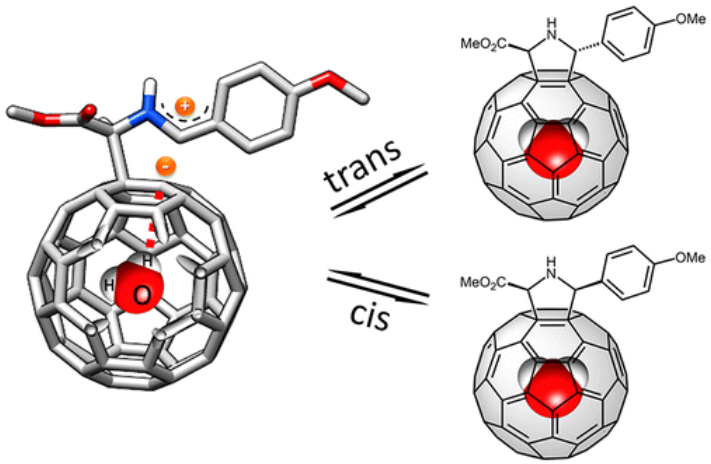

Endohedral fullerenes are a singular scenario to test stereoselective methods and explore the contributions of the entrapped species. In this sense, the proposed goals in this topic are the following:

- Synthesis of enantiomerically enriched pyrrolidino[60]fullerenes and pyrrolidino[70]fullerenes considering chiral metal-ligands in 1,3-dipolar cycloadditions of N-metalated azomethine ylides.
- Synthesis of the endohedral fullerene $H_2O@C_{60}$ by molecular surgery.
- Stereodivergent synthesis of $H_2O@C_{60}$ stereoisomers.
- Investigation of the *cis/trans* isomerization reaction from enantiomerically enriched fullerene derivatives (C_{60}, C_{70} and $H_2O@C_{60}$).
- Study of the contribution of the inner water molecule in the *cis/trans* isomerization by kinetic and theoretical investigation.

2.3. Results and discussion

2.3. RESULTS AND DISCUSSION

2.3.1. UNPRECEDENTED HYDROGEN ADDITION IN THE 1,3-DIPOLAR CYCLOADDITION REACTION ON La@C_s-C_{82}

Although La@C_{2v}-C_{82} is one of the most investigated EMFs and is considered a prototype of paramagnetic EMF, another isomer (La@C_s-C_{82}) has been comparatively less studied and is the molecule used in the present study. 1,3-dipolar cycloaddition of suitably functionalized azomethine ylides, also known as Prato reaction was performed on this almost unexplored isomer,[148] finding an unprecedented H-addition on the cage. Considering the 44 non-equivalent carbon atoms, the results disclosed a remarkable selectivity under certain conditions (Figure 2.3-1). This work was carried out in collaboration with the group of Prof. Akasaka in the Tsukuba Life Science Center for Advanced Research at Tsukuba University, where a short stay was accomplished and served as the beginning of the project.

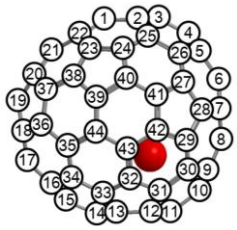

Figure 2.3-1. La@C_s-C_{82} structure. View from its only symmetry plane indicating its 44 non-equivalent carbon atoms.

a) Synthesis and isolation of the La@C_s-C_{82} Prato adducts

Firstly, the 1,3-dipolar cycloaddition reaction on La@C_s-C_{82} (denoted as La@C_{82} hereafter for simplicity) was conducted using an azomethine ylide as 1,3-dipole utilizing *o*-DCB as solvent (Figure 2.3-2).

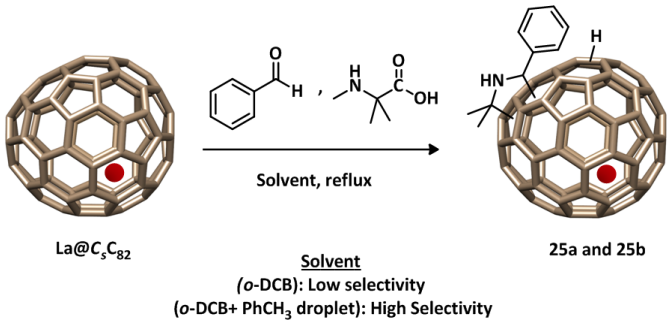

Figure 2.3-2. 1,3-Dipolar cycloaddition on La@C_s-C_{82}.

After 15 minutes of reaction, the crude reaction HPLC profiles showed different peaks with high consumption of the starting La@C_{82} (Figure 2.3-3,

upper). The appearance of several shoulder peaks indicated that the selectivity of the addition reaction to the fullerene was quite low under these conditions. The reaction was tried again but adding a toluene droplet into the *o*-DCB solution before refluxing. The selectivity was drastically improved as confirmed by the HPLC profiles (Figure 2.3.3, lower). After refluxing for one hour, a 50 % of the starting fullerene was consumed and two products were dominantly formed.

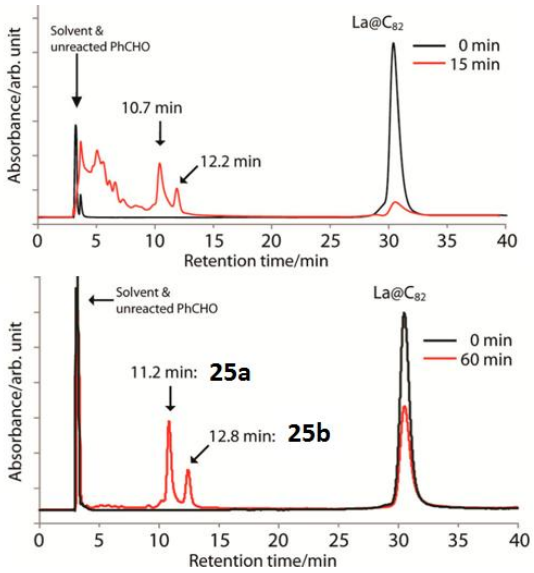

Figure 2.3-3. HPLC profile exhibiting differences in regioselectivity for each reaction solvent conditions. *o*-DCB (upper) and *o*-DCB + toluene droplet (lower) as solvent. Analysis conditions: Buckyprep column (ϕ 4.6 × 250 mm); eluent, toluene; flow rate, 1.0 mL/min; wavelength, 330 nm; temperature, 40 ^{o}C.

The two products were successfully isolated from the non-reacted starting materials and by-products by using multi-step high performance liquid chromatography (HPLC). Conversion yields for main product (**25a**) and for the minor product (**25b**) were 45 % and 20 %, respectively, based on the consumed La@C_{82}.

b) Characterization of the main product

The main product **25a** was characterized by Matrix Assisted Laser Desorption Ionization coupled to Time-of-Flight analyzer (MALDI-TOF). Its mass spectrum showed a molecular ion peak at 1285 *m/z* and a fragment peak at 1123 *m/z* which came from pristine La@C_{82} formed by the loss of the addend during laser desorption (Figure 2.3-4). A detailed analysis on peaks between 1284 to 1289 *m/z* revealed a different isotopic distribution pattern on the expected Prato adduct. This result suggests that **25a** is a 1,3-dipolar cycloadduct which is accompanied by an additional hydrogen atom, and the small peak at 1284 *m/z*

would be originated from the loss of the hydrogen atom of **25a**. Furthermore, the electron spin resonance (ESR) resulted on a close-shell configuration in contrast with the starting EMF and the previously reported Prato adducts for La@C_{2v}-C_{82},[185] which is in line with the proposed unexpected addition of H to the cage.

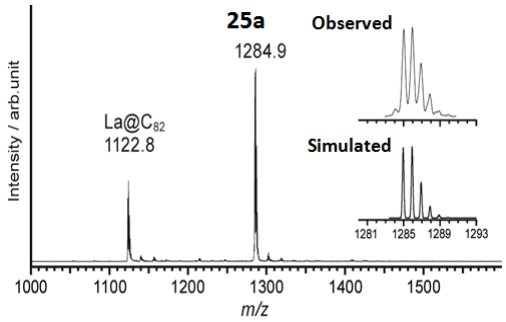

Figure 2.3-4. MALDI-TOF analysis showing the results for the just isolated **25a** product.

Several 1D and 2D NMR analyses were performed on **25a**. The ^{1}H and ^{13}C-NMR spectra, respectively, demonstrated characteristic signals of the pyrrolidine ring, phenyl group and the hydrogen atom (Figure 2.3-5 and Experimental Section). Final assignments were confirmed by DEPT 135, HSQC and HMBC (Figure 2.3-6 and Experimental Section), certifying that a hydrogen atom was attached on the cage. The ^{1}H-NMR signal of the hydrogen atom at 3.19 ppm shows the clear correlation with carbon atoms of the fullerene cage both in HSQC and HMBC.

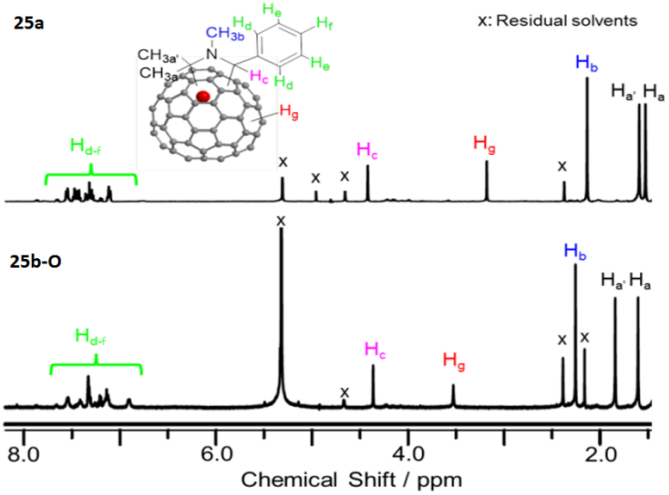

Figure 2.3-5. ^{1}H-NMR spectra of **25a** and **25b**-O in CS_2/CD_2Cl_2 = 3/1 (v/v).

[185] Chai, Y., Guo, T., Jin, C., Haufler, R. E., Chibante, L. P. F., Fure, J., Wang, L., Alford, J. M. and Smalley, R. E., *J. Phys. Chem.* **1991**, *95*, 7564.

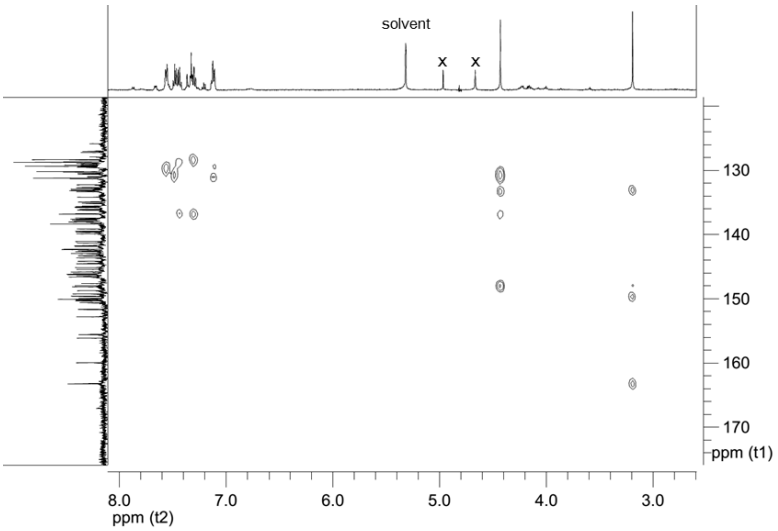

Figure 2.3-6. HMBC spectrum of **25a** showing the correlation of the H at 3.19 ppm to the C atoms on the cage CS_2/CD_2Cl_2 = 3/1 (v/v).

c) Characterization of the minor product

Just after the isolation by HPLC, **25b** mainly showed a molecular ion peak at 1285 *m/z* and a fragment peak at 1123 *m/z* in MALDI-TOF mass measurement as well as **25a** (Figure 2.3-7, upper). However, after a few minutes from the isolation under ambient conditions, the minor product showed a new signal at 1301 *m/z* attributed to an oxidized **25b** (**25b-O**) (Figure 2.3-7, lower).

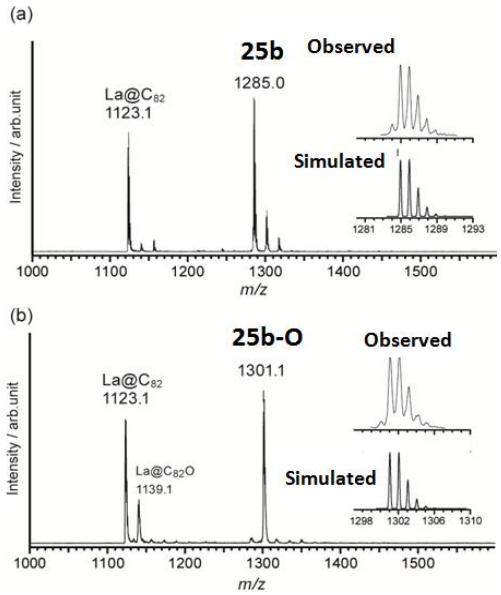

Figure 2.3-7. MALDI-TOF analysis showing the results for the just isolated **25b** product (a) and a few minutes later (b).

Additionally, HPLC analyses were performed on **25b-O** resulting in an extended elution time from 12.8 min. to 13.2 min. as consequence of the oxidation process. In contrast, in absence of light, product **25a** exhibits a pronounced stability with no significant changes in HPLC analysis after days. This significant different stability in **25a** and **25b** is still not completely clear. The different direction of the addend, in particular the phenyl ring close to the attached H in **25a** and in the opposite location in **25b**, might be an explanation as discussed later by DFT calculations.

Because of the instability of **25b**, characterization of **25b-O** provided enough structural information. **25b-O** has also a closed shell structure as well as **25a** and, therefore, NMR measurements were performed. The ^{1}H and ^{13}C-NMR spectra were distinguishable from those of **25a**, and all characteristic peaks of the addend and the hydrogen atom were discernible. Meanwhile, the HSQC spectra of **25b-O** did not show any correlation between the hydrogen atom and the carbon atoms of the C_{82} cage, suggesting that the oxidized position is the carbon where the H atom is attached, resulting in a hydroxyl group (Annexe 1, Figure A1-18). When **25b-O** was mixed with D_2O, the signal at 3.4 ppm disappeared, thus corroborating the OH group hypothesis (Figure 2.3-8).

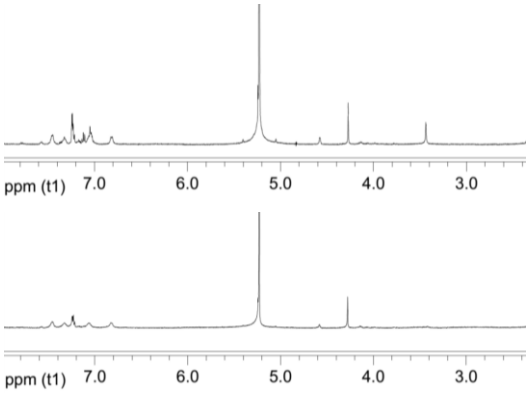

Figure 2.3-8. ^{1}H-NMR spectra of **25b-O** before (upper) and after (bottom) mixing of the sample solution with D_2O, in CS_2/CD_2Cl_2 = 3/1 (v/v). Disappearance of the signal at 3.4 ppm, which is attributed to the hydrogen atom, after mixing strongly with D_2O, suggests that the hydrogen atom is part of a hydroxyl group.

d) Discussion on the reaction mechanism and molecular structures of the Prato adducts

To this point, results suggest that in the absence of toluene the reaction affords a vast number of regioisomers, poly-adducts and a variety of oxidized compounds involving a rapid high consumption of the starting material and low regioselectivity. Furthermore, the origin of the H, the role of toluene and the two different pathways in the product formation (Figure 2.3-9) were not totally understood and complementary experiments were necessary.

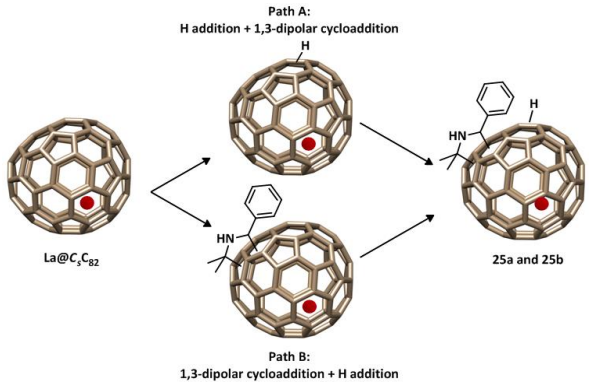

Figure 2.3-9. Two possible pathways in the products formation. Path A (H addition prior to 1,3-dipolar cycloaddition) and path B (1,3-dipolar cycloaddition prior to H addition).

Initially, the H was considered to derive from H_2O released from the azomethine ylide formation. To get rid of the first possibility, the 1,3-dipolar cycloaddition reaction was performed in an *o*-DCB solution containing D_2O and a droplet of toluene. No evidence of deuterium addition on the cage was found, discarding the possibility of H_2O as source of the H atom. To explore the possibility of toluene as H source, the reactivity of La@C_{82} was examined by heating La@C_{82} with a droplet of toluene in carefully degassed *o*-DCB. After an hour of reaction a very small portion was found to react resulting in an unknown product (HPLC t_R: 15 min, Figure 2.3-10, left), what indicates that cycloaddition should be prior to H addition. Moreover, MALDI-TOF analysis on this reaction mixture showed a peak at 1156 *m/z*, attributed to La@$C_{82}HO_2$, with a small fragment peak at 1155 *m/z* which stems from the loss of the hydrogen atom (Figure 2.3-10, right). The formation of La@$C_{82}HO_2$ implies that La@C_{82}H may be formed under these reaction conditions and readily oxidized under ambient atmosphere, as previously reported for La@C_{2v}-C_{82}.

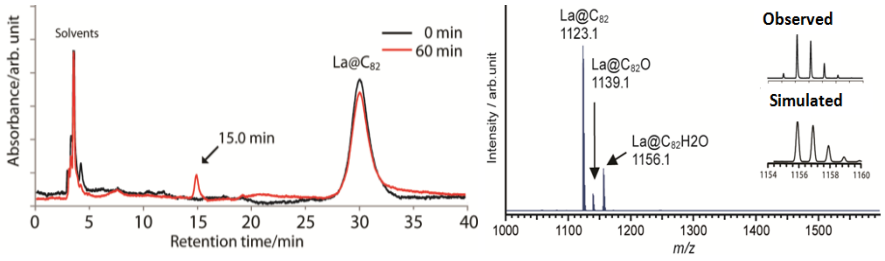

Figure 2.3-10. HPLC profiles of the thermal reaction of La@C_{82} with a droplet of toluene in *o*-DCB. Conditions: Buckyprep column (ϕ 4.6 × 250 mm); eluent, toluene; flow rate, 1.0 mL/min; wavelength, 330 nm; temp., 40 °C (Left). MALDI-TOF mass spectrum of the reaction mixture result of the thermal reaction of La@C_{82} with a droplet of toluene, in negative linear mode using 1,1,4,4-tetraphenyl-1,3-butadiene as a matrix (Right).

The similar features in **25a** and **25b-O** absorption spectra revealed an identical addition pattern in both products, so they can be considered as site-isomers (Annexe 1, Figure A1-21).[186] DFT calculations give us sufficient criteria for the prediction of the addition sites of the substituents according to two different criteria.[187]

i) LUMO distribution on the dipolarophile surface: It is well known in this kind of reaction that the dipolarophile LUMO plays an important role in diamagnetic EMF,[188] and when a carbon atom exhibits high positive charge and high POAV[189] value simultaneously, and the adjacent carbon atom shows a relatively negative charge, those use to be the most feasible candidate site for the cycloaddition, as it is fulfilled in C20-C21 for La@C_{82} (view Table 2.3-1 and 2.3-2).[169b]

ii) *Radical character of the azomethine ylide*: It has been reported that the intrinsic radical character of azomethine ylides may play an important role in 1,3-dipolar cycloadditions on paramagnetic endohedral metallofullerenes.[190] In this case, the feasible addition site contains the carbon atom which has the largest POAV and spin density, in addition to an adjacent carbon atom with a relatively large negative charge, and it is fulfilled in C22-C23. (view Table 2.3-1 and 2.3-3).

On the basis of the first criterion, the bond between C20-C21 potentially affords four regioisomers, each one having two conformers (Figure 2.3-11). The relative formation energies were calculated for the possible eight optimized structures. It is found in all cases that the more stable structure has the methyl group connected to the nitrogen atom, located far away from the phenyl group. Among the most stable four structures, *A1* and *B1* demonstrate better stabilities and may be considered as the intermediates for **25b** and **25a**, respectively, based on the relative formation energies. However, a remarkable difference was not found in the charge density, spin density or POAV values among these possible intermediates and the starting La@C_{82} (Table 2.3-3). Therefore, the subsequent selective addition of H atom cannot be rationalized by this first criterion.

---

[186] Maroto, E. E., de Cózar, A., Filippone, S., Martín-Domenech, Á., Suarez, M., Cossío, F. P. and Martín, N., *Angew. Chem., Int. Ed.* **2011**, *50*, 6060.
[187] Zhao, Y. and Truhlar, D., *Theor. Chem. Acc.* **2008**, *120*, 215.
[188] Coldham, I. and Hufton, R., *Chem. Rev.* **2005**, *105*, 2765.
[189] Haddon, R. C., *Science* **1993**, *261*, 1545.
[190] [(a)]Tsuchiya, T., Rudolf, M., Wolfrum, S., Radhakrishnan, S. G., Aoyama, R., Yokosawa, Y., Oshima, A., Akasaka, T., Nagase, S. and Guldi, D. M., *Chem. Eur. J.* **2013**, *19*, 558; [(b)]Braida, B., Walter, C., Engels, B. and Hiberty, P. C., *J. Am. Chem. Soc.* **2010**, *132*, 7631.

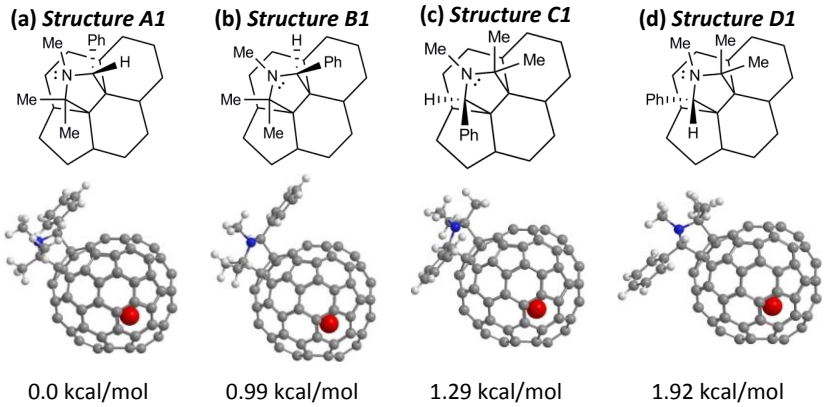

Figure 2.3-11. Four possible structures of the site-isomer intermediate based on the LUMO distribution of dipolarophile (C20-C21). Optimized at the M06-2X/3-21G [C, H, N], SDD [La] level of theory. The numbers in kcal/mol indicate their M06-2X/6-31G* [C, H, N], SDD [La] relative energies of formation.

The second criterion considering the radical reactivity suggests the feasibility of C22-C23 as the addition site. Moreover, it is supported by the ROESY measurements on **25a** which demonstrate a correlation between the hydrogen atom in the pyrrolidine ring and the hydrogen atom on the fullerene cage (Annexe 1, Figure 2.1-20). This result indicates the fact that the pyrrolidine moiety and the hydrogen atom of **25a** must locate within a distance for nuclear Overhauser effect, that is usually within 5 Å, being consistent in the addition position of C22-C23. Judging from the optimized structures by the DFT calculations , firstly, the stable conformation of the pyrrolidine ring is the same to those in the adducts based on C20-C21. The relative energies suggest that the most feasible structures are structures *A'1* and *B'1*.

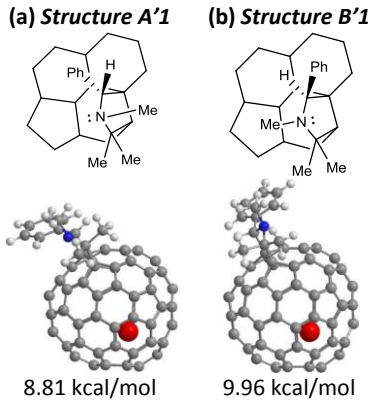

Figure 2.3-12. Two possible structures of the intermediate based on the second criterion in which the radical character of the azomethine ylide is important. Site addition on C22-C23. Optimized at the M06-2X/3-21G [C, H, N], SDD [La] level of theory. The numbers in kcal/mol indicate their M06-2X/6-31G* [C, H, N], SDD [La] relative energies of formation in comparison with *Structure A1* in Figure 2.3-11.

Although these energies are higher than those based on C20-C21, it is safe to conclude that the relative energies are not significant enough for the determination of the structure because the second criterion is based on the radical reactivity, in which kinetic products are favourable rather than the thermodynamic products. In addition, in sharp contrast to structures *A1* and *B1*, *structures A'1* and *B'1* explain the selectivity of the following hydrogen addition.

Regarding the addition position of the hydrogen atom, the carbon atom C3 is the best candidate because it has the highest spin density and POAV values both in pristine La@C_{82} and the intermediates (Table 2.3-3 and 2.3-4). Moreover, the spin density is remarkably increased in the intermediates (0.12-0.14) relative to pristine fullerene (0.09), rationalizing the site-selective addition of the hydrogen atom. It has previously been reported that radical addition on La@C_{82} occurs on the carbon atom having the highest spin density and POAV values. Taking all together, the molecular structures of **25a** and **25b** are concluded to be structures *A'1*+H_{C3} and B'1+H_{C3}, respectively, as it is shown in Figure 2.3-13. This result is in good agreement with the experimental findings where the two adducts were obtained in a selective way as a result of the addition reaction by an asymmetric azomethine ylide and in different yields.

Carbon numb.	Charge density	POAV value	Carbon numb.	Charge density	POAV value	Carbon numb.	Charge density	POAV value
C1	0.006	9.78	**C16**	0.008	11.11	**C31**	-0.091	10.54
C2	0.001	10.59	**C17**	-0.006	11.69	**C32**	-0.039	8.58
C3	-0.006	11.14	**C18**	-0.004	11.44	**C33**	-0.013	8.32
C4	-0.014	10.67	**C19**	-0.003	11.61	**C34**	-0.037	7.76
C5	0.006	10.73	**C20**	0.009	10.90	**C35**	-0.024	7.44
C6	-0.005	10.62	**C21**	-0.015	7.35	**C36**	0.008	10.96
C7	-0.055	8.65	**C22**	0.009	7.47	**C37**	-0.007	10.82
C8	-0.061	8.75	**C23**	0.009	11.23	**C38**	-0.010	10.62
C9	-0.106	10.98	**C24**	-0.001	10.52	**C39**	0.007	11.11
C10	-0.138	11.75	**C25**	-0.028	8.44	**C40**	-0.007	11.12
C11	-0.148	13.13	**C26**	-0.037	8.35	**C41**	-0.013	10.97
C12	-0.156	10.51	**C27**	0.007	11.21	**C42**	0.012	11.03
C13	-0.086	10.19	**C28**	-0.003	10.61	**C43**	-0.047	7.82
C14	-0.084	9.09	**C29**	-0.024	9.65	**C44**	-0.027	7.36
C15	-0.004	10.25	**C30**	-0.153	9.33			

Table 2.3-1. Mulliken charge densities and the POAV values in La@C_s-C_{82} calculated at the M06-2X/3-21G [C, H, N], SDD [La] level of theory.

Carbon number	Charge density	POAV value
C42	0.012	11.03
C23	0.009	11.23
C20	0.009	10.90
C16	0.008	11.11
C27	0.007	11.21

Table 2.3-2. The five highest Mulliken charge densities, the five highest charge densities and their POAV values in La@C_s-C_{82} calculated at the M06-2X/3-21G [C, H, N], SDD [La] level of theory.

La@C_s-C_{82}					Structure A1	Structure B1
Carbon number	**POAV value**	**Spin density**	**Carbon number**	**POAV value**	**Spin density**	**Spin density**
C3	11.14	0.090	**C3**	11.03	0.095	0.091
C23	11.23	0.068	**C23**	11.57	0.070	0.072
C40	11.12	0.061	**C23'**	11.12	0.069	0.067
C1	9.78	0.059	**C1**	9.19	0.066	0.063
C29	9.65	0.053	**C1'**	10.09	0.062	0.062

Table 2.3-3 The five highest Mulliken atomic spin density values and their POAV values in pristine La@C_s-C_{82} and intermediates calculated at the M06-2X/3-21G [C, H, N], SDD [La] level of theory considering first criteria (dipolarophile LUMO) For the intermediates, carbon numbers with prime indicate each another unequivalent carbon atom which originate from a set of two equivalent carbons because of the symmetrical change in the fullerene cage from C_s to C_1.

		Structure A'1	Structure B'1
Carbon number	**POAV value**	**Spin density**	**Spin density**
C3	10.82	0.135	0.123
C5	10.58	0.105	0.099
C6	10.54	0.068	0.072
C23'	11.32	0.065	0.059
C25	8.80	0.048	0.044

Table 2.3-4 The five highest Mulliken atomic spin density values and their POAV values in pristine La@C_s-C_{82} and intermediates calculated at the M06-2X/3-21G [C, H, N], SDD [La] level of theory. considering the second criteria (radical character). For the intermediates, carbon numbers with prime indicate each another unequivalent carbon atom which originate from a set of two equivalent carbons because of the symmetrical change in the fullerene cage from C_s to C_1.

Carbon number	Charge density
C22	-0.030
C24	-0.001
C38	-0.001

Table 2.3-5. The Mulliken charge densities of the adjacent carbon atoms of C23 in La@C_s-C_{82} calculated at the M06-2X/3-21G [C, H, N], SDD [La] level of theory.

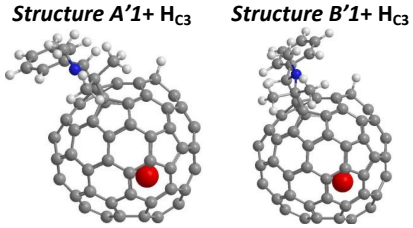

Figure 2.3-13. The two most feasible structures for **25a** and **25b** optimized at the M06-2X/3-21G[C, H, N], SDD [La] level of theory. The numbers in kcal/mol indicate their M06-2X/6-31G* [C, H, N], SDD [La] relative energies of formation.

e) Optoelectronic properties of 25a and 25b-O

UV-vis-NIR absorption spectra of **25a** and **25b-O** revealed changes in the electronic properties of the fullerene cage from pristine La@C_{82} (Annexe 1,Figure A1-21). In both compounds, the absorbance onsets show remarkable hypsochromic shifts from *ca.* 2000 nm in pristine La@C_{82} to 1070 nm, which is attributed to the loss of open-shell electronic structure and the formation of closed-shell structures. Electrochemical measurements of **25a** and **25b-O** were performed by cyclic voltammetry (CV) and differential pulse voltammetry (DPV) (Figure 2.3-14). The redox potentials were determined by DPV (Table 2.3-6). The first reduction and the first and second oxidation potentials are comparable between **25a** and **25b-O**. These experimental findings are consistent with the absorption spectra, which demonstrate the similar electronic properties in both compounds.

	$E_{ox}^{(2)}$	$E_{ox}^{(1)}$	$E_{red}^{(1)}$	$E_{red}^{(2)}$
25a	0.80[a]	-0.02[a]	-1.39	
25b-O	0.80[a]	-0.03[a]	-1.40	
La@C_s-C_{80}[b]	1.08	-0.07	-0.47	-1.40

Table 2.3-6. Redox potentials. Values are given in volts relative to a $Fc^{0/+}$ redox couple and were obtained from DPVs. Conditions: working electrode and counter electrode, platinum wires; reference electrode, SCE; supporting electrolyte, 0.1 M $TBAPF_6$ in *o*-DCB. CV: scan rate, 50 mV s^{-1}. DPV: pulse amplitude, 50 mV; scan rate, 20 mV s^{-1}. [a] Irreversible. [b] Data from ref.[191]

[191] Kikuchi, K., Nakao, Y., Suzuki, S., Achiba, Y., Suzuki, T. and Maruyama, Y., *J. Am. Chem. Soc.* **1994**, *116*, 9367.

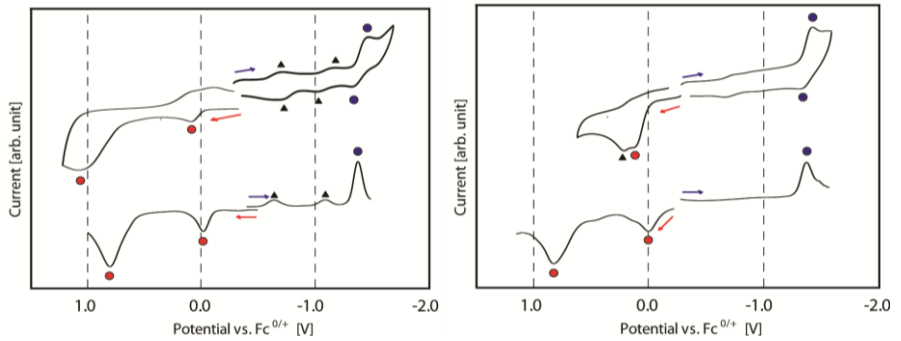

Figure 2.3-14. CV (upper) and DPV (lower) of **25a** (left) and **25b-O** (right) measured in 0.1 M $TBAPF_6$ in *o*-dichlorobenzene. Circle and triangle symbols indicate redox peaks and the peaks from the compound generated during measurements, respectively.

Meanwhile, **25a** and **25b-O** revealed distinguishable electrochemical stability in *o*-DCB. **25a** showed two small peaks at -0.35 and -0.80 V vs. Fc/Fc^+ couple when a freshly prepared sample was measured. Then two peaks were found to become larger after scanning a more positive region than the first oxidation peak (0.27 V), which was confirmed by multiple scan in CV (Figure 2.3-15). **25b-O** demonstrated a similar behavior after the scan of the first oxidation peak. In addition, a new peak, which was not clearly detected in DPV but in CV measurements, appeared in the anodic region close to the oxidation peak during the scanning. These results suggest that the first oxidation step is attributable to the oxidation on the hydrogen atom, which leads to an irreversible reaction of decomposition of **25a** and **25b-O** afforded new products which possess similar reduction potentials to those of paramagnetic pristine $La@C_{82}$. Moreover, it was revealed that the carbon bearing the hydrogen atom of **25a** and **25b-O** is still reactive towards oxidation reactions.

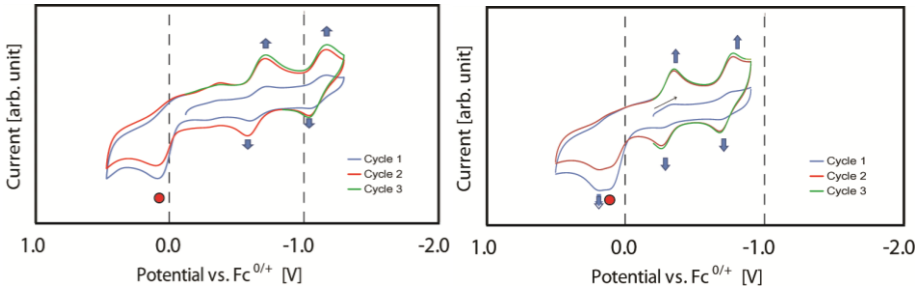

Figure 2.3-15. Cyclic voltammograms of **25a** (left) and **25b**-O (right) in multiple scans between the first oxidation peak and the second peak of the appeared compound measured in 0.1 M $TBAPF_6$ in *o*-DCB. Circle symbol indicates the original oxidation peak.

2.3.2. STUDY OF THE ENCAPSULATED H_2O MOLECULE IN THE *CIS/TRANS* ISOMERIZATION PROCCESS OF PYRROLIDINO[3,4:1,2][60]FULLERENES

During the last years, with the aim to investigate the almost unexplored chirality in fullerenes, our research group has utilized different cages as benchmark for testing several catalyzed cycloadditions. In this sense, we have contributed to develope an outstanding methodology for the synthesis of chiral pyrrolidinofullerenes by metal catalyzed enantioselective 1,3-dipolar cycloaddition of *N*-metalated azomethine ylides, being able to control the stereochemical result by means of the use of different metals (Ag or Cu) and chiral ligands.[192] Moreover this process was found to be reversible and quasi-enantiomeric.[193] This methodology has also been successfully extended to higher fullerenes and EMF (C_{70} and La@C_{72}($C_6H_3Cl_2$).[186,194]

We went a step further reporting organocatalytic methods for the synthesis of chiral [60]fullerene derivatives by a convergent phosphine-catalyzed [3+2] cycloaddition of allenoates onto C_{60}.[195] Recently, both metal and organocatalytic methodologies have been applied for the enantioselective [3+2] cycloaddition of münchnones onto fullerenes and olefins.[196]

Considering this recent outstanding progress of in the development of a high efficient methodology to prepare enantiopure pyrrolidinofullerenes,[186,197] in this work an enantiospecific selective *cis/trans* isomerization process of these derivatives has been found. A systematic study of the process at different levels (Figure 2.3-16) has been accomplished, which has been complemented with further DFT calculations that support the experimental results.

[192] Filippone, S., Maroto, E. E., Martin-Domenech, A., Suarez, M. and Martin, N., *Nat Chem* **2009**, *1*, 578.
[193] Maroto, E. E., Filippone, S., Suárez, M., Martínez-Álvarez, R., de Cózar, A., Cossío, F. P. and Martín, N., *J. Am. Chem. Soc.* **2013**, *136*, 705.
[194] Sawai, K., Takano, Y., Izquierdo, M., Filippone, S., Martín, N., Slanina, Z., Mizorogi, N., Waelchli, M., Tsuchiya, T., Akasaka, T. and Nagase, S., *J. Am. Chem. Soc.* **2011**, *133*, 17746.
[195] Marco-Martínez, J., Marcos, V., Reboredo, S., Filippone, S. and Martín, N., *Angew. Chem., Int. Ed.* **2013**, *52*, 5115.
[196] Marco-Martínez, J., Reboredo, S., Izquierdo, M., Marcos, V., López, J. L., Filippone, S. and Martín, N., *J. Am. Chem. Soc.* **2014**, *136*, 2897.
[197] Maroto, E. E., Filippone, S., Martín-Domenech, A., Suarez, M. and Martín, N., *J. Am. Chem. Soc.* **2012**, *134*, 12936.

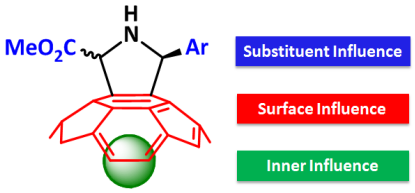

Figure 2.3-16. "Three levels" approach that may influence the stereochemical result of the *cis*/*trans* isomerization in pyrrolidinofullerenes.

Firstly, a series of enantiopure pyrrolidino[60]fullerenes with different aromatic groups were synthesized under the previously optimized catalytic systems and conditions reported, affording derivatives with an optical purity about 80-99 % (Figure 2.3-17).

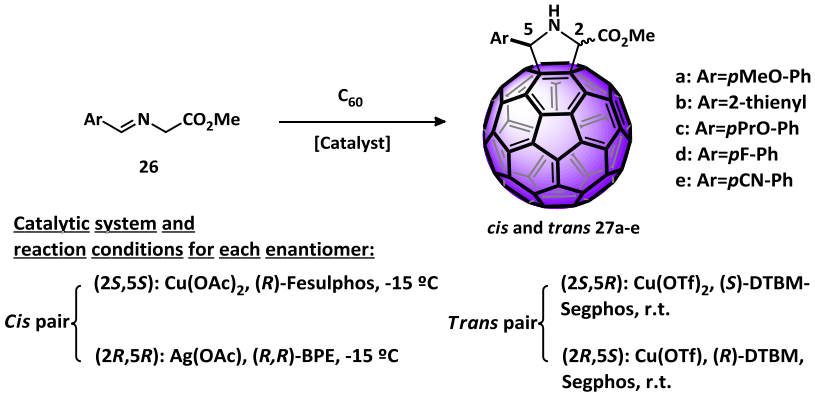

Figure 2.3-17. Conditions for preparing optically pure [60]-pyrrolidinofullerenes.

a) Screening and optimal conditions for the isomerization

Next, the conditions for the *cis/trans* isomerization study were optimized (Table 2.3-7). The (2*S*,5*S*)-*cis*-pyrrolidino[60]fullerenes **27a** was utilized as benchmark, except for entry 12-14. The diastereomers ratio was determined by ^{1}H-NMR spectroscopy of the crude whereas the enantiomer excess was determined by chiral HPLC.

According to the obtained results, it can be stated that (2*S*,5*S*)-*cis*-**27a** isomerizes to the corresponding (2*S*,5*R*)-*trans*-**27a** to reach an equilibrium where the *cis* adduct is the major product in a 7:3 ratio, a surprising result if we consider that it is the kinetically control product. The obtained *trans* product exhibited a configuration retention in C2 while C5 changes its configuration. Side processes of racemization and retrocycloaddition may compete at temperatures over 35 ºC. As a final conclusion of these experiment, best solvent conditions found were 1-Cl-Np:acetonitrile and toluene:acetonitrile (Table 2.3-7, entries 10-11). The experiments were extended to the related enantiomer (2*R*,5*R*)-cis-**27a** (Table 2.3-7, entry 12) and very similar values and retention in the configuration of C2 was observed

again. When (2*S*,5*S*)-*cis*-**27a** was used in a higher optical purity (99 %) the same result is obtained (Table 2.3-7, entry 13) affording both diastereomers with a 97 % enantiomeric excess. Going further, to check the reversibility of the isomerization, (2*S*,5*R*)-*trans*-**27a** was employed as starting material (Table 2.3-7, entry 14) reaching the same 7:3 ratio between *cis* and *trans* with a C2 configuration retention and almost the same enantiomeric excess that the starting material.

Entry	Solvent (1:10)	t (days)	T (ºC)	*cis*:*trans*	*e.e.cis*(%)	*e.e.trans*(%)
1	-	0	-	99:1	92 (2S,5S)	-
2	Toluene	20	50	73:27	35 (2*S*,5*S*)	47 (2*S*,5*R*)
3	Toluene	25	35	87:13	61 (2*S*,5*S*)	65 (2*S*,5*R*)
4	MeOH	40	50	92:8	65(2*S*,5*S*)	-
5	Tol/MeOH	40	50	83:17	64(2*S*,5*S*)	60(2*S*,5*R*)
6	MeCN	40	50	70:30	72 (2S,5S)	70(2S,5R)
7	Cl-Nap/MeCN	5	50	70:30	81 (2*S*,5*S*)	80 (2*S*,5*R*)
8	Tol/MeCN	8	50	70:30	70 (2*S*,5*S*)	70(2*S*,5*R*)
9	Cl-Nap/MeCN	25	20	75:25	87 (2*S*,5*S*)	87 (2*S*,5*R*)
10	Cl-Nap/MeCN	6	35	72:28	90 (2*S*,5*S*)	90 (2*S*,5*R*)
11	Tol/MeCN	9	35	71:29	89 (2*S*,5*S*)	89 (2*S*,5*R*)
12[a]	Cl-Nap/MeCN	6	35	66:34	88 (2*R*,5*R*)	88 (2*R*,5*S*)
13[b]	Cl-Nap/MeCN	6	35	72:28	97 (2*S*,5*S*)	97 (2*S*,5*R*)
14[c]	Cl-Nap/MeCN	6	35	70:30	93 (2*S*,5*S*)	93 (2*S*,5*R*)

[a] (2*R*,5*R*)-*cis*-pyrrolidinofullerene **27a** (90% optical purity) employed as starting material.
[b] (2*S*,5*S*)-*cis*-pyrrolidinofullerene **27a** (99% optical purity) employed as starting material.
[c] (2*S*,5*R*)-*trans*-pyrrolidinofullerene **27a** (95% optical purity) employed as starting material.

Table 2.3-7. Representative results for the screening of reaction conditions for the isomerization of (2*S*,5*S*)-*cis*-**27a**.

b) Influence of the different aryl groups on the *cis/trans* isomerization

Once established the conditions for the isomerization experiments, the influence of the different electronic nature of substituents was examined on pyrrolidino[60]fullerenes **27a-e** (Figure 2.3-18)

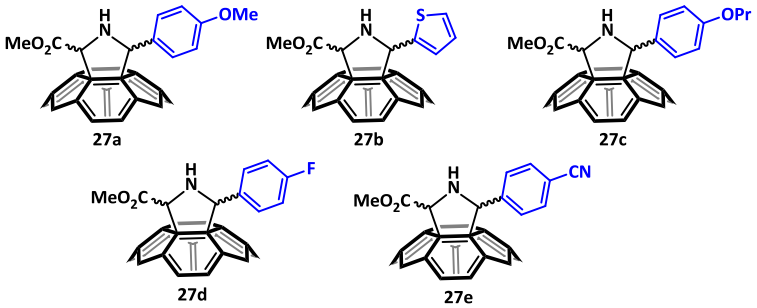

Figure 2.3-18. Optically pure pyrrolidino[60]fullerenes synthesized.

Electron-releasing substituted pyrrolidinofullerenes (**27b-c**) exhibited analogous results to the reference **27a**, demonstrating an excellent enantiocontrol and getting the same 7:3 ratio between *cis/trans* isomers (Table 2.3-8, entries 1-8). This behaviour was observed using both *cis* or *trans* isomers as starting material. When electron-withdrawing substituents were utilized (**27d-e**) different results were observed. Either *cis* or *trans* isomerized under optimized conditions (Table 2.3-8, entries 9-16). When higher temperatures are utilized (60 ºC), *cis*-**27e** leads to a 5 % of *trans*-**27e** whereas *cis*-**27d** afforded a 17 % of *trans*-**27d** (Table 2.3-8, entries 17-18). Moreover, this isomerization at higher temperatures involved a decrease in the enantiomeric excess as a consequence of the racemization and retrocycloaddition reactions.

Entry	Starting derivative	t(days)	*cis*:*trans*	*e.e.cis*(%)	*e.e.trans*(%)
1	*cis*-**27b**	0	99:1	90(2*S*,5*R*)	-
2	*cis*-**27b**	7	68:32	88(2*S*,5*R*)	87(2*S*,5*S*)
3	*trans*-**27b**	0	1:99	-	90 (2*R*,5*R*)
4	*trans*-**27b**	7	70:30	84 (2*R*,5*S*)	84 (2*R*,5*R*)
5	*cis*-**27c**	0	99:1	90 (2*R*,5*R*)	-
6	*cis*-**27c**	6	71:29	89 (2*R*,5*R*)	89 (2*R*, 5*S*)
7	*trans*-**27c**	0	1:99	-	90 (2*R*,5*S*)
8	*trans*-**27c**	6	68:32	90 (2*R*,5*R*)	90 (2*R*,5*S*)
9	*cis*-**27d**	0	99:1	90 (2*S*,5*S*)	-
10	*cis*-**27d**	10	99:1	87 (2*S*,5*S*)	-
11	*trans*-**27d**	0	1:99	-	94 (2*S*,5*R*)
12	*trans*-**27d**	10	2:98	-	91 (2*R*,5*S*)
13	*cis*-**27e**	0	99:1	88 (2*S*,5*S*)	-
14	*cis*-**27e**	10	99:1	85 (2*S*,5*S*)	-
15	*trans*-**27e**	0	1:99	-	91 (2*S*,5*R*)
16	*trans*-**27e**	10	1:99	-	88 (2*R*,5*S*)
17[a]	*cis*-**27d**	10	83:17	65 (2*S*,5*S*)	64 (2*S*,5*R*)
18[a]	*cis*-**27e**	10	95:5	69 (2*S*,5*S*)	-

Table 2.3-8. Representative results for the isomerization of (2*S*,5*S*)-*cis*-**27b-e**. [a] Carried out at 60 ºC).

Taking in mind these experimental results, it can be assumed that C2 is unaltered during the isomerization while the C5-cage bond must be broken. A zwitterionic intermediate where fullerene stabilizes the anion and a benzylic cation is formed, allowing the rotation around the C2-N bond to afford the opposite diastereomer. The stability of the carbocation is the determining issue to the extension of the process, and it will be more favourable when carried out under the presence of electron-rich rings. In this sense, the retention in the C2 configuration and the low extension of the diastereomer conversion in electron-poor derivatives corroborate this

proposal. Moreover, the higher energy necessary for these derivatives will promote the racemization and retrocycloaddition processes that lead to lower enantiomeric excess, as experimentally observed.

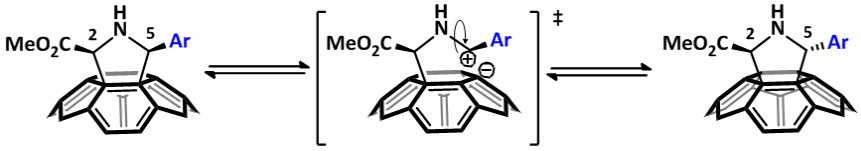

Figure 2.3-19. Stepwise isomerization reaction involving a zwitterionic intermediate.

c) Influence of the cage surface on the *cis/trans* isomerization

The optimized conditions were extended to the isomerization study of pyrrolidino[70]fullerenes derivatives **28** and **29** in all their *cis* forms. The synthesis of these compounds was accomplished with a high optical purity following the conditions previously reported by our group (Figure 2.3-20).[186]

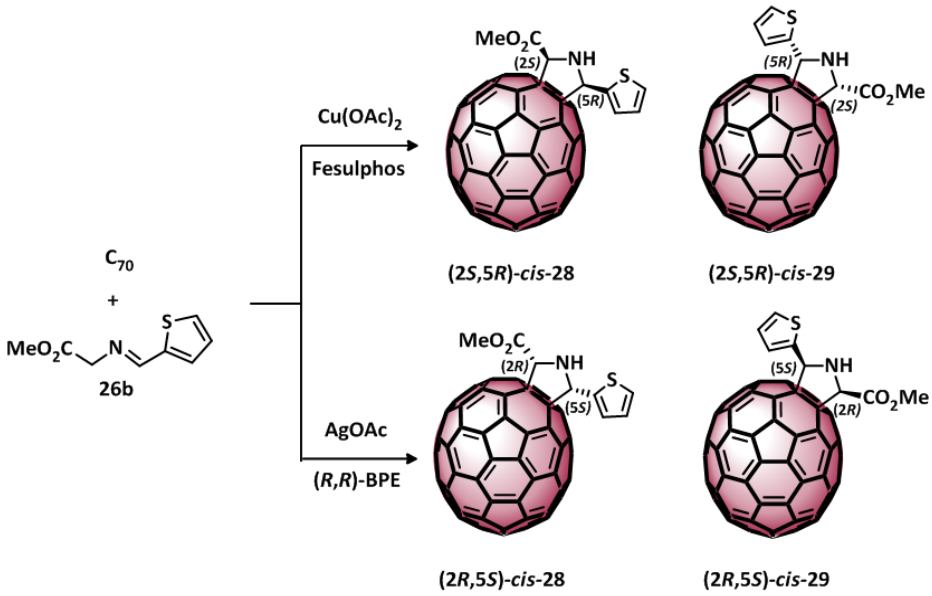

Figure 2.3-20. Synthesis of pyrrolidino[70]fullerenes utilized for the isomerization study.

When (2*S*,5*R*)-*cis*-**28** was submitted to the experimental conditions, a faster isomerization to the corresponding *trans* diastereomer was observed, reaching the same 7:3 ratio and configuration retention at C2 as observed in C_{60} derivatives (Table 2.3-9, entries 1-2). It is necessary to remark the absence of any byproducts as consequence of the formation of site- or regioisomers, what indicates a different level of stereospecificity of the process. In contrast, the regioisomer (2*S*,5*R*)-*cis*-**29**, bearing the carboxylate

motif close to the equatorial region exhibited a slower isomerization, needing 9 days to reach the equilibrium rate. (Table 2.3-9, entries 3-4).

Entry	Starting derivative	t(days)	*cis*:*trans*	*e.e.cis*(%)	*e.e.trans*(%)
1	*cis*-**28**	0	99:1	96 (2*S*,5*R*)	-
2	*cis*-**28**	2	69:31	96 (2*S*,5*R*)	96 (2*S*,5*S*)
3	*cis*-**29**	0	99:1	94 (2*R*,5*S*)	-
4	*cis*-**29**	9	71:29	91 (2*R*,5*S*)	92 (2*S*,5*R*)

Table 2.3-9. Representative results for the isomerization of *cis*-**28** and *cis*-**29**.

The isomerization for process of **28** and **29** afforded different structures for each zwitterionic intermediate, localized in C8 and C25, respectively. It is well known that carbanions are better stabilized in more planar systems because of their larger *s* character and are destabilized in more pyramidilized carbons because of its larger *p* character.[186] Taking these considerations in mind, more equatorial carbon atoms in C_{70} are more planar compared to those close to the cage poles. Consequently, C8 would stabilize the carbanion better than C25, providing a higher isomerization rate, which is consistent with the experimental results.

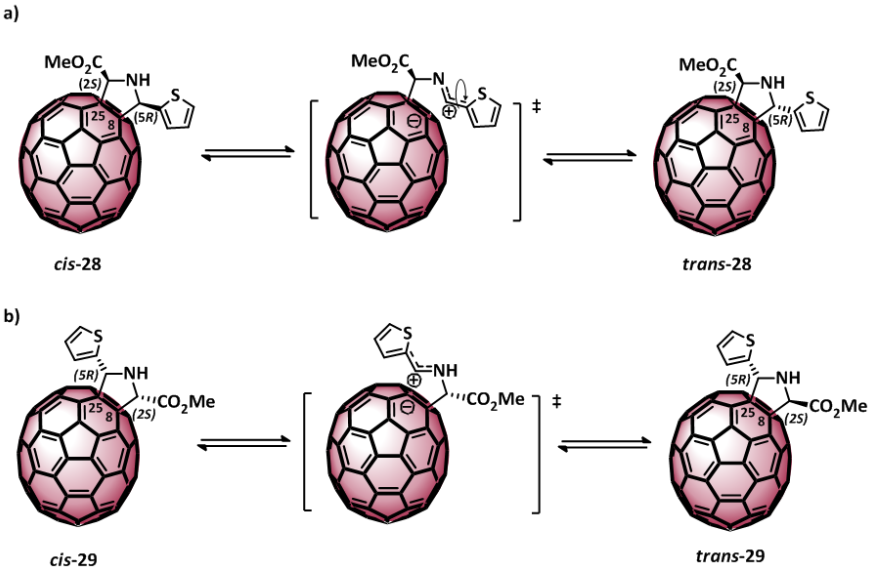

Figure 2.3-21. Stepwise isomerization reaction involving a zwitterionic intermediate for the different regioisomers in C_{70}.

d) Influence of the inner H_2O molecule on the *cis/trans* isomerization

In order to study the influence of an encapsulated polar molecule in the isomerization, the synthesis of several analogous pyrrolidinofullerenes on an endohedral fullerene was proposed. Previous to this synthesis, the preparation of the endohedral $H_2O@C_{60}$ was necessary (Figure 2.3-22). A

research stay at the laboratory of Prof. Murata (Institute for Chemical Research, Kyoto University) was carried out to accomplished the preparation of this novel endohedral fullerene, following the reported procedure based on molecular surgery.[184]

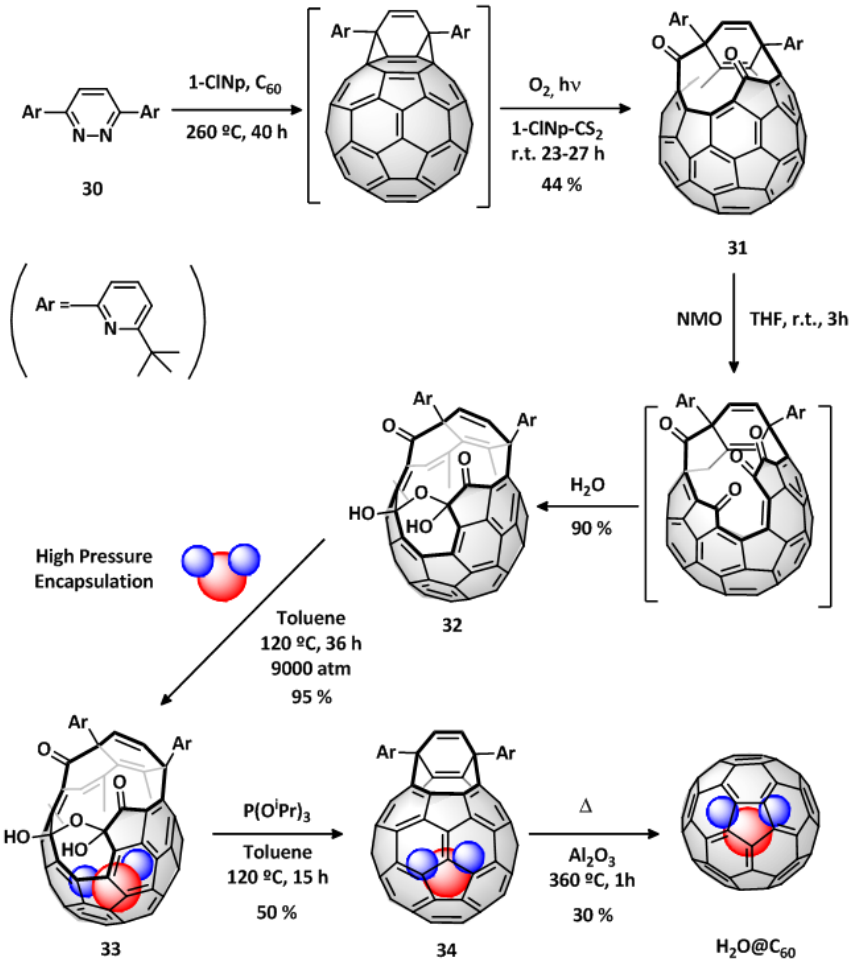

Figure 2.3-22. Procedure for the synthesis of $H_2O@C_{60}$ by molecular surgery.

Under the same conditions utilized for **27**, the $H_2O@C_{60}$-pyrrolidines **35a** were obtained in an enantioespecific manner (Figure 2.3-23).

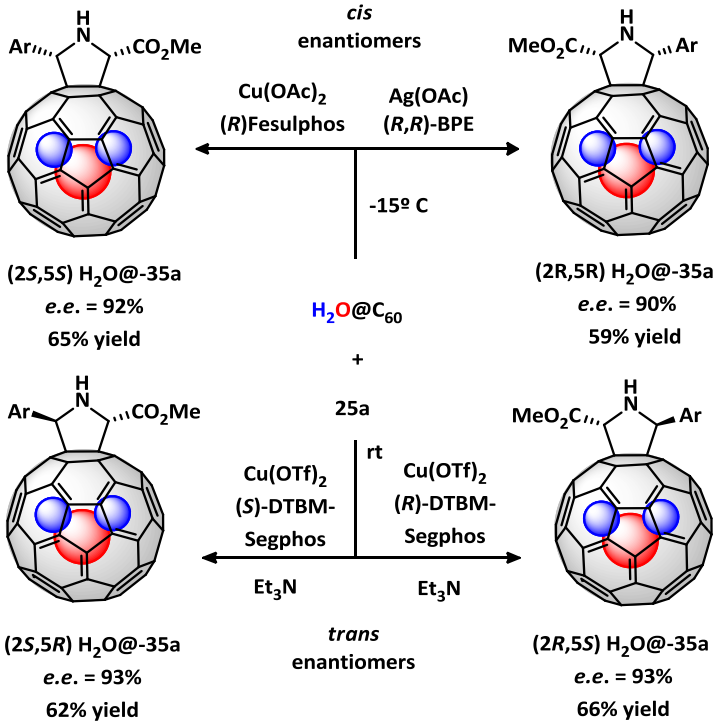

Figure 2.3-23. Synthesis of endohedral $H_2O@C_{60}$-pyrrolidines utilized for the isomerization study.

Once the synthesis and characterization was accomplished, the *cis/trans* isomerization was studied and excellent results were obtained, observing the expected 7:3 ratio and a retention in enantiomeric excess for both *cis* and *trans* pairs (Table 2.3-8).

Entry	Starting derivative	t(days)	*cis*:*trans*	*e.e.cis*(%)	*e.e.trans*(%)
1	*cis*-**35a**	0	99:1	92 (2*S*,5*S*)	-
2	*cis*-**35a**	6	66:34	92 (2*S*,5*S*)	92 (2*S*,5*R*)
3	*cis*-**35a**	0	99:1	90 (2*R*,5*R*)	-
4	*cis*-**35a**	6	68:32	90 (2*R*,5*R*)	90 (2*R*,5*S*)
5	*trans*-**35a**	0	1:99	-	93 (2*S*,5*R*)
6	*trans*-**35a**	6	71:29	93 (2*S*,5*S*)	93 (2*R*,5*S*)

Table 2.3-10. Representative results for the isomerization of the endohedral derivatives **35a**.

Going further, a comparative study between the empty and endohedral related isomers was accomplished. The *cis*/*trans* ratio was measured during 6 days revealing an enhancement in the results in the endohedral derivatives. The results suggested that the inner water molecule is not inert and can play a role in favour of the isomerization.

Entry	Starting derivative	t(d)	*cis:trans*
1	*cis*-**27a**	0	99:1
2	*cis*-**35a**	0	99:1
3	*cis*-**27a**	1	99:1
4	*cis*-**35a**	1	97:3
5	*cis*-**27a**	2	98:2
6	*cis*-**35a**	2	95:5
7	*cis*-**27a**	3	92:8
8	*cis*-**35a**	3	87:13
9	*cis*-**27a**	4	85:15
10	*cis*-**35a**	4	80:20
11	*cis*-**27a**	5	76:24
12	*cis*-**35a**	5	71:29

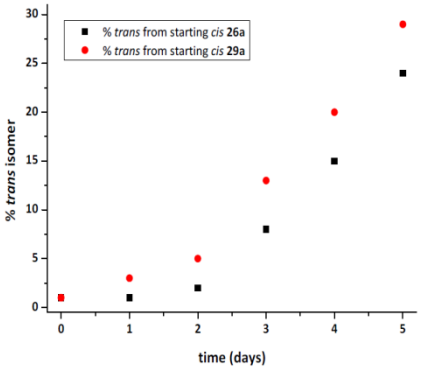

Table 2.3-11. Representative results for the time dependent ratio *cis/trans* for derivatives **27a** and **35a**.

Since the experimental conditions are exactly the same and the only modification is the inner water hosted inside the cage, the enhancement in the isomerization rates can only be rationalized by a H assistance in the stabilization of the zwitterionic intermediate. Interestingly, the stereochemical outcome also seems to be influenced by the entrapped H_2O.

e) Theoretical calculations

To support this experimental findings, several DFT calculations at the M06-2X/6-311+G(d,p)//OLYP/TZP level of theory were performed by the group of Prof. Solá at Girona University. The study started on **27a** and the possible competition of the retro-Prato reaction. As experimental results revealed, calculations set a lower energy for the *cis* adduct (1.6 Kcal/mol more estable), attributed to the repulsion between the N lone pairs and carbonyl groups. Two zwitterionic intermediates were proposed (INT(2S,5S)-*cis* and INT(2S,5R)-*trans*) where a fullerene anion and benzyl cation are formed (Figure 2.3-24).

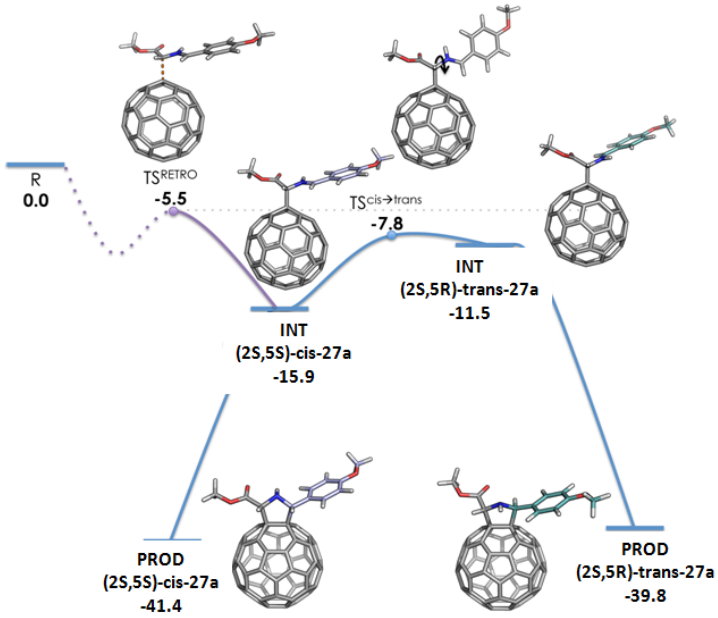

Figure 2.3-24. DFT mechanism for the *cis/trans* **27a** isomerization (represented using a blue line) and retro-Prato process (in purple). All energies are expressed in kcal/mol.

Both intermediates (INT(2S,5S)-*cis* and INT(2S,5R)-*trans*) are calculated to be -16 and -12 kcal/mol more stable than isolated reactants. Once INT-cis has been formed, two possible pathways should be considered: i) the cis/*trans* isomerization to achieve INT-*trans*, and ii) the retro-Prato process to recover the initial reactants. The most favourable isomerization process involves the rotation of the C2-N single bond, and has an activation barrier of ca. 8 kcal/mol with respect to INT-*cis* (and of about 4 kcal/mol with respect to INT-*trans*). It should be emphasized that the isomerization process through the N-C5 bond is extremely unfavourable due to its higher double bond character (Figure 2.3-25). In contrast, the retro-Prato reaction presents an activation barrier of ca. 10.5 kcal/mol. This is ca. 2.5 kcal/mol higher than the one corresponding to the *cis-trans* isomerization. These observations indicate that: i) the retro-Prato could compete with the isomerization process at high temperatures (as observed experimentally for instance in the cases **27d** and **27e**), and ii) the stabilities of the intermediate INT(2S,5R)-*trans* give a reasonable estimate of the activation barrier of the isomerization process (less than 4.0 kcal/mol of difference between the activation barrier and relative stability of the *cis-trans* intermediates).

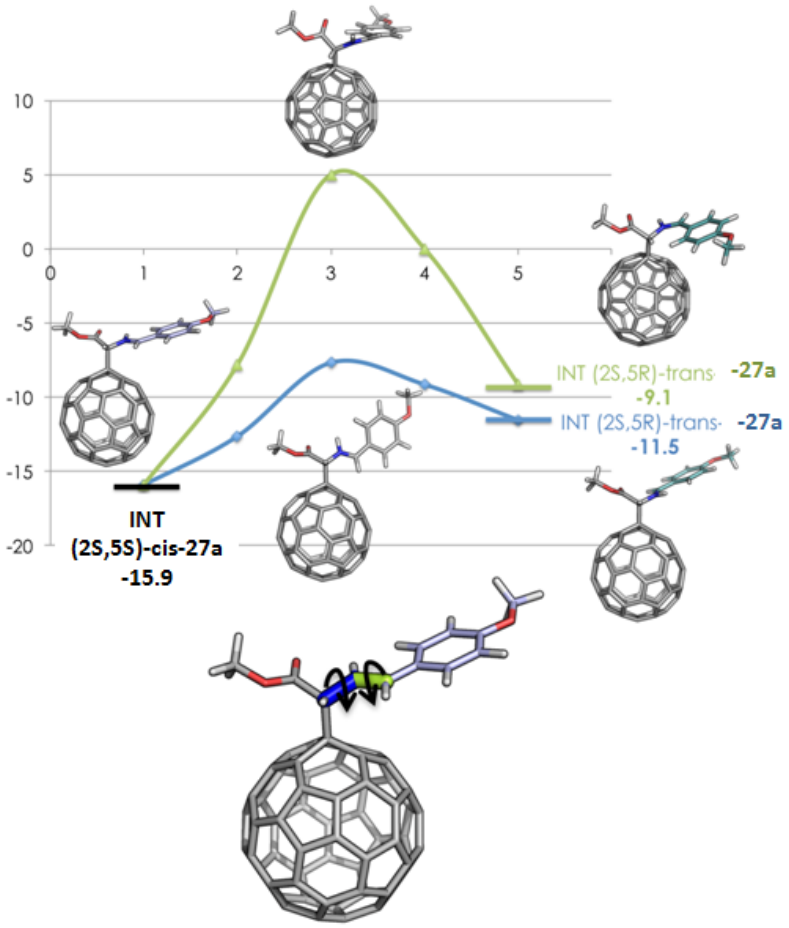

Figure 2.3-25. Linear transit calculations for the two possible isomerization processes: in green the rotation along the double bond N-C5, and in blue along the single N-C2 bond. All energies are expressed in kcal/mol

The effect of the substituent, fullerene surface, and inner water molecule on the isomerization process has also been studied computationally (Figure 2.3-26). In Table 2.3-12, the relative stabilities of *cis-trans* products and their respective intermediates for the rest of the studied systems are represented. In all cases, the *trans* product is ca. 1.5 kcal/mol less stable than the *cis* one, showing that the same *cis/trans* ratio will be obtained in all cases. As observed experimentally, the presence of electron-withdrawing groups in the benzyl substituent destabilizes the formed intermediates by approximately 2-3 and 5-6 kcal/mol for **27d** and **27e**, respectively. Under these conditions, the isomerization and retro-Prato reaction are both plausible, which is in line with the experimental observations.

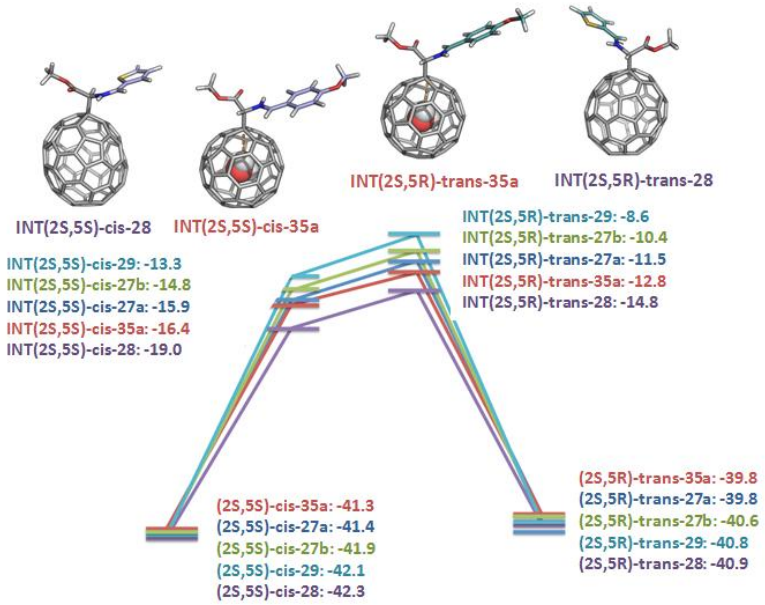

Figure 2.3-26. Representation of the *cis-trans* isomerization process for the C_{60}-based systems **27a** (in blue), and **27b** (green), the $H_2O@C_{60}$ **35a** (in red), and the C_{70}-based cases **28** (purple) and **29** (cyan). All energies are expressed in kcal/mol.

	C_{60}				$H_2O@C_{60}$	C_{70}	
	26a	**26d**	**26e**	**26b**	**35a**	**28**	**29**
PROD-cis	-41.4	-42.0	-41.1	-41.9	-41.3	-42.3	-42.1
INT-cis	-15.9	-13.3	-11.4	-14.8	-16.4	-19.0	-13.3
INT-trans	-11.5	-7.6	-3.0	-10.4	-12.8	-14.8	-8.6
PROD-trans	-39.8	-40.2	-39.4	-40.6	-39.8	-40.9	-40.8

Table 2.3-12. M06-2X/6-311+G(d,p)//OLYP/TZP relative stabilities of *cis*/*trans* products and intermediates with respect to isolated reactants for C_{60}, $H_2O@C_{60}$, and C_{70} systems. All energies in kcal/mol.

The effect of the fullerene surface has been investigated considering the bigger [70]-fullerene. DFT calculations indicate that INT(2S,5S)-*cis*-**28** (-19.0 kcal/mol with respect to C_{70} + dipole) and INT(2S,5R)-*trans*-**28** (-14.8 kcal/mol) correspond to the most stable intermediates among all considered cases. In contrast, the corresponding intermediates for **29**, which bear the ester substituent on the equatorial region of C_{70} are ca. 6 kcal/mol less stable than **28** (-13.3 and -8.6 kcal/mol for INT-*cis* and INT-*trans*, respectively). In comparison, the relative stabilities of the latter thiophene-based intermediates in the case of C_{60} are -14.8 and -10.4 kcal/mol respect to isolated reactants, respectively. The difference in reactivity for INT-(2S,5S)-*cis*-**27b**, **28**, and **29** can be rationalized by considering the average

pyramidalization angle of the carbon atoms of the pentagonal ring where the new C-C bond is formed (10.0°, 10.8°, and 10.4° for **28**, **29**, and **27b**, respectively). In the most stable adduct **27** the negative charge is located in a more planar region, INT-*cis*-[60]-**27b** presents an intermediate pyramidalization angle, and the least planar geometry is found for the least stable **29**.

Finally, the effect on the isomerization process of having a water molecule in the fullerene inner cavity has been investigated. Several orientations of the inner molecule have been considered (Figure 2.3-27). By comparing the relative stabilities of both *cis* and *trans* endohedral intermediates **35** with respect to empty cages **27b**, a slight stabilization of INT-*cis* (0.5 kcal/mol), but a substantial stabilization of INT-*trans* (ca. 1.3 kcal/mol) is observed for the H_2O molecule orientation leading to the most stable structure.

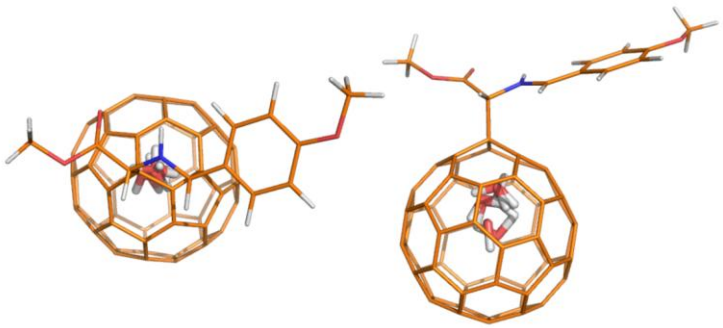

Figure 2.3-27. Superposition of the 8 different orientations studied for the inner H_2O molecule in the endohedral system $H_2O@C_{60}$.

As it can be seen in Figure 2.3-28, the inner water molecule is assisting the isomerization process by stabilizing the formed fullerene anion, where a hydrogen atom of the water molecule is directly pointing to the negatively charged carbon atom on the fullerene surface. The distance between the hydrogen atom of the inner H_2O and the carbon atom where the addition would take place to form PROD-*trans* is ca. 2.7 Å in both *cis* and *trans* intermediates. The O-H distance in *cis* and *trans* intermediates is 0.967 Å, slightly elongated as compared to that in $H_2O@C_{60}$ (0.965 Å). In this latter species the C・・・HO interaction was classified as a weak H-bond in a previous work.[198] In *cis* and *trans* intermediates this H-bond is somewhat stronger. The H-C and O-H values in the *cis* and *trans* intermediates correspond to the usually observed hydrogen bond distances, thus clearly showing that this H-bond stabilization is the main force that favours the isomerization process.

[198] Aroua, S., Garcia-Borràs, M., Osuna, S. and Yamakoshi, Y., *Chem. Eur. J.* **2014**, *20*, 14032.

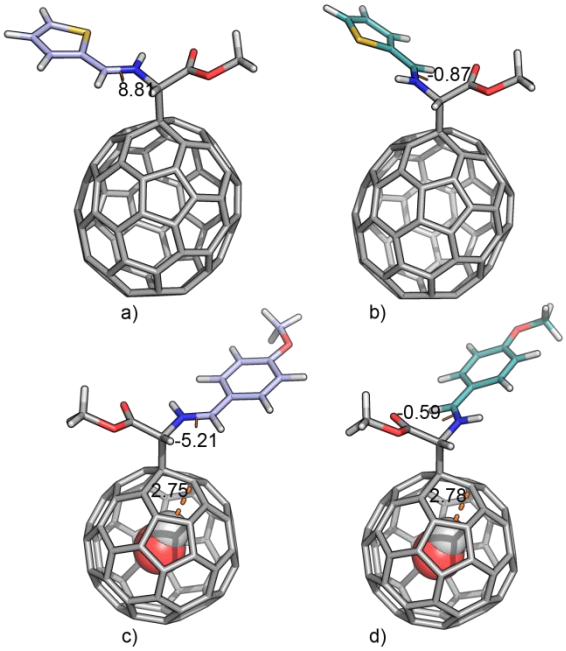

Figure 2.3-28. DFT optimized *cis-trans* intermediates for: a) INT(2S,5S)-*cis*-**28**, b) INT(2S,5R)-*trans*-**28**, c) INT(2S,5S)-*cis*-**35a**, and d) INT(2S,5R)-*trans*-**35a**. H_{H2O}-C_{full} distance in angstroms and ∠CNCH dihedral angle in degrees.

2.4. Experimental section

2.4. EXPERIMENTAL SECTION

2.4.1. UNPRECEDENTED HYDROGEN ADDITION IN THE 1,3-DIPOLAR CYCLOADDITION REACTION ON La@C_s-C_{82}

General methods

Materials

All chemicals and solvents were obtained from Wako Inc. and used without further purification unless otherwise stated. La@C_s-C_{82} was synthesized and isolated by using a La-graphite rod in an electric arc discharge Krätschmer–Huffman generator.[199] The resulting crude was extracted by Soxhlet with different solvents and filtered to afford a multi-step HPLC separation. The isolate crude was clearly identified by Mass Spectrometry and Uv-vis by comparison with the reported features by this isomer.

Instruments

HPLC (Analytical and preparative) were performed on a JASCO HPLC apparatus or JAI LC-908. Toluene was used as the eluent.

NMR analyses (^{1}H, ^{13}C and 2D NMR measurements) were carried out on a Bruker AVANCE 500 spectrometer with a CryoProbe system, where TMS was used as an internal reference (d = 0.00 ppm).

UV-vis spectra were recorded in a SHIMADZU UV-3150 spectrophotometer.

Mass spectrometry was performed on a Bruker BIFLEX III, using 1,1,4,4-tetraphenyl-1,3-butadiene as a matrix. The samples were prepared by drop casting in ambient conditions.

Cyclic voltammetry and **differential pulse voltammetry** were recorded on a BAS CV50W electrochemical analyzer. Platinum wires were used as the working and counter electrodes. The reference electrode was a saturated calomel reference electrode (SCE) filled with 0.1 M (n-Bu)$_4$NPF$_6$ (TBAPF$_6$) in o-DCB. CVs were recorded using a scan rate of 50 mV/s, and DPVs were obtained using a pulse amplitude of 50 mV, a pulse width of 50 ms a pulse period of 200 ms, and a scan rate of 20 mV/s. The solution was purged for 20 min. with argon prior to the electrochemical measurements.

[199] Yamamoto, K., Funasaka, H., Takahasi, T., Akasaka, T., Suzuki, T. and Maruyama, Y., *J. Phys. Chem.* **1994**, *98*, 12831.

a) Synthesis, isolation and characterization of the Prato adducts

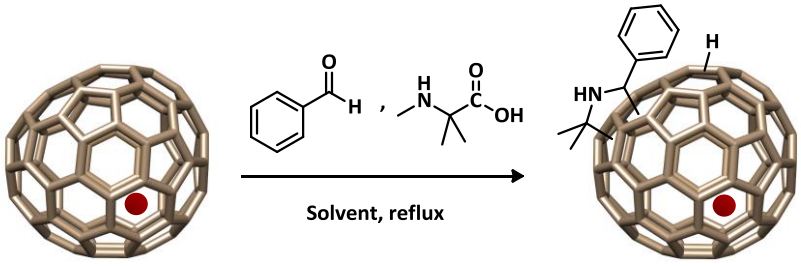

La@C_s-C_{82} 25a and 25b

Solvent
***(o*-DCB): Low selectivity**
(*o*-DCB+ $PhCH_3$ droplet): High Selectivity

- In the absence of toluene:

1.0 mL *o*-DCB solution containing 0.25 mg of La@C_s-C_{82} (2.3×10^{-4} mmol) was carefully degassed and refluxed with 6 equivalents of 2-(methylamino)isobutyric acid and 2 equivalents of benzaldehyde under argon atmosphere. After cooling to the room temperature, the reaction mixture was analyzed by HPLC (Figure 2.4-1).

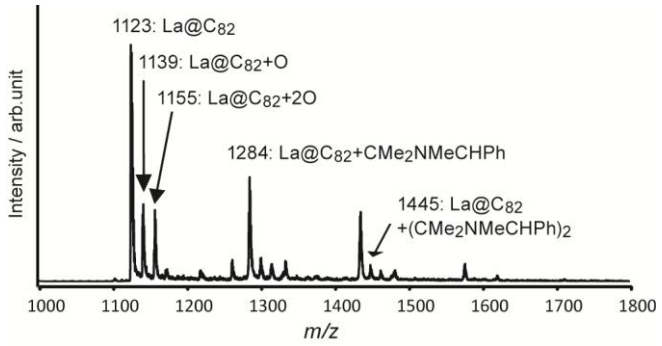

Figure 2.4-1. MALDI-TOF mass spectrum of the reaction mixture of the Prato reaction using La@C_{82} in the absence of toluene, in negative linear mode using 1,1,4,4-tetraphenyl-1,3-butadiene as a matrix.

- In the presence of toluene:

25 mL *o*-DCB solution containing 6.4 mg of La@C_s-C_{82} (5.7×10^{-3} mmol) and 50 μL of toluene was carefully degassed and refluxed with 6.0 equivalents of 2-(methylamino)isobutyric acid and 2.0 equivalents of benzaldehyde under argon atmosphere. After cooling to room temperature, the solvent was removed under reduced pressure and the reaction mixture was subjected to multi step preparative HPLC as shown in Figure 2.4-2 for the isolation of the target compound from byproducts and unreacted starting materials. As the result, **25a** was obtained in 45% yield based on the consumed starting

fullerene, which was confirmed by the HPLC analyses. **25b** was also obtained after the HPLC separation and was found to become oxidized (**25b-O**) in a few minutes. The conversion yield of **25b-O** was 20% based on the recovered fullerene.

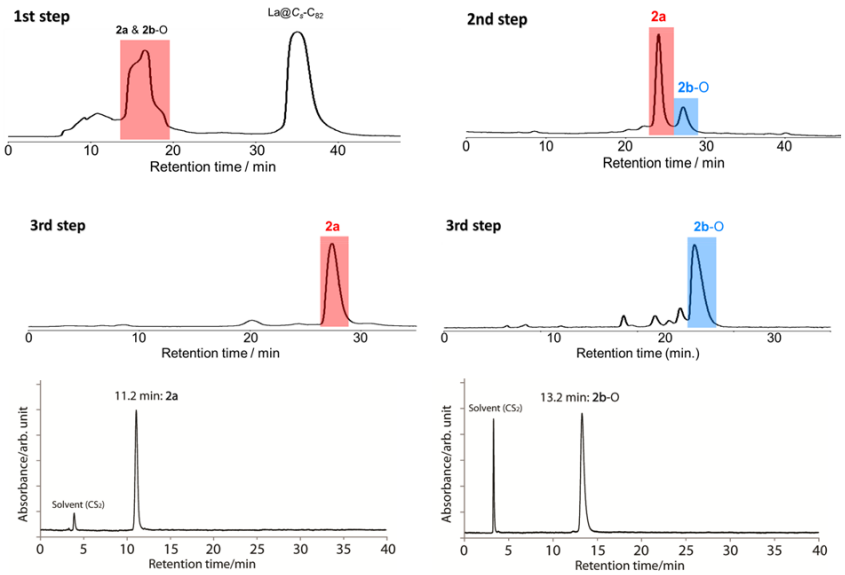

Figure 2.4-2. Upper part: HPLC profiles for purification of **25a** and **25b**-O. Conditions; eluent: toluene, flow rate: 1.0 mL/min, wavelength: 330 nm, temperature: r.t., column: (1st step) 5PYE (ϕ 20 × 250 mm), (2nd step) Buckprep (ϕ 20 × 250 mm), (3rd for **25a**) Buckyprep-M (ϕ 10 × 250 mm), and (3rd for **25b**-O) 5NPE (ϕ 10 × 250 mm). Lower part: HPLC profiles of isolated (left) **25a** and (right) **25b**-O. Conditions: Buckyprep column (ϕ 4.6 × 250 mm); eluent, toluene; flow rate, 1.0 mL/min; wavelength, 330 nm; temperature, 40 °C.

*La@C_{82}CHMe$_2$NMeCHPh (**25a**)*:

^{1}H NMR (CS_2/CD_2Cl_2 = 3/1 (v/v), 500 MHz), δ: 7.56 (d, *J* = 7.3 Hz, 1H), 7.46 (m, 2H), 7.33 (m, 1H), 7.13 (t, *J* = 7.2 Hz, 1H), 4.43 (s, 1H, C*H*), 3.19 (s, 1H, C*H* on the cage), 2.39 (s, 3H, NCH_3), 1.61 (s, 3H, CCH_3), 1.54 (s, 3H, CCH_3).

^{13}C NMR (CS_2/CD_2Cl_2 = 3/1 (v/v), 125 MHz), δ: 163.24, 156.13, 155.59, 152.80, 151.66, 150.63, 150.35, 150.22, 150.08, 149.94, 149.62, 149.25, 148.76, 148.15, 147.99, 147.63, 146.62, 146.60, 146.45, 146.24, 146.16, 146.10, 145.85, 145.81, 145.42, 145.13, 144.54, 144.17, 143.63, 143.32, 142.98, 142.95, 142.67, 142.52, 142.36, 142.31, 141.81, 141.74, 141.33, 141.10, 139.89, 139.65, 139.50, 139.13, 138.33, 138.05, 138.00, 137.92, 137.73, 137.71, 137.63, 137.59, 137.45, 136.80, 136.18, 136.07, 135.80, 135.74, 135.63, 135.54, 135.16, 134.93, 134.17, 133.32, 133.17, 133.11, 132.90, 132.70, 132.26, 131.26, 131.20, 130.59, 130.50, 129.55, 129.47, 129.35,

129.28, 129.15, 129.02, 128.96, 128.73, 128.34, 127.94, 127.20, 127.02, 77.91 (*C*H), 68.23 (*C*$(CH_3)_2$), 64.76, 62.57, 47.62 (*C*H on the cage), 32.13(NCH_3), 26.78 (*C*H_3), 16.26 (*C*H_3).

DEPT135 (CS_2 with acetone-d_6 in a capillary tube, 125 MHz) δ: 131.17 (*C*H), 130.50 (*C*H), 129.28 (*C*H), 128.72 (*C*H), 128.34 (*C*H), 77.91 (*C*H), 47.62 (*C*H on the cage), 32.13 (NCH_3), 26.78 (*C*H_3), 16.26 (*C*H_3).

UV-vis-NIR (in CS_2) λ_{max}: 520, 944.

MALDI-TOF: mass calculated for $C_{93}H_{16}LaN$ ([*M*]$^-$): 1285.0, found: 1285.2 *m/z*.

*La@C_{82}COHMe$_2$NMeCHPh (**25b-O**)*:

^{1}H NMR (CS_2/CD_2Cl_2 = 3/1 (v/v), 500 MHz), δ:7.54 (m, 1H), 7.42 (m, 1H), 7.33 (m, 1H), 7.14 (m, 1H), 6.90 (m, 1H), 4.36 (s, 1H, C*H*), 3.53 (s, 1H, CO*H*), 2.26 (s, 3H, NCH_3), 1.84 (s, 3H, CCH_3), 1.60 (s, 3H, CCH_3);

^{13}C NMR (CS_2 with acetone-d_6 in a capillary tube, 125 MHz) δ: 159.82, 158.59, 156.12, 155.78, 153.78, 152.71, 151.68, 150.85, 150.43, 150.35, 149.96, 149.89, 149.24, 149.12, 148.86, 148.70, 148.59, 147.81, 147.11, 146.94, 146.45, 146.28, 145.96, 145.79, 145.74, 145.58, 145.02, 144.66, 144.22, 143.53, 143.39, 143.24, 143.01, 142.82, 142.72, 142.06, 141.86, 141.62, 141.02, 140.92, 140.87, 140.33, 140.00, 139.51, 139.44, 139.07, 138.93, 138.60, 137.88, 137.84, 137.69, 137.55, 137.47, 137.35, 137.22, 137.19, 136.93, 136.65, 136.16, 135.61, 135.51, 135.35, 135.20, 135.06, 134.63, 134.59, 134.10, 133.25, 132.59, 132.25, 131.66, 131.32, 131.01, 130.82, 130.46, 130.36, 130.07, 129.42, 128.06, 127.89, 127.38, 127.14, 125.78, 77.77 (*C*H), 73.52 (*C*OH), 68.99, 68.97 (*C*$(CH_3)_2$), 59.40, 32.17 (NCH_3), 26.04 (*C*H_3), 17.08 (*C*H_3);

UV-vis-NIR (in CS_2) λ_{max}: 525, 945.

MALDI-TOF: mass calculated for $C_{93}H_{16}OLaN$ ([*M*]$^-$): 1301.0, found: 1301.1 *m/z*.

b) Thermal experiments

Thermal reaction of La@C_{82} with a droplet of toluene in o-ODCB

1.0 mL *o*-DCB solution containing 0.25 mg of La@C_s-C_{82} (2.3×10^{-4} mmol) and 5 μL of toluene was carefully degassed and refluxed under argon atmosphere. After cooling to the room temperature, the reaction mixture was analyzed by HPLC.

Thermal reaction of La@C_{82} with o-ODCB containing D_2O

1.0 mL *o*-DCB was stirred with 0.5 mL of D_2O for 15 min, then the organic layer was corrected and used for the reaction as below. 1.0 mL of the *o*-DCB solution containing 0.25 mg of La@C_s-C_{82} (2.3×10^{-4} mmol) and 5 μL of toluene was carefully degassed and refluxed under argon atmosphere. After cooling to the room temperature, the reaction mixture was analyzed by HPLC and MALDI-TOF mass measurements.

2.4.2. STUDY OF THE ENCAPSULATED H_2O MOLECULE IN THE *CIS/TRANS* ISOMERIZATION PROCCESS OF PYRROLIDINO[3,4:1,2] [60]FULLERENES

General methods

All reactions were performed using an atmosphere of argon and oven-dried glassware. Solvents were treated prior to use according to the standard methods. The commercially available reagents were used without further purification.

NMR spectra were recorded on a BRUKER AVANCE 300, 500 or a BRUKER AVANCE 700 in $CDCl_3$, and referenced to $CDCl_3$.

TLC was performed using aluminum coated Merck Kieselgel 60 F254 to check the evolution of the reactions. Visualization was made by UV-light (λ = 254 or 365nm).

Flash column chromatography were performed using silica gel (230-400 mesh).

Optical rotations were measured using a polarimeter with a thermally jacketed 10 cm cell at 25ºC (concentration given as g/100mL).

HPLC chromatrography was utilized for the determination the *de* and *ee* values (*Buckyprep Waters* and 5YPE *Waters* for *de* and *Pirkle Covalent (R,R) Whelk-02 10/100 FEC* for *ee*). All these values were monitored in a 320 nm spectrophotometer detector for fullerenic products and in a 230 nm one for non fullerenic products. Semipreparative HPLC was carried out using *5PYE Waters* whose dimensions were 10 x 20 mm.

a) Synthesis of α-iminoesters 26a-e

All α-iminoesters were synthesized following a modified procedure reported in the bibliography.[200]

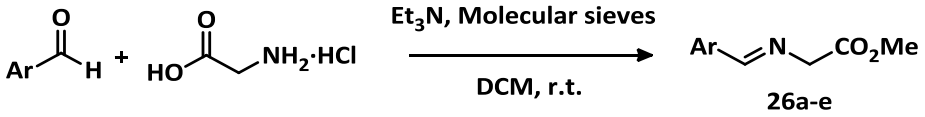

26a-e

To a suspension of methyl glycinate hydrochloride (1.50 mmol) and in dry CH_2Cl_2 (10 mL) over molecular sieves, Et_3N (0.2 mL, 1.5 mmol) was added. The mixture was stirred at room temperature for 1 h, and the corresponding benzaldehyde (1.00 mmol) was added. After 12h at room temperature the mixture was filtered off and water (5 mL) was added. The organic layer was separated and the aqueous phase was extracted with CH_2Cl_2 (10 mL). The

[200] [(a)]López-Pérez, A., Adrio, J. and Carretero, J. C., *Angew. Chem., Int. Ed.* **2009**, *48*, 340; [(b)]Wang, C.-J., Liang, G., Xue, Z.-Y. and Gao, F., *J. Am. Chem. Soc.* **2008**, *130*, 17250.

combined organic layers were washed with brine, dried over $MgSO_4$, and evaporated under reduced pressure to afford the desired α-iminoesters without further purification.

26a	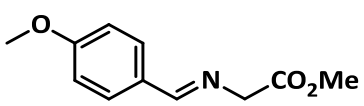	^{1}H-NMR ($CDCl_3$, 300 MHz), δ: 8.09 (s, 1H), 7.62 (d, *J*=8.4 Hz, 2H), 6.82 (d, *J*=8.4 Hz, 2H), 4.27 (s, 2H), 3.71 (s, 3H), 3.66 (s, 3H).
26b	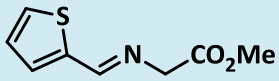	^{1}H-NMR ($CDCl_3$, 300 MHz), δ: 8.38 (d, *J*=0.9 Hz, 1H), 7.45 (d, *J*=4.9 Hz, 1H), 7.37 (dd, *J*=3.6, 0.9 Hz, 1H), 7.08 (dd, *J*=4.9, 3.6 Hz, 1H), 4.37 (d, *J*=0.9 Hz, 2H), 3.76 (s, 3H).
26c	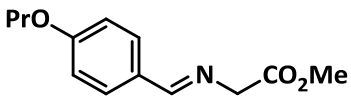	^{1}H-NMR ($CDCl_3$, 300 MHz), δ: δ 8.05 (s, 1H), 7.58 (d, J=8.7 Hz, 2H), 6.78 (d, J=8.7 Hz, 2 H), 4.23 (s , 2H), 3.80 (m, 2H), 3.62 (s, 3H), 1.67 (m, 2H), 0.91(m, 3H).
26d	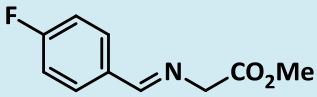	^{1}H-NMR ($CDCl_3$, 300 MHz), δ:8.25 (s, 1H), 7.76-7.79 (m, 2H), 7.08-7.12 (m, 2H), 4.40 (s, 2H),3.77 (s, 3H).
26e	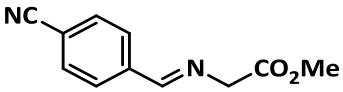	^{1}H-NMR ($CDCl_3$, 300 MHz), δ: 8.35 (s, 1H), 7.90 (d, *J*=8.3 Hz, 2H), 7.72 (d, *J* = 8.3 Hz, 2H), 4.48 (s, 2H), 3.79 (s, 3H).

Table 2.4-1. ^{1}H-NMR characterization for each α-iminoester **26a-e**.

b) Synthesis of enantiomerically pure pyrrolidino[60]fullerenes 27a-e

Enantiomerically pure pyrrolidino[60]fullerenes **27a-e** were synthesized from the corresponding α-iminoesters **26a-e** according to the method previously reported by our group. [197]

General procedure for *trans* adducts 27a-e:

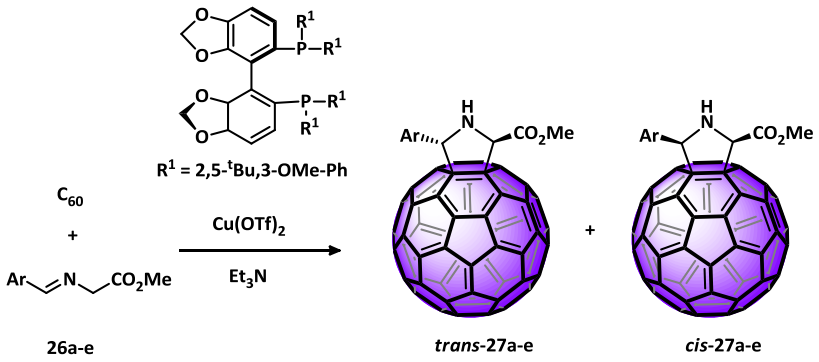

Figure 2.4-3. Enantioselective synthesis of *trans*-pyrrolidino[60]fullerenes utilizing (R)-DTBM-Segphos as ligand.

(*R*)- or (*S*)-DTBM-Segphos chiral ligand (0.0028 mmol) and copper(II)triflate (0.0025 mmol) were dissolved in toluene (7 mL). The solution was stirred for 30 min. at room temperature getting a bright blue colour, and then, a solution of α-iminoester **26a-e** (0.028 mmol) in toluene (1.5 mL) was added obtaining a yellow mixture. Finally, C_{60} (0.025 mmol) and triethylamine (0.0051 mmol) were added. The reaction mixture was stirred for a variable time and, afterwards, it was quenched with a saturated ammonium chloride solution (40 mL). The mixture was extracted with toluene (3 x 20 mL), and the combined extracts were washed with brine (30 mL). The organic layer was dried over $MgSO_4$ and concentrated *in vacuo*. The crude product was purified by silica gel flash chromatography.

Entry	Product	*trans:cis*	*e.e.trans* (%)	*e.e.cis* (%)	Yield [b] (%)
1	**27a**	95:5	95(2*R*,5*S*)	n.d.	55
2	**27b**	90:10	91(2*R*,5*R*)	n.d.	68
3	**27c**	95:5	92(2*R*,5*S*)	n.d.	57
4	**27d**	50:50	95(2*R*,5*S*)	95(2*R*,5*R*)	51
5	**27e**	30:70	91(2*R*,5*S*)	93(2*R*,5*R*)	59

[a] Same results were obtained with the opposite (*S*)-ligand for (2*S*,5*R*)*trans* and (2*S*,5*S*)*trans* in **27b**. [b] Yields calculated on the total amount of monoadduct.

Table 2.4-2. *trans*-selective cycloaddition of *N*-metalated azomethine ylides onto C_{60} fullerene using the complex Copper(II)-(*R*)-DTBM-Segphos.

***trans*-27a**	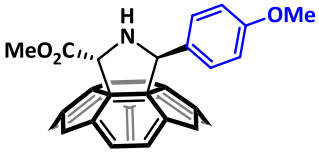	^{1}H-NMR ($CDCl_3$, 300 MHz), δ: 7.80 (d, 2H, *J* = 8.5 Hz, H-Ar), 6.94 (d, 2H, *J*=8.5 Hz, H-Ar), 6.52 (s, 1H, CH-N), 5.83 (s, 1H, CH-N), 3.96 (s, 3H, CH_3O), 3.84 (s, 3H, $COOCH_3$).
***trans*-27b**	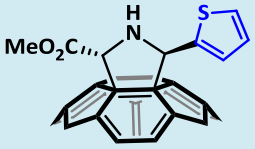	^{1}H-NMR ($CDCl_3$, 300 MHz), δ: 7.46 (d, 1H, *J*=3.5 Hz, H-Ar), 7.39 (dd, 1H, *J*=5.1, 1.1 Hz, H-Ar), 7.10 (dd, 1H, *J*=5.1, 3.6 Hz, H-Ar), 6.90 (s, 1H, CH-N), 5.85 (s, 1H, CH-N), 3.96 (s, 3H, $COOCH_3$).
***trans*-27c**	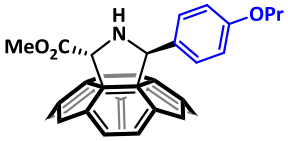	^{1}H-NMR ($CDCl_3$, 300 MHz), δ: 7.77 (d, 2H, *J*=8.7 Hz, H-Ar), 6.94 (d, 2H, *J*=8.7 Hz, H-Ar), 6.51 (s, 1H, CH-N), 5.82 (s, 1H, CH-N), 3.95 (s, 3H, $COOCH_3$), 3.94 (t, 2H, *J*=6.8 Hz, OCH_2), 1.84 (q, 2H, *J*=7.1 Hz, OCH_2-CH_2), 1.08 (t, 3H, *J*=7.2 Hz, CH_3).
***trans*-27d**	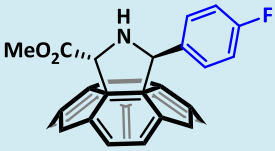	^{1}H-NMR ($CDCl_3$, 300 MHz), δ: 7.87 (dd, 2H, *J*=8.7, 5.5 Hz, H-Ar), 7.13 (t, 2H, *J*=8.7 Hz, H-Ar), 6.56 (s, 1H, CH-N), 5.83 (s, 1H, CH-N), 3.95 (s, 3H, $COOCH_3$).
***trans*-27e**	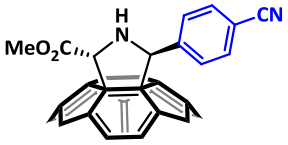	^{1}H-NMR ($CDCl_3$, 300 MHz), δ: 8.01 (d, 2H, *J*=8.3 Hz, H-Ar), 7.75 (d, 2H, *J*=8.3 Hz, H-Ar), 6.64 (s, 1H, CH-N), 5.84 (s, 1H, CH-N), 3.96 (s, 3H, $COOCH_3$), 2.39 (s, 1H, NH).

Table 2.4-3. ^{1}H-NMR characterization for each *trans*-pyrrolidino[60]fullerenes 27a-e.[197]

General procedure for *cis* adducts 27a-e:

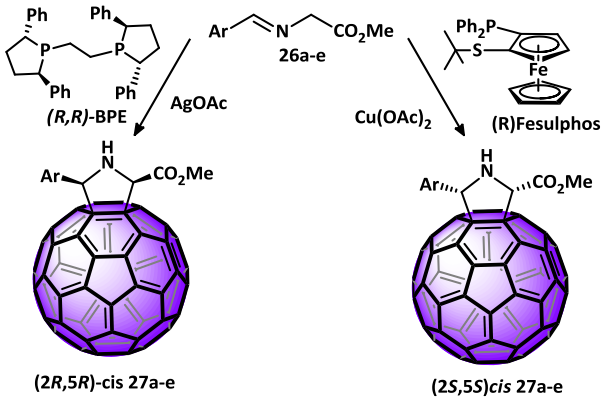

Figure 2.4-4. *Cis*-selective cycloaddition of *N*-metalated azomethine ylides onto [60]fullerene.

The chiral ligand (0.0028 mmol) and metal salt (0.0025 mmol) were dissolved in toluene (7 mL). The solution was stirred for 1h at room temperature, the mixture was cooled to -15º C, and then, a solution of α-iminoester **26a-e** (0.028 mmol) in toluene (1 mL) was added. Finally, C_{60} (0.025 mmol) was added. The reaction mixture was stirred for 2h, and afterwards, it was quenched with a saturated ammonium chloride solution (40 mL). The mixture was extracted with toluene (3 x 20 mL), and the combined extracts were washed with brine (30 mL). The organic layer was dried over $MgSO_4$ and concentrated *in vacuo*. The crude product was purified by silica gel flash chromatography.

Entry	Product	Chiral ligand	Metal salt	*cis:trans*	*e.e.cis* (%)	Yield (%)
1	**27a**	(*R*)Fesulphos	$Cu(OAc)_2$	99:1	92(2*S*,5*S*)	61
2	**27b**	(*R*)Fesulphos	$Cu(OAc)_2$	99:1	90(2*S*,5*R*)	45
3	**27c**	(*R*)Fesulphos	$Cu(OAc)_2$	99:1	90(2*S*,5*S*)	68
4	**27d**	(*R*)Fesulphos	$Cu(OAc)_2$	99:1	90(2*S*,5*S*)	46
5	**27e**	(*R*)Fesulphos	$Cu(OAc)_2$	99:1	88(2*S*,5*S*)	63
6	**27a**	(*R,R*)-BPE	AgOAc	99:1	90(2*R*,5*R*)	57
7	**27b**	(*R,R*)-BPE	AgOAc	99:1	80(2*R*,5*S*)	47
8	**27c**	(*R,R*)-BPE	AgOAc	99:1	90(2*R*,5*R*)	57
9	**27d**	(*R,R*)-BPE	AgOAc	99:1	85(2*R*,5*R*)	60
10	**27e**	(*R,R*)-BPE	AgOAc	99:1	86(2*R*,5*R*)	55

Table 2.4-4. Catalytic systems for the *cis*-pyrrolidino[60]fullerenes **27a-e** synthesis.

***cis*-27a**	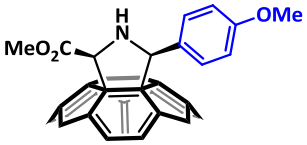	^{1}H-NMR ($CDCl_3$, 300 MHz), δ: 7.73 (d, 2H, *J* 8.6 Hz , H-Ar), 6.98 (d, 2H, *J*=8.6 Hz, H-Ar), 5.87 (s, 1H, CH-N), 5.70 (s, 1H, CH-N), 3.93 (s, 3H, CH_3O), 3.83 (s, 3H, $COOCH_3$), 1.76 (s, 1H, N-H).
***cis* -27b**	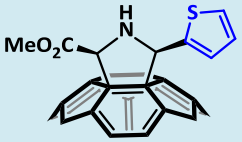	^{1}H-NMR ($CDCl_3$, 300 MHz), δ: 7.47 (d, 1H, *J* = 3.4 Hz, H-Ar), 7.40 (d, 1H, *J*=5.1 Hz, H-Ar), 7.12 (dd, 1H, *J*=5.0 Hz, 3.4 Hz, H-Ar), 6.19 (s, 1H, CH-N), 5.67 (s, 1H, CH-N), 3.94 (s, 3H, $COOCH_3$).
***cis*-27c**	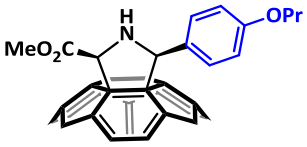	^{1}H-NMR ($CDCl_3$, 300 MHz), δ: 7.70 (d, 2H, *J* = 8.7 Hz, H-Ar), 6.97 (d, 2H, *J*=8.7 Hz, H-Ar), 5.84 (s, 1H, CH-N), 5.67 (s, 1H, CH-N), 3.95 (t, 2H, *J* 6.8 Hz, OCH_2), 3.93 (s, 3H, $COOCH_3$), 1.84 (q, 2H, *J*=7.2 Hz, OCH_2-CH_2), 1.07 (t, 3H, *J*=7.4 Hz, CH_3).
***cis* -27d**	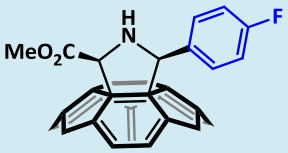	^{1}H-NMR ($CDCl_3$, 300 MHz), δ: 7.81 (dd, 2H, *J*=8.9, 5.3 Hz, H-Ar), 7.17 (t, 2H, *J*=8.9 Hz, H-Ar), 5.86 (s, 1H, CH-N), 5.67 (s, 1H, CH-N), 3.93 (s, 3H, $COOCH_3$).
***cis* -27e**	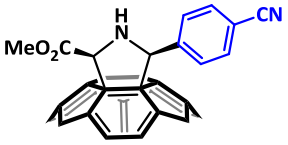	^{1}H-NMR ($CDCl_3$, 300 MHz), δ: 7.98 (d, 2H, *J*=8.2 Hz, H-Ar), 7.77 (d, 2H, *J*=8.2 Hz, H-Ar), 5.92 (s, 1H, CH-N), 5.67 (s, 1H, CH-N), 3.94 (s, 3H, $COOCH_3$), 2.37 (s, 1H, N-H).

Table 2.4-5. ^{1}H-NMR characterization for each *trans*-pyrrolidino[60]fullerenes **27a-e**.

c) Synthesis of enantiomerically pure pyrrolidino[70]fullerenes 28 and 29.[197]

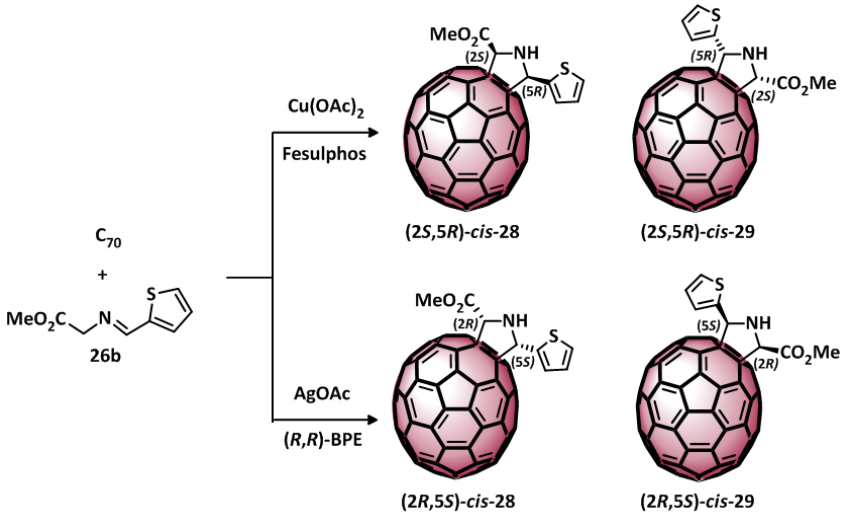

Figure 2.4-5. *Cis*-selective cycloaddition of *N*-metalated azomethine ylides onto [70]-fullerene.

Chiral ligand (0.0028 mmol) and metal salt (0.0025 mmol) were dissolved in toluene (7 mL). The solution was stirred for 1h. at room temperature, and then, a solution of α-iminoester **26b** (0.028 mmol) in toluene (1.5 mL) was added. The reaction mixture was cooled to -40º C and finally, C_{70} (0.025 mmol) was added. The reaction mixture was stirred overnight, and afterwards, it was quenched with a saturated ammonium chloride solution (40 mL). The mixture was extracted with toluene (3 x 20 mL), and the combined extracts were washed with brine (30 mL). The organic layer was dried over $MgSO_4$ and concentrated *in vacuo*. The crude product was purified by silica gel flash chromatography.

Entry	Product	Chiral ligand	Metal salt	*cis:trans*	*ee cis*(%)	Yield[a](%)
1	**28**	(*R*)Fesulphos	$Cu(OAc)_2$	99:1	96(2*S*,5*R*)	57
2	**28**	(*R*,*R*)-BPE	AgOAc	99:1	81(2*R*,5*S*)	60
3	**29**	(*R*)Fesulphos	$Cu(OAc)_2$	99:1	94 (2*S*,5*R*)	49
4	**29**	(*R*,*R*)-BPE	AgOAc	99:1	81(2*R*,5*S*)	55

[a] Yields calculated on the base of the total amount of monoadduct

Table 2.4-6. *Cis*-selective cycloaddition of *N*-metalated azomethine ylides onto C_{70}-fullerene.

***cis*-27**	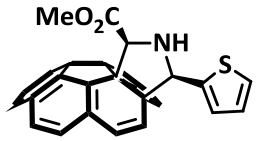	^{1}H-NMR ($CDCl_3/CS_2$, 700 MHz), δ: 7.45 (dd, 1H, *J*=3.5, 5.2 Hz, H-Ar), 7.16 (d, 1H, *J*=3.5 Hz, H-Ar), 6.97 (dd, 1H, *J*=3.6, 5.2 Hz, H-Ar), 5.32 (d, 1H, *J*=10.7 Hz, CH-N), 4.94 (d, 1H, *J*=10.7 Hz, CH-N), 4.23 (s, 3H, $COOCH_3$), 3.05 (t, 1H, *J*=10.6 Hz, NH)
***cis*-28**	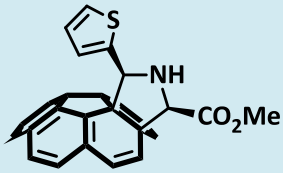	^{1}H-NMR ($CDCl_3/CS_2$, 700 MHz), δ: 7.58 (d, 1H, *J*=3.4 Hz, H-Ar), 7.55 (dd, 1H, *J*=1.1, 5.1 Hz, H-Ar), 7.31 (dd, 1H, *J*=3.4, 5.1 Hz, H-Ar), 5.44 (d, 1H, *J*=10.8 Hz, CH-N), 4.68 (d, 1H, *J*=10.8 Hz, CH-N), 3.79 (s, 3H, $COOCH_3$), 3.03 (t, 1H, *J*=10.8 Hz, NH)

Table 2.4-7. ^{1}H-NMR characterization for each *cis*-C_{70}-pyrrolidinofullerenes **28** and **29**. [186]

d) Molecular surgery based procedure for the synthesis of the endohedral $H_2O@C_{60}$ [184]

Synthesis of 3,6-bis(6'-*t*-butylpyridin-2'-yl)pyridazine (30)

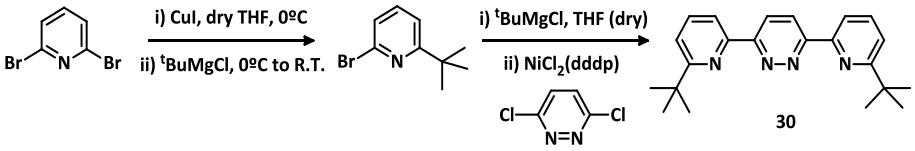

A mixture of 2,6-dibromopyrimidine (5.00 g, 21.29 mmol) and CuI (0.192 g, 1.01 mmol) in dry THF (20 mL) was degassed and charged with Ar and took it to 0ºC into a ice bath. A volume of 19.25 mL of a ^{t}BuMgCl (1.74 M in THF) was added dropwise and kept stirring during 5 hours. The reaction was stopped and 50 mL of NH_4Cl solution was added. The aqueous layer was extracted with ether (3 x 50 mL) and the mixture of organic layers was dried with Na_2SO_4, filtered and the solvent was removed. A dark oil was obtained and was purified by medium pressure column chromatography over silica gel using hexane as solvent to yield a colourless oil.

Then, the in situ synthesis of (6-*t*-butylpyridin-2-yl)magnesium bromide was accomplished from the 2-bromo-6-*tert*-butylpyridine (2.87, 13.4 mmol) previously prepared and magnesium powder (0.32 g, 13.5 mmol) in dry THF (20 mL) under reflux conditions. To a mixture of 3,6-dichloropyridazine (0.74 g, 5.00 mmol) and $NiCl_2$(dppp) (546 mg, 1.01 mmol) in dry THF (25 mL), the magnesium reagent was added and the mixture was stirred for 7 h at 65 °C. Saturated $NaHCO_3$ aqueous solution (50 mL) was added to the reaction mixture and the aqueous layer was extracted with $CHCl_3$ (50 mL × 3). The combined organic solution was dried over anhydrous Na_2SO_4. The solution was concentrated and the residue was purified by column chromatography

(silica gel, hexane / AcOEt = 5 / 1 as eluent) to provide the product as white powder (40%).

^{1}H-NMR ($CDCl_3$, 300 MHz), δ: 8.77 (s, 2H, H-4 and H-5 of pyridazine), 8.56 (d, 2H, J = 7.3 Hz, H-3' of pyridyl), 7.81 (t, 2H, J = 7.8 Hz, H-4' of pyridyl), 7.44 (d, 2H, J = 7.4 Hz, H-5' of pyridyl), 1.45 (s, 18H).

Synthesis of the 12-member open cage (31)

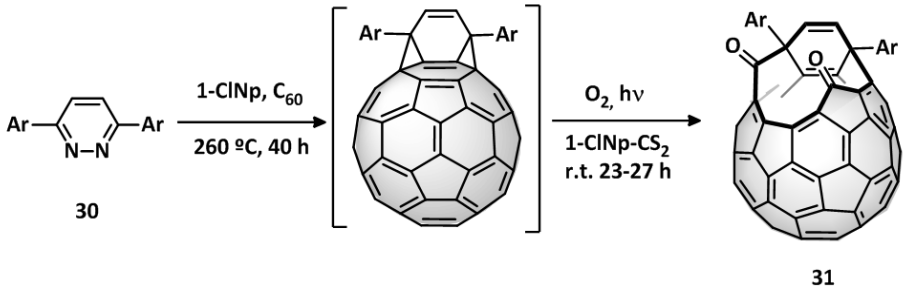

30 31

C_{60} (2.00 g, 2.78 mmol) and 3,6-bis(6-*tert*-butylpyridin-2-yl)pyridazine **30** (1.200 g, 3.46 mmol) was dissolved into 1-chloronaphthalene (80 mL) and the mixture was degassed under the reduce pressure, and then charged with argon gas for 5 times. The resulting mixture was refluxed at 260 °C for 40 h. Before carrying out the photochemical cleavage, the reaction mixture was checked by HPLC (Buckyprep, 30ºC, o-DCB), observing the intermediate product signal at t_R=3.68 min (80 %) and the remaining C_{60} at 8.00 min. (20 %). After cooling to room temperature, CCl_4 (220 mL) was added, the solution was purged with O_2, stirred during 30 minutes and then irradiated with 2 lamps (Xe, 500 W) during 24 hours, when total consumption of the intermediate is observed by HPLC. The desired product was isolated by column chromatography (silica gel, toluene as eluent) and CH_3CN was added to precipitate the product and centrifuged during 10 minutes to remove the remaining Cl-Naphtalene (44 %).

^{1}H-NMR ($CDCl_3$, 300 MHz), δ: 7.68 (t, 1H, *J* = 7.8 Hz, H-4 or H-4' of pyridyl), 7.65 (t, 1H, *J* = 7.8 Hz, H-4 or H-4' of pyridyl), 7.50 (dd, 1H, *J* = 0.7 Hz, 7.8 Hz, H-3 or H-3' of pyridyl), 7.38 (dd, 1H, *J* = 0.7 Hz, 7.8 Hz, H-3 or H-3' of pyridyl), 7.23 (d, 2H, *J* = 7.8 Hz, H-5 and H-5' of pyridyl), 7.21 (d, 1H, *J* = 10.0 Hz, vinylene), 7.17 (d, 1H, *J* = 10.0 Hz, vinylene), 1.26 (s, 9H, *t*-butyl), 1.17 (s, 9H, *t*-butyl).

Synthesis of the 16/13-member dynamic hole open cage (32)

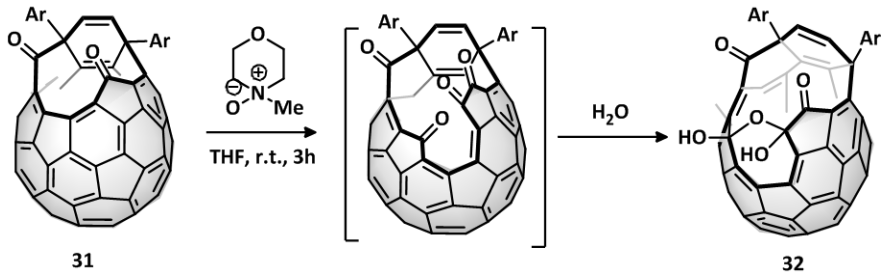

31 32

To a solution of **31** (1.3 g, 1.21 mmol) in dry THF (125 mL), *N*-methylmorpholine *N*-oxide (50.3 mg, 2.78 mmol) and distilled water (21.78 µl, 1.21 mmol) were added under argon atmosphere and the resulting mixture was stirred at room temperature for 3 h. After concentration of the reaction mixture under the reduced pressure, the residue was purified by column chromatography (silica gel, toluene/AcOEt = 5/1 as eluent). The second fraction was concentrated to provide the desired product as brown powder (90 %).

^{1}H-NMR ($CDCl_3$, 300 MHz), δ: 7.62 (t, 1H, J = 7.8 Hz, H-4 or H-4' of pyridyl), 7.56 (t, 1H, *J* = 7.8 Hz, H-4 or H-4' of pyridyl), 7.44 (d, 1H, J = 7.8 Hz, H-3 or H-3' of pyridyl), 7.21 (d, 2H, *J* = 7.8 Hz, H-5 and H-5' of pyridyl), 7.16 (d, 1H, *J* = 7.8 Hz, H-3 or H-3' of pyridyl), 7.09 (d, 1H, *J* = 10.0 Hz, vinylene), 6.95 (d, 1H, *J* = 10.0 Hz, vinylene), 1.22 (s, 9H, *t*-butyl), 1.16 (s, 9H, *t*-butyl).

Synthesis of the 16/13-member dynamic hole open cage with encapsulated H_2O (33)

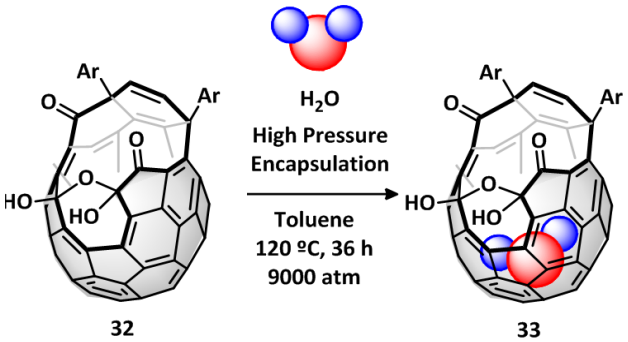

32 33

To a Teflon container a solution of **32** (350.0 mg, 0.3121 mmol) in toluene (10 mL) and distilled water (15 µL) were added and the lid was closed. The container was kept at 120 °C under 9,000 bar for 36 h. After getting back to ambient conditions, the resulting mixture was concentrated and the residue was dissolved in $CHCl_3$ (5 mL). The solution was mixed with CH_3CN (10 mL) and centrifuged . The resulting precipitates were collected and washed with

CH_3CN (5 mL × 3) to provide the water-encapsulating product as brown powder (95 %).

^{1}H-NMR ($CDCl_3$, 300 MHz), δ: 7.62 (t, 1H, *J* = 7.8 Hz, H-4 or H-4' of pyridyl), 7.56 (t, 1H, *J* = 7.8 Hz, H-4 or H-4' of pyridyl), 7.43 (d, 1H, *J* = 7.8 Hz, H-3 or H-3' of pyridyl), 7.21 (d, 2H, *J* = 7.8 Hz, H-5 and H-5' of pyridyl), 7.16 (d, 1H, *J* = 7.8 Hz, H-3 or H-3' of pyridyl), 7.09 (d, 1H, *J* = 10.0 Hz,vinylene), 6.94 (d, 1H, *J* = 10.0 Hz, vinylene), 1.22 (s, 9H, *t*-butyl), 1.16 (s, 9H, *t*-butyl), –9.87 (s, 2H, H_2O).

Synthesis of the 8-member open cage with encapsulated H_2O (34)

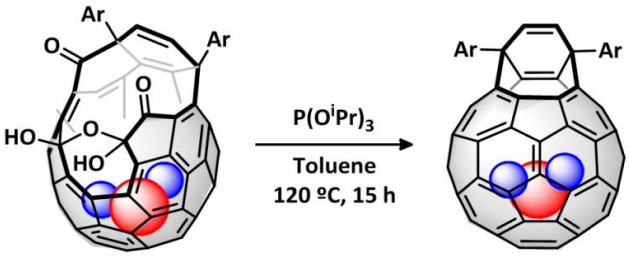

33 **34**

In a Schlenk tube, a solution of **33** (280.0 mg, 0.24 mmol) in dry toluene (34 mL) was bubbled with argon to remove oxygen. To the solution, P(O*i*Pr)$_3$ (5.0 mL, 20.27 mmol) was added and the mixture was stirred at 120 °C for 15 h. The reaction mixture was concentrated and the residue was purified by column chromatography (silica gel, toluene as eluent) to provide a product as brown oil. The oil was dissolved in $CHCl_3$ (5 mL) and mixed with CH_3CN (10 mL). The resulting precipitates were collected and washed with CH_3CN (5 mL × 3) to provide the product as brown powder (50% yield).

^{1}H-NMR ($CDCl_3$, 300 MHz), δ: 7.77 (t, 2H, *J* = 7.8 Hz, H-4 of pyridyl), 7.70 (d, 2H, *J* = 7.1 Hz, H-3 of pyridyl), 7.32 (d, 2H, *J* = 7.6 Hz, H-5 of pyridyl), 6.46 (s, 2H, vinylene), 1.35 (s, 18H, *t*-butyl), –6.10 (s, 2H, H_2O).

Synthesis of $H_2O@C_{60}$

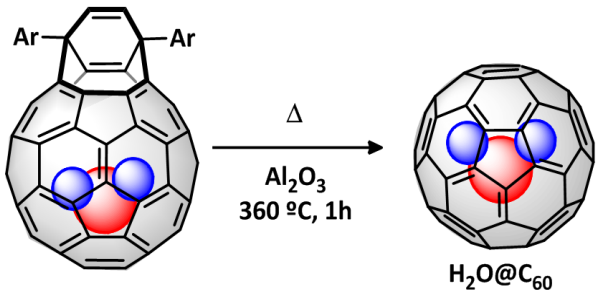

34 **35**

A mixture of **34** (49.9 mg, 0.0472 mmol) and neutral alumina (1.005 g) (mixed with a mortar and a pestle) was lightly wrapped with an aluminum foil and heated at 360 °C for 1 h under vacuum (< 1 mm Hg). The reaction mixture was mixed with CS_2 (3 mL) and the resulting mixture was poured onto column chromatography (silica gel, CS_2/hexane = 1/1 as eluent) to separate products. The first fraction was concentrated to provide the desired product as brown powder (30 %).

^{1}H-NMR ($CDCl_3$, 300 MHz), δ: –4.81 (s, 2H, H_2O).

e) Synthesis of enantiomerically pure endohedral pyrrolidinofullerenes 35a

Synthesis of (2*R*,5*R*) *cis*-35a

(*R*,*R*)-BPE (8.1 μmol) and silver acetate (8.0 μmol) were dissolved in toluene (20 mL). The solution was stirred for 45 min. at room temperature. Then, 1 mL of this solution was mixed with a solution of α-iminoester **26a** (4.5 μmol) in toluene (1 mL) and cooled to -15º C. Finally, $H_2O@C_{60}$ (4.1 μmol) was also added. The reaction mixture was stirred for two hours, and afterwards, it was quenched with a saturated ammonium chloride solution (3 mL). The mixture was extracted with toluene (3 x 2 mL), and the combined extracts were washed with brine (3 mL). The organic layer was dried over $MgSO_4$ and concentrated *in vacuo*. The crude product was purified by semipreparative HPLC chromatography.

Synthesis of (2*S*,5*S*) *cis*-35a

(*R*)-Fesulphos (4.1 μmol) and copper (II) acetate (4.0 μmol) dissolved in toluene (10 mL) were stirred for 45 min. at room temperature. Then, 1 mL of this solution were mixed with a solution of α-iminoester **26a** (4.5 μmol) in toluene (1 mL), and the mixture was cooled at -15º C. Finally $H_2O@C_{60}$ (4.1 μmol) was also added. The reaction was stirred for two hours, and afterwards, it was quenched with a saturated ammonium chloride solution (3 mL). The mixture was extracted with toluene (3 x 2mL), and the combined extracts were washed with brine (3 mL). The organic layer was dried over $MgSO_4$ and concentrated *in vacuo*. The crude product was purified by semipreparative HPLC chromatography.

Cis-2-methoxycarbonyl-5-(_p_-methoxyphenyl)pyrrolidino[3,4:1,2]H_2O@C_{60} (_cis_-35a)

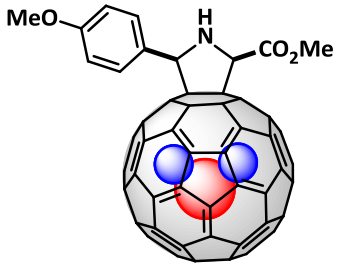

^{1}H-NMR ($CDCl_3$, 700 MHz), δ: 7.77 (d, 2H, *J*=8.6 Hz , H-Ar), 7.00 (d, 2H, *J*=8.6 Hz, H-Ar), 5.94 (s, 1H, CH-N), 5.77 (s, 1H, CH-N), 3.96 (s, 3H, CH_3O), 3.85 (s, 3H, $COOCH_3$), -7.87 (s, 2H, H_2O@).

^{13}C NMR (175 MHz, $CDCl_3$), δ: 170.12, 159.74, 153.31, 152.81, 152.71, 151.25, 150.89, 148.43, 147.36, 147.27, 147.02, 146.85, 146.47, 146.42, 146.38, 146.33, 146.26, 146.23, 146.18, 146.10, 146.00, 145.74, 145.69, 145.60, 145.58, 145.55, 145.52, 145.45, 145.42, 145.33, 145.28, 144.69, 144.58, 144.50, 144.41, 144.34, 143.64, 143.24, 143.19, 143.16, 143.10, 143.06, 142.84, 142.81, 142.54, 142.51, 142.43, 142.40, 142.14, 142.11, 142.06, 141.82, 141.69, 140.35, 140.12, 139.88, 139.85, 139.60, 137.45, 137.13, 136.23, 135.64, 132.33, 130.14, 129.36, 128.12, 123.57, 122.64, 79.41, 75.80, 75.77, 73.34, 55.29, 52.83.

MS (MALDI-TOF): calculated for $C_{71}H_{16}NO_4$ $[M+H]^+$ 946.1079, found 946.1091.

HPLC: *Buckyprep Waters* 4.6 x 250 mm toluene/acetonitrile 9:1 flow rate 0.75 mL/min; t_R = 6.9 min; Chiral HPLC *Pirkle Covalent (R,R) Whelk-02*; hexane/methanol 97:3, flow rate 1.25 mL/min, t_R = 24.0 min isomer *(2R, 5R)* and 28.1 min isomer *(2S, 5S)*; $[\alpha]_D^{20}$: +17.5 (c 0.08 $CHCl_3$) for *(2R, 5R)*; $[\alpha]_D^{20}$: -17.5 (c 0.08 $CHCl_3$) for *(2S, 5S)*.

e.e.=94% (2*S*,5*S*) with $Cu(OAc)_2$/(*R*)Fesulphos; 90% (2*R*,5*R*) with AgOAc/(*R,R*)-BPE

Synthesis of (2*S*,5*R*) or (2*R*,5*S*)-*trans*-35a

(*R*) or (*S*)-DTBM-Segphos (2.9 μmol) and copper(II)triflate (2.8 μmol) were dissolved in toluene (10 mL). The solution was stirred for 30 min at room temperature getting a slight blue colour. Then, 1 mL of this solution was mixed with a solution of α-iminoester **26a** (2.8 μmol) in toluene (1 mL) obtaining a yellow mixture. Finally, H_2O@C_{60} (2.5 μmol) and 1mL of a solution of triethylamine in toluene (10.5 μmol in 20 mL) were added. The reaction mixture was stirred for one hour, and afterwards, it was quenched with a saturated ammonium chloride solution (3 mL). The mixture was extracted

with toluene (3 x 1mL), and the combined extracts were washed with brine (3 mL). The organic layer was dried over $MgSO_4$ and concentrated *in vacuo*. The crude product was purified by semipreparative HPLC chromatography.

***Trans*-2-methoxycarbonyl-5-(*p*-methoxyphenyl)pyrrolidino[3,4:1,2]-H_2O@C_{60} (*trans*-35a)**

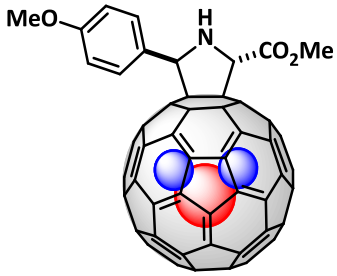

^{1}H-NMR ($CDCl_3$, 700 MHz), δ: 7.81 (d, 2H, *J*=8.4 Hz , H-Ar), 6.98 (d, 2H, *J*=8.5 Hz, H-Ar), 6.54 (s, 1H, CH-N), 5.85 (s, 1H, CH-N), 3.96 (s, 3H, CH_3O), 3.84 (s, 3H, $COOCH_3$), -7.87 (s, 2H, H_2O@).

MS (MALDI-TOF): calculated for $C_{71}H_{16}NO_4$ $[M+H]^+$ 946.1079, found 946.1092.

HPLC: *Buckyprep Waters* 4.6 x 250 mm toluene/acetonitrile 9:1 flow rate 0.75 mL/min; t_R = 6.3 min; Chiral HPLC *Pirkle Covalent (R,R) Whelk-02*; hexane/methanol 97:3, flow rate 1.25 mL/min, t_R = 15.9 min isomer *(2S, 5R)* and 17.6 min isomer *(2R, 5S*); $[\alpha]_D^{20}$: +133 (c 0.06 $CHCl_3$) for *(2S, 5R)*; $[\alpha]_D^{20}$: -133 (c 0.06 $CHCl_3$) for *(2R, 5S*).

e.e.=93% (2*S*,5*R*) with (*S*)-DTBM-Segphos; 93% (2*R*,5*S*) with (*R*)-DTBM-Segphos

f) *Cis-trans* isomerization experiments

A freshly prepared 0.4 mM solution of diastereo and enantiomerically pure *cis* or *trans* fulleropyrrolidine in 1-chloronaphthalene/acetonitrile 1/10 (or toluene/acetonitrile 1/10) was stirred at 35ºC. The reaction was monitored by TLC, ^{1}H NMR and HPLC. In the case of kinetic experiments for comparing the endohedral and the empty derivatives, following the general procedure, two solutions of (2*S*,5*S*)*cis*-**27a** and (2*S*,5*S*)*cis*-**35a** were prepared at the same time and with exactly the same molar concentration (0.35mM). They were stirred at 35ºC and the reaction progress was analyzed every 24h by HPLC.

Conclusions and remarks

CONCLUSIONS AND REMARKS

In the light of the results obtained during this thesis work, the next conclusions can be established.

Conclusions to ***Chapter 1: Carbon nanotubes and graphene chemistry***

A series of nanoconjugates containing the latest discovered carbon nanoforms (SWNT, MWNT and graphene) and bearing π-exTTF motifs have been synthesized and characterized by the main techniques for this kind of materials (FTIR, Raman spectroscopy, TGA, and XPS analysis as well as by TEM microscopy).

A comprehensive study of the different chemical reactivity against arylation and CuAAC reactions has been accomplished. The results revealed SWNT to be more reactive against arylation reactions compared to MWNT and graphene. In contrast, the major density of phenyl groups containing alkyne groups in **SWNT-1** seems to involve a hindrance in the subsequently CuAAC reactions. The lower functionalization degree in **MWNT-1** and its better solubility compared to **SWNT-1** seems to avoid this problem leading to excellent yields in the CuAAC reaction. The graphene planarity combined with its high tendency to stack afforded a lower reactivity in both type of reactions.

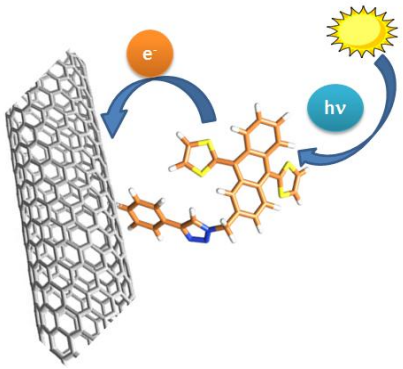

- Depictive image of **SWNT-2** in the process of charge transfer.

The presence of π-exTTF motifs in **CNF-2** and **CNF-3** was expected to involve an electronic communication between the donor units (π-exTTF) and the acceptor units (SWNT, MWNT and graphene). This fact was investigated in **SWNT-2**, **MWNT-2** and **GR-2** by cyclic voltamperometry, observing the corresponding π-exTTF oxidations waves. In the case of **SWNT-2**, which exhibits a major functionalization degree, this finding was corroborated by photophysical measurements. A new transition absorption maximum around 600 to 800 nm range is observed upon photoexcitation. This latter

was an unequivocal probe of the one-electron oxidized π-exTTF, what confirms the formation of the charge separated state in the nanoconjugate.

The improvement in the dispersibility was clearly observed in SWNT, where TEM images revealed a higher disaggregation and the presence of smaller bundles of nanotubes.

Several experiments were performed in order to check the ability of CNF containing a molecular tweezer to recognize C_{60} fullerene. The preliminary titration experiment of the isolated tweezer **18** vs. C_{60} by UV-vis spectroscopy revealed a moderate binding constant K_a. The interaction of both **SWNT-3** and **MWNT-3** with C_{60} was clearly corroborated by the same technique by observing a quenching in the CNF absorption features upon the C_{60} additions at the time that the π-exTTF absorption decreased and a new charge transfer band is generated, as observed in the titration experiment [**18**·C_{60}].

A comprehensive study in the nature of the interaction π-exTTF tweezer- C_{60} was performed by ^{1}H-NMR. Two new analogous receptors containing TCAQ (**22**) and benzene (**24**) units as recognition motifs were synthesized and compared with the above mentioned **18**. The ^{1}H-NMR titrations experiments revealed very similar values for K_a and a major role of the central phenyl and the C-H in triazole rings in the interaction, whereas the role of the benzene rings of the anthracene units is significantly less important.

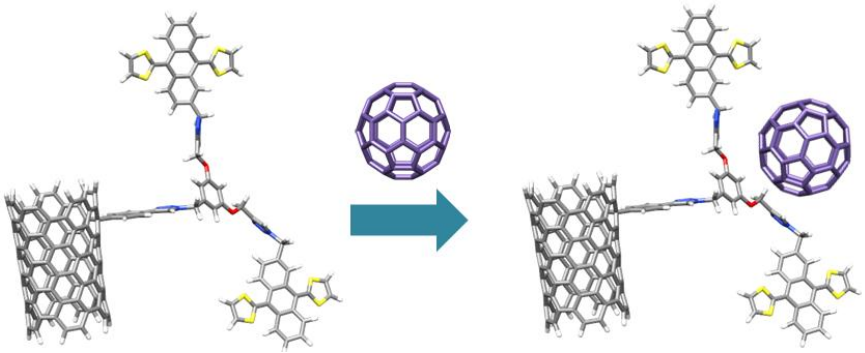

- Formation of the supramolecular complex between **CNF-3** and C_{60}.

These observations were underpinned by theoretical calculations by means of the Density Functional Theory (DFT) using the dispersion-corrected exchange-correlation B97D functional with the 6-31G** basis set. The very similar values found for K_a were explained by the large inner reorganization in the free state of **18** and **22** tweezers, what produced a considerable reduction of the interaction energy in the dimer complex.

Conclusions to ***Chapter 2: Chemical reactivity of endohedral fullerenes***

Unprecedented hydrogen addition in the 1,3-dipolar cycloaddition reaction on La@C_s-C_{82}.

The almost unexplored La@C_s-C_{82} has been studied upon *Prato* reactions and an expected selectivity has been found in the reaction, affording only two products with the highest reported yields to the date in this EMF. This finding was only observed when a droplet of toluene is added to the reaction medium.

The ESR analysis, MALDI-TOF MS, 1D and 2D-^{1}H-NMR experiments on these cycloadducts of La@C_s-C_{82} (**25a** and **25b-O**) revealed the presence of an unexpected H atom on the cage what stabilize the starting paramagnetic cage in a diamagnetic product by means of a radical addition process.

Derivative **25a** demonstrated a good stability under ambient conditions while **25b** was rapidly oxidized by nucleophilic substitution affording product **25b-O**.

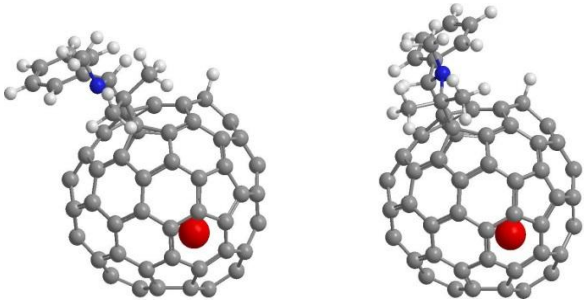

- Structure for **25a** and **25b** elucidated by means of the combination of NMR, MS, ESR and DFT-theoretical calculations.

The order in the reactions (i: Cycloaddition reaction + H-addition or ii: H-addition + Cycloaddition *reaction*) was studied by different thermal experiments using deuterated solvents, revealing that the H-addition is a very slow process and takes place after the *Prato* reaction.

DFT calculations were performed in order to unveil the addition pattern of both derivatives utilizing different criteria where the radical character seems to be the driving force and the different orientation of the phenyl substituent may be the reason of the rapid oxidation of **25b** in contrast to **25a**.

Study of the encapsulated H_2O molecule role in the cis/trans isomerization proccess of pyrrolidinofullerenes

A novel enantiospecific *cis-trans* isomerization in optically pure pyrrolidinofullerenes under mild conditions in polar solvents has been described. The process was found to involve a C2 configuration retention

and a mechanism involving a zwitterionic intermediate was proposed and studied at three different levels: i) different electron character of the substituent, ii) different cage geometry and iii) influence of inner species in the cage.

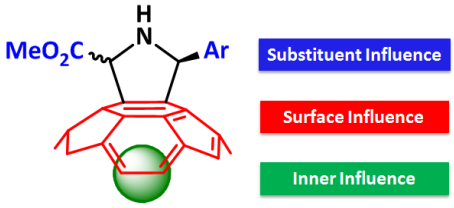

- Three different levels studied for the isomerization process in fulleropyrrolidines.

Pyrrolidino[60]fullerenes bearing substituents with different electronic character were synthesized and its isomerization process was studied revealing that electron-releasing substituents in the aryl group favour the process in contrast to that found for electron-withdrawing substituents.

Pyrrolidino[70]fullerenes were studied under the same conditions revealing that the zwitterionic intermediate is more stabilized when the charge is localized on the equatorial carbon atoms, favouring the isomerization process.

Analogous fulleropyrrolidine derivatives were synthesized on endohedral fullerene $H_2O@C_{60}$ and the isomerization process was studied under the same conditions. The process demonstrated to be more favourable in the endohedral derivatives by means of H bond assistance. This interaction may stabilize the zwitterionic intermediate, setting a precedent to the development of a novel “inner” manner to influence the stereochemical outcome in fullerene chemistry.

DFT calculations corroborate the enantiospecific result of the isomerization and the relative stabilities of reaction intermediates, thus supporting the proposed stepwise mechanism involving a zwitterionic intermediate with a C2 retention.

Annexe 1: Molecular materials spectra gallery and related data

Compound 17

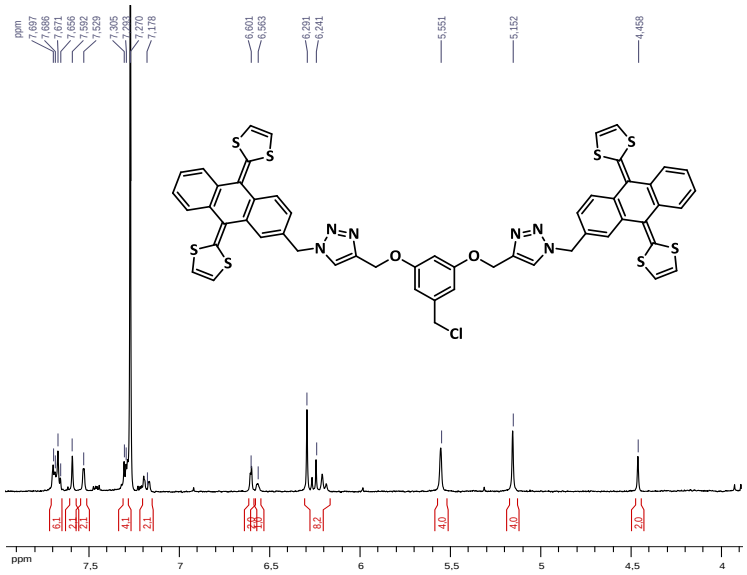

Figure A1-1. ^{1}H-NMR ($CDCl_3$, 300 MHz) of compound **17**.

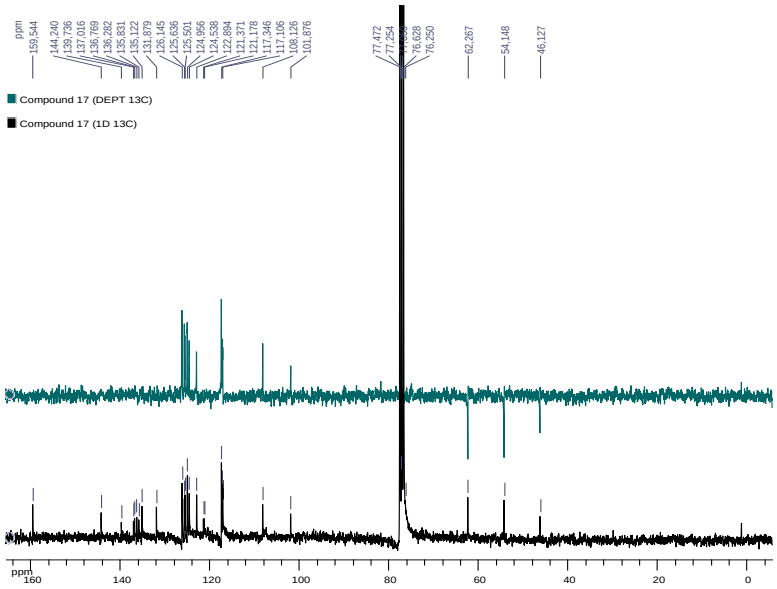

Figure A1-2. ^{13}C-NMR ($CDCl_3$, 75MHz) of compound **17**.

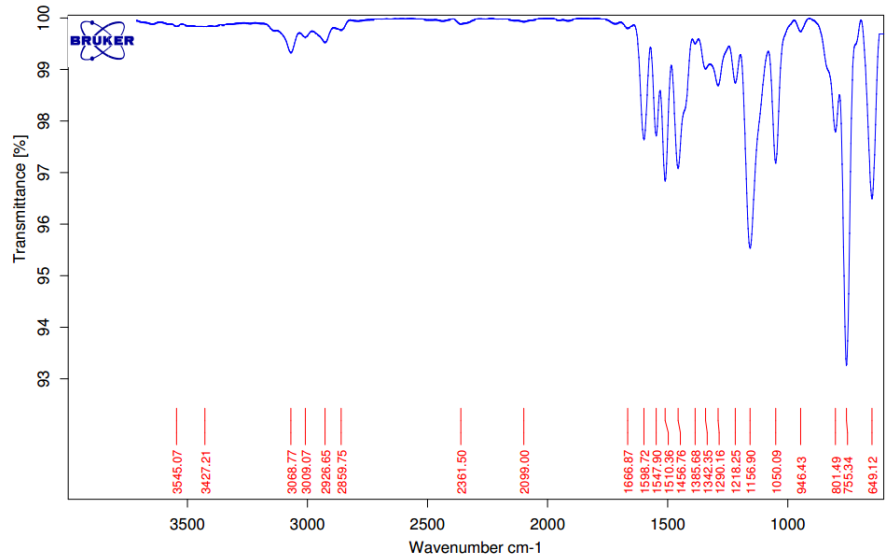

Figure A1-3. FTIR in $CHCl_3$ of compound **17**.

Compound 18

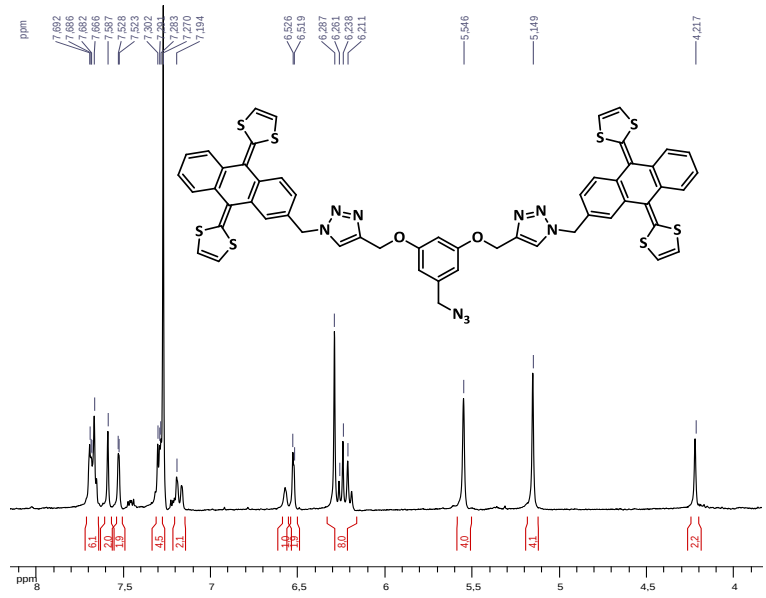

Figure A1-4. ^{1}H-NMR ($CDCl_3$, 300 MHz) of compound **18**.

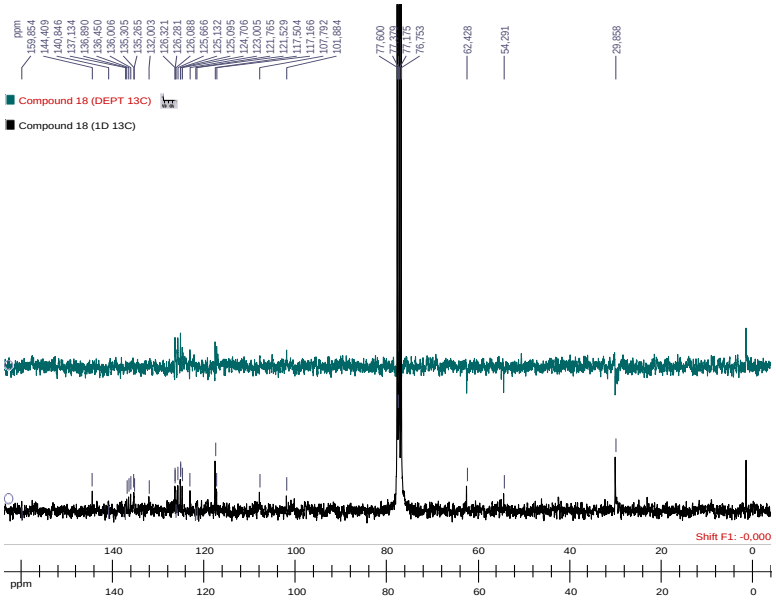

Figure A1-5. ^{13}C-NMR ($CDCl_3$, 75 MHz) of compound **17**.

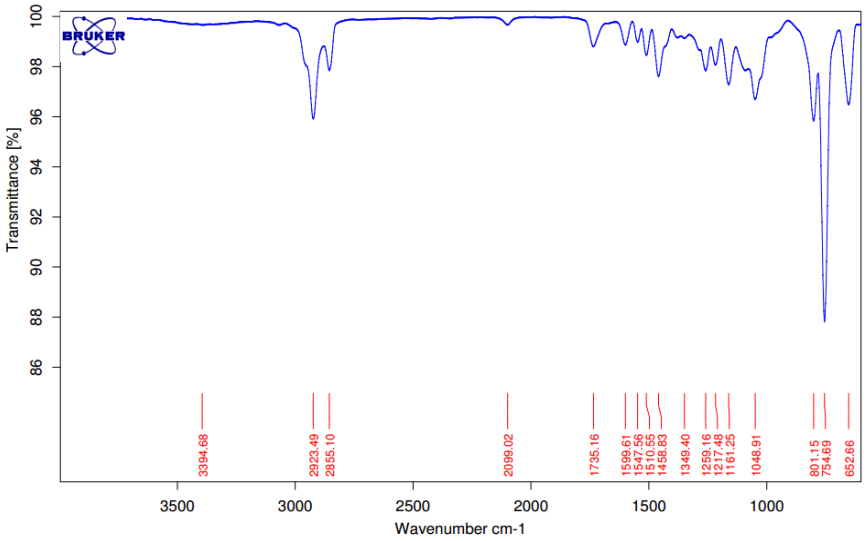

Figure A1-6. FTIR in $CHCl_3$ of compound **17**.

Compound 19

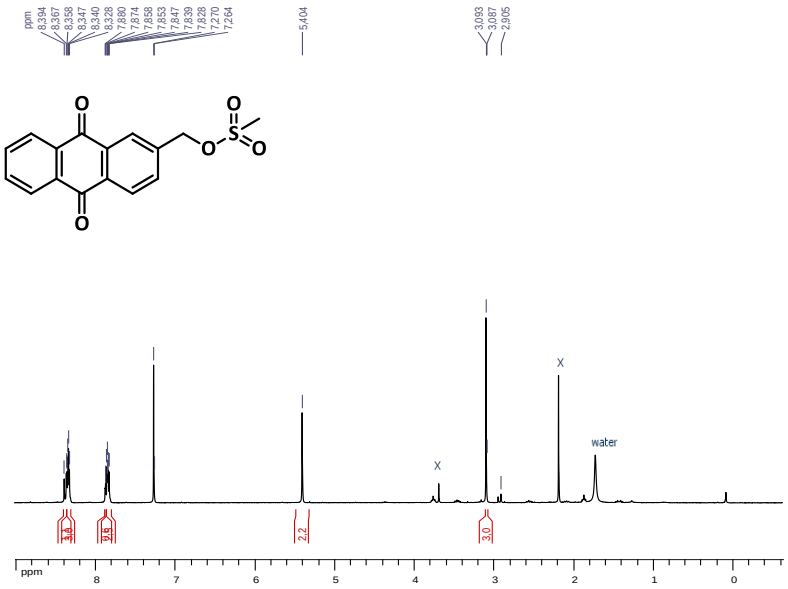

Figure A1-7. ^{1}H-NMR ($CDCl_3$, 300 MHz) of compound **19**.

Compound 21

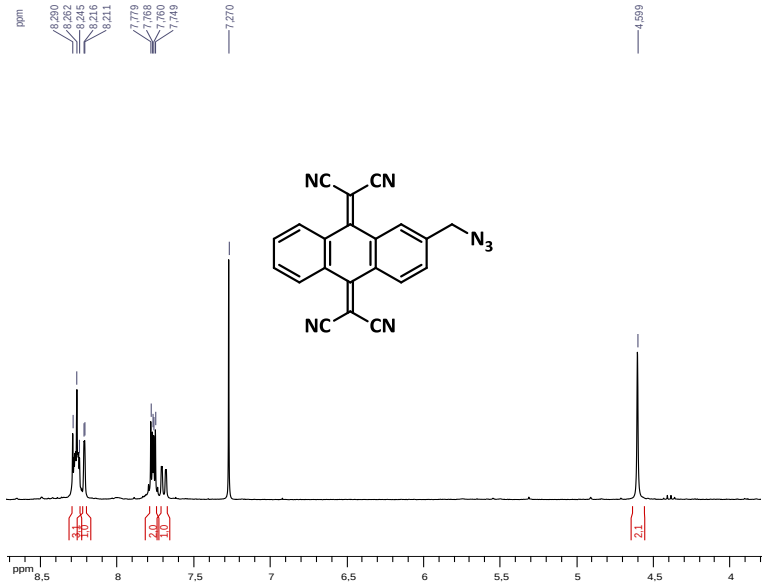

Figure A1-8. ^{1}H-NMR ($CDCl_3$, 300 MHz) of compound **21**.

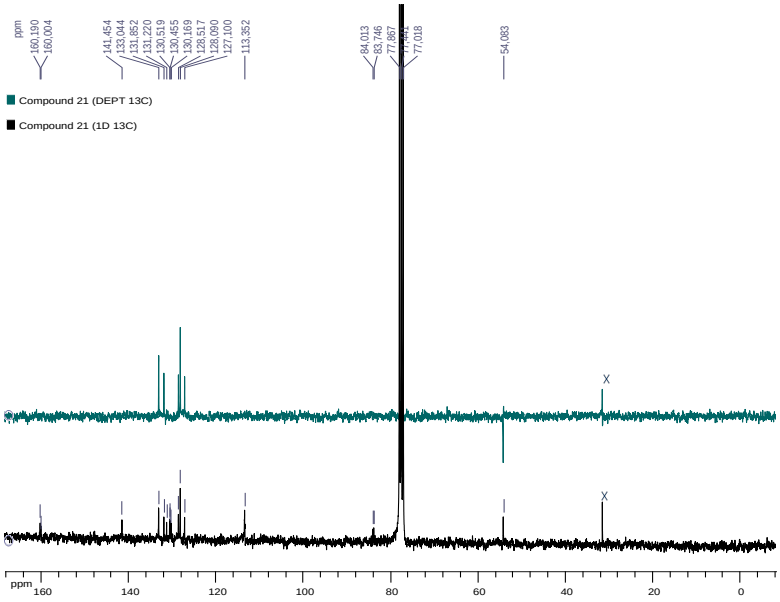

Figure A1-9. ^{13}C-NMR ($CDCl_3$, 75 MHz) of compound **21**.

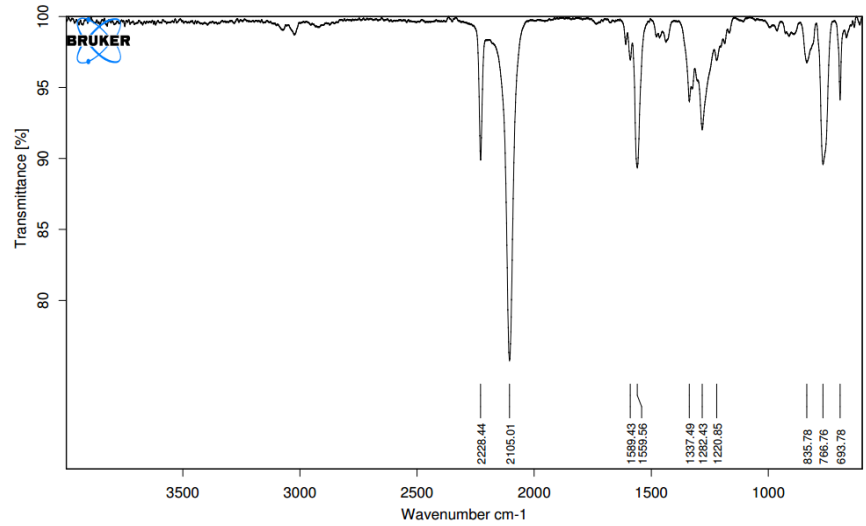

Figure A1-10. FTIR in $CHCl_3$ of compound **21**.

Compound 22

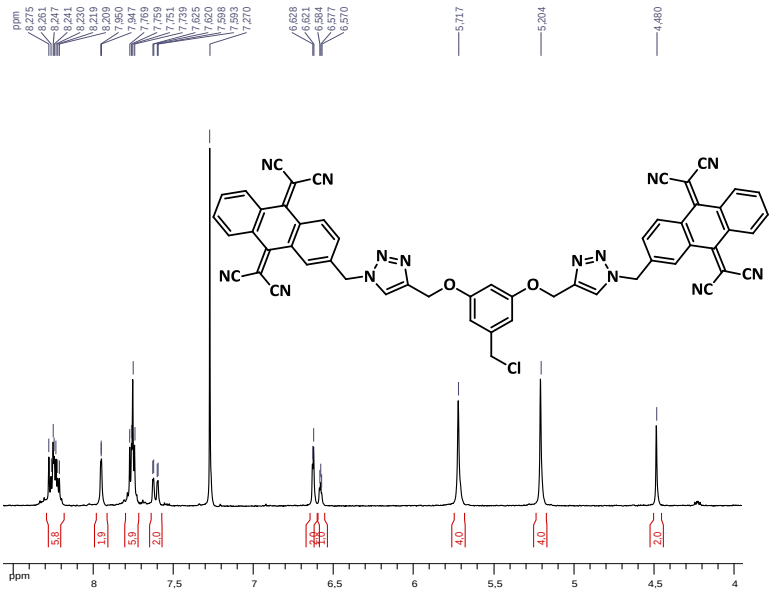

Figure A1-11. ^{1}H-NMR ($CDCl_3$, 300 MHz) of compound **22**.

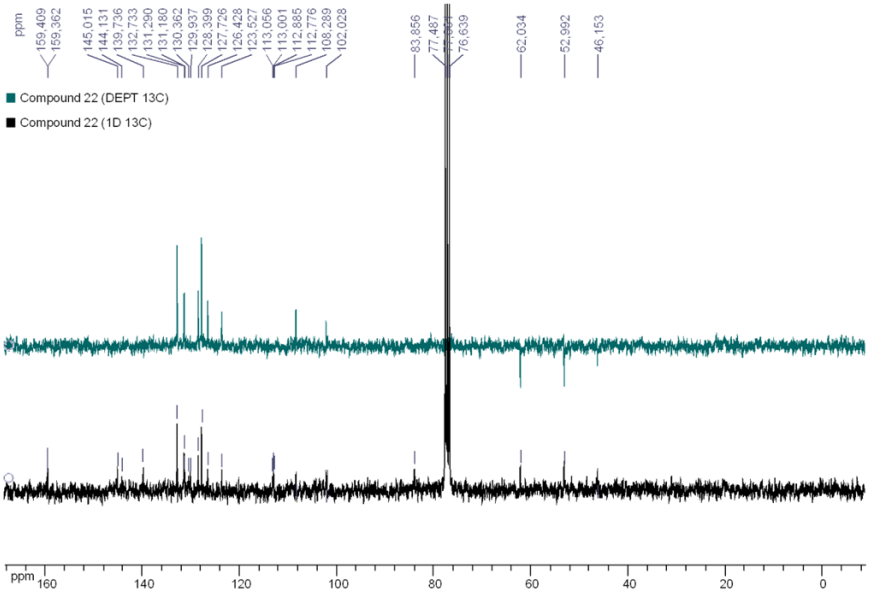

Figure A1-12. ^{13}C-NMR ($CDCl_3$, 75 MHz) of compound **22**.

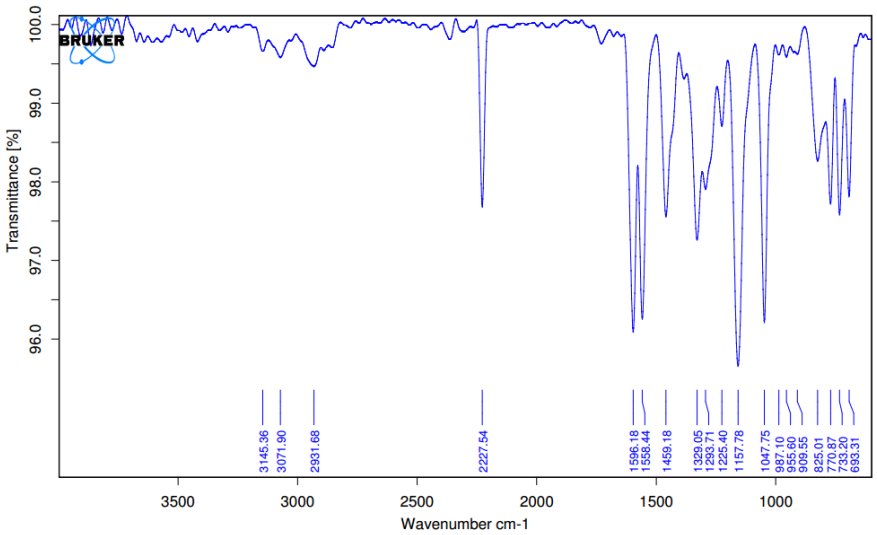

Figure A1-13. FTIR in $CHCl_3$ of compound **22**.

Compounds 25a and 25b

^{1}H-NMR

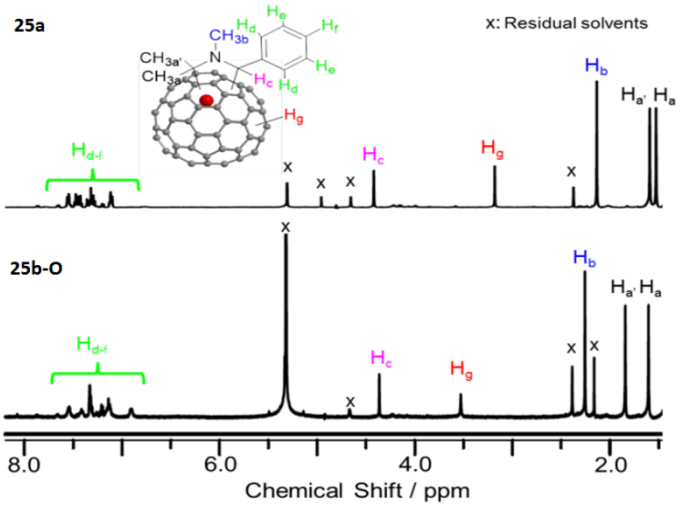

Figure A1-14. ^{1}H-NMR (500 MHz, CS_2/CD_2Cl_2 (3:1)) of compounds **25a** and **25b-O**.

^{13}C-NMR

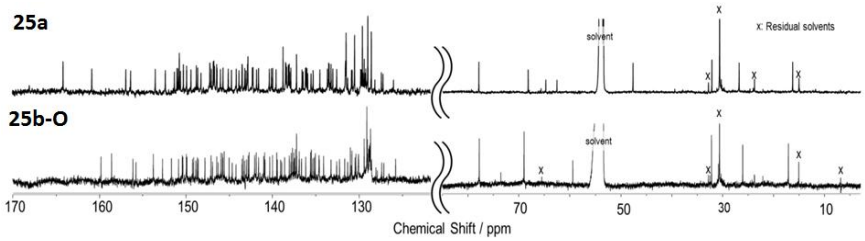

Figure A1-15. ^{13}C-NMR (125 MHz, CS_2/CD_2Cl_2 (3:1)) of compounds **25a** and **25b-O**.

DEPT-135

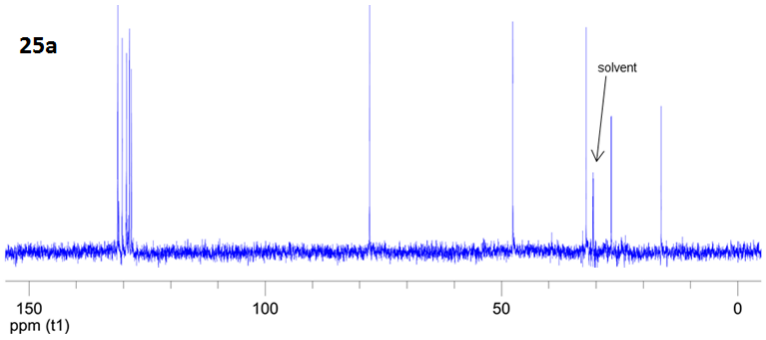

Figure A1-16. DEPT-135 (125 MHz, CS_2/CD_2Cl_2 = 3/1 (v/v)) of compounds **25a**.

HSQC

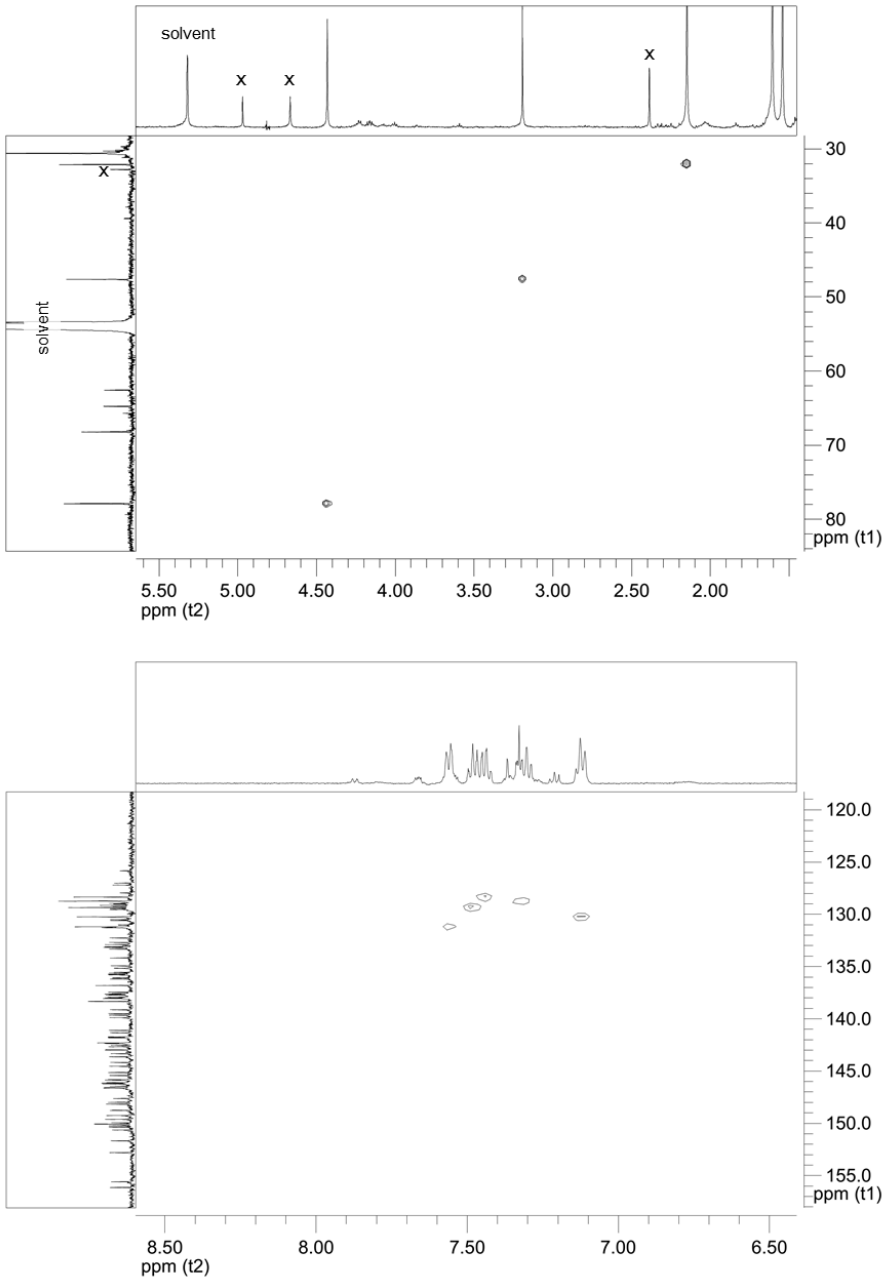

Figure A1-17. HSQC spectra of **25a** in CS_2/CD_2Cl_2 = 3/1 (v/v).

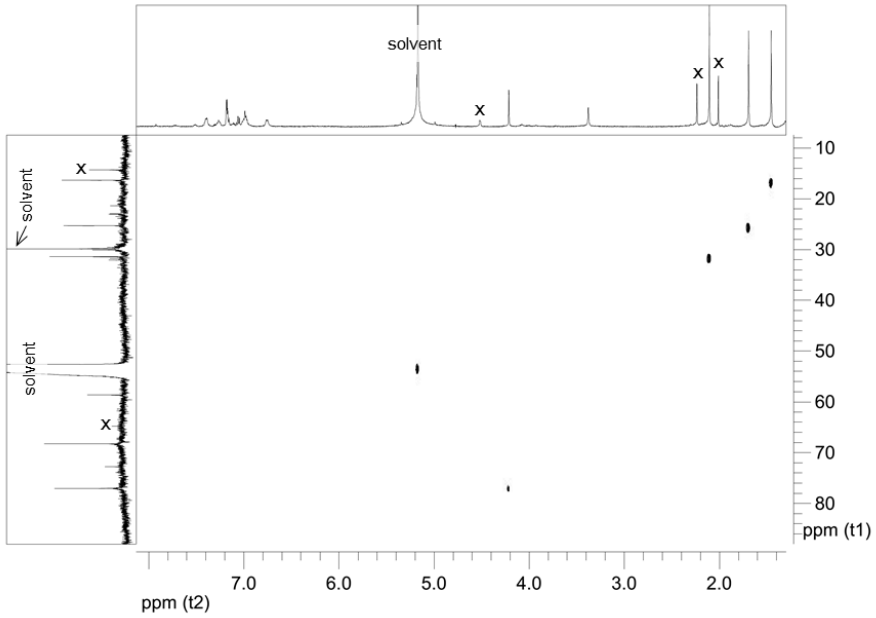

Figure A1-18. HSQC spectrum of **25b-O** in CS_2/CD_2Cl_2 = 3/1 (v/v).

HMBC

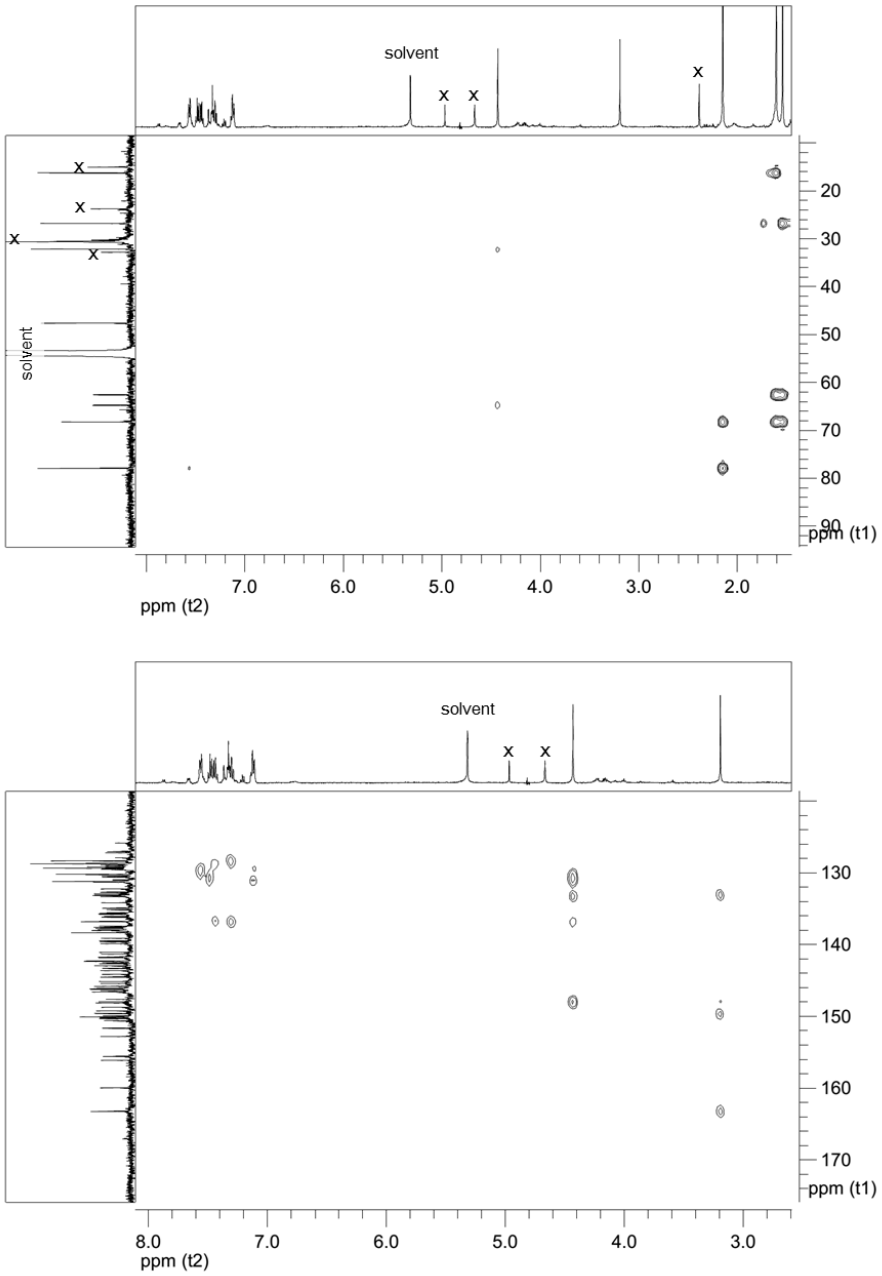

Figure A1-19. HMBC spectrum of **25a** in CS_2/CD_2Cl_2 = 3/1 (v/v).

ROESY

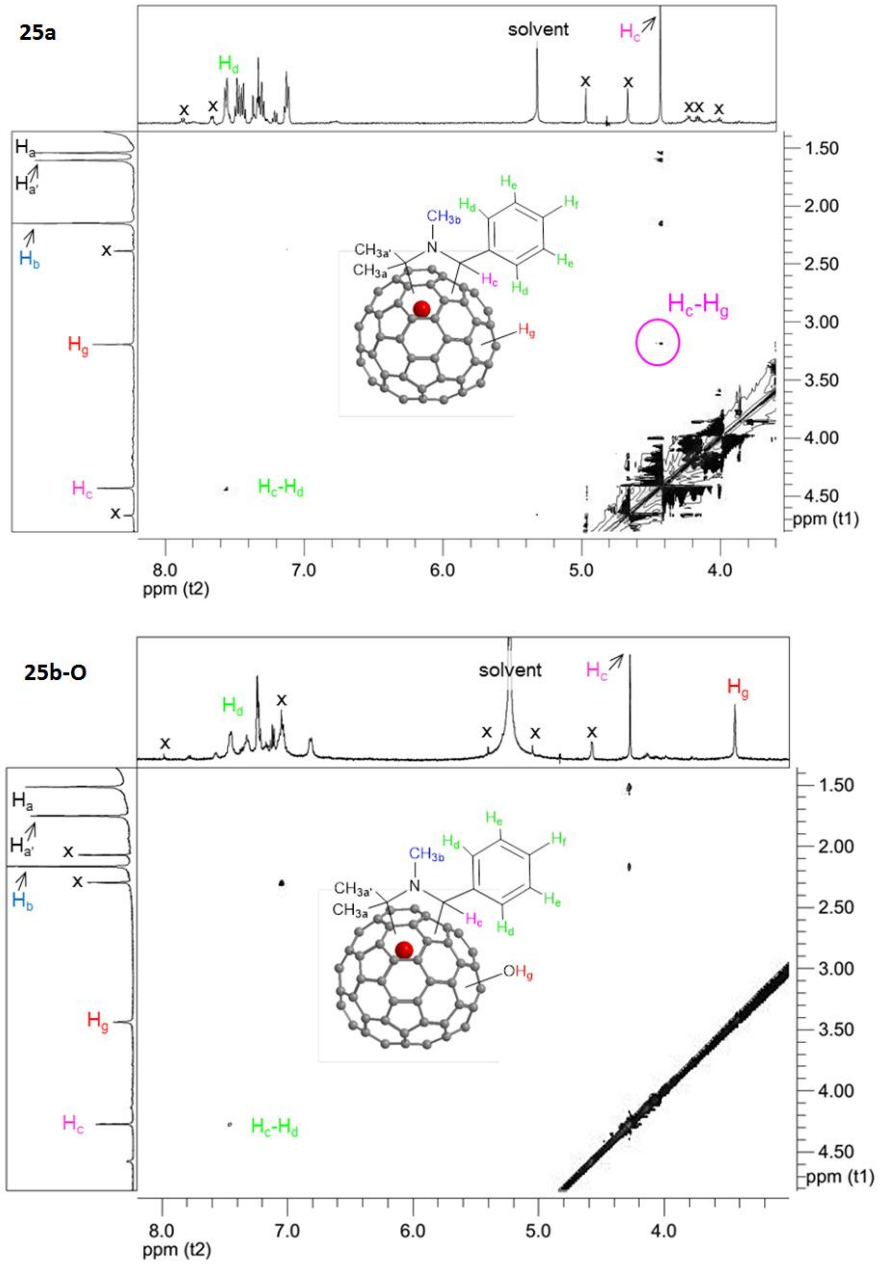

Figure A1-20. ROESY spectrum of **25a** (upper) and **25b**-O (bottom) in CS_2/CH_2Cl_2 = 3/1 (v/v) at 500 MHz. **25a** shows a correlation between H_c and H_g whereas **25b-O** does not show it.

UV-Vis SPECTROSCOPY

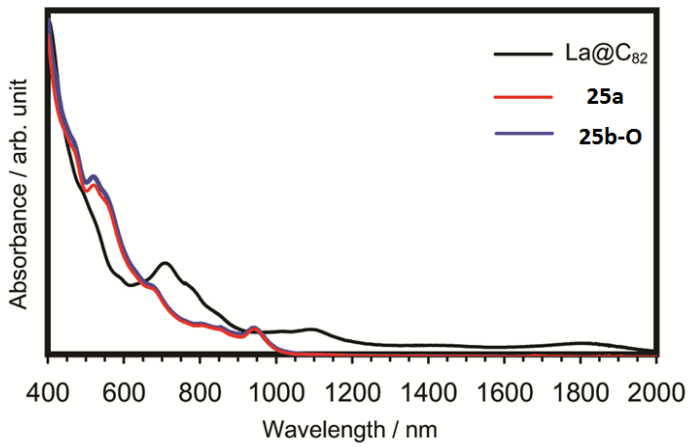

Figure A1-21. UV-Vis spectroscopy for compounds **25a** and **25b-O** (bottom).

Compounds *cis*-**35a** and *trans*-**35a**

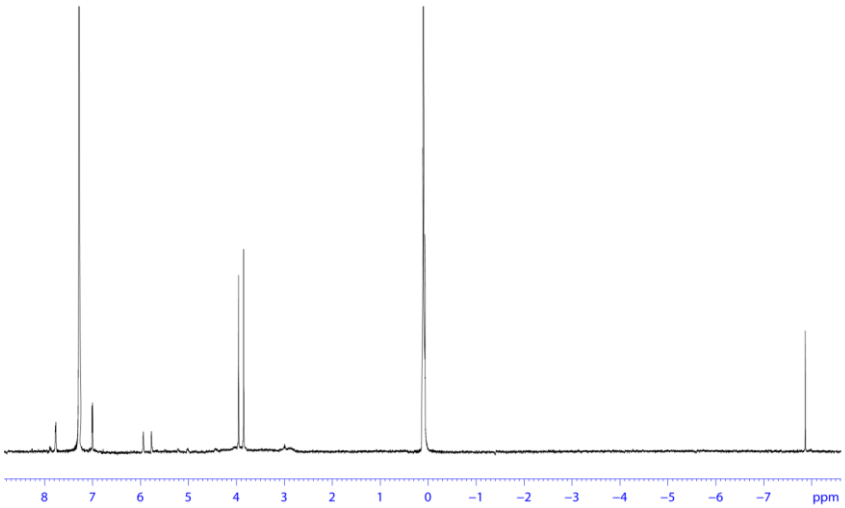

Figure A1-22. ^{1}H-NMR spectrum (700 MHz, $CDCl_3$) of *cis*-**35a**.

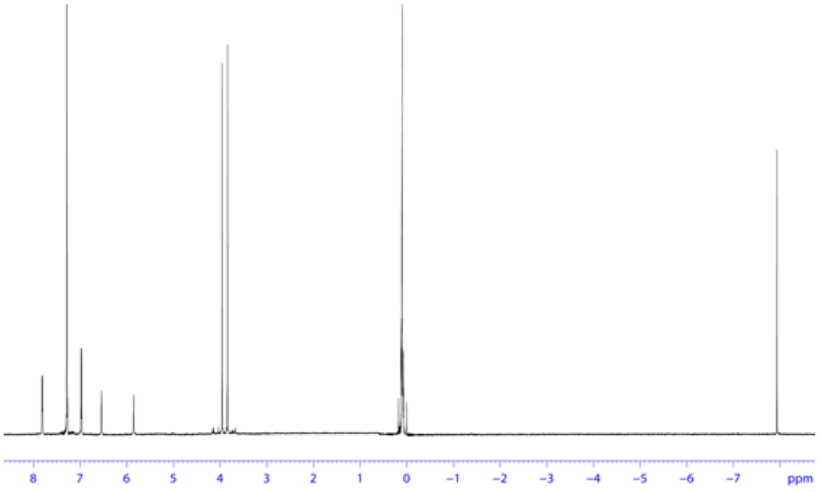

Figure A1-23. ^{1}H-NMR spectrum (700 MHz, $CDCl_3$) of *trans*-**35a**.

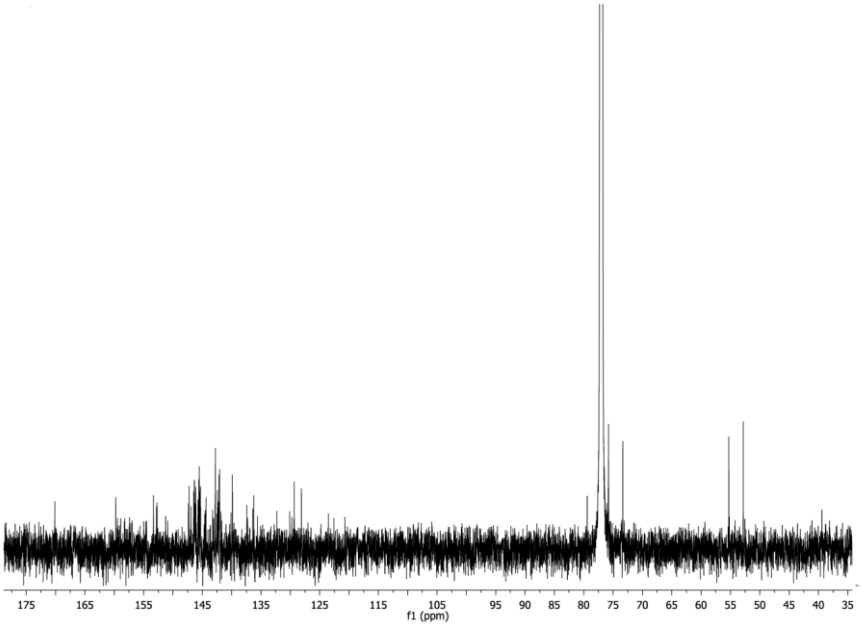

Figure A1-24. ^{13}C-NMR spectrum (175 MHz, CDCl3) of *cis*-**35a**.

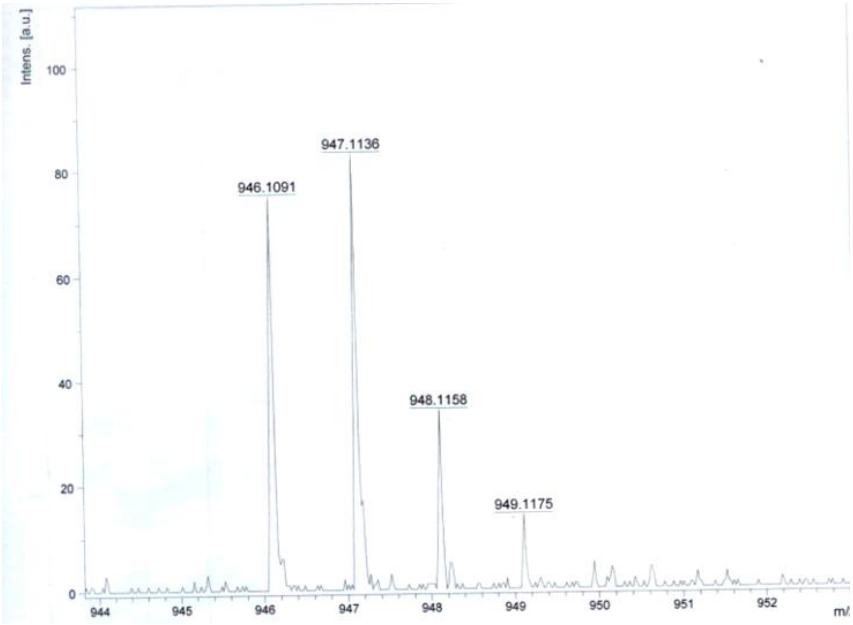

Figure A1-25. MS (MALDI-TOF) spectrum for *cis*-3**5a**.

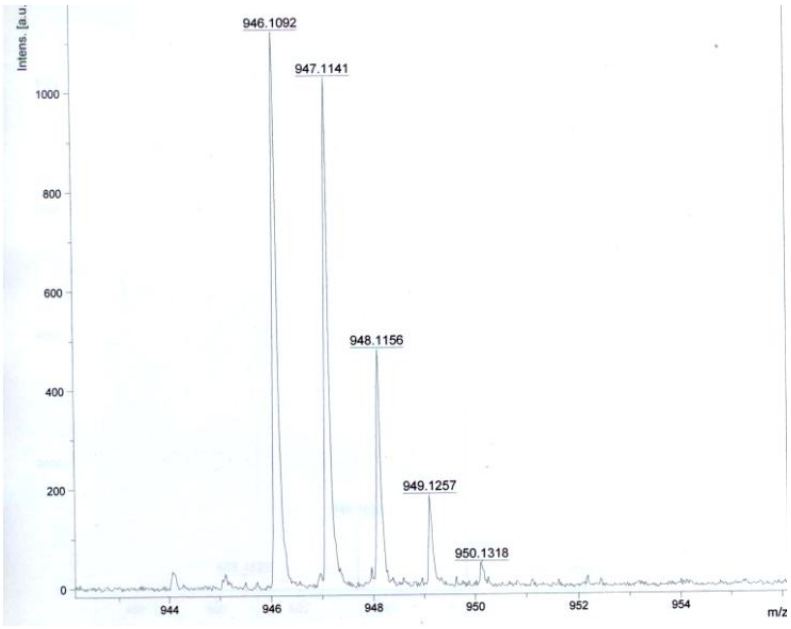

Figure A1-26. MS (MALDI-TOF) spectrum for *trans*-**35a**.

Representative spectra from the *cis/trans* isomerization experiments

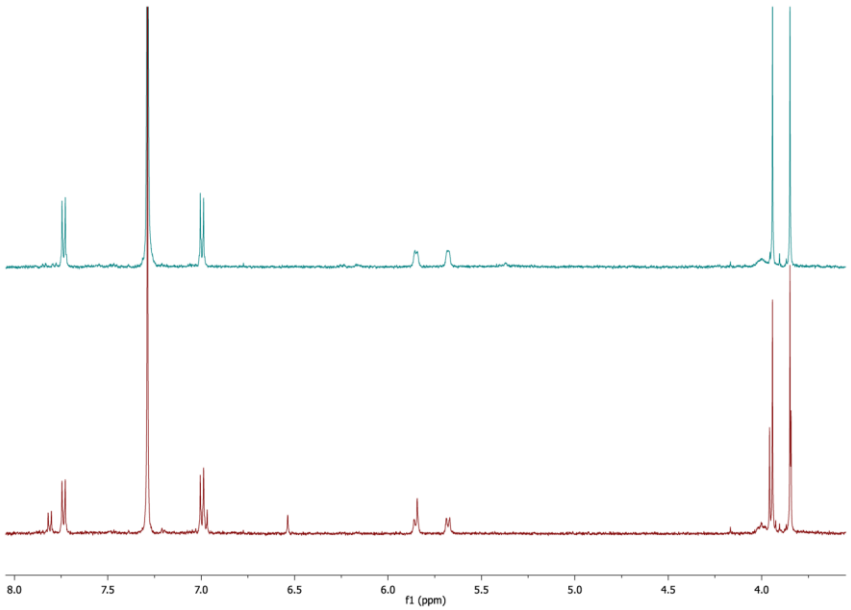

Figure A1-27. ^{1}H-NMR spectra (500 MHz, $CDCl_3$) of starting *cis*-**27a** (in blue) and *cis-trans*-**27a** equilibrium mixture (in red).

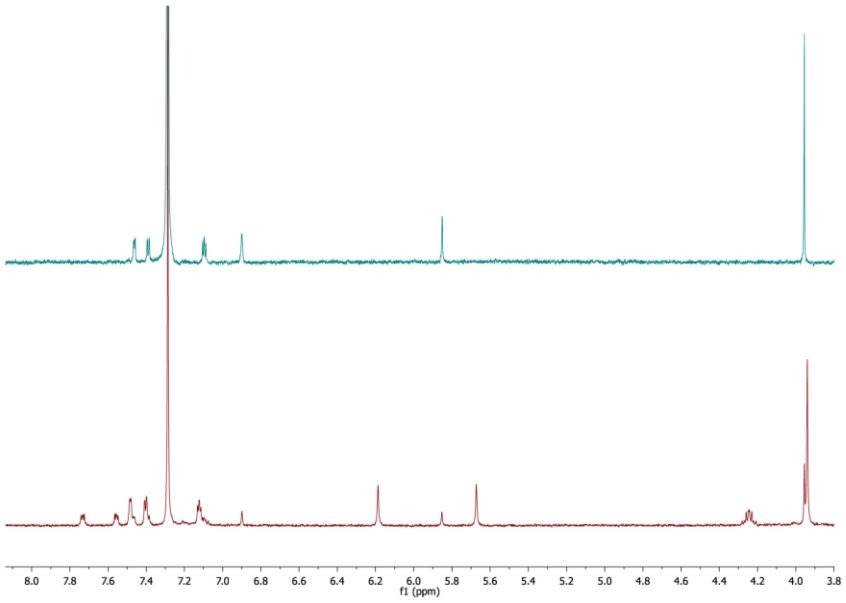

Figure A1-28. ^{1}H-NMR spectra (500 MHz, $CDCl_3$) of starting *trans*-**27b** (in blue) and *cis-trans*-**27b** equilibrium mixture (in red).

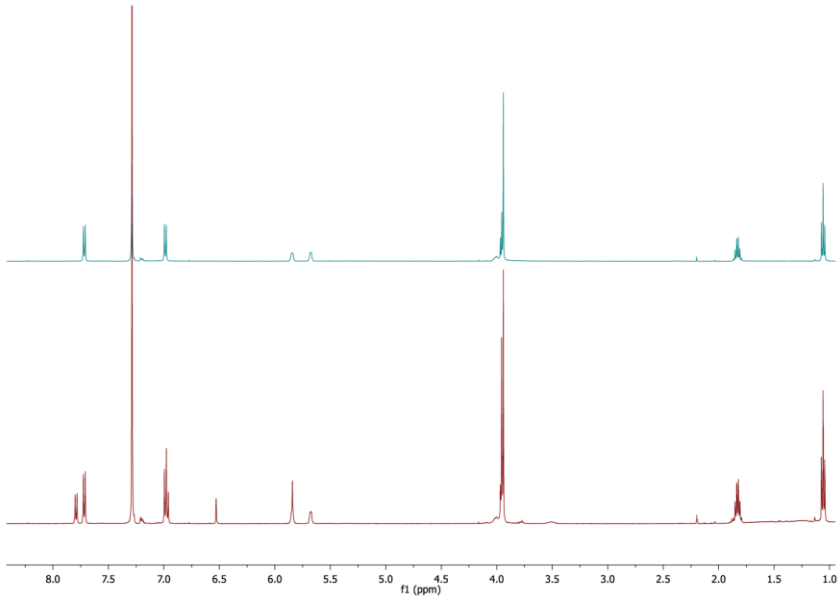

Figure A1-29. ^{1}H-NMR spectra (500 MHz, $CDCl_3$) of starting *cis*-**27c** (in blue) and *cis-trans*-**27c** equilibrium mixture (in red).

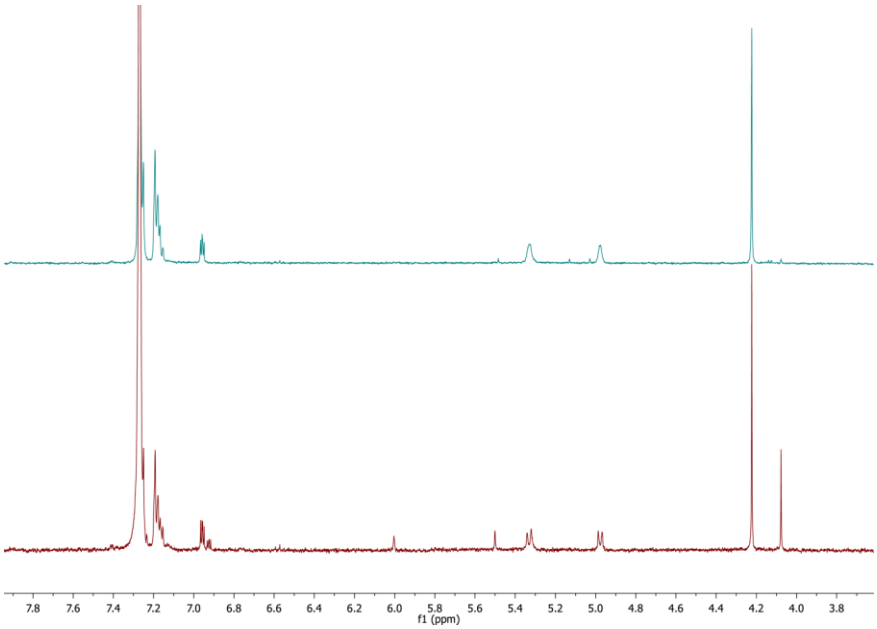

Figure A1-30. ^{1}H-NMR spectra (500 MHz, $CDCl_3$) of starting *cis*-**28** (in blue) and *cis-trans*-**28** equilibrium mixture (in red).

Time (days)	Experiment: *cis*-27a to *trans*-27a	Result (*de*)
4	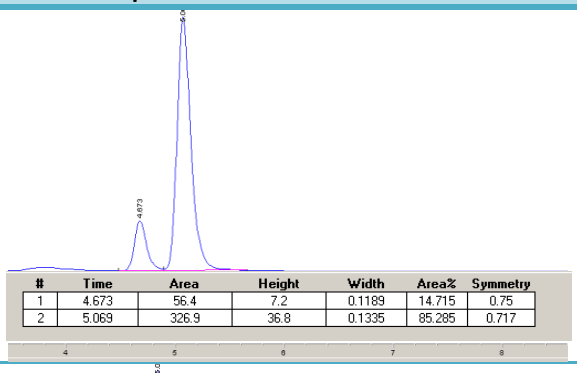 \# | Time | Area | Height | Width | Area% | Symmetry 1 | 4.673 | 56.4 | 7.2 | 0.1189 | 14.715 | 0.75 2 | 5.069 | 326.9 | 36.8 | 0.1335 | 85.285 | 0.717	***Cis*: 85 %** ***Trans*: 15 %**
5	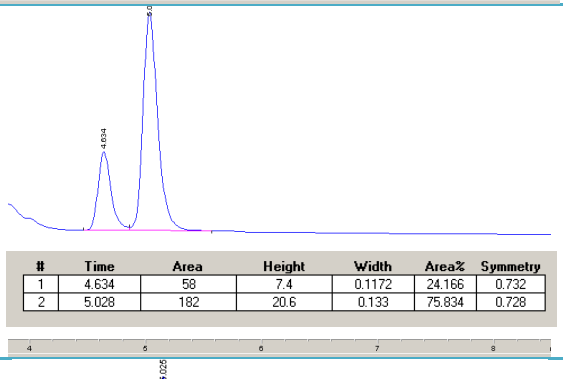 \# | Time | Area | Height | Width | Area% | Symmetry 1 | 4.634 | 58 | 7.4 | 0.1172 | 24.166 | 0.732 2 | 5.028 | 182 | 20.6 | 0.133 | 75.834 | 0.728	***Cis*: 76 %** ***Trans*: 24 %**
6	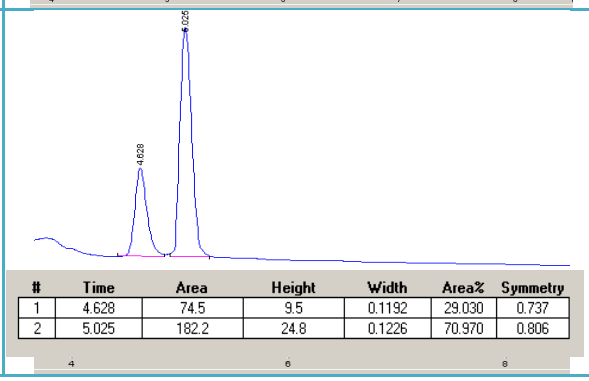 \# | Time | Area | Height | Width | Area% | Symmetry 1 | 4.628 | 74.5 | 9.5 | 0.1192 | 29.030 | 0.737 2 | 5.025 | 182.2 | 24.8 | 0.1226 | 70.970 | 0.806	***Cis*: 71 %** ***Trans*: 29 %**

Table A1-1. Isomerization reaction from *cis*-**27a** after 4, 5 and 6 days (equilibrium) respectively, affording 15, 24 and 29 % of *trans*-**27a** (*Buckyprep Waters* toluene:acetonitrile 9:1; 1mL/min).

<table>
<tr><th>Time (days)</th><th>Experiment: cis-27a to trans-27a</th><th>Result (de)</th></tr>
<tr><td>0</td><td> 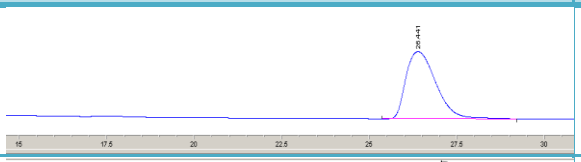 </td><td>Cis: 99 %
Trans: - %</td></tr>
<tr><td>2</td><td> 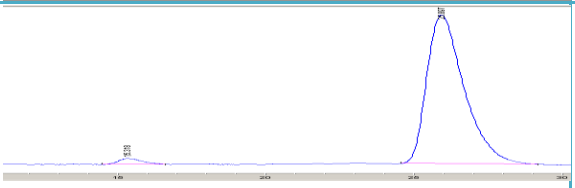
<table>
<tr><th>#</th><th>Time</th><th>Area</th><th>Height</th><th>Width</th><th>Area%</th><th>Symmetry</th></tr>
<tr><td>1</td><td>15.318</td><td>66.1</td><td>1.2</td><td>0.9543</td><td>2.620</td><td>0.677</td></tr>
<tr><td>2</td><td>25.897</td><td>2457.9</td><td>28</td><td>1.045</td><td>97.380</td><td>0.632</td></tr>
</table></td><td>Cis: 97 %
Trans: 3 %</td></tr>
<tr><td>5</td><td> 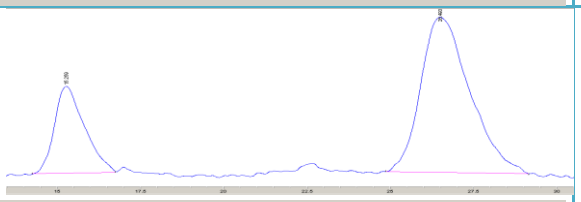
<table>
<tr><th>#</th><th>Time</th><th>Area</th><th>Height</th><th>Width</th><th>Area%</th><th>Symmetry</th></tr>
<tr><td>1</td><td>15.259</td><td>549.6</td><td>8.7</td><td>1.0513</td><td>25.562</td><td>0.631</td></tr>
<tr><td>2</td><td>26.493</td><td>1600.5</td><td>15.6</td><td>1.2184</td><td>74.438</td><td>0.667</td></tr>
</table></td><td>Cis: 74 %
Trans: 26 %</td></tr>
<tr><td>6</td><td> 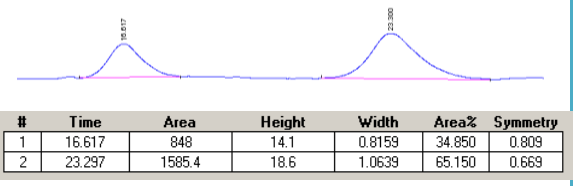
<table>
<tr><th>#</th><th>Time</th><th>Area</th><th>Height</th><th>Width</th><th>Area%</th><th>Symmetry</th></tr>
<tr><td>1</td><td>16.617</td><td>848</td><td>14.1</td><td>0.8159</td><td>34.850</td><td>0.809</td></tr>
<tr><td>2</td><td>23.297</td><td>1585.4</td><td>18.6</td><td>1.0639</td><td>65.150</td><td>0.669</td></tr>
</table></td><td>Cis: 66 %
Trans: 34 %</td></tr>
</table>

Table A1-2. Isomerization reaction from enantiopure (2*R*,5*R*)*cis*-**27a**. Starting enantiopure material and state of reaction after 2, 5 and 6 days, affording 3%, 26% and 34% respectively of (2*R*,5*S*)*trans*-**27a** (*Pirkle Covalent (R,R) Whelk-02* hexane:methanol 97:3; 1.25mL/min).

<table>
<tr><th>Time (days)</th><th>Experiment: trans-27c to cis-27c</th><th>Result (de)</th></tr>
<tr><td>3</td><td> 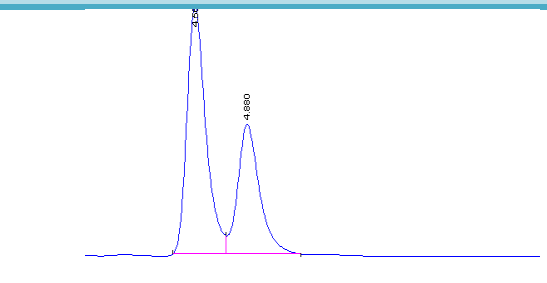

<table>
<tr><th>#</th><th>Time</th><th>Area</th><th>Height</th><th>Width</th><th>Area%</th><th>Symmetry</th></tr>
<tr><td>1</td><td>4.569</td><td>747.2</td><td>95.8</td><td>0.13</td><td>62.261</td><td>0.718</td></tr>
<tr><td>2</td><td>4.88</td><td>452.9</td><td>50.2</td><td>0.1504</td><td>37.739</td><td>0.745</td></tr>
</table></td><td>Cis: 38 %
Trans: 62 %</td></tr>
<tr><td>6</td><td> 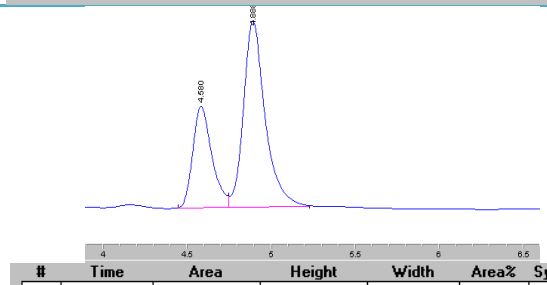

<table>
<tr><th>#</th><th>Time</th><th>Area</th><th>Height</th><th>Width</th><th>Area%</th><th>Symmetry</th></tr>
<tr><td>1</td><td>4.58</td><td>114.4</td><td>14.5</td><td>0.1179</td><td>32.234</td><td>0.712</td></tr>
<tr><td>2</td><td>4.888</td><td>240.5</td><td>26.7</td><td>0.1351</td><td>67.766</td><td>0.701</td></tr>
</table></td><td>Cis: 68 %
Trans: 32 %</td></tr>
</table>

Table A1-3. Isomerization reaction from *trans*-**27c** after 3 and 6 days (equilibrium), affording 38% and 68% respectively of *cis*-**27c** (*Buckyprep Waters* toluene:acetonitrile 9:1; 1mL/min).

Time (days)	Experiment: *cis*-27e to *trans*-27e	Result (*de*)
4	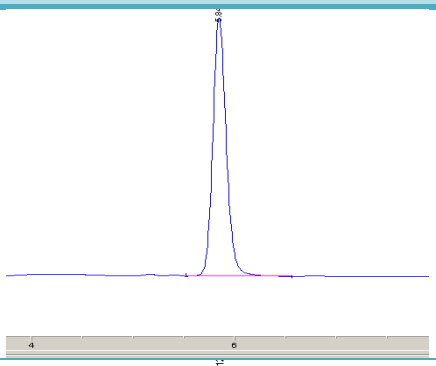	***Cis*: 99 %** ***Trans*: --**
10	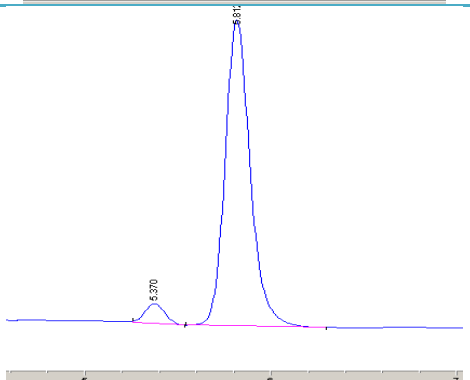 5.370 5.812 4 5 6 7	***Cis*: 95 %** ***Trans*: 5 %**

#	Time	Area	Height	Width	Area%	Symmetry
1	5.37	45.9	6.2	0.1165	4.968	0.907
2	5.812	877.7	93.7	0.1433	95.032	0.814

Table A1-4 Isomerization reaction from *cis*-**27e** after 4 and 10 days at 60º C, showing the slow and small rate of interconversion compared to the other derivatives of the series (*Buckyprep Waters* toluene:acetonitrile 9:1; 1mL/min).

Time (h)	Experiment: *cis*-28 to *trans*-28	Result (*de*)
12	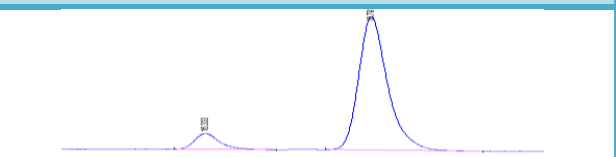 | # | Time | Area | Height | Width | Area% | Symmetry | |---|---|---|---|---|---|---| | 1 | 16.333 | 168.1 | 6.5 | 0.3782 | 9.331 | 0.696 | | 2 | 18.791 | 1633.4 | 54.8 | 0.454 | 90.669 | 0.728 |	***Cis*: 91 %** ***Trans*: 9 %**
36	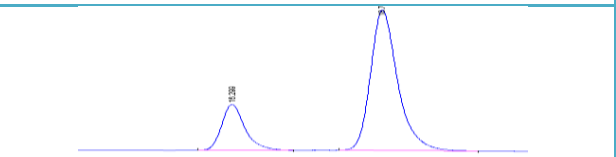 | # | Time | Area | Height | Width | Area% | Symmetry | |---|---|---|---|---|---|---| | 1 | 16.299 | 242.2 | 9.2 | 0.4008 | 21.773 | 0.754 | | 2 | 18.75 | 870.2 | 28.2 | 0.4681 | 78.227 | 0.732 |	***Cis*: 78 %** ***Trans*: 22 %**
36	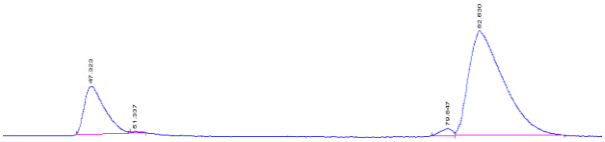 | # | Time | Area | Height | Width | Area% | Symmetry | |---|---|---|---|---|---|---| | 1 | 47.323 | 546.5 | 4.2 | 2.1625 | 19.295 | 0.479 | | 2 | 51.337 | 10.2 | 1.7E-1 | 1.0068 | 0.359 | 0.468 | | 3 | 79.847 | 31.8 | 6.6E-1 | 0.8033 | 1.122 | 0 | | 4 | 82.63 | 2243.7 | 9.2 | 4.0453 | 79.224 | 0.518 |	***Cis*: ee 99 %** ***Trans*: ee 99 %**
48	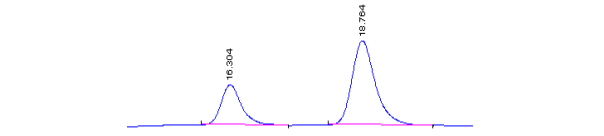 | # | Time | Area | Height | Width | Area% | Symmetry | |---|---|---|---|---|---|---| | 1 | 16.304 | 106.9 | 4.1 | 0.3874 | 29.386 | 0.732 | | 2 | 18.764 | 256.9 | 8.5 | 0.4522 | 70.614 | 0.743 |	***Cis*: 71 %** ***Trans*: 29 %**

Table A1-5. Isomerization reaction from *cis*-**28** after 12h, 36h and 48h, showing the equilibrium mixture (5YPE *Waters* toluene:acetonitrile 6:4; 0.8mL/min). The enantiomerical excess is shown for 36h, (*Pirkle Covalent (R,R) Whelk-02* hexane:methanol:toluene 96.5:2:1.5; 0.6mL/min).

Time (days)	Experiment: *cis*-29 to *trans*-29	Result (*de*)
5	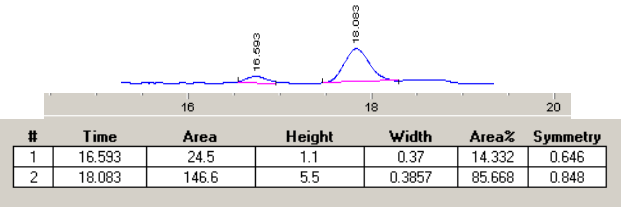 \# Time Area Height Width Area% Symmetry 1 16.593 24.5 1.1 0.37 14.332 0.646 2 18.083 146.6 5.5 0.3857 85.668 0.848	***Cis*: 85 %** ***Trans*: 15**

Table A1-6. Isomerization reaction from *cis*-**29** after 5 days, affording 14% of *trans*-**4** (5YPE *Waters* toluene:acetonitrile 6:4; 0.8mL/min).

Time (days)	*cis*-27a to *trans*-27a	*cis*-35a to *trans*-35a
0	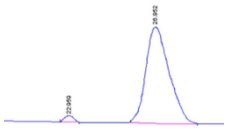 ***ee (cis)*=92 %**	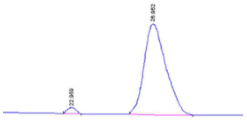 ***ee (cis)*=92 %**
6	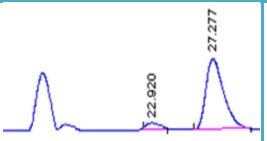 ***ee (cis)*=90 %**	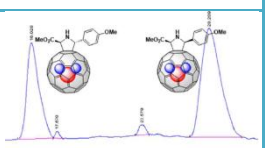 ***ee*=92 %**

Table A1-7. *ee* for the starting materials *cis*-**27a** and *cis*-**35a** and *ee* for the mixture after 6 days.

Time (days)	***cis*-27a to *trans*-27a**	***cis*-35a to *trans*-35a**
0	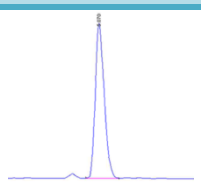 ***de*=99:1**	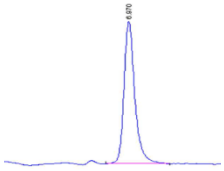 ***de*=99:1**
1	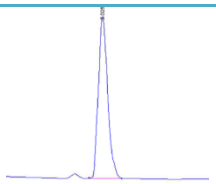 ***de*=99:1**	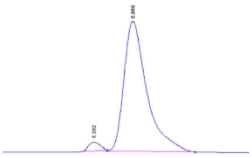 ***de*=97:3**
2	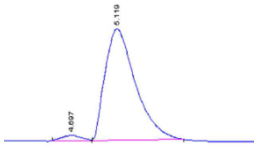 ***de*=98:2**	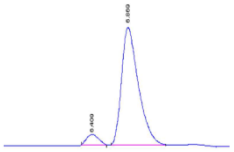 ***de*=95:5**
3	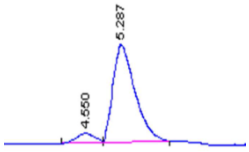 ***de*=92:8**	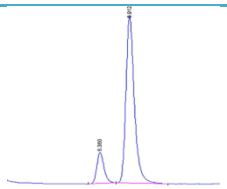 ***de*=86:14**
4	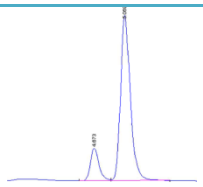 ***de*=85:15**	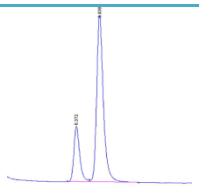 ***de*=78:22**
5	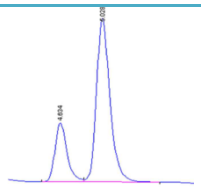 ***de*=76:24**	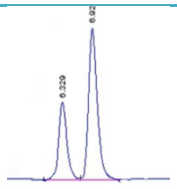 ***de*=70:30**

Table A1-8. Comparison of isomerization rates for empty and endohedral related **27a** and **35a**.

Annexe 2: Carbon nanoforms characterization

For most organic chemists or simply non-related with materials science some of the techniques utilized in this PhD work may result unknown. In order to lighten the comprehension of these techniques, a brief description of the fundamentals and the information that provide us applied to carbon nanostructures, is commented in next pages.

Fourier transform infrared spectroscopy (FTIR)

FTIR is a technique utilized to record different infrared spectra (emission, absorption, photoconductivity) of a sample by collecting simultaneously a wide wavelengths range data, in contrast to dispersive techniques that need a long time to analyze the same range. The term *Fourier transform* is referred to the mathematical process utilized to convert the sinusoidal recorded wave into a understandable spectrum.

Although not many structural information about the CNF can be collected by using FTIR, it allows to observe characteristic bands from the organic functional groups decorating the nanoconjugates. In the case of the prepared **CNF-1**, **CNF-2** and **CNF-3** the appearance and disappearance of the alkyne group is corroborated by the stretching band observed about 2100-2200 cm^{-1} (ν, C≡C), in a very clean an defined region. In Figures A2-1 and A2-2 this band is observed in the blue spectra as a consequence of the Tour reaction. In the red and green spectra, when the CuAAC cycloaddition is performed, this band disappears. Moreover, the stretching and bending modes for group C-H (2900 and 1600) attributed to the defects in the material are clearly observed.

This qualitative information does not allow to extract any conclusion about the functionalization degree but it is a powerful and simple tool to follow the course of the reactions .

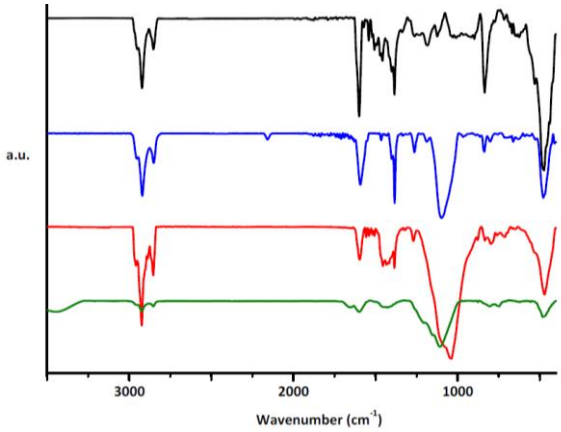

Figure A2-1. Comparative FTIR spectra for all SWNT nanoconjugates. Pristine **SWNT** (black), **SWNT-1** (blue), **SWNT-2** (red) and **SWNT-3** (green).

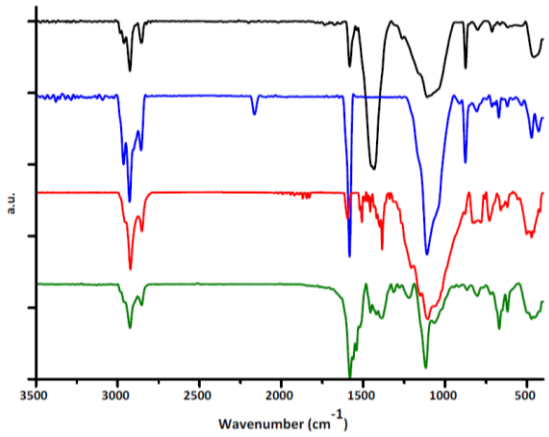

Figure A2-2. Comparative FTIR spectra for all graphene nanoconjugates. Pristine **GR** (black), **GR-1** (blue), **GR-2** (red) and **GR-3** (green).

Raman spectroscopy[121,123]

It is a spectroscopic technique used to observe vibrational, rotational, and other low-frequency modes in a system. A laser source is utilized, and its inelastic interaction with vibrations and phonons results in shifts that provide information about vibrational and rotational modes in the system. Applied to carbon materials, it may be a more complex topic than expected because many features are related to their phonon modes. The importance of the phonon modes in the material properties, such as electronic, electrical or thermal make Raman spectroscopy to provides much more information than only structural features, but its understanding could require many pages on the physical treatment of the electronic structure of CNF. In the next lines we describe the most relevant observed modes that provide important chemical and structural information.

There are several characteristics bands that provide important information:

RBM

The radial breathing mode (RBM) corresponds to the vibration of carbon atoms in the radial direction making change the SWNT diameter as a consequence of a "breathing" movement. These features appear between 100 and 260 cm^{-1}. This mode can be used to study the nanotube diameter and checking the electronic structure through perform an *(n,m)* assignment in single isolated SWNT . Unfortunately samples are not made of isolated nanotubes and all features are contribution of each different type of SWNT present in the sample and a diameter characterization is not so trivial.

G-mode

it is associated with the longitudinal optical (LO) phonon mode, (around 1580 cm^{-1}) between the two non-equivalent carbons in the graphite unit cell, sometimes so called tangential vibration mode. When this term is extended to CNT, the single peak found in graphite turns to a more complex signal composed of several peaks associated to the SWNT curvature. This feature makes this band useful for diameter assignation, distinguish between metallic and semiconducting SWNT and to probe the charge transfer arising from SWNT doping .

The G band consists of two components: G^+ (1590 cm^{-1}) is more related to the LO phonon mode and is up-shifted for electron-acceptor dopants and down-shifted for electron-donor dopants, and G^- (1570 cm^{-1}) is associated with vibrations of carbon atoms along the circumferential direction of the SWNT (TO phonon), and its shape is depending on the metallic or semiconducting character of the SWNT. While in smaller SWNT the observance of the two different contributions is more clear (Figure A2-3), in larger diameter SWNT and MWNT this mode is more similar to graphite and

graphene, observing a sharp peak as represented in the Figure A2-3 and observed at 1590 cm^{-1} in Figure A2-5 and Figure A2-6.

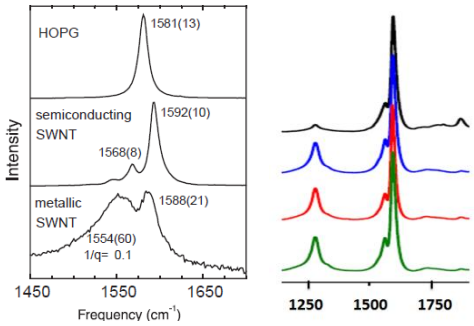

Figure A2-3. Comparative G-band shape between graphite, semiconducting SWNT and metallic SWNT and D and G modes for pristine **SWNT** (black), **SWNT-1** (blue), **SWNT-2** (red) and **SWNT-3** (green).

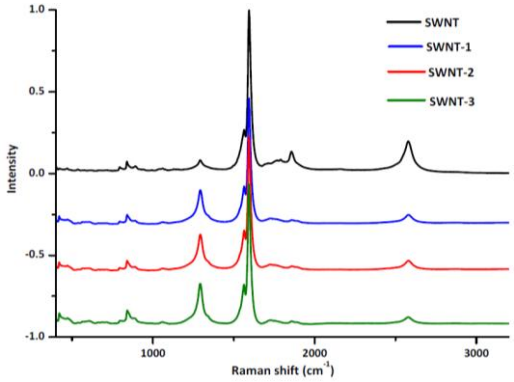

Figure A2-4. Comparative Raman spectra for all SWNT nanoconjugates. Pristine **SWNT** (black), **SWNT-1** (blue), **SWNT-2** (red) and **SWNT-3** (green).

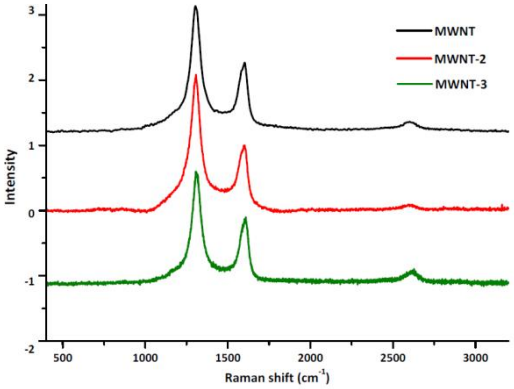

Figure A2-5. Comparative Raman spectra for MWNT nanoconjugates. Pristine **MWNT** (black), **MWNT-2** (red) and **MWNT-3** (green).

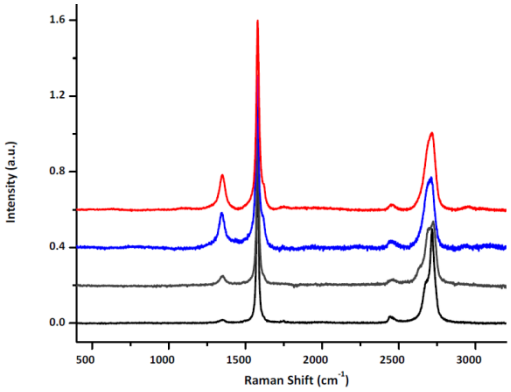

Figure A2-6. Comparative Raman spectra for GR nanoconjugates. Graphite (black), **GR**, **GR-1** (blue) and **GR-2** (red).

D-mode

The disorder induced band or D band (1350 cm^{-1}) appears as a consequence of the interruption in the sp^2 network. In SWNT this mode depends on the diameter and chirality. In finite-size graphene appears as a consequence of the edges with special shapes, stacking disorder between two layers, and atomic defects within the layer. For such a disordered carbon, the relative intensity of D to G provides a good indicator for determining the in-plane crystallite size or the degree of disorder.

G' or 2D mode

The second order mode for D, G' or 2D (2700 cm^{-1}) is specially intense and depends on the laser excitation energy. In monolayer graphene, the G' band is stronger than the G band, whereas for bilayer graphene or multilayer graphene, the G' band is broader and weaker than the G band. It used to be accompanied by a small peak at 2450 cm^{-1}. (Figure A2-6). In 3D graphitic materials it may be observed as a doublet because of an interlayer coupling mechanism.

Other features and remarks in Raman spectroscopy

Other overtones and combinations of Raman and phonon modes can be observed. As example, the *M overtone* (1750 cm^{-1}, Figure A2-4) in SWNT, that is enhanced by symmetry-breaking effects associated with SWNT curvature. It is important to remark that MWNT are composed of an outer tube with a large diameter and inner tubes with smaller diameters what made that those Raman features that are univocal for SWNT and graphene respectively, in the MWNT Raman spectrum may be not so clear.

Thermogravimetric analysis (TGA)

This technique consist in the measurement of the weight loss of a sample when is progressively heated until a certain temperature under air or inert atmospheres. It allows to determine the decomposition temperature, range of stabilities, desorption temperatures or dryness degree of a substance. Applied to CNF, it provides information about the amount of organic residues attached on them (in other words, the degree of functionalization) and the desorption temperature of these addends.

With the aim of getting reliable analyses, a previous treatment by heating at temperatures about 90-100ºC is performed in order to remove any possible residual solvent that may interfere in the analysis. As observed in Figure A2-7, the starting pristine SWNT exhibits a very slight weight loss compared to the functionalized materials **SWNT-1** and **SWNT-3**. The derivative graph allows to find the desorption temperature for a certain compound. In the case of SWNT, which are usually highly aggregated and addends are intercalated, the desorption process is progressive and is difficult to assign a well defined temperature range. In MWNT, where the degree of aggregation is lower than in SWNT, the analysis on **MWNT-3** allows to observe a first maximum in the weight loss at 255 ºC that may be attributed to the π-exTTF units. The second maximum is found at 365 ºC that corresponds with the maximum in **MWNT-2** (Figure A2-8). An intermediate situation occurs on **GR-1**, **GR-2** and **GR-3** derivatives, where the high tendency to aggregation of graphene flakes results in a progressive weight loss but allowing the observation of the corresponding maximas (Figure A2-9).

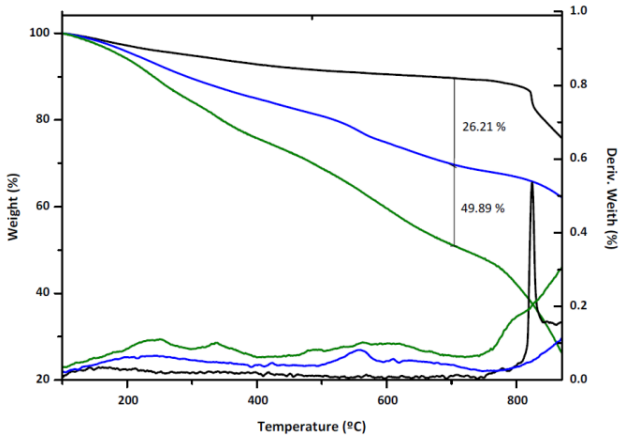

Figure A2-7. Comparative TGA analyses for SWNT (black), **SWNT-1** (blue) and **SWNT-3** (green)

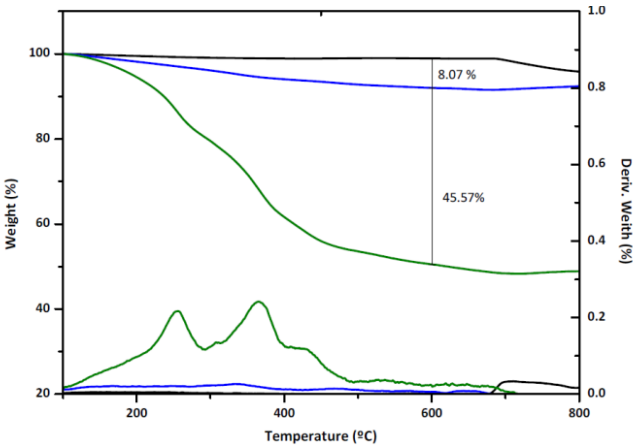

Figure A2-8. Comparative TGA analyses for MWNT (black), **MWNT-1** (blue) and **MWNT-3** (green)

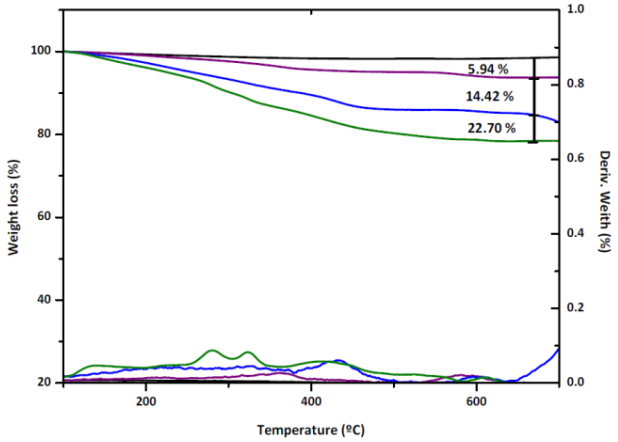

Figure A2-9. Comparative TGA analyses for graphite (black), graphene (purple), **GR-1** (blue) and **GR-3** (green)

X-Ray photoelectron spectroscopy (XPS)

XPS is a surface-sensitive semi-quantitative spectroscopic technique that measures the elemental composition at the parts per thousand range in a solid sample. The XPS spectra are obtained by irradiating a material with a beam of X-ray while simultaneously measuring the kinetic energy and number of electrons that escape from the first 10 nm of the material surface. The binding energy expressed in eV allows determining the different elements, the electronic state and type of hybridization by comparison with tabulated values. It helps determining the presence of different functionalities (i.e. distinguishing between amine and amides).

When this technique is applied to CNF it is possible to identify certain elements present in the attached functionalities. For example, the presence of S because of the attachment of π-exTTF or remaining F from TBAF or glass. More important is the possibility of deconvoluting a certain peak in different contributions depending on the oxidation state of the element. In Figure A2-10 and Figure A2-11, in right spectra, the N peak deconvolution afforded the contribution from the **N=N** and **N-N** in the triazole rings. The C signal deconvolution afforded the contribution of carbonyl, alcohols or sp^3 carbon (Figure A2-11).

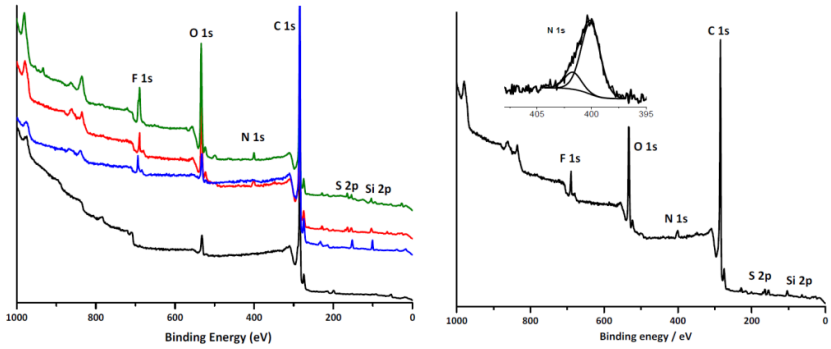

Figure A2-10. Left: Comparative XPS analyses for SWNT (black), **SWNT-1** (blue), **SWNT-2** (red) and **SWNT-3** (green)). Right: Deconvolution at core level for N 1s peaks in **SWNT-2**.

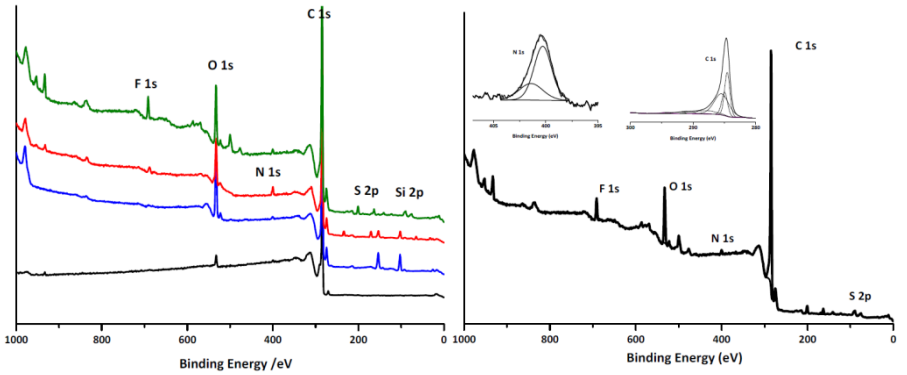

Figure A2-11. Left: Comparative XPS analyses for Graphene (black), **GR-1** (blue), **GR-2** (red) and **GR-3** (green). Right: Deconvolution at core level for C 1s and N 1s peaks in **GR-3**.

Transmission electron microscopy (TEM)

TEM is a microscopic technique that uses electrons beams as irradiation sources. The electrons are transmitted through an ultra-thin species (i.e: SiO_2 wafers, biological tissues, nanoparticles), interacting with them as electrons pass through. The image is magnified and focused onto an imaging device, such as a fluorescent screen, on a layer of photographic film. Because of the small wavelength associated to electrons, it is possible to obtain a high resolution image species at the nanoscale.

When SWNT are studied by TEM, bundles of nanotubes are usually observed with some isolated small bundles and even individual nanotubes among them. The funtionalization leads to bundles coformed by a lower number of nanotubes compared to pristine SWNT (Figure A2-12).

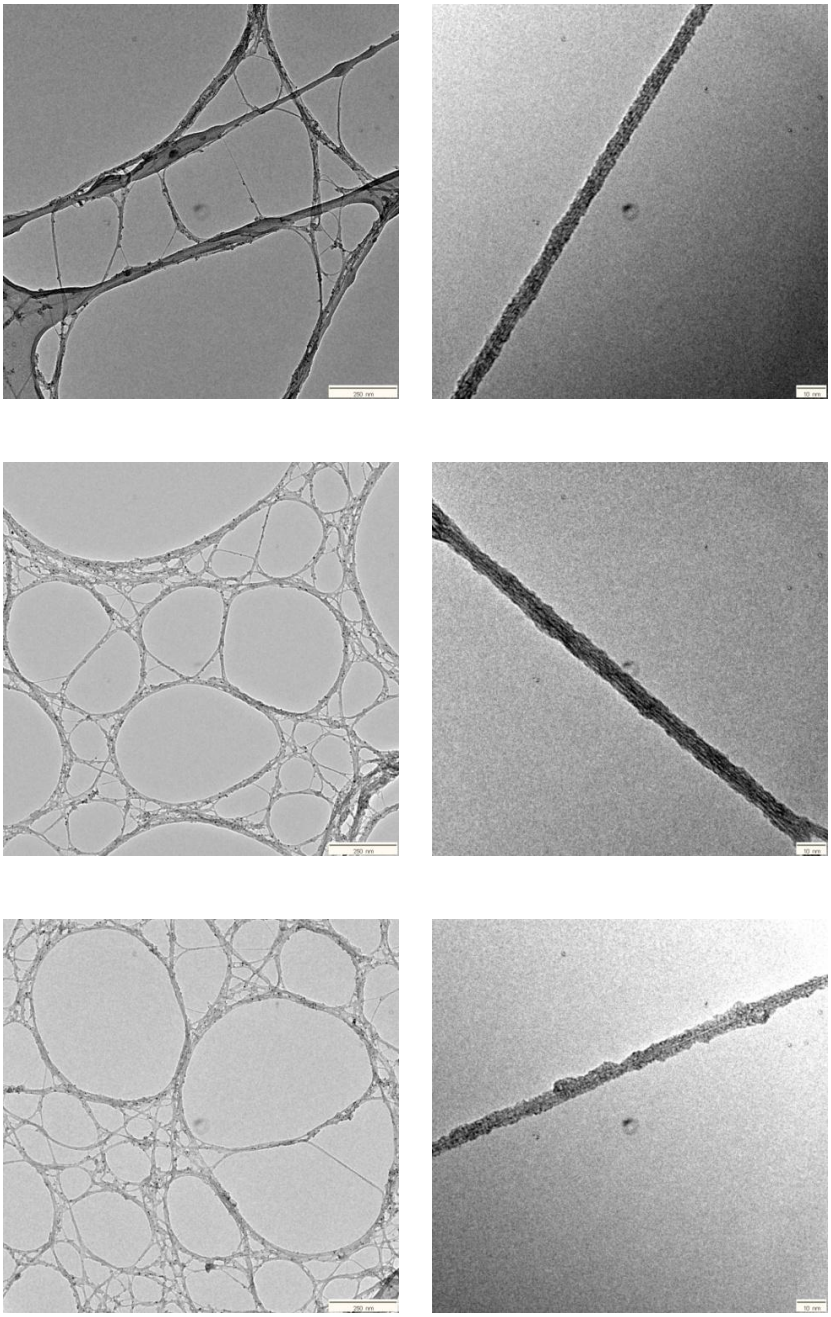

Figure A2-12. Representative TEM images on holey carbon grids with scale bars of 250 nm (left) and 10 nm (right) of pristine SWNT (upper part), **SWNT-1** (central part) and **SWNT-2** (lower part).

MWNT are easier to be dispersed than SWNT, so they usually do not exhibit remarkable differences in morphology upon functionalization (Figure A2-13).

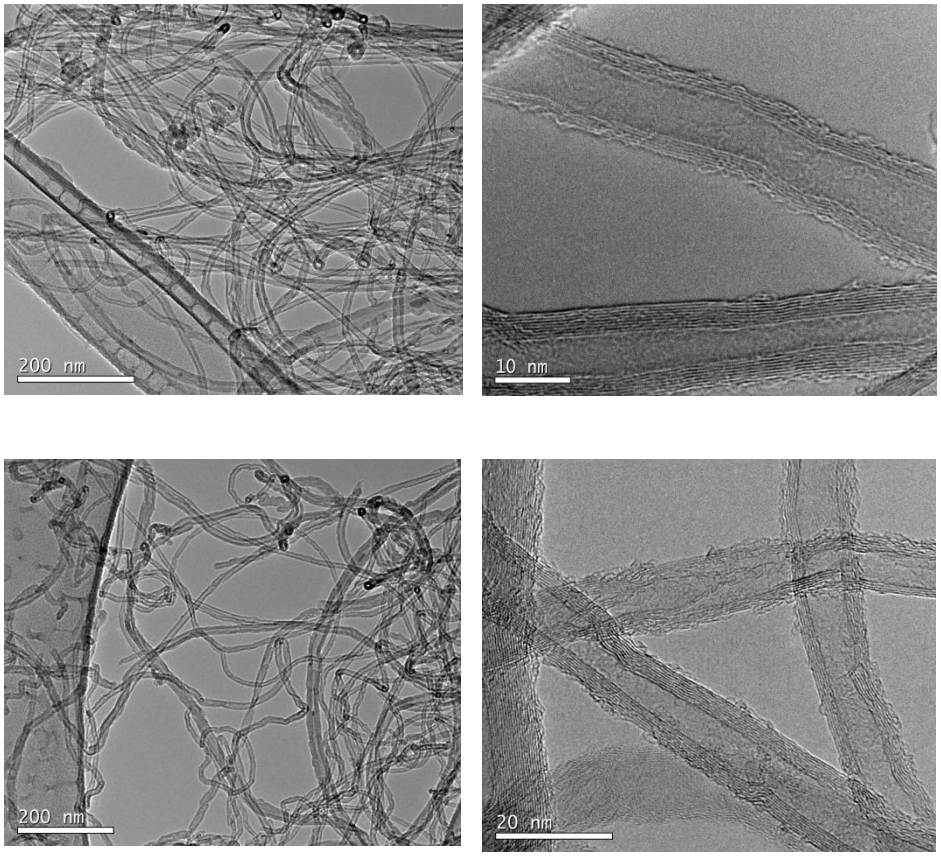

Figure A2-13. Representative TEM images on holey carbon copper grids, with scale bars of 200 nm (left) and 10 or 20 nm (right) of pristine MWNT (upper part) and **MWNT-2** (lower part).

TEM analysis on graphite or graphene provide important information about their structure and morphology. When exfoliation is effective affording few layer graphene samples, the TEM images show a diffuse shadow that correspond to the edge of the flakes, while in graphite sheets are clearly observable. In Figure A2-14 (left), at a 200 nm scale, a few layer graphene sample is observed with two well defined regions. In the upper part, darker, a major number of flakes are stacked as in the lower part, lighter, the number of flakes may be very low. In the right image, the graphene edges can be observed as parallel lines.

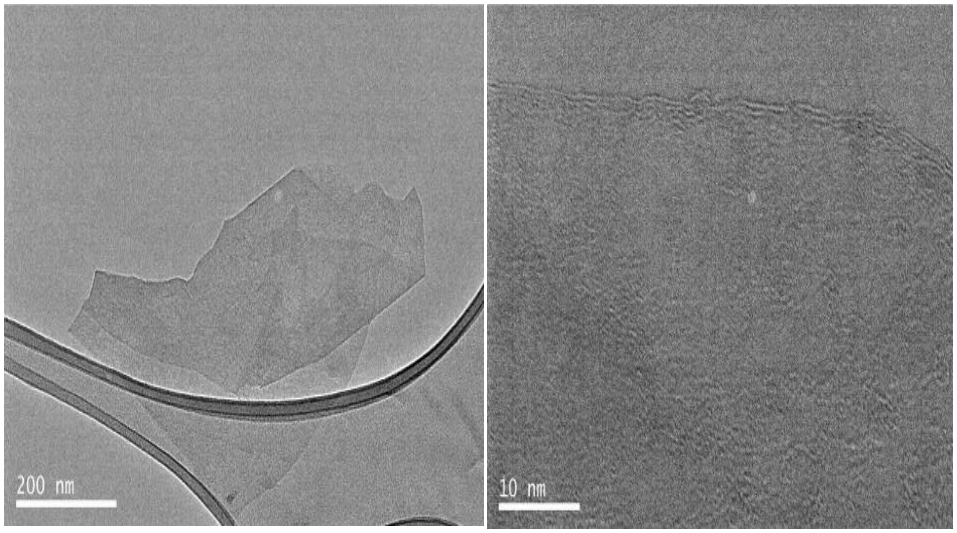

Figure A2-14. TEM image of graphene obtained after the exfoliation procedure (left) and magnification of the upper part where can be observed the graphene layers (right).

Photophysical measurements

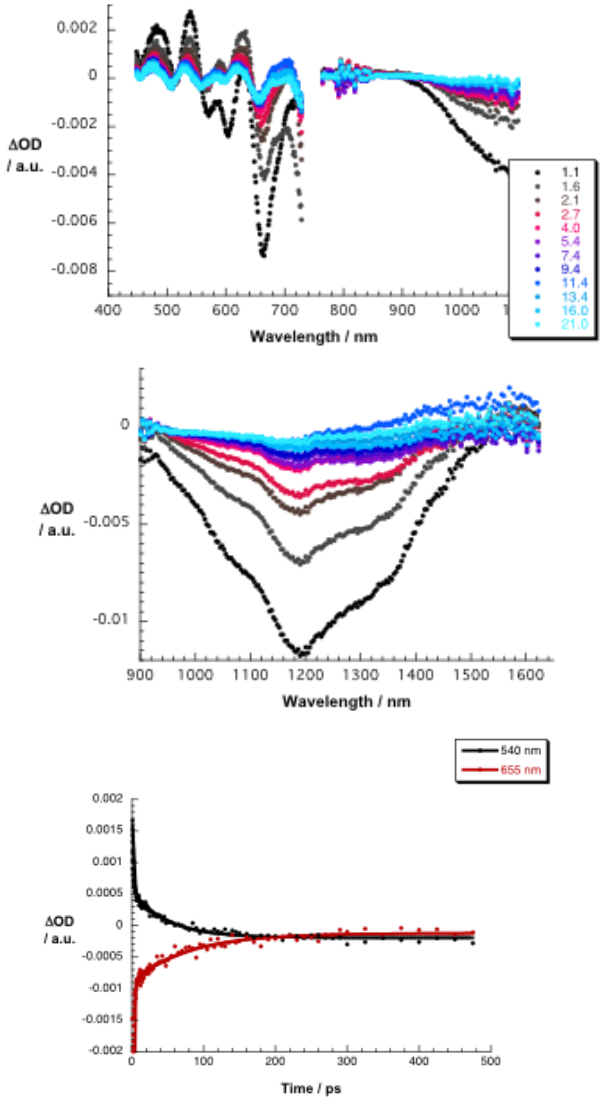

Figure A2-15. Differential absorption spectra (visible and near-infrared) obtained upon femtosecond pump probe experiments (387 nm) of pristine SWCNT with several time delays between 1.1 and 21.0 ps at room temperature (upper). Differential absorption spectra (extended near-infrared) obtained upon femtosecond pump probe experiments (387 nm) of pristine SWCNT with several time delays between 1.1 and 21.0 ps at room temperature (central). Time absorption profiles of the spectra shown in the upper part at 540 and 655 nm monitoring the excited state decay (lower).

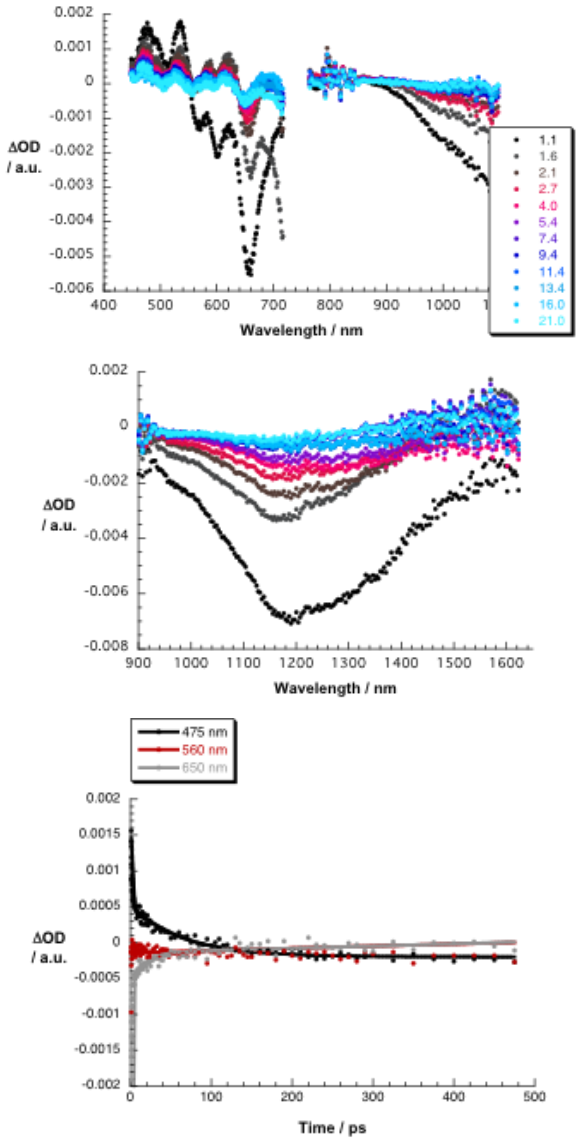

Figure A2-16. Differential absorption spectra (visible and near-infrared) obtained upon femtosecond pump probe experiments (387 nm) of **SWNT-1** with several time delays between 1.1 and 21.0 ps at room temperature (upper). Differential absorption spectra (extended near-infrared) obtained upon femtosecond pump probe experiments (387 nm) of **SWNT-1** with several time delays between 1.1 and 21.0 ps at room temperature (central). Time absorption profiles of the spectra shown in the upper part at 475, 560, and 650 nm monitoring the excited state decay (lower).

Annexe 3:

Experimental determination of binding constants in supramolecular complexes

Annexe 3: Experimental determination of binding constants

A supramolecular system is defined by a host molecule (H, usually our synthesized receptor), a guest molecule (G, fullerene C_{60} in this case) that associates by one or several binding sites to afford a complex (H_mG_n). The extension of the formation of the complex is determined by β_{mn}.

$$mH+nG \underset{}{\overset{\beta_{mn}}{\rightleftharpoons}} H_mG_n$$

$$\beta_{mn} = \frac{[H_mG_n]}{[H]^m[G]^n}$$

Considering the simpler case, when m=n=1, the equation is reduced to the form:

$$K_a = \frac{[HG]}{[H][G]} \text{ or the inverse form: } K_d = \frac{[H]\cdot[G]}{[HG]}$$

When the fraction of total binding sites occupied θ is defined, a plot θ versus [*G*] at a constant concentration of $[H]_{total}$ will yield a hyperbola whose midpoint will surrender K_d.

$$\theta = \frac{[G]_{bound}}{[H]_{total}} = \frac{[HG]}{[H]+[HG]} = \frac{[G]}{K_d+[G]} = \frac{K_a\cdot[L]}{1+K_a\cdot[L]}$$

The θ values are proportional to any physical or chemical properties that may be modified upon the addition of ligands (UV-Vis absorbance, fluorescence, δ in NMR), so, if we are able to monitorize these changes we can obtain a K_a value. By using different simplifications working in a range of concentrations where the [G] is larger than the [H], equations may be simplified to other forms that are experimentally more useful:[130]

$$\Delta Abs = \Delta Abs_{max}\frac{K\cdot[G]+K[H]+1-\sqrt{(K\cdot[G]+K[H]+1)^2-4\cdot K^2\cdot[G]\cdot[H]}}{2\cdot K\cdot[H]}$$

$$\Delta\delta = \Delta\delta_{max}\frac{K\cdot[G]-K[H]-1+\sqrt{(K\cdot[G]+K[H]+1)^2-4\cdot K^2\cdot[G]\cdot[H]}}{K\cdot[G]-K[H]+1+\sqrt{(K\cdot[G]+K[H]+1)^2-4\cdot K^2\cdot[G]\cdot[H]}}$$

In the case of the existence of several binding sites in a host, it can be found that the effectiveness of the binding sites is dependent upon each other. This phenomenon is named as allosterism and is well known in the biological systems, for example, in enzymes, hormones or cell recognition. In these cases, a particularly useful multi-site model is the Hill plot, and applied to UV-vis spectroscopy affords the equation, where:

$$\Delta Abs = \frac{Abs_{max} \cdot [G]^{n_h} \cdot K_n}{1 + [G]^{n_h} \cdot K_n} \quad \textbf{(Hill's equation)}$$

The Hill coefficient, n_h, is a qualitative parameter that measures the degree of cooperativity and it is smaller than the number of present binding sites. When $n_h>1$ it is said that the system is positively cooperative, in other words, the entrance of a ligand into a binding site is facilitated by a previous H-G interaction. When $n_h<1$ the system is said to be anticooperative because the entrance of a first guest hinder the interaction of more ligands in other binding sites.

Once the theoretical and mathematical bases are established it is found that obtaining reliable experimental results is not an easy topic. Firstly, the expected K_a value determines the more suitable technique for determining its value. Considering that NMR is a good method for $K_a < 10^5$ M^{-1} and UV-vis for $10^3 \leq K_a \leq 10^7$ M^{-1} and fluorescence for $K_a > 10^6$ M^{-1} and the related reported systems commented in the background section afforded values about 10^3-10^4, it may be acceptable utilizing UV-Vis spectroscopy or ^{1}H-NMR. Another important consideration is the low solubility of fullerene in common organic solvents which limits the experiment to the utilization of CS_2, toluene, chlorobenzene and other low volatile aromatic solvents. Moreover, the expected K_a value determines the spectroscopic technique and the range of concentrations to be used. A very useful rule is utilizing a concentration of host equal or slightly higher than the reciprocal of the expected binding constant.

Determination of binding constants by UV-vis spectroscopy

When UV-Vis titration experiments were considered, we started the search of conditions utilizing [**18**] = 10^{-4} M and [C_{60}] = 10^{-2} M in chlorobenzene to ensure an excess of guest. After a series of trial and error experiments, $[H]^0/[G]^0$ = 1/77 seems to provide better experimental conditions. An important matter is how to keep a constant [**18**] during the experiment. To overcome this problem the host solution is utilized as solvent for the C_{60} solution. An illustrative table of the concentrations and parameters for a typical titration experiment is shown in Figure A3-1.

C60	Mw	720,64	L=1 mm	[18]	Mw	1111,5		
	weight(mg)	2,9			weight	0,485		
	volume(mL)	3			volume(mL)	25		
	concentratio	1,34E-03			concentration	1,75E-05		
	solvent	solution of clip			solvent	clph		

Volume add	Equiv. C60	mmol C60	Volume (mL	Equiv REC	mmol REC	Final Volum	Final Conc C	Final Conc REC (M)
0	0,0000	0	*1*	*1,00*	*0,000018*	1	0,00E+00	1,75E-05
0,003	0,2376	0,00000417	*1*	*1,00*	*0,000018*	1,003	4,16E-06	1,75E-05
0,005	0,3952	0,00000695	*1*	*1,00*	*0,000018*	1,005	6,92E-06	1,75E-05
0,01	0,7864	0,0000139	*1*	*1,00*	*0,000018*	1,01	1,38E-05	1,75E-05
0,015	1,1738	0,00002085	*1*	*1,00*	*0,000018*	1,015	2,05E-05	1,75E-05
0,02	1,5574	0,0000278	*1*	*1,00*	*0,000018*	1,02	2,73E-05	1,75E-05
0,025	1,9373	0,00003475	*1*	*1,00*	*0,000018*	1,025	3,39E-05	1,75E-05
0,03	2,3135	0,0000417	*1*	*1,00*	*0,000018*	1,03	4,05E-05	1,75E-05
0,05	3,7823	0,0000695	*1*	*1,00*	*0,000018*	1,05	6,62E-05	1,75E-05
0,07	5,1963	0,0000973	*1*	*1,00*	*0,000019*	1,07	9,09E-05	1,75E-05
0,09	6,5583	0,0001251	*1*	*1,00*	*0,000019*	1,09	1,15E-04	1,75E-05
0,11	7,8713	0,0001529	*1*	*1,00*	*0,000019*	1,11	1,38E-04	1,75E-05
0,13	9,1378	0,0001807	*1*	*1,00*	*0,000020*	1,13	1,60E-04	1,75E-05
0,15	10,3602	0,0002085	*1*	*1,00*	*0,000020*	1,15	1,81E-04	1,75E-05
0,18	12,1162	0,0002502	*1*	*1,00*	*0,000021*	1,18	2,12E-04	1,75E-05
0,21	13,7851	0,0002919	*1*	*1,00*	*0,000021*	1,21	2,41E-04	1,75E-05

Figure A3-1. Illustrative table containing the concentrations, equivalents, volumes and more related conditions for a typical UV-vis titration experiment.

The absorbance at 438 nm for each addition (Figure 1.3-15) were utilized after subtraction of the C_{60} contribution to plot and fit the binding isotherm to the Hill equation mentioned above utilizing *Origin Microcal 8.0*.

$$\Delta Abs = \frac{Abs_{max} \cdot [G]^{n_h} \cdot K_n}{1 + [G]^{n_h} \cdot K_n}$$

The data were treated by *Specfit*, a software that use previous recorded spectra of host and guest to perform the calculations.

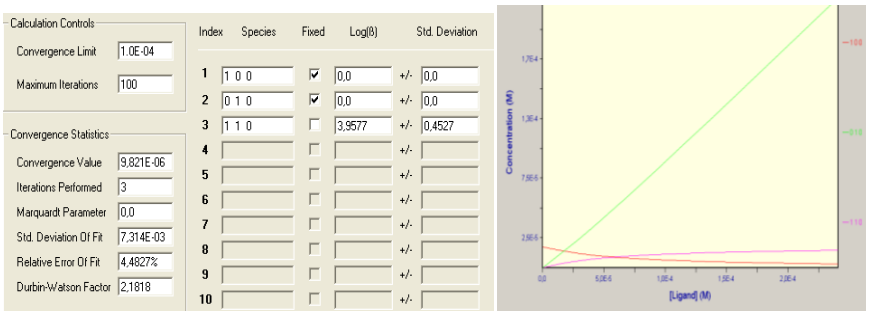

Figure A3-2. Results predicted by *Specfit* software (left). Concentration of the three species present during the experiment (**18** in red, C_{60} in green and [**18**-C_{60}] in pink)

Determination of binding constants by ^{1}H-NMR.

The ^{1}H-NMR titration experiments were performed utilizing a **18**, **22** or **24** solution in a mixture $CS_2/CDCl_3$ (1:1) as solvent. This solution was utilized as solvent for the C_{60} solution in order to keep the host in a constant concentration during the experiment. After each addition the spectra were recorded at 300 MHz and 25 ºC. All the spectra were carefully compared and studied and calculating all the shifts in the signals. Only signals with a significant shift (over 0.005 ppm from the blank to the last addition) were considered for further calculations.

The different shifts in the NMR signals were plotted and fitted to the next equation using *Origin Microcal 8.0*.

$$\Delta\delta = \Delta\delta_{max}\frac{K\cdot[G]-K[H]-1+\sqrt{(K\cdot[G]+K[H]+1)^2-4\cdot K^2\cdot[G]\cdot[H]}}{K\cdot[G]-K[H]+1+\sqrt{(K\cdot[G]+K[H]+1)^2-4\cdot K^2\cdot[G]\cdot[H]}}$$

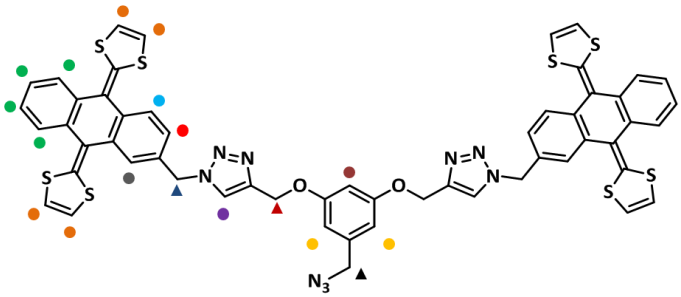

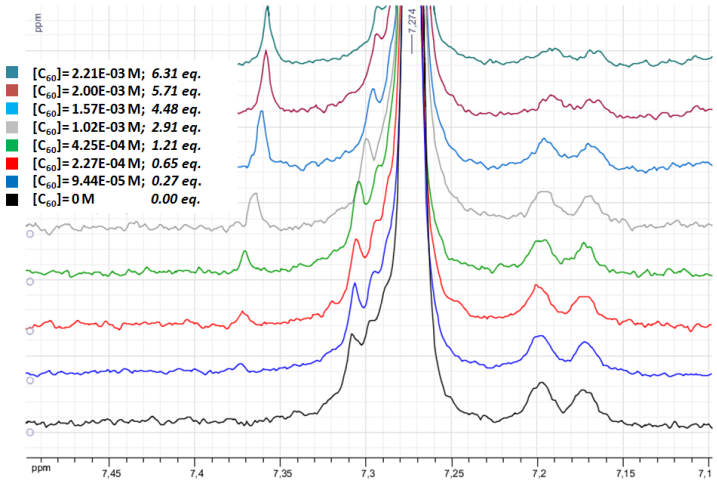

Figure A3-3. ^{1}H-NMR spectrum enhancing the change in the position 3 in the **18** anthracene skeleton.

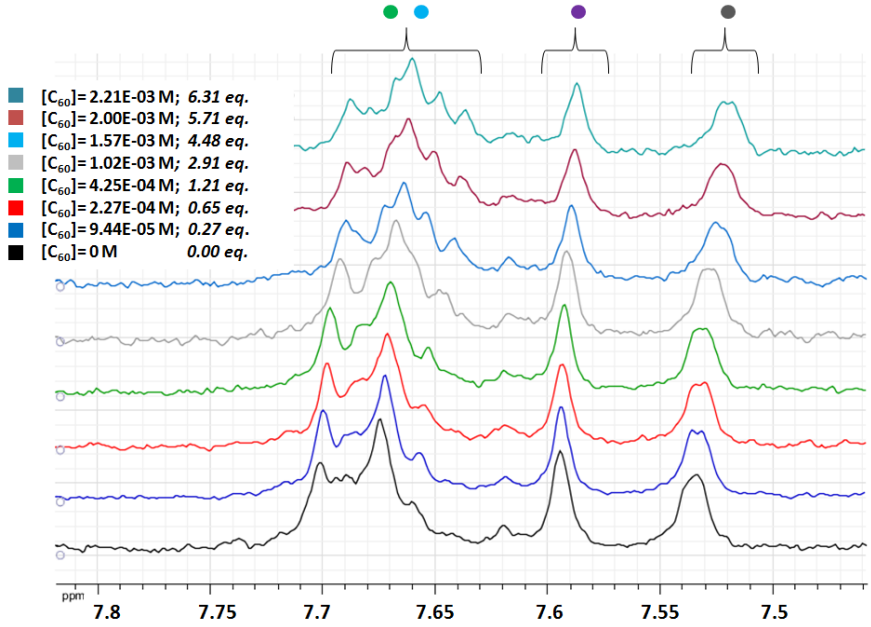

Figure A3-4. ^{1}H-NMR titration experiment for system **[18·C_{60}]** enhancing the change in some of the anthracene skeleton signals of π-exTTF (blue, red and grey) and in the triazole signal (purple).

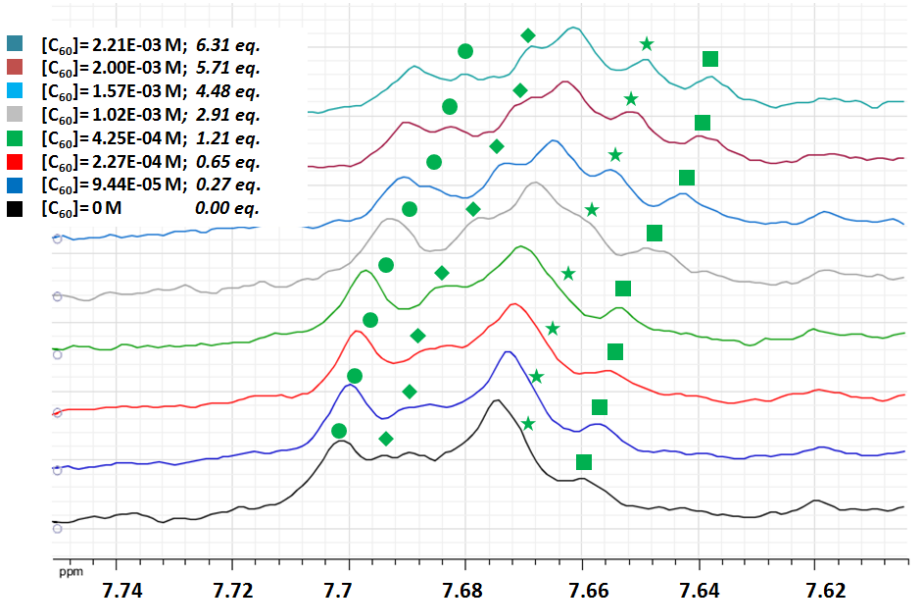

Figure A3-5. ^{1}H-NMR titration experiment for system **[18·C_{60}]** enhancing the change in some of the anthracene skeleton signals of π-exTTF. Enlarged zone indicating the shift of some of the peaks utilized for calculations.

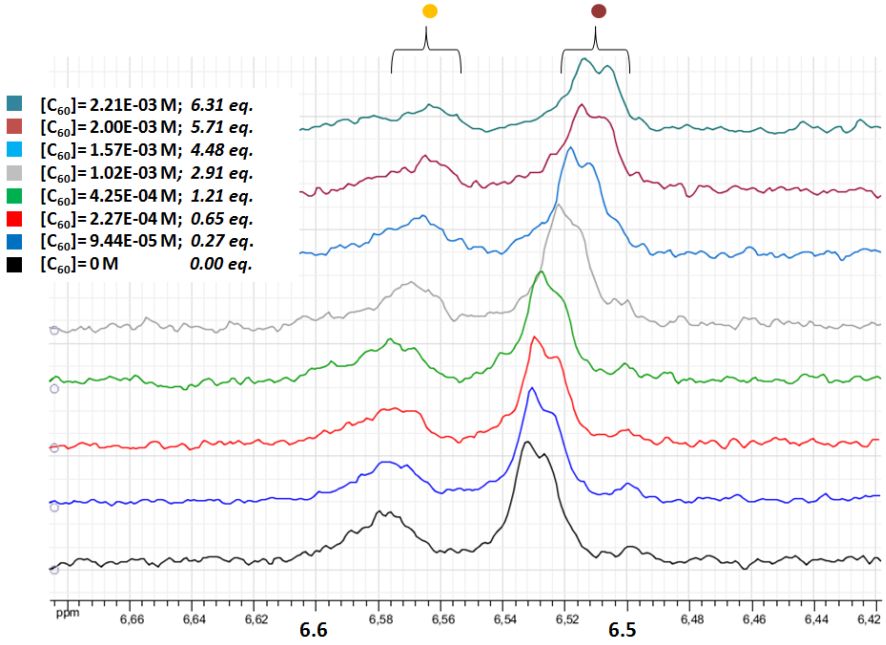

Figure A3-6. ^{1}H-NMR titration experiment for system **[18·C_{60}]** enhancing the change in the doublet and triplet of the central phenyl ring.

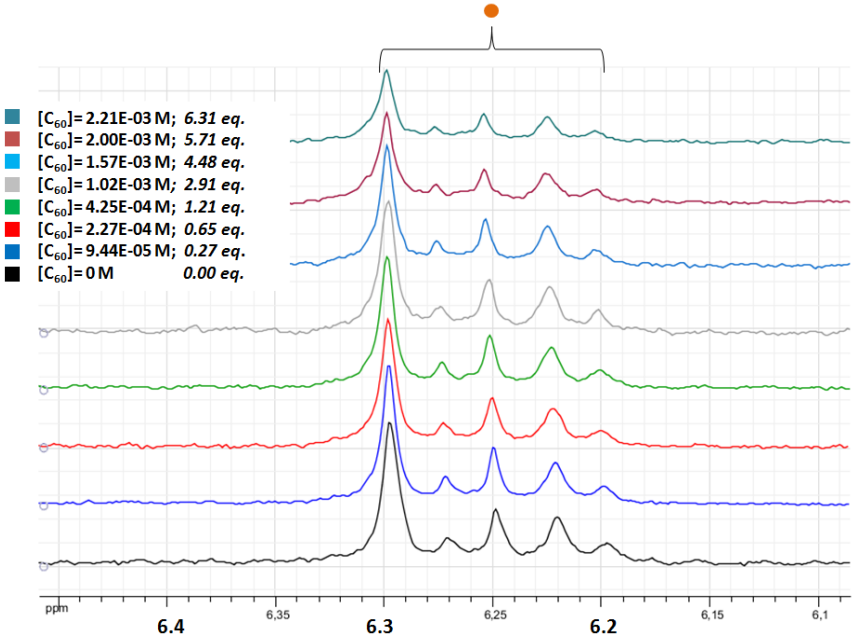

Figure A3-7. ^{1}H-NMR titration experiment for system **[18·C_{60}]** enhancing the no modification of the 1,3-dithiole ring signals in the π-exTTF.

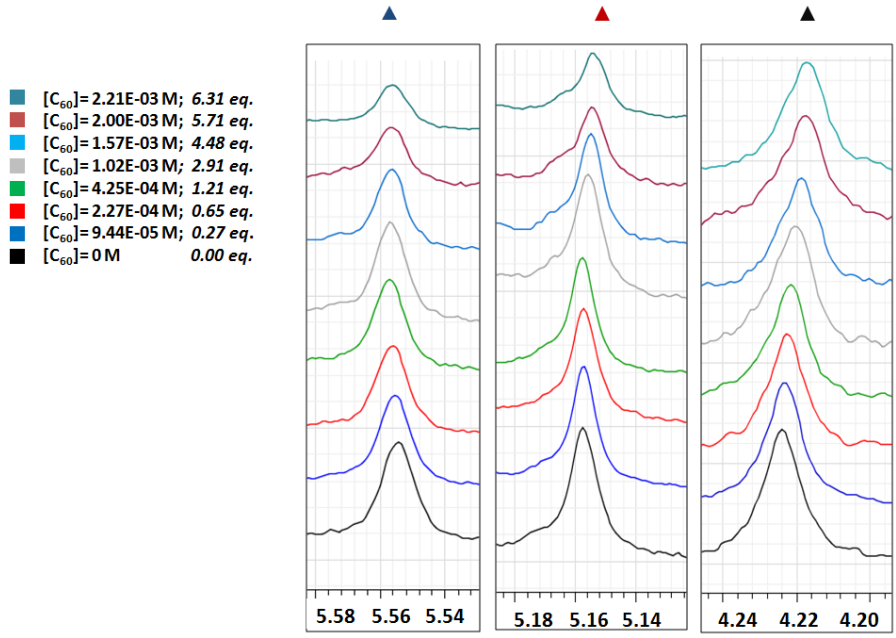

Figure A3-8. ^{1}H-NMR titration experiment for system **[18-C_{60}]** enhancing the no modification in the CH_2-triazole and the CH_2-O, and the notable shift in CH_2-N_3.

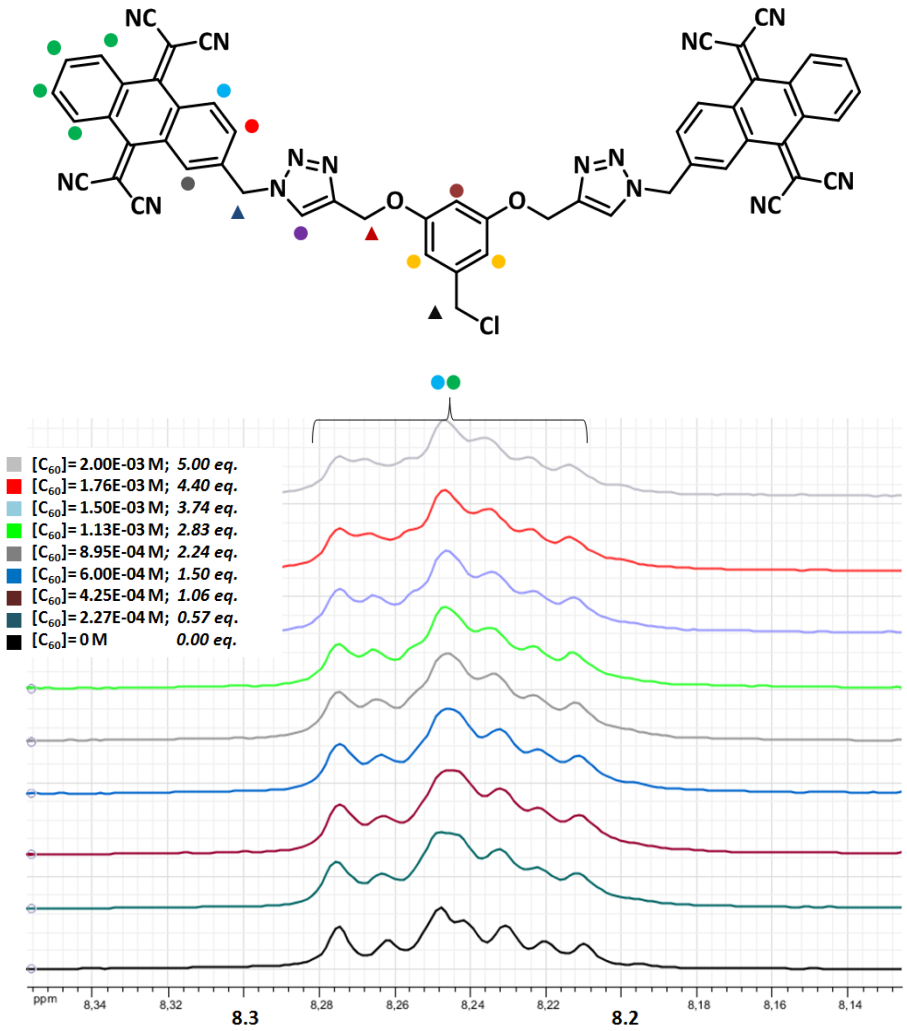

Figure A3-9. ^{1}H-NMR titration experiment for system **[22·C_{60}]** enhancing the no change in the anthracene skeleton signals of TCAQ.

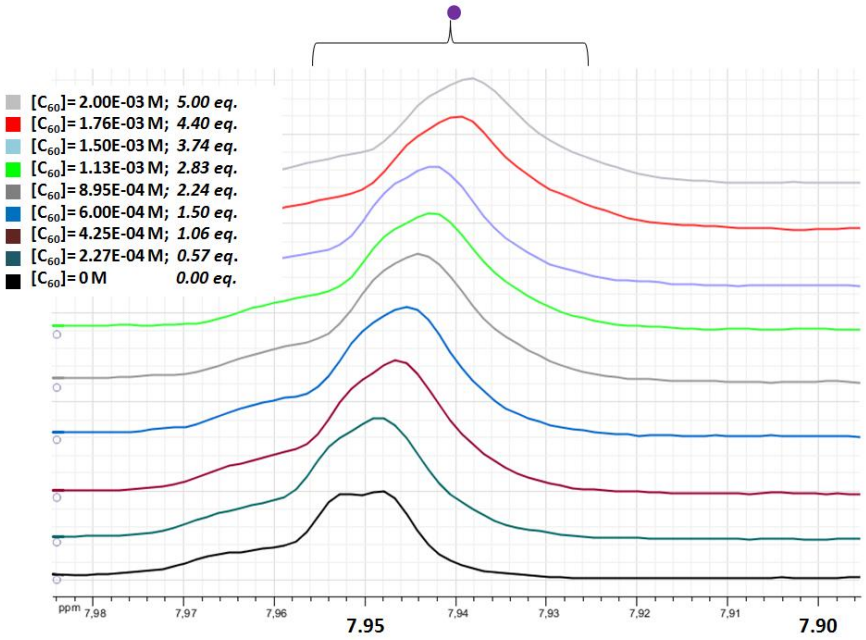

Figure A3-10. ^{1}H-NMR titration experiment for system **[22·C_{60}]** enhancing the change in the triazole signal.

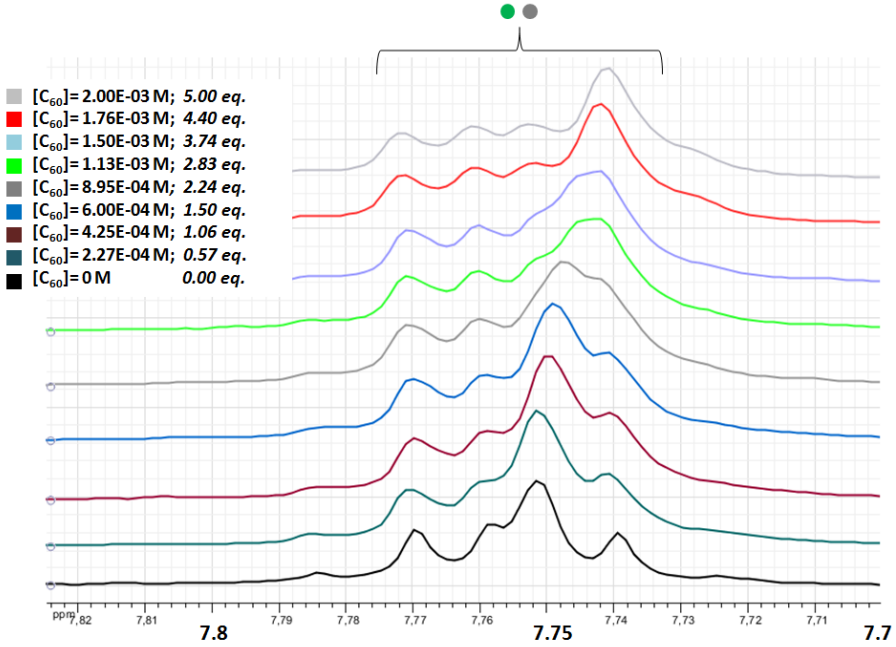

Figure A3-11. ^{1}H-NMR titration experiment for system **[22·C_{60}]** enhancing the slight change in the anthracene skeleton signals of TCAQ.

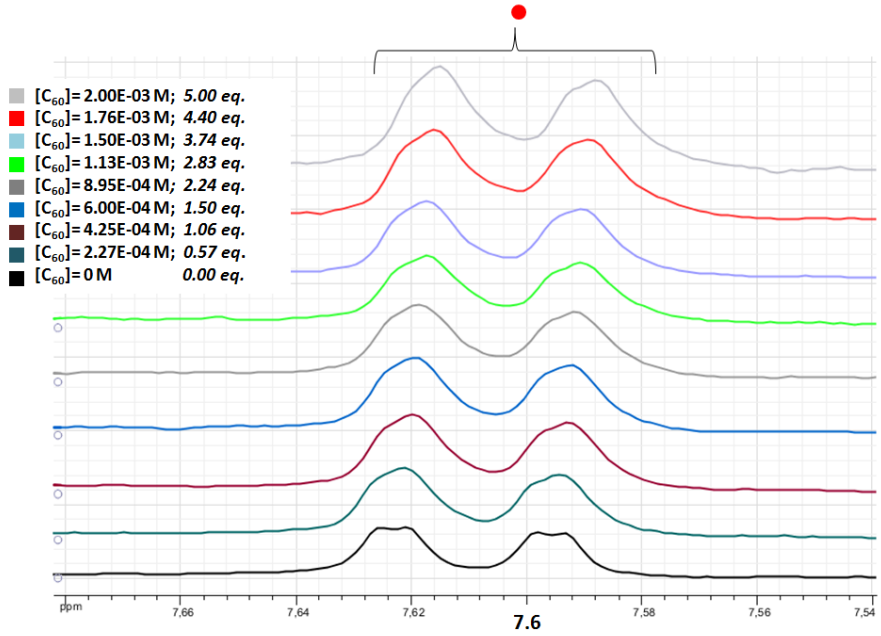

Figure A3-12. ^{1}H-NMR titration experiment for system **[22·C_{60}]** enhancing the no change in the anthracene skeleton signals of TCAQ.

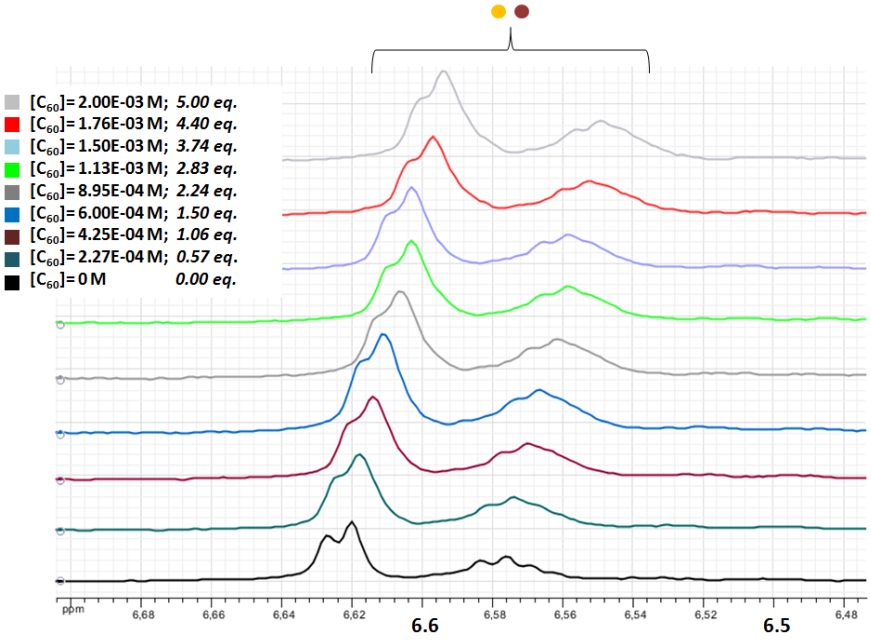

Figure A3-13. ^{1}H-NMR titration experiment for system **[22·C_{60}]** enhancing the change in the doublet and triplet of the central phenyl ring.

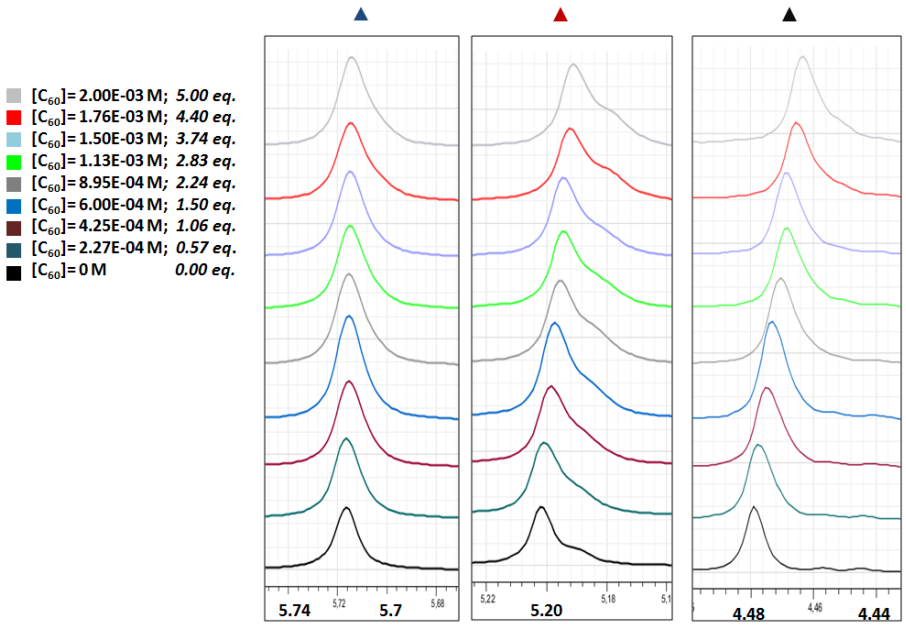

Figure A3-14. ^{1}H-NMR titration experiment for system **[22·C_{60}]** enhancing the almost imperceptible modification in the CH_2-triazole (left), the very small modification in CH_2-O (centre), and the notable shift in CH_2-Cl (right).

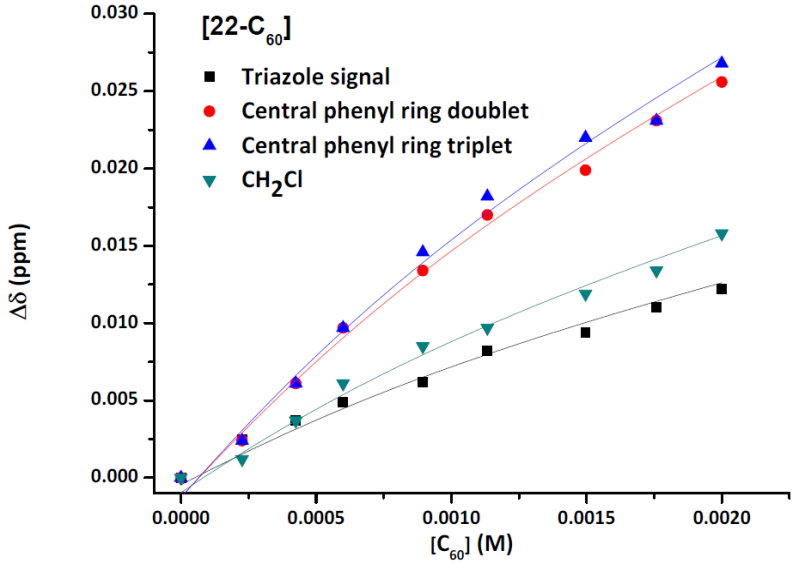

Figure A3-15. Data fitting for the signals change in the ^{1}H-NMR spectrum upon the addition of C_{60} to **22**.

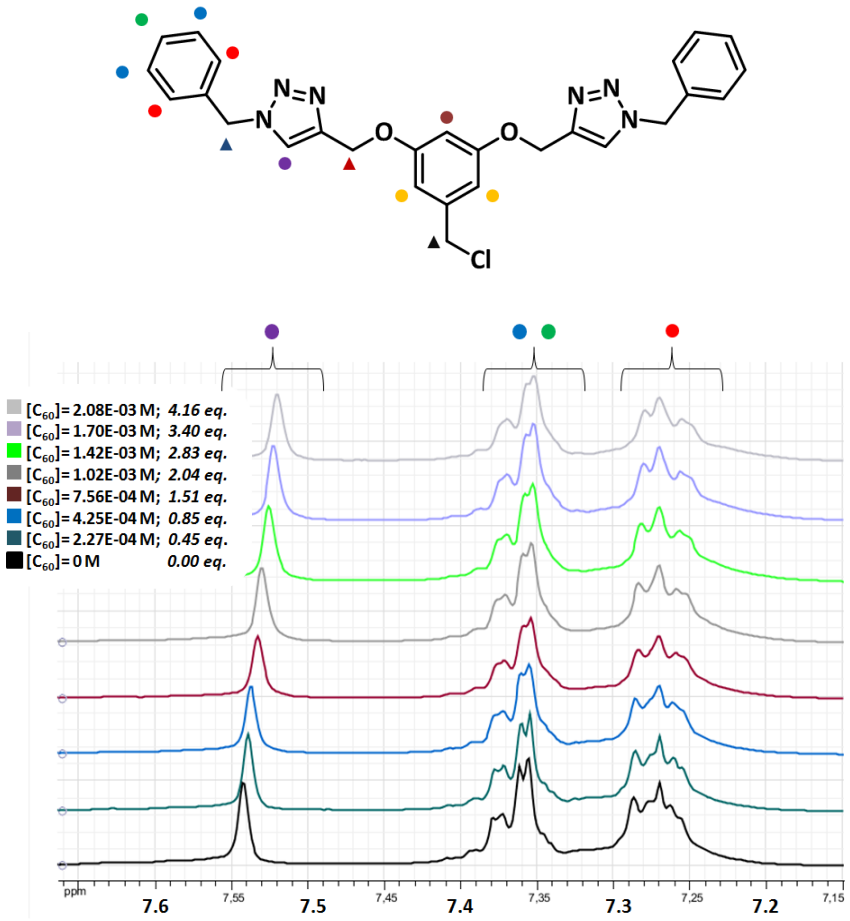

Figure A3-16. ^{1}H-NMR titration experiment for system **[24·C_{60}]** enhancing the change in the triazole signal (purple) as the side phenyl rings signals (blue, green and red) remain almost unaltered.

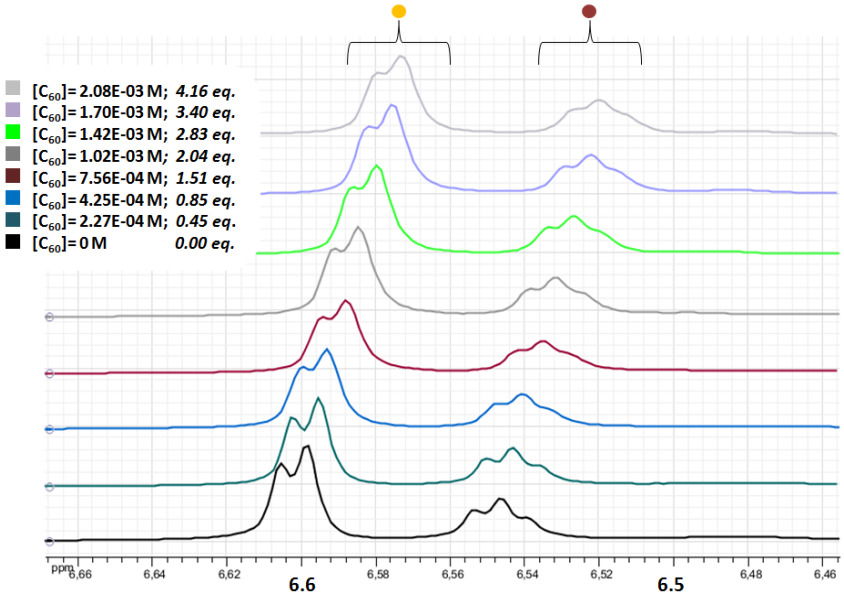

Figure A3-17. ^{1}H-NMR titration experiment for system **[24·C_{60}]** enhancing the change in the doublet and triplet of the central phenyl ring.

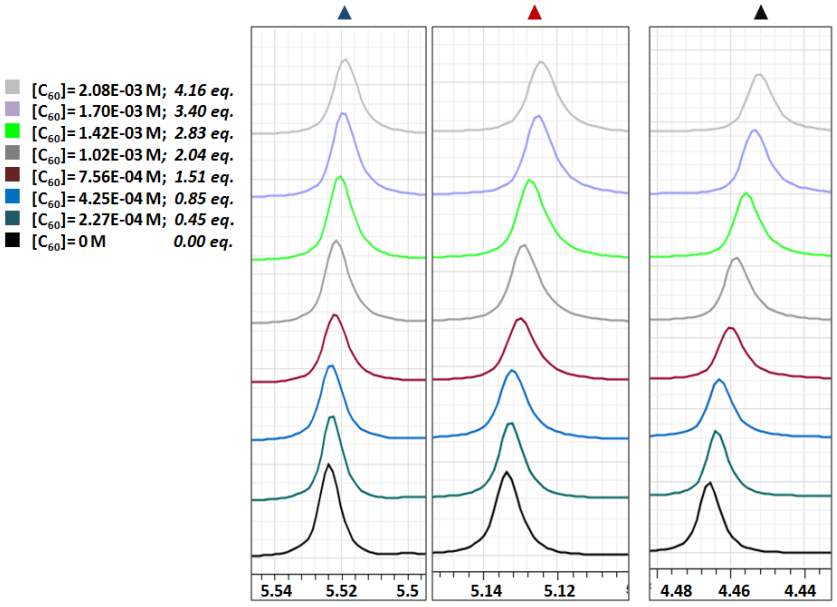

Figure A3-18. ^{1}H-NMR titration experiment for system **[24·C_{60}]** enhancing the almost imperceptible modification in the CH_2-triazole (left), the small modification in CH_2-O (centre), and the notable shift in CH_2-N_3 (right).

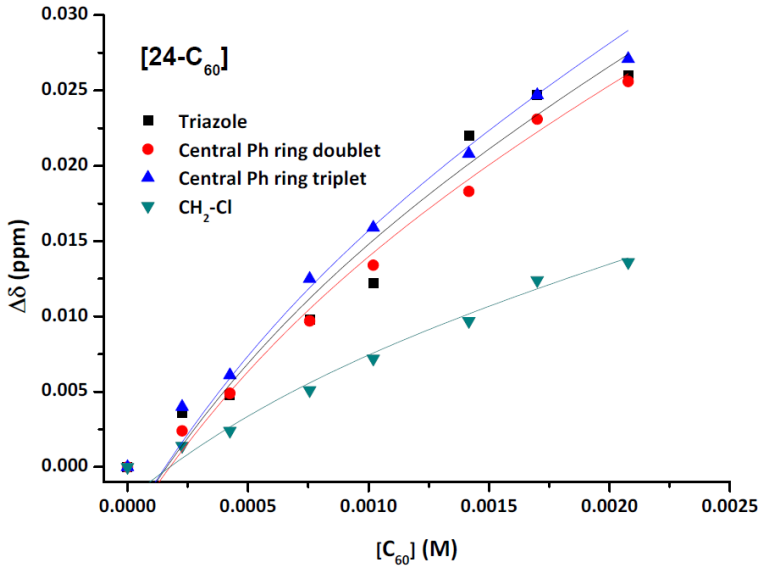

Figure A3-19. Data fitting for the signals change in ^{1}H-NMR spectrum upon addition of C_{60} to **24**.

Summary

INTRODUCTION

The development of new tools and the knowledge of new materials has been crucial to the evolution of mankind, trying to obtain lighter and more resistant materials and, also, searching for new applications to improve living conditions.

In the last decades of the 20th century a new family of carbon structures (*fullerenes*, *carbon nanotubes* (CNT) and *graphene*) emerged arousing a huge interest (Figure 1).[3,6,7] This fact is evidenced by the large number of publications about these materials during the last years, reported by scientists from different fields such as biomedicine, electronics, materials science, optics, etc.[10]

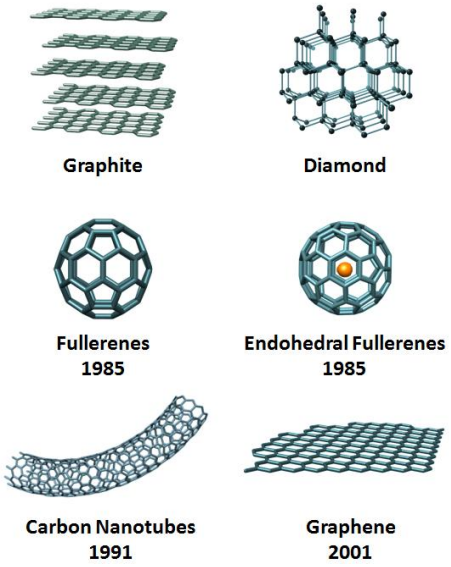

Figure 1. Structure and year of discovery for the main carbon allotropes.

On the one hand, this interest in CNT and graphene lies in their remarkable properties. It can be highlighted, for example, their highest current density, ballistic transport, ultrahigh thermal conductivity, and extremely high mechanical strength, just to name a few.[12] In fact, several experimental and commercially available products containing CNT and graphene have been developed (wind turbine blades, carbon bicycles or field emission displays).[15]

On the other hand, with the aim of exploiting and modulating fullerene properties, the *chemistry of fullerenes* has emerged as a relevant research field, leading to interesting new reactions and methodologies for its exohedral functionalization.[201] In contrast to the well known C_{60} fullerene,

[201] Filippone, S., Maroto, E. E., Martín-Domenech, Á. and Martín, N., in *Advances in Organometallic Chemistry and Catalysis*, John Wiley & Sons, Inc., **2013**, pp. 459.

the novel *endohedral fullerenes* (carbon cages containing atoms or small molecules inside) have not been so deeply studied. Those endohedral fullerenes containing metals or clusters inside, named as endohedral metallofullerenes (EMF), are usually obtained during the fabrication process utilizing a Krätschmer–Huffman generator. Furthermore, a novel methodology known as *molecular surgery*, allows the encapsulation of small molecules and non-metal species (i.e. He, H_2, N_2 or H_2O).[172-179] This methodology is based on the utilization of chemical reactions to open the fullerene cage, enlarge the hole to a suitable size, incarcerate the desired chemical specie and, a final closure of the hole by different chemical rearrangements. These strategies open the possibility of modulating fullerene properties by changing the encapsulated species.

Considering the possibilities that CNT, graphene and endohedral fullerenes offer to the society, it may seem strange not to be surrounded by many devices and products based on them. Unfortunately, as prepared CNT and graphene samples are polydisperse materials with different sizes and properties, in addition to the presence of fabrication impurities, that require separation procedures for most of the potential applications. Moreover, CNT and graphene exhibit a low solubility in water and common organic solvents what makes their chemistry and processability quite challenging. In the case of endohedral fullerenes, the low availability of these materials for extensive research is probably the most critical point that still hampers the development of these unprecedented systems.

Although scientists from different fields, and in particular chemists, have offered several procedures and methodologies to the purification and functionalization of CNT, [17,20] graphene[74] and endohedral fullerenes,[138] there is still so much work to do. In this sense, chemists must play a leading role and synthetic methodologies accompanied by the latest techniques in materials science are considered powerful tools. The aim of this work is to contribute to the development of these intriguing materials by means of their chemical modification.

OBJECTIVES

Firstly, in *Chapter 1*, we set as main goals the development of the first comparative study on the chemical reactivity of SWNT, MWNT and graphene by means of arylation/click reactions, the photophysical study of the synthesized nanoconjugates and the supramolecular study of those nanoconjugates suitable for the recognition of fullerenes.

In *Chapter 2*, we established as main objective the study of cycloaddition reactions in two different types of endohedral fullerenes, that is, on La@C_{82} as example of EMF and in H_2O@C_{60} as example of non-metal endohedral fullerene.

RESULTS AND DISCUSSION

Chapter 1: Carbon nanotubes and graphene chemistry

i) Comparative study on the covalent modification of SWNT, MWNT and graphene with π-exTTF derivatives

A set of analogous nanoconjugates of SWNT, MWNT and graphene (CNF) was synthesized (Figure 2). Firstly, 4-[(trimethylsilyl)ethynyl]aniline was attached to CNF to yield **CNF-1** by arylation reactions that involve the *in situ* formation of arenediazonium salts.[45,46] Next, two different π-exTTF based azide derivatives (**12** and **18**) were reacted with **CNF-1** by a Cu(I)- catalyzed 1,3-dipolar cycloaddition reaction (CuAAC), affording **CNF-2** and **CNF-3**.[49,113]

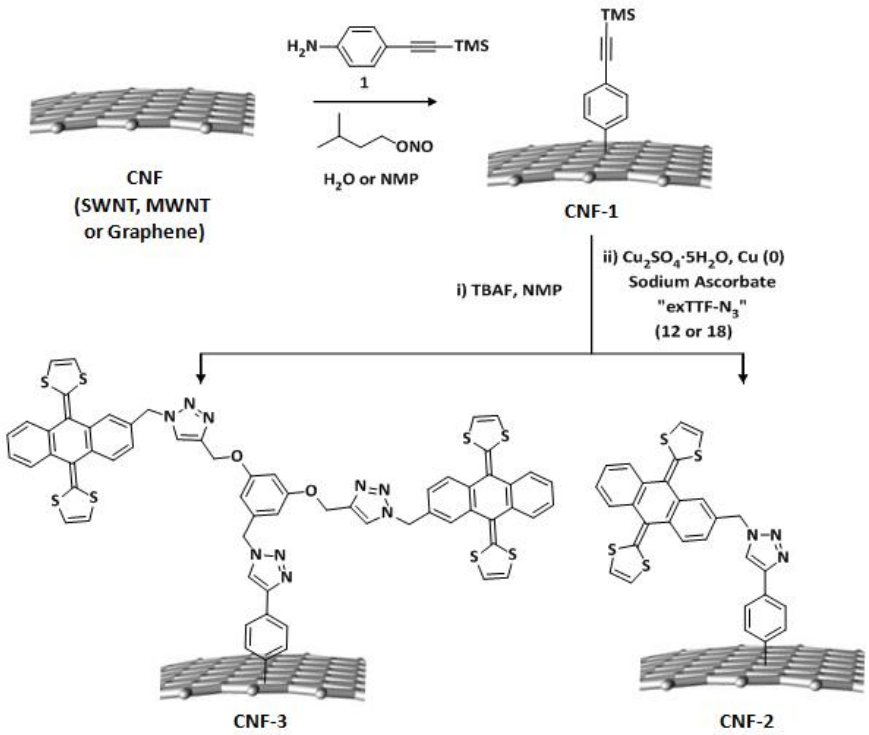

Figure 2. Synthetic procedure for the covalent modification of CNF.

All the obtained nanoconjugates were fully characterized by a thorough set of analytical, spectroscopic and microscopic techniques (TGA, FTIR, Raman, UV-Vis-NIR, cyclic voltammetry, TEM and XPS). All the experimental data suggested the correct functionalization of SWNT, MWNT and graphene.

The obtained values for the functionalization degree of each CNF, extracted from the weight loss results (% W.L.) of TGA analysis, were compared. These results suggested a higher reactivity of SWNT against arylation reactions

compared to MWNT and graphene. When the CuAAC reaction was accomplished, a higher increase in the % W.L. (**CNF-2**) was observed for **MWNT-2**, a fact that may be attributed to the better solubility of this material compared to SWNT and graphene. The same tendency was observed when the analysis on **CNF-3** were considered.

ii) Photophysical study of the synthesized nanoconjugates

Because of the electron-donor character of π-exTTF, several experiments to study the electronic communication between the π-exTTF motifs and the carbon nanoforms were performed. The electrochemical properties of **SWNT-2**, **MWNT-2** and **GR-2** samples were investigated by cyclic voltammetry (CV) and compared with **12** as a reference. In all samples, the formation of the π-exTTF dication species was clearly discernible, noticeably broader and positively shifted by 220-270 mV relative to the reference system **12**, which is likely to be a result of the intramolecular electronic interaction between CNF and π-exTTF, as previously observed in related systems.[32]

Several photophysical measurements (absorption, emission and transient absorption) were carried out in the group of Prof. D.M. Guldi, Erlangen University. The analyses by absorption spectroscopy revealed that covalently functionalized SWNT were notably blue shifted when compared to a pristine sample.[127] The fluorescence intensities of **SWNT-1** and **SWNT-2** are quenched with values of 82 and 63 %, respectively, relative to pristine SWNT. The electronic communication between π-exTTF and SWNT in **SWNT-2** was corroborated by femtosecond transient absorption measurements, where new conduction bands are observed, electrons injected from π-exTTF are shifting the transitions to lower energies, resulting in the generation of a charge separated state, with a lifetime about 250 ps.

iii) Supramolecular study of CNF as receptors for fullerenes

Many different molecular receptors for the selective recognition of fullerenes have been described and some of them, based on π-exTTF, with promising results.[107-112] However, there are no studies of these receptors anchored on CNF. Considering these points, **CNF-3** may be suitable candidates for the supramolecular study of the interaction with C_{60}.

A preliminary titration experiment by UV-vis spectroscopy was performed utilizing a free state receptor, not anchored to CNF, and C_{60} as guest. The recorded spectra exhibited a decrease in the π-exTTF absorption band and the occurrence of a new charge transfer band. The extension of the interaction was evaluated by fitting the corrected absorbance to the Hill equation, affording a log K_a= 3.51. The Job plot experiment revealed a 1:1 stoichiometry in the interaction. The titration was performed on **SWNT-3** and

MWNT-3, observing the same features that in the free-state receptor form and an additional cross-point in the recorded spectra at 630 nm. These findings may involve the formation of a supramolecular complex between the anchored receptor and the guest fullerene (Figure 3).

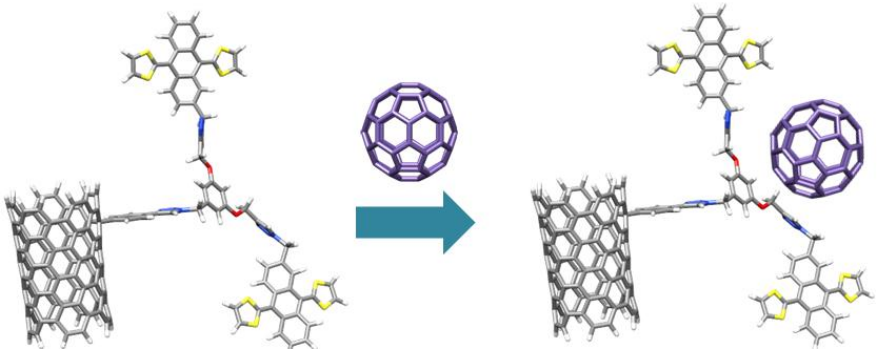

Figure 3. Depictive picture of the fullerene recognition by **CNF-3**.

Going further, a comprehensive study of the supramolecular interaction of the π-exTTF based "tweezer" system by comparison with other related receptors containing tetracyanoanthraquinodimethane (TCAQ) and benzene rings as recognition motifs was performed by ^{1}H-NMR and theoretical methods (Figure 4). The theoretical calculations were carried out in the group of Prof. Enrique Ortí at the Institut de Ciència Molecular, Universitat de València. The results revealed the importance of the central phenyl ring and the C-H of the triazole ring in the interaction. The closer phenyl ring in the anthracene skeleton demonstrated to contribute to the global interaction but in a lower extension.

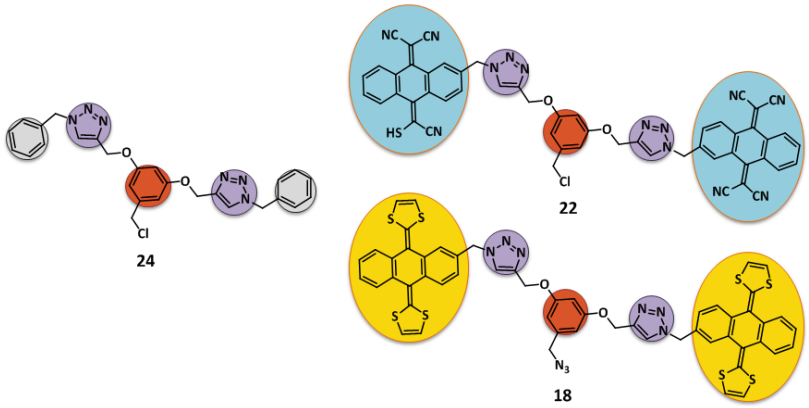

Figure 4. Three different hosts studied by ^{1}H-NMR titration experiments.

***Chapter 2:* Chemical reactivity of endohedral fullerenes**

i) Unprecedented hydrogen addition in the 1,3-dipolar cycloaddition reaction on La@C_s-C_{82}

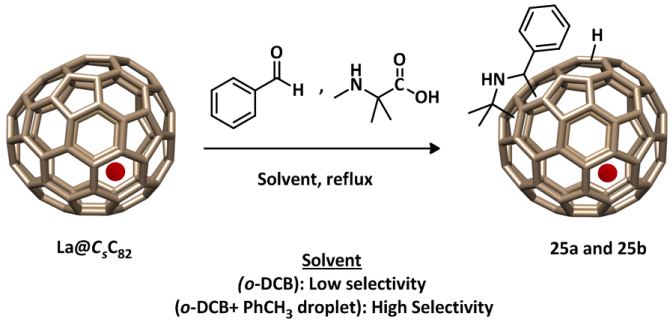

Figure 5. 1,3-dipolar cycloaddition on La@C_s-C_{82}.

In contrast to the C_{2v} isomer, a much lower number of reports are available for the chemical derivatization of La@C_s-C_{82}, mainly owing to the presence of 44 non-equivalent carbon atoms and the relatively poor selectivity of La@C_s-C_{82} in addition reactions. When this isomer was reacted with an azomethine ylide using o-DCB as solvent a poor regioselectivity is observed. In contrast, when a droplet of toluene was added, the reaction afforded only two products (**25a** and **25b**). While **25a** exhibited a good stability, **25b** was rapidly oxidized to afford **25b-O** (Figure 5).

Both **25a** and **25b-O** were fully characterized. Firstly, MALDI-TOF mass spectrometry analysis suggests the presence of an additional H. Furthermore, electron spin resonance (ESR) showed a closed-shell configuration, in contrast with the starting EMF and the previously reported cycloadducts of La@C_{2v}-C_{82}.185 These data is in line with the proposed unexpected addition of H to the cage.

Several 1D and 2D NMR analysis were performed on **25a** (^{1}H, ^{13}C-NMR, DEPT 135, HSQC and HMBC) certifiyng that a hydrogen atom was attached on the cage. The ^{1}H-NMR signal of the hydrogen atom at 3.19 ppm shows the clear correlation with carbon atoms of the fullerene cage both in HSQC and HMBC. The same analysis on **25b-O** suggested that the H atom was substituted by an OH group.

The H was firstly considered to derive from H_2O released from the azomethine ylide formation, but several experiments ruled out this possibility, (no evidence of deuterium addition on the cage was found when D_2O and a droplet of toluene were added). In contrast, when the starting La@C_s-C_{82} was heated in *o*-DCB and in the presence of toluene, a small portion was found to react resulting in an unknown product (1156 *m/z*, attributed to La@$C_{82}HO_2$).

UV-vis spectroscopy revealed identical features for both **25a** and **25b-O**, what involves the same addition pattern for both derivatives, which can be considered site isomers. In order to predict the addition sites, DFT calculations were performed considering two different criteria:[187] i) the LUMO distribution on the dipolarophile surface and ii) the radical character of the azomethine ylide. The second criteria was found to predict a more reasonable addition pattern (positions of the cage C22 and C23 for cycloaddition and C3 for the H radical addition) that matched with the results found in the ROESY spectroscopy.

This work was carried out in collaboration with the group of Prof. Akasaka in the Tsukuba Life Science Center for Advanced Research at Tsukuba University, where a three month stay was accomplished and served as the beginning of the project.

***ii) Study of the encapsulated H_2O molecule role in the cis/trans isomerization process of* pyrrolidinofullerenes**

Considering the recent outstanding progress of our group in the development of an efficient methodology to prepare enantiopure fulleropyrrolidines,[192,193,197] in complementary work, we have found an enantiospecific selective *cis/trans* isomerization process of these derivatives. A systematic study of the process at different levels has been accomplished and validated with further DFT calculations that support the experimental results (Figure 6).

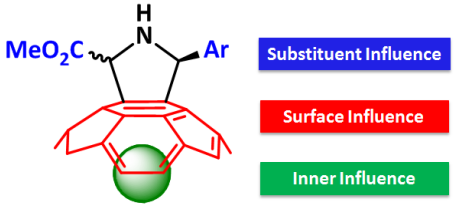

Figure 6. "Three levels" approach that may influence the stereochemical result of the *cis*/*trans* isomerization in fulleropyrrolidines.

Firstly, a series of enantiopure C_{60}-fulleropyrolidines with different aromatic groups were synthesized under the previously optimized catalytic systems and conditions reported, affording derivatives with an optical purity about 80-99 % (Figure 7). The conditions for study the isomerization process were established at 35 ºC, utilizing toluene/acetonitrile as solvent.

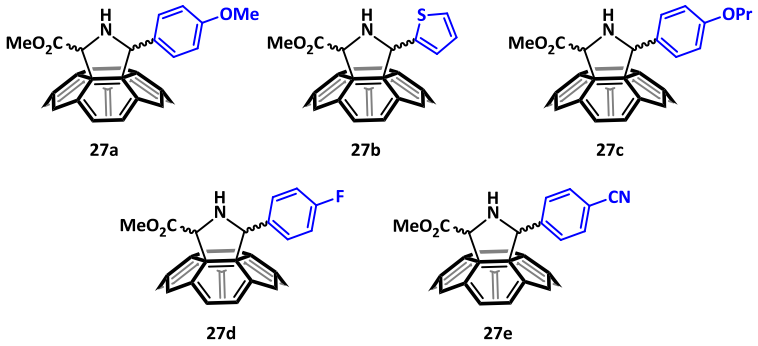

Figure 7. Optically pure pyrrolidino[60]fullerenes synthesized.

When enantiopure *cis*-pyrrolidino[60]fullerenes bearing electron-releasing groups (**27a-c**) were submitted to isomerization, a 70:30 (*cis/trans*) equilibrium was reached, observing a retention in the configuration of C2. The same result was observed when the corresponding *trans* pair was utilized. In contrast, when electron-withdrawing groups are present (**27d-e**), no isomerization was observed. These experimental finding, where C2 is unaltered during the isomerization while the C5-cage must be broken, suggested the formation of a zwitterionic intermediate where fullerene stabilizes the anion and a benzylic cation is formed, allowing the rotation around the C2-N bond to afford the opposite diastereomer (Figure 8). The stability of the carbocation is the determining issue to the extension of the process, and it will be more favourable when carried out under the presence of electron-rich rings. In this sense, the retention in the C2 configuration and the lower extension of the diastereomer conversion in electron-poor derivatives corroborate this proposal. Moreover, the higher energy necessary for these derivatives will promote the racemization and retrocycloaddition processes that lead to lower enantiomeric excess, as experimentally observed.

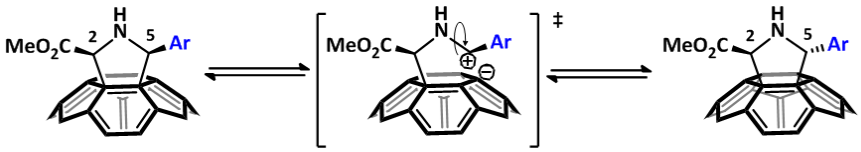

Figure 8. Stepwise isomerization reaction involving a zwitterionic intermediate.

Going to the next level, the same experiment was performed on *cis*-pyrolidino[70]fullerenes. These derivatives, where the electron-releasing group are differently oriented (close to the equatorial region in **28** and close to the pole in **29**) exhibited a similar diastereomerical result (70:30, *cis/trans*). However, while *cis*-**28** reached this ratio in two days, *cis*-**29** required nine days to reach the same ratio.

Following the same reasoning that in *cis*-[60]-fulleropyrolidines, the isomerization of **28** and **29** afforded different structures for each zwitterionic intermediate, localized in C8 and C25, respectively (Figure 9). It is well known that carbanions are better stabilized in more planar systems because of their larger *s* character and are destabilized in more pyramidilized carbons because of its larger *p* character. Taking these considerations in mind, equatorial carbon atoms in C_{70} are more planar compared to those close to the cage poles. Consequently, C8 would stabilize the carbanion better than C25, providing a higher isomerization rate, which is consistent with the experimental results.

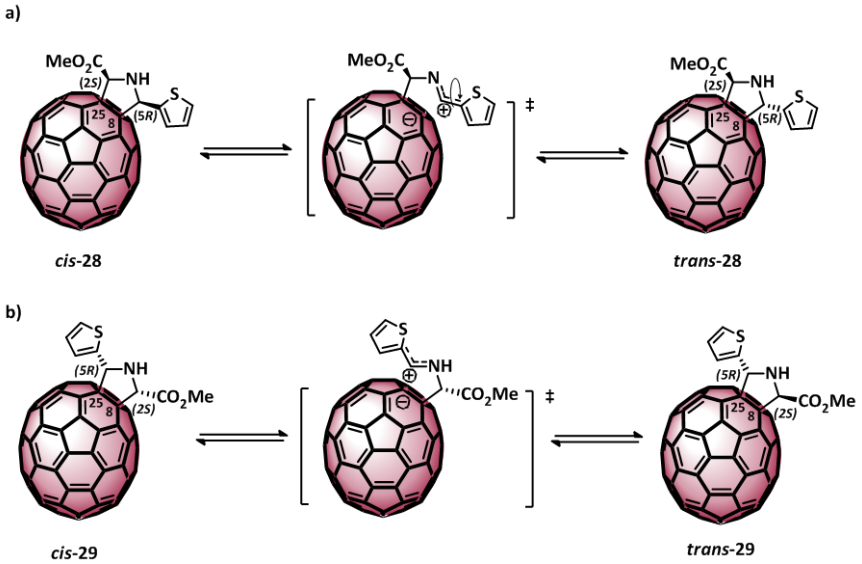

Figure 9. Stepwise isomerization reaction involving a zwitterionic intermediate for the different regioisomers in C_{70}.

In order to study the influence of an encapsulated polar molecule in the isomerization, enantiopure $H_2O@C_{60}$-pyrrolidines were synthesized. Previous to this synthesis, the preparation of the endohedral $H_2O@C_{60}$ was performed during a research stay at the laboratory of Prof. Murata (Institute for Chemical Research, Kyoto University).

Under the same conditions utilized for **27**, the $H_2O@C_{60}$-pyrrolidines **35a** were obtained in an enantioespecific manner (Figure 10).

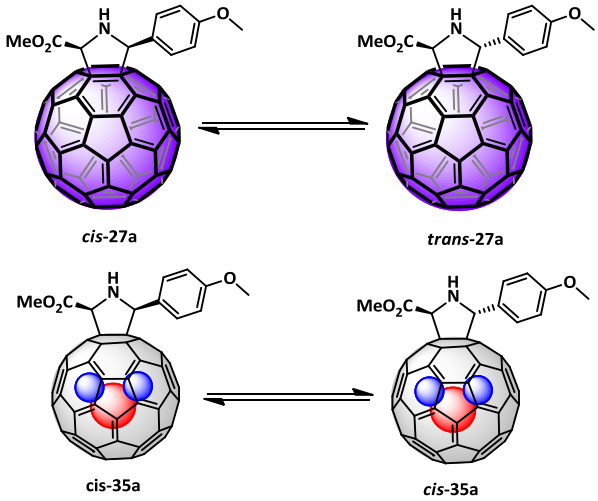

Figure 10. Synthesis of endohedral $H_2O@C_{60}$-fulleropyrrolidines utilized for the isomerization study.

Once the synthesis and characterization was accomplished, the *cis/trans* isomerization was studied and excellent results were obtained, observing the expected 7:3 ratio and a retention in enantiomeric excess for both *cis* and *trans* pairs. Going further, a comparative study between the empty and endohedral related isomers was accomplished. The *cis*/*trans* ratio was measured during 6 days revealing an enhancement in the results in the endohedral derivatives (Figure 11). The results suggested that the inner water molecule is not inert and can play a role in favour of the isomerization.

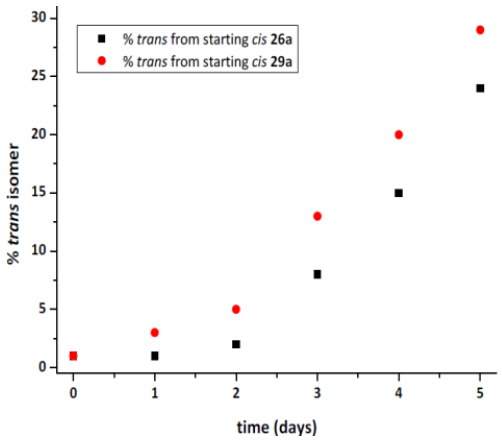

Figure 11. Results for the *cis/trans* isomerization in derivatives **27a** and **35a** along the time.

Since the experimental conditions are exactly the same and the only modification is the inner water hosted inside the cage, the enhancement in the isomerization kinetic rates can only be rationalized by a H assistance in

the stabilization of the zwitterionic intermediate. Interestingly, the stereochemical outcome also seems to be influenced by the entrapped H_2O.

Complementary DFT theoretical calculations were performed by the group of Prof. Solá at Girona University. The relative energies for both diastereomer intermediates and the possible contribution of side processes (retro-cycloaddition or racemization) were considered and, results corroborated the proposed zwitterionic intermediate with the retention in C2, thus that the role of H_2O in the major stabilization of the carbanion when **27a** and **35a** are compared.

CONCLUSIONS

Chapter 1: Carbon nanotubes and graphene chemistry

A set of nanoconjugates bearing π-exTTF motifs and different carbon nanostructures (SWNT, MWNT and graphene) were synthesized and fully characterized (**CNF-2** and **CNF-3**). A comparative study on the different reactivity against arylation and CuAAC cycloaddition reaction was accomplished. Considering the results, it can be stated a higher reactivity of SWNT against arylation reaction compared to MWNT and graphene. In contrast, the better solubility of MWNT make this CNF to react under CuACC conditions with a better efficiency than SWNT and graphene.

The electronic communication between π-exTTF and CNF was clearly corroborated by cyclic voltammetry and several photophysical measurements (absorption, emission and transient absorption).

The ability of **CNF-3** to recognize fullerenes and establish a supramolecular interaction was evidenced by titration experiments utilizing UV-vis-NIR spectroscopy. A comprehensive study about the nature of the interaction was performed by ^{1}H-NMR and theoretical methods. The three analogous **18**, **22** and **24**, bearing different recognition motifs (π-exTTF, TCAQ and phenyl), were studied and the results revealed the leading role of the central phenyl ring and the C-H in the triazole ring in the formation of the complex.

Chapter 2: Chemical reactivity of endohedral fullerenes

i) Unprecedented hydrogen addition in the 1,3-dipolar cycloaddition reaction on La@C_s-C_{82}.

The almost unexplored La@C_s-C_{82} has been considered in 1,3-dipolar cycloaddition reactions and an expected selectivity has been found in the reaction, affording only two products with the highest reported yields to date for this EMF. This finding was only observed when a droplet of toluene is added to the reaction medium.

ESR analysis, MALDI-TOF MS, 1D and 2D-^{1}H-NMR experiments on these cycloadducts, obtained with La@C_s-C_{82}, (**25a** and **25b-O**) revealed the presence of an unexpected H atom on the cage. The radical addition of the H atom stabilizes the starting paramagnetic cage yielding a diamagnetic product.

Derivative **25a** demonstrated a good stability under ambient conditions while **25b** was rapidly oxidized by nucleophilic substitution affording product **25b-O**.

The order in the reactions (i: cycloaddition reaction + H-addition or ii: H-addition + cycloaddition reaction) was studied by different thermal experiments using deuterated solvent. The H-addition revealed to be a very slow process that take place after the cycloaddition reaction.

DFT calculations were performed in order to unveil the addition pattern of both derivatives. The radical character seems to be the driving force and the different orientation of the phenyl substituent may be the reason of the rapid oxidation of **25b** in contrast to **25a**.

ii) Study of the encapsulated H_2O molecule role in the cis/trans isomerization proccess of pyrrolidinofullerenes

A novel enantiospecific *cis-trans* isomerization in optically pure fulleropyrrolidines under mild conditions in polar solvents has been described. The process was found to involve a C2 configuration retention and a mechanism involving a zwitterionic intermediate was proposed and studied at three different levels: i) different electron character of the substituent, ii) different cage geometry and iii) influence of inner species in the cage.

It was demonstrated that pyrrolidino[60]fullerenes bearing electron-releasing substituents in the aryl group favour the process in contrast to that found for electron-withdrawing substituents.

[70]-fulleropyrrolidines were studied under the same conditions revealing that the zwitterionic intermediate is more stabilized when the charge is localized on the equatorial carbon atoms, favouring the isomerization process.

Analogous fulleropyrrolidine derivatives were synthesized on endohedral fullerene $H_2O@C_{60}$. and the isomerization process was demonstrated to be more favourable in the endohedral derivatives by means of H bond assistance. This interaction may stabilize the zwitterionic intermediate, setting a precedent to the development of a novel “inner” manner to influence the stereochemical outcome in fullerene chemistry.

DFT calculations corroborate the enantiospecific result of the isomerization and the relative stabilities of reaction intermediates, thus supporting the proposed stepwise mechanism involving a zwitterionic intermediate with a C2 retention.

Resumen

INTRODUCCIÓN

El desarrollo de nuevas herramientas y el conocimiento de nuevos materiales ha sido crucial para la evolución de la humanidad, tratando de obtener materiales más ligeros y más resistentes, así como buscando nuevas aplicaciones para mejorar las condiciones de vida.

En las últimas décadas del siglo XX una nueva familia de estructuras de carbono (fullerenos, nanotubos de carbono (CNT) y grafeno) surgió despertando un enorme interés (Figura 1).[3,6,7] Este hecho se evidencia por el gran número de publicaciones sobre estos materiales durante los últimos años por científicos de diferentes campos como la biomedicina, la electrónica, la ciencia de materiales, la óptica, etc.[10]

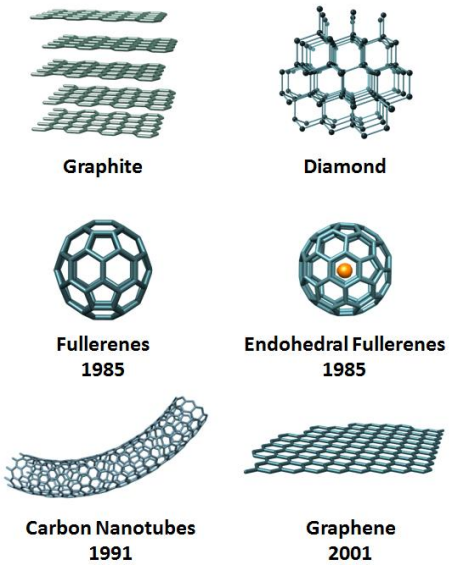

Figure 1. Estructura de los alótropos de carbono descubiertos recientemente.

Por un lado, el interés en CNT y grafeno reside principalmente en sus interesantes propiedades.[12] Entre éstas, puede destacarse su alta densidad de corriente, conducción balística, conductividad térmica ultra-alta y una extremada resistencia mecánica. De hecho, varios dispositivos experimentales e incluso algunos productos comerciales han sido desarrollados (turbinas eólicas, bicicletas de carbono o dispositivos de emisión de campo).[15]

Por otro lado, con objeto de explotar y modular las propiedades de los fullerenos, la *química de* fullerenos ha emergido como un importante campo de investigación, conduciendo a nuevas e interesantes reacciones para su funcionalización exoédrica.[201]

Al contrario que el fullereno C_{60}, cuya química es bien conocida, los fullerenos endoédricos (jaulas de carbono que contienen átomos o moléculas pequeñas en su interior) no han sido estudiados en tanta profundidad. Aquellos fullerenos endoédricos que contienen metales o clústers en su interior, denominados metalofullerenos endoédricos (EMF), se obtienen normalmente durante el proceso de fabricación en reactores Krätschmer–Huffman. Por otro lado, una novedosa metodología denominada cirugía molecular, permite el encapsulado de gases y otras pequeñas moléculas (ej: He, H_2, N_2 or H_2O).[172-179] El proceso de obtención de este tipo de fullerenos endoédricos se basa en cuatro etapas: uso de reacciones químicas para abrir un orificio en la jaula de carbono, seguido de otras reacciones que permiten expandir dicho orificio hasta un tamaño adecuado, encapsulado de la especie deseada y cierre final mediante sucesivas reacciones de reordenamiento. Estos dos procedimientos abren la posibilidad de modular la reactividad y las propiedades de los fullerenos en función de la especie encapsulada en su interior.

En vista de las posibilidades que CNT, grafeno y fullerenos endoédricos ofrecen a la sociedad, puede resultar extraño que no estemos rodeados de dispositivos y productos basados en estas estructuras. Desafortunadamente, CNT y grafeno son materiales polidispersos con diferentes tamaños y propiedades que además presentan impurezas resultantes de su fabricación, cuya separación es necesaria para múltiples aplicaciones. Además, CNT y grafeno presentan una baja solubilidad tanto en agua como en los disolventes orgánicos más comunes, lo que hace que su química y su tratamiento sea bastante tedioso. En el caso de los fullerenos endoédricos, su baja disponibilidad es probablemente el punto más crítico que aún imposibilita el desarrollo de estos novedosos sistemas.

Aunque investigadores de diferentes campos, y en particular químicos, han ofrecido diversos procedimientos y metodologías para la purificación y funcionalización de CNT[17,20] grafeno[74] y fullerenos endoédricos,[138] todavía hay mucho trabajo por hacer. En este sentido, la química debe jugar un papel principal de la mano de estrategias sintéticas y las últimas técnicas en ciencia de materiales. El objeto de este trabajo es contribuir al desarrollo de estos curiosos materiales mediante su modificación química.

OBJECTIVOS

En el Capítulo 1 se establece como objetivos principales el desarrollo del primer estudio comparativo sobre la reactividad química de SWNT, MWNT y grafeno mediante reacciones de arilación/click, el estudio fotofísico de los nanoconjugados sintetizados así como estudio supramolecular de aquellos sistemas adecuados para el reconocimiento de fullerenos.

En el Capítulo 2, se establece como principal objetico el estudio de reacciones de cicloadición en los dos diferentes tipos de fullerenos endoédricos, es decir sobre La@C_{82} como ejemplo de EMF, y sobre H_2O@C_{60} como ejemplo de fullereno endoédrico no metálico.

RESULTADOS Y DISCUSIÓN

<u>Capítulo 1:</u> Química de nanotubos de carbono y grafeno

i) Estudio comparativo de la modificación covalente de SWNT, MWNT y grafeno con derivados de π-exTTF

Se ha llevado a cabo la síntesis de una serie de nanoconjugados de SWNT, MWNT y grafeno (Figura 2). En primer lugar, mediante reacciones de arilación que implican la generación *in situ* de sales de arenodiazonio, la 4-[(trimetilsilil)etinil]anilina se adiciona sobre las diferentes nanoformas de carbono (CNF) para dar lugar a los correspondientes **CNF-1**.[45,46] Posteriormente, dos azidas diferentes derivadas de π-exTTF (**12** and **18**) se hacen reaccionar con las diferentes **CNF-1** mediante una cicloadición dipolar 1,3 catalizada por Cu(I) (CuAAC), obteniéndose los correspondientes nanoconjugados **CNF-2** y **CNF-3**.[49,113]

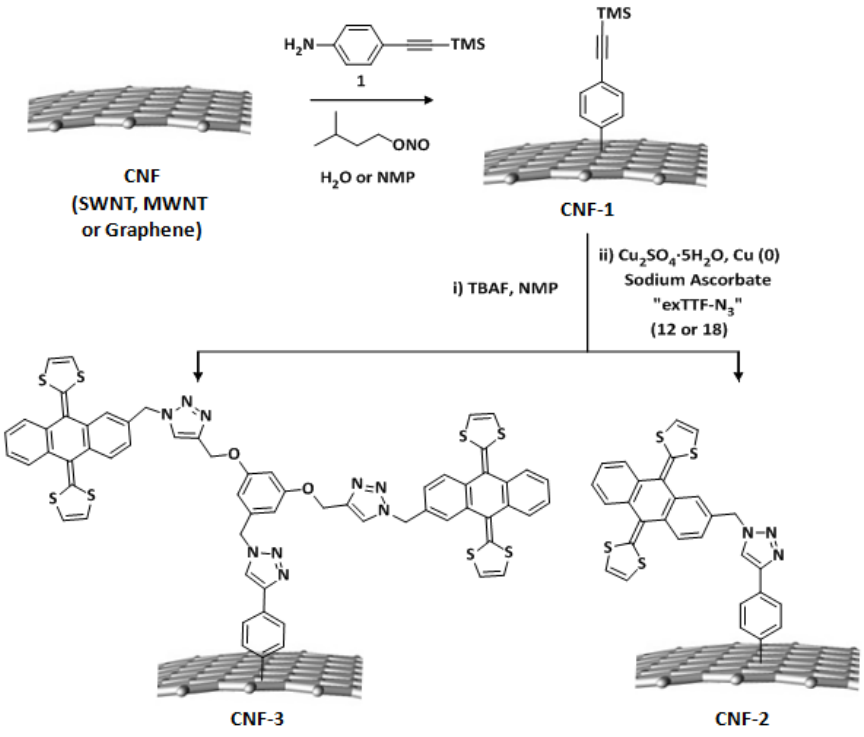

Figura 2. Estrategia sintética para la modificación covalente de CNF.

Todos los nanoconjugados sintetizados se caracterizaron minuciosamente mediante técnicas analíticas, espectroscópicas y microscópicas (TGA, FTIR, Raman, UV-Vis-NIR, voltametría cíclica, TEM y XPS). Todos los resultados experimentales certificaron la correcta funcionalización de SWNT, MWNT y grafeno.

El grado de funcionalización de cada nanoconjugado, extraído del porcentaje de masa perdida en los análisis termogravimétricos, fue analizado y comparado. Los valores sugieren una mayor reactividad de SWNT frente a la reacción de arilación en comparación con MWNT y grafeno. Sin embargo, cuando se llevaron a cabo las reacciones CuAAC, el incremento en la pérdida de masa es notablemente mayor en los derivados de MWNT que en los de SWNT y grafeno (**CNF-2**), hecho atribuible a una mejor solubilidad de MWNT en comparación con el resto así como a una mayor distancia entre grupos alquino en **MWNT-2** que favorece la adición de la azida. La misma tendencia se observó en **CNF-3**.

ii) Estudio fotofísico de los nanoconjugados sintetizados

Debido al carácter electro-dador del π-exTTF, se llevaron a cabo varios experimentos con objeto de estudiar la comunicación electrónica entre las unidades de π-exTTF y las diferentes CNF. Las propiedades electroquímicas de **SWNT-2**, **MWNT-2** y **GR-2** se analizaron mediante voltametría cíclica (CV) y comparadas con el sistema **12** como referencia. En todas ellas se pudo observar la formación de la especie dicatiónica del π-exTTF, cuya oxidación se encontró notablemente más ancha y desviada positivamente entre 220-270 mV en comparación con el sistema de referencia **12**. Este hecho puede atribuirse a la comunicación intramolecular entre CNF y π-exTTF.[32]

Varios análisis fotofísicos (absorción, emisión y absorción transitoria) fueron llevados a cabo por el grupo del Prof. D.M. Guldi, Erlangen University. La espectroscopia de absorción reveló que los sistemas funcionalizados covalentemente (**SWNT-1** y **SWNT-2**) se encontraban desplazadas hacia energías más altas en comparación con SWNT.[127] Las intensidades de fluorescencia de dichos sistemas mostraron una disminución en torno al 82 y 63 % para **SWNT-1** y **SWNT-2**, respectivamente, en relación al material de partida. En el caso de **SWNT-2**, mediante medidas de absorción transitoria, se observaron nuevas bandas de conducción como consecuencia de los electrones inyectados por las unidades de π-exTTF que desplazan las transiciones a valores de energía más bajos dando como resultado un estado de separación de carga con valores de vida media alrededor de los 250 ps.

iii) Estudio supramolecular de CNF como receptores de fullerenos

Hasta la fecha se han descrito múltiples receptores moleculares para el reconocimiento selectivo de fullerenos e incluso varios de ellos basados en π-

exTTF.[107-112] Sin embargo, no existen estudios de estos receptores anclados sobre CNF. En vista de ello, se consideró que los sistemas **CNF-3** podrían ser unos candidatos idóneos para llevar a cabo un estudio supramolecular sobre su interacción con C_{60}.

En primer lugar se llevó a cabo una valoración preliminar mediante espectroscopia UV-vis utilizando el receptor en estado libre, sin anclar a CNF, y C_{60} como molécula huésped. Los espectros registrados mostraron como una de las bandas asociadas al π-exTTF disminuía su intensidad al mismo tiempo que se generaba una nueva banda de transferencia de carga como consecuencia de la interacción. La extensión de dicha interacción se evaluó mediante el ajuste de la absorbancia corregida a la ecuación de Hill, obteniéndose un valor para log K_a= 3.51. Además, los experimentos *Job plot* revelaron la formación de una especie de estequiometria 1:1. La valoración se llevo a cabo entonces utilizando los sistemas **SWNT-3** y **MWNT-3**, observándose las mismas características que en la valoración del receptor en estado libre, así como la aparición de un nuevo punto de corte sobre 630 nm. Estos hechos implicarían la formación de un complejo supramolecular entre el receptor anclado a CNF y la especie huésped (Figura 3).

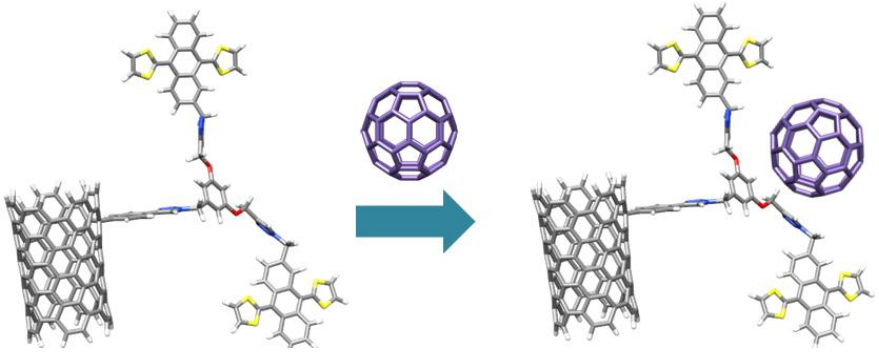

Figura 3. Imagen descriptiva del reconocimiento de fullereno por **CNF-3**.

Con objeto de investigar más en la naturaleza de la interacción que se establece entre este tipo de receptores y fullereno, se llevó a cabo un estudio comparativo mediante ^{1}H-RMN y cálculos teóricos con otros sistemas análogos donde las unidades de π-exTTF fueron reemplazadas por tetraciano-antraquinodimetano (TCAQ) y anillos de benceno (Figure 4). Dichos cálculos teóricos fueron desarrollados en el grupo de Prof. Enrique Ortí at the Institut de Ciència Molecular, Universitat de València. Los cálculos teóricos revelaron la importancia del anillo central de benceno y el C-H del anillo de triazol en la interacción. El anillo aromático del esqueleto antraquinónico más cercano al anillo de triazol también demostró contribuir a la estabilización de la interacción, pero en menor extensión.

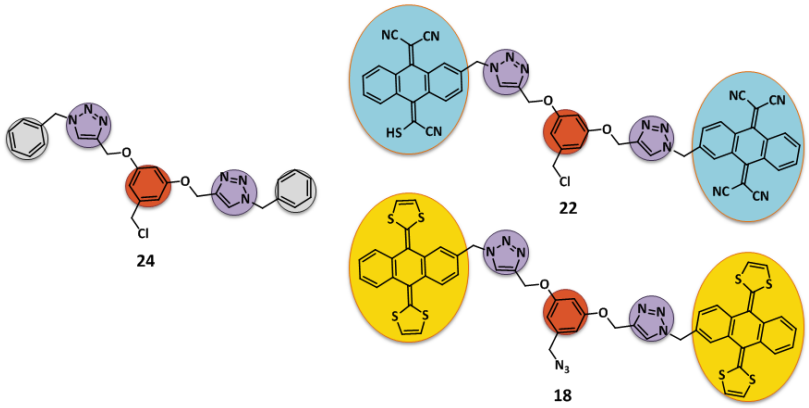

Figura 4. Estructura de los tres diferentes sistemas estudiados mediante valoraciones por ^{1}H-RMN.

***Capítulo 2:* Reactividad química de fullerenos endoédricos**

i) Adición de H en la reacción de cicloadición 1,3 dipolar sobre La@C_s-C_{82}

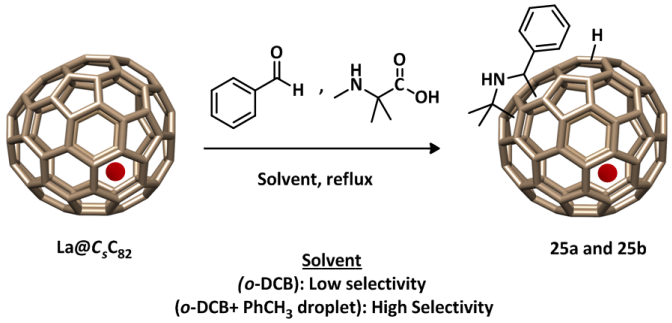

Figura 5. Cicloadición 1,3-dipolar sobre La@C_s-C_{82}.

Mientras que existen diversas reacciones descritas sobre el isómero C_{2v} del La@C_{82}, el isómero C_s permanece prácticamente inexplorado, principalmente debido a la presencia de 44 átomos de carbono no equivalentes y la relativa baja selectividad que presenta en las reacciones de adición. En este trabajo dicho isómero se hizo reaccionar con un iluro de azometino utilizando o-DCB como disolvente dando lugar a una mezcla de productos como consecuencia de la baja selectividad. Sin embargo, cuando se adicionó una alícuota de tolueno a la reacción en idénticas condiciones se obtuvieron solamente dos productos (**25a** y **25b**). El producto mayoritario **25a** presentaba una buena estabilidad mientras que el producto **25b** se oxidaba rápidamente para dar lugar al producto **25b-O** (Figura 5).

Ambos productos **25a** y **25b-O** fueron caracterizados. En primer lugar, los análisis de espectrometría de masas mediante MALDI-TOF sugirieron la presencia de un átomo de H adicional. Además, los resultados de ESR

concordaban con un sistema diamagnético, en contraste con el paramagnetismo del material de partida y de los cicloaductos descritos que suelen obtenerse con el isómero La@C_{2v}-C_{82}.185 Este resultado obtenido mediante ESR corroboraría la inesperada presencia de un H adicional sobre el producto obtenido.

Los análisis llevados a cabo mediante 1D y 2D-RMN sobre el producto **25a** (^{1}H, ^{13}C-NMR, DEPT 135, HSQC and HMBC) certificaron dicha presencia del átomo de H (3.19 ppm) y su clara correlación mediante HSQC y HMBC con alguno de los átomos de carbono de la jaula fullerénica. Dichos análisis sobre el producto **25b-O** sugirieron la sustitución del H por un grupo OH durante el proceso de oxidación.

Como primera hipótesis sobre la procedencia del átomo de H, se postuló que podría tener origen en el H_2O que se desprende de la formación del iluro de azometino. Sin embargo, se llevaron a cabo diversos experimentos que no pudieron corroborar dicha hipótesis (por ejemplo, no se observó presencia de deuterio cuando se adicionó D_2O y tolueno en el medio de reacción). Por otro lado, cuando el producto inicial, La@C_s-C_{82}, se llevó a alta temperatura utilizando o-DCB como disolvente y en presencia de una alícuota de tolueno, se observó la formación de un nuevo producto, cuyo análisis mediante espectrometría de masas dio lugar un valor de 1156 *m/z*, que puede atribuirse a La@$C_{82}HO_2$.

Cuando los productos **25a** y **25b-O** fueron analizados mediante espectroscopia UV-vis se pudieron observar características idénticas en ambos espectros, lo que implicaría un patrón idéntico de adición en los dos productos, pudiéndose considerar loco-isómeros. Con objeto de predecir el sitio de adición, se llevaron a cabo una serie de cálculos teóricos DFT utilizando dos criterios diferentes:[187] i) La distribución del LUMO en la superficie del dipolarófilo y ii) el carácter radicálico del iluro de azometino. Este segundo criterio resultó ser más razonable en la predicción del sitio de adición (C22 y C23 para la cicloadición y C3 para la adición radicálica del átomo de H) , predicción en línea con los resultados obtenidos mediante espectroscopia ROESY.

Todo este trabajo se desarrolló en colaboración con el grupo de Prof. Akasaka en el Tsukuba Life Science Center for Advanced Research de la Universidad de Tsukuba, donde se realizó una estancia de tres meses que sirvió como inició de este proyecto.

ii) Estudio sobre la influencia de la molécula de H_2O encapsulada en los procesos de isomerización cis/trans en pirrolidinofullerenos

Considerando los últimos avances en desarrollo de metodologías eficientes en la síntesis de pirrolidinofullerenos enantiopuros,[192,193,197] se encontró que los procesos de isomerización *cis/trans* en estos derivados transcurrían de una manera selectiva y enantioespecífica. En este sentido, se ha desarrollado un estudio de este proceso a tres niveles diferentes, complementándose con una serie de cálculos teóricos mediante DFT (Figura 6).

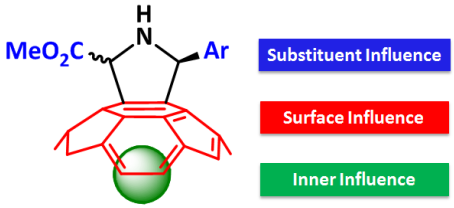

Figura 6. Esquema de los tres niveles sobre los que se ha estudiado la posible influencia en el resultado estereoquímico de la isomerización *cis/trans* pirrolidinofullerenos.

Inicialmente, se sintetizó una serie de pirrolidino[60]fullerenos enantiopuros con diferentes grupos aromáticos, utilizando las condiciones previamente descritas, y dando lugar a los correspondientes derivados con una pureza óptica sobre 80-99 % (Figura 7). Las condiciones para el estudio de la isomerización se establecieron a 35 ºC, utilizando tolueno/acetonitrilo como disolvente.

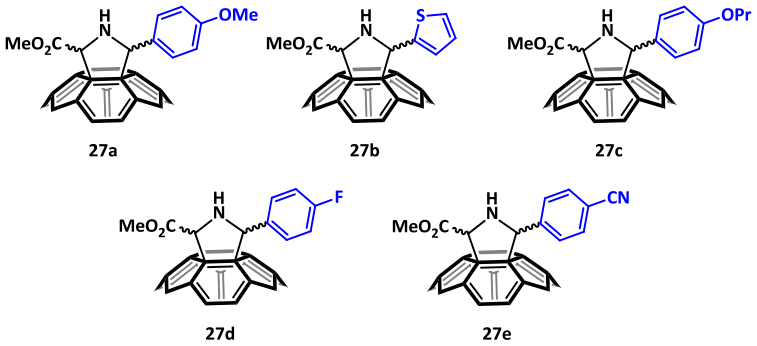

Figura 7. Estructura de los pirrolidino[60]fullerenos sintetizados.

Cuando los *cis*-pirrolidino[60]fullerenos con grupos electro-dadores (**27a-c**) fueron sometidos a las condiciones de isomerización, se alcanzó un equilibrio entre los dos diastereómeros en una proporción 70:30 (*cis/trans*), observándose además una retención en la configuración del C2. Cuando el experimento se llevó a cabo utilizando el isómero *trans* como producto inicial, se obtuvo idéntico resultado. Sin embargo, cuando se sometió al mismo experimento a aquellos derivados que presentaban grupos electro-

aceptores (**27d-e**), el proceso de isomerización no se llevaba a cabo. Este resultado experimental, que indica una retención en la configuración de C2 mientras que se invierte en el C5, debe implicar la ruptura del enlace de este último, formándose un intermedio zwitterionico donde el fullereno estabiliza la carga negativa y se forma un catión bencílico. Este intermedio permitiría la rotación alrededor del enlace C2-N para dar lugar al diastereómero opuesto (Figura 8). La extensión del proceso vendría determinada por la estabilidad del carbocatión, la cual está favorecida ante la presencia de anillos con mayor densidad de carga. Esta propuesta se confirma por el hecho de la baja extensión de la isomerización en aquellos derivados con baja densidad de carga en el anillo aromático. Además, la elevada energía que se requiere para que se de el proceso implicaría procesos secundarios de racemización y retro-cicloadición, dando lugar a bajos excesos enantioméricos, como se observa experimentalmente.

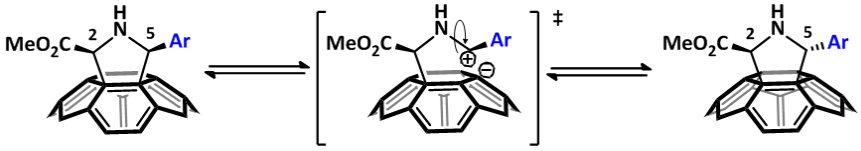

Figura 8. Proceso de isomerización por pasos que implica la formación de un intermedio zwitterionico.

Llevando este estudio a un segundo nivel, los mismos experimentos se llevaron a cabo en *cis*-pyrrolidino[70]fullerenos con grupos electro-dadores orientados de diferente manera (próximos a la región ecuatorial en **28** y próximos a los polos en **29**). Dichos derivados presentaron un resultado diastereomérico similar al observado previamente (70:30, *cis/trans*) pero con una cinética diferente, donde el derivado *cis*-**28** alcanzó dicho equilibrio en dos días y el derivado *cis*-**29** necesitó nueve días.

Siguiendo un razonamiento similar al empleado en los *cis*-pyrrolidino[60]fullerenos, la isomerización en **28** y **29** daría lugar a dos intermedios zwitterionicos con las cargas localizadas en C8 y C25 respectivamente (Figura 9). Se sabe que los carbaniones estabilizan mejor la carga en sistemas planos, debido a su mayor carácter *s*, y se desestabiliza en sistemas más piramidalizados, debido a su mayor carácter *p*. Teniendo en mente esta consideración, los carbonos ecuatoriales en C_{70} presentan una mayor planaridad que aquellos más localizados en los polos. Consecuentemente, el carbanión se encontraría mejor estabilizado en C8 que en C25, dando lugar a una mayor isomerización como corroboran los resultados experimentales.

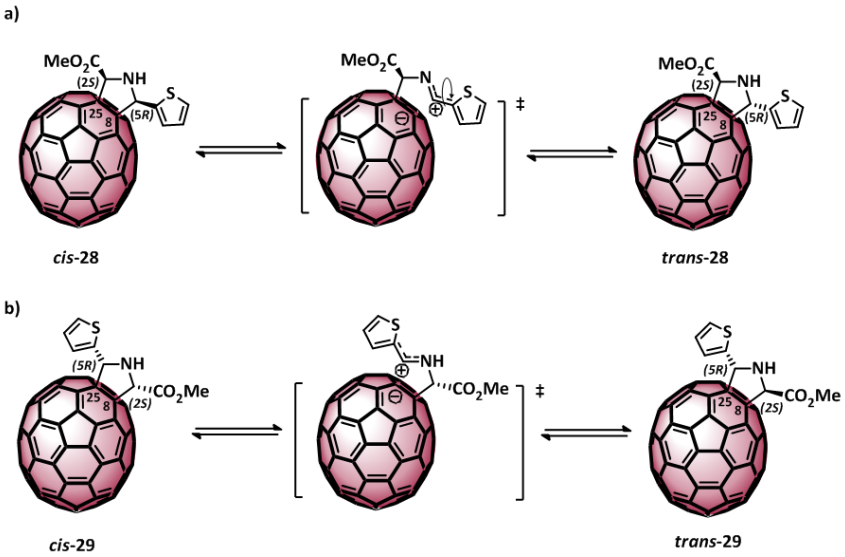

Figura 9. Proceso de isomerización por pasos que implica la formación de un intermedio zwitterionico en C_{70}.

Considerando un tercer nivel en el estudio de la isomerización *cis/trans*, se sintetizó una serie de $H_2O@C_{60}$-pirrolidinofullerenos. Para dicha síntesis, fue necesaria una estancia previa en el laboratorio del Prof. Murata (Institute for Chemical Research, Kyoto University) con objeto de preparar el fullereno endoédrico $H_2O@C_{60}$ mediante cirugía molecular. Bajo las mismas condiciones utilizadas para la síntesis de **27a** se obtuvieron los correspondientes $H_2O@C_{60}$-pirrolidinofullereno **35a**. de forma enantioespecífica (Figura 10).

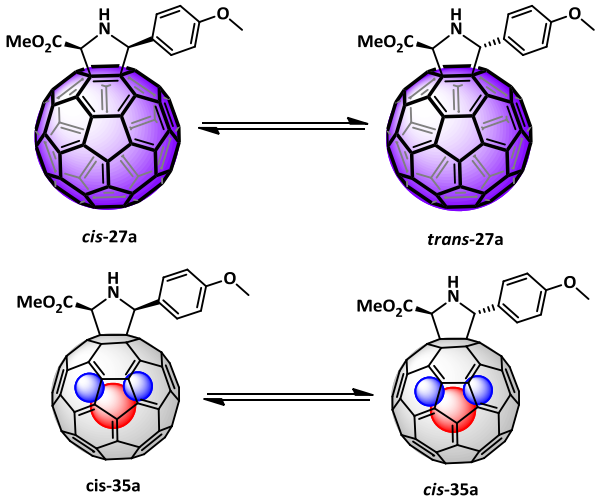

Figura 10. Estudio comparativo de la isomerización entre pirrolidinofullerenos derivados de C_{60} y $H_2O@C_{60}$.

Una vez sintetizados y caracterizados los correspondientes $H_2O@C_{60}$-pirrolidinofullerenos, se estudió el proceso de isomerización *cis/trans* con excelentes resultados, observándose la misma proporción 7:3 que en los casos anteriores, con retención en el exceso enantiomérico para los dos diastereómeros. Los dos sistemas análogos derivados de C_{60} y $H_2O@C_{60}$ fueron comparativamente estudiados, evaluando la proporción *cis*/*trans* durante seis días. Los resultados mostraron valores más altos para el derivado de $H_2O@C_{60}$, lo que implicaría una clara influencia de la molécula de H_2O en favor del proceso de isomerización (Figure 11).

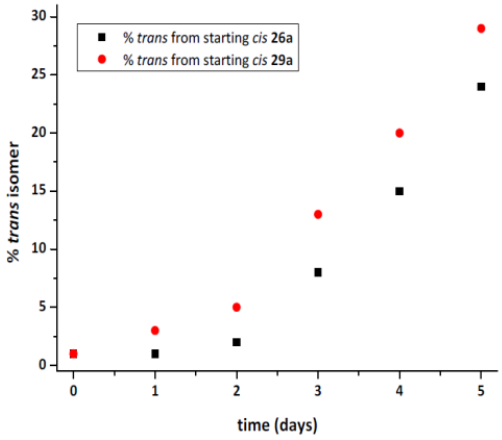

Figura 11. Resultados obtenidos para la isomerización *cis/trans* en **27a** y **35a** en función del tiempo.

Puesto que las condiciones experimentales para ambos derivados son idénticas y la única diferencia es la presencia de dicha molécula de H_2O en el interior del fullereno, esta mejora en la cinética de isomerización solo puede ser racionalizada mediante la asistencia de uno de los átomos de H de la molécula de H_2O en la estabilización del intermedio zwitterionico. Además, el resultado estereoquímico parece estar influenciado por la molécula encapsulada.

Cálculos teóricos complementarios mediante DFT fueron llevados a cabo por el grupo del Prof. Solá en la Universidad de Girona. Se consideró la energía relativa de los intermedios de ambos diastereómeros así como la posible contribución de posibles procesos secundarios (retro-cicloadición o racemización). Los resultados corroboraron la formación de un intermedio zwitterionico con retención en C2, así como una mayor estabilización en el carbanión en **35a** respecto a **27a**.

CONCLUSIONES

Capítulo 1: Química de nanotubes de carbono y grafeno

Se han sintetizado y caracterizado una serie de nanoconjugados formados por unidades de π-exTTF y diferentes nanoestructuras de carbono (**CNF-2** y **CNF-3**). Dichos sistemas han servido para llevar a cabo un estudio comparativo sobre la diferente reactividad de estas nanoestructuras de carbono frente a reacciones de arilación y tipo "click" (CuAAC). En vista de los resultados, se puede afirmar que los SWNT presentan una mayor reactividad frente a reacciones de arilación en comparación con MWNT y grafeno. En cambio, la mejor solubilidad de MWNT así como una mayor distancia entre los grupos alquino, pueden ser las causas de la mayor eficiencia de las reacciones CuAAC sobre MWNT en comparación con SWNT y grafeno. La comunicación electrónica entre las unidades de π-exTTF y las correspondientes CNF fue contrastada mediante CV y análisis fotofísicos (absorción, emisión y absorción transitoria).

Los nanoconjugados **CNF-3** fueron evaluados como candidatos para el reconocimiento de fullerenos mediante interacciones supramoleculares. Las valoraciones mediante espectroscopia UV-Vis evidenciaron dicha interacción entre los receptores y el C_{60}. Con objeto de investigar sobre la naturaleza de las interacciones entre receptor y fullereno, se llevó a cabo un estudio exhaustivo mediante ^{1}H-NMR y cálculos teóricos. Tres sistemas análogos con diferentes grupos de reconocimiento (**18**, basado en π-exTTF, **22**, basado en TCAQ y **24**, basado en anillos de benceno) fueron estudiados. Los resultados del estudio revelaron el papel fundamental del anillo central de benceno y los C-H presentes en el anillo de triazol en la formación del complejo.

Capítulo 2: Reactividad Química de fullerenos endoédricos

i) Adición de H en la reacción de cicloadición 1,3 dipolar sobre La@C_s-C_{82}

Uno de los fullerenos endoédricos menos estudiado hasta la fecha, LaC_s-C_{82}, ha sido el objeto de estudio en este capítulo, encontrando una inesperada selectividad en la reacción de adición 1,3-dipolar. Se obtuvieron únicamente dos productos con el rendimiento más alto encontrado en EMF. Este hecho solamente fue observado cuando se adicionó una alícuota de tolueno al medio de reacción.

Los diferentes análisis llevados a cabo (ESR, MALDI-TOF MS, 1D y 2D-^{1}H-NMR) sobre los dos cicloaductos obtenidos (**25a** y **25b-O**) revelaron la inesperada presencia de un átomo de H sobre la jaula de carbono. Esta adición de H vía radicálica resultó ser la responsable del diamagnetismo de dichos aductos en comparación con el carácter paramagnético del material de partida.

Mientras que el producto **25a** demostró una buena estabilidad, el producto **25b** resultó ser rápidamente oxidado mediante una sustitución nucleófila que dio lugar al producto **25b-O**.

El orden de las sucesivas reacciones que se dan (i: cicloadición + adición de H o ii: adición de H + cicloadición) fue estudiado mediante diferentes experimentos utilizando disolventes deuterados. Dicha adición radicálica de H demostró ser un proceso comparativamente más lento.

Los diferentes cálculos DFT llevados a cabo desvelaron el patrón de adición de ambas reacciones, así como que la adición radicálica parece ser la responsable de dicha selectividad. La diferente orientación de los sustituyentes fenilo es responsable de la rápida oxidación de **25b** en comparación con **25a**.

ii) Estudio sobre la influencia de la molécula de H_2O encapsulada en los procesos de isomerización cis/trans en pirrolidinofullerenos

Se ha descrito un novedoso proceso de isomerización enantioespecífica *cis*/*trans* en pirrolidinofullerenos en presencia de disolventes polares y condiciones suaves de reacción. Se observó que dicho proceso implicaba la retención de la configuración en C2 y la formación de un intermedio zwitterionico, llevándose a cabo un estudio en tres niveles diferentes: i) diferente carácter electrónico de los sustituyentes, ii) diferente geometría de la jaula y iii) influencia de especies encapsuladas en la jaula.

Se ha demostrado que los pirrolidino[60]fullerenos con sustituyentes electro-dadores en los grupos arilo favorecen el proceso de isomerización en contraste con lo observado en aquellos con sustituyentes electro-aceptores.

Derivados de pirrolidino[70]fullereno fueron estudiados bajo las mismas condiciones demostrando como el intermedio zwitterionico que se forma se encuentra más estabilizado cuando la carga se localiza en carbonos ecuatoriales, favoreciendo el proceso de isomerización.

Del mismo modo, los derivados análogos sintetizados sobre $H_2O@C_{60}$ demostraron que el proceso de isomerización se ve favorecido en la especie endoédrica como resultado de la asistencia de un átomo de H de la molécula de H_2O encapsulado que estabiliza el carbanión. Dicha observación sienta un precedente en la asistencia interna sobre el resultado estereoquímico en la química de fullerenos.

Estos resultados fueron apoyados por cálculos DFT, corroborando el resultado enantioespecífico del proceso, las energías relativas de estabilización de los intermedios y por lo tanto el mecanismo basado en un intermedio zwitterionico con retención en la configuración de C2.

Bibliography

[1] [(a)] Bernal, J. D., *The Structure of Graphite*, *Proc. R. Soc. London, A*, **1924**, *106*, 749; [(b)] Debye, P., Scherrer, P., *Interferenz an regellos orientierten Teilchen im Röntgenlicht I*, *Physik. Z.*, **1916**, *17*, 277; [(c)] Bragg, W. H., Bragg, W. L., *The Structure of the Diamond*, *Proc. R. Soc. London, A*, **1913**, *89*, 277.

[2] [(a)] Tennant, S., *On the nature of the diamond*, *Philos. Trans. R. Soc. London, A*, **1797**, *87*, 123; [(b)] Lavoisier, A., *Premier mémoire sur la destruction du diamant par le feu*, *Hist. Acad. Roy. Sci. Mém. Math. Phys.*, **1772**, *Part 2*.

[3] Kroto, H. W., Heath, J. R., O'Brien, S. C., Curl, R. F., Smalley, R. E., *C_{60}: Buckminsterfullerene*, *Nature*, **1985**, *318*, 162.

[4] Kroto, H. W., *Carbon onions introduce new flavour to fullerene studies*, *Nature*, **1992**, *359*, 670.

[5] [(a)] Li, Y., in *Endohedral Fullerenes*, World Scientific Publishing Co., **2014**, pp. 417; [(b)] Murata, M., Murata, Y., Komatsu, K., in *Organic Nanomaterials*, John Wiley & Sons, Inc., **2013**, pp. 225.

[6] [(a)] Iijima, S., Ichihashi, T., *Single-shell carbon nanotubes of 1-nm diameter*, *Nature*, **1993**, *363*, 603; [(b)] Iijima, S., *Helical microtubules of graphitic carbon*, *Nature*, **1991**, *354*, 56.

[7] Novoselov, K. S., Geim, A. K., Morozov, S. V., D. Jiang, Zhang, Y., S. V. Dubonos, Grigorieva, I. V., Firsov, A. A., *Electric Field Effect in AtomicallyThin Carbon Films*, *Science*, **2004**, *306*, 666.

[8] [(a)] Bacon, R., *Growth, Structure, and Properties of Graphite Whiskers*, *J. Appl. Phys.*, **1960**, *31*, 283; [(b)] Sears, G. W., *Growth Mechanism for Graphite Whiskers*, *J. Chem. Phys.*, **1959**, *31*, 358; [(c)] Davis, W. R., Slawson, R. J., Rigby, G. R., *An Unusual Form of Carbon*, *Nature*, **1953**, *171*, 756.

[9] Radushkevich, L. V., Lukyanovich, V. M., *O strukture ugleroda, obrazujucegosja pri termiceskom razlozenii okisi ugleroda na zeleznom kontakte*, *Zurn. Fisic. Chim.*, **1952**, *26*, 88.

[10] Delgado, J. L., Herranz, M. A., Martín, N., *The nano-forms of carbon*, *J. Mater. Chem.*, **2008**, *18*, 1417.

[11] Haley, M. M., *Synthesis and properties of annulenic subunits of graphyne and graphdiyne nanoarchitectures*, *Pure Appl. Chem.*, **2008**, *80*, 519.

[12] Bhushan, B., Luo, D., Schricker, S. R., Sigmund, W., Zauscher, S., *Handbook of Nanomaterials Properties*, Springer Berlin Heidelberg, **2014**.

[13] Yang, N., *Novel Aspects of Diamond: From Growth to Applications, Vol. 121*, Springer International Publishing, **2015**.

[14] Prasek, J., Drbohlavova, J., Chomoucka, J., Hubalek, J., Jasek, O., Adam, V., Kizek, R., *Methods for carbon nanotubes synthesis-review*, *J. Mater. Chem.*, **2011**, *21*, 15872.

[15] De Volder, M. F. L., Tawfick, S. H., Baughman, R. H., Hart, A. J., *Carbon Nanotubes: Present and Future Commercial Applications*, *Science*, **2013**, *339*, 535.

[16] Coleman, J. N., Khan, U., Blau, W. J., Gun'ko, Y. K., *Small but strong: A review of the mechanical properties of carbon nanotube–polymer composites*, *Carbon*, **2006**, *44*, 1624.

[17] [(a)] Langa, F., Nierengarten, J. F., *Fullerenes: Principles and Applications* The Royal Society of Chemistry, **2012**; [(b)] Akasaka, T., Wudl, F., Nagase, S., *Chemistry of Nanocarbons*, John Wiley & Sons, Ltd, **2010**; [(c)] Guldi, D. M., Martín, N., *Carbon Nanotubes and Related Structures*, Wiley-VCH Verlag GmbH & Co. KGaA, **2010**.

[18] [(a)] Hirsch, A., Vostrowsky, O., *Functionalization of Carbon Nanotubes*, *Top. Curr. Chem.*, **2005**, *245*, 193; [(b)] Chen, Z., Thiel, W., Hirsch, A., *Reactivity of the Convex and Concave Surfaces of Single-Walled Carbon Nanotubes (SWCNTs) towards Addition Reactions: Dependence on the Carbon-Atom Pyramidalization*, *ChemPhysChem*, **2003**, *4*, 93.

[19] [(a)] Li, J., Jia, G., Zhang, Y., Chen, Y., *Bond-Curvature Effect of Sidewall [2+1] Cycloadditions of Single-Walled Carbon Nanotubes: A New Criterion To the Adduct Structures*, *Chem. Mater.*, **2006**, *18*, 3579; [(b)] Li, I. L., Li, G. D., Liu, H. J., Chan, C. T., Tang, Z. K., *Chirality-dependent curvature effect in smallest single-walled carbon nanotubes*, *Appl. Phys. Lett.*, **2003**, *82*, 1467.

[20] [(a)] Vazquez, E., Giacalone, F., Prato, M., *Non-conventional methods and media for the activation and manipulation of carbon nanoforms*, *Chem. Soc. Rev.*, **2014**, *43*, 58; [(b)] Hodge, S. A., Bayazit, M. K., Coleman, K. S., Shaffer, M. S. P., *Unweaving the rainbow: a review of the relationship between single-walled carbon nanotube molecular structures and their chemical reactivity*, *Chem. Soc. Rev.*, **2012**, *41*, 4409; [(c)] Singh, P., Campidelli, S., Giordani, S., Bonifazi, D., Bianco, A., Prato, M., *Organic functionalisation and characterisation of single-walled carbon nanotubes*, *Chem. Soc. Rev.*, **2009**, *38*, 2214; [(d)] Zhao, Y.-L., Stoddart, J. F., *Noncovalent Functionalization of Single-Walled Carbon Nanotubes*, *Acc. Chem. Res.*, **2009**, *42*, 1161; [(e)] Tasis, D., Tagmatarchis, N., Bianco, A., Prato, M., *Chemistry of Carbon Nanotubes*, *Chem. Rev.*, **2006**, *106*, 1105.

[21] [(a)] Carlsson, J. M., *Curvature and chirality dependence of the properties of point defects in nanotubes*, *Phys. Stat. Sol. (B),*, **2006**, *243*, 3452; [(b)] Charlier, J. C., *Defects in Carbon Nanotubes*, *Acc. Chem. Res.*, **2002**, *35*, 1063; [(c)] Ebbesen,

T. W., Takada, T., *Topological and SP3 defect structures in nanotubes*, *Carbon*, **1995**, *33*, 973.

[22] Wang, C., Zhou, G., Liu, H., Wu, J., Qiu, Y., Gu, B.-L., Duan, W., *Chemical Functionalization of Carbon Nanotubes by Carboxyl Groups on Stone-Wales Defects: A Density Functional Theory Study*, *J. Phys. Chem. B*, **2006**, *110*, 10266.

[23] Mahalingam, P., Parasuram, B., Maiyalagan, T., Sundaram, S., *Chemical Methods For Purification Of Carbon Nanotubes-A Review*, *J. Environ. Nanotechnol.*, **2012**, *1*, 53.

[24] Liu, J., Rinzler, A. G., Dai, H., Hafner, J. H., Bradley, R. K., Boul, P. J., Lu, A., Iverson, T., Shelimov, K., Huffman, C. B., Rodriguez-Macias, F., Shon, Y.-S., Lee, T. R., Colbert, D. T., Smalley, R. E., *Fullerene pipes*, *Science*, **1998**, *280*, 1253.

[25] Hong, S. Y., Tobias, G., Ballesteros, B., El Oualid, F., Errey, J. C., Doores, K. J., Kirkland, A. I., Nellist, P. D., Green, M. L. H., Davis, B. G., *Atomic-Scale Detection of Organic Molecules Coupled to Single-Walled Carbon Nanotubes*, *J. Am. Chem. Soc.*, **2007**, *129*, 10966.

[26] Alvaro, M., Atienzar, P., de la Cruz, P., Delgado, J. L., Troiani, V., Garcia, H., Langa, F., Palkar, A., Echegoyen, L., *Synthesis, Photochemistry, and Electrochemistry of Single-Wall Carbon Nanotubes with Pendent Pyridyl Groups and of Their Metal Complexes with Zinc Porphyrin. Comparison with Pyridyl-Bearing Fullerenes*, *J. Am. Chem. Soc.*, **2006**, *128*, 6626.

[27] Chopra, N., Majumder, M., Hinds, B. J., *Bifunctional Carbon Nanotubes by Sidewall Protection*, *Adv. Funct. Mater.*, **2005**, *15*, 858.

[28] [(a)] Ahmad, R., Soni, U., Srivastava, R., Singh, V. N., Chand, S., Sapra, S., *Investigation of the Photophysical and Electrical Characteristics of CuInS2 QDs/SWCNT Hybrid Nanostructure*, *J. Phys. Chem. C*, **2014**, *118*, 11409; [(b)] Li, W., Gao, C., Qian, H., Ren, J., Yan, D., *Multiamino-functionalized carbon nanotubes and their applications in loading quantum dots and magnetic nanoparticles*, *J. Mater. Chem.*, **2006**, *16*, 1852; [(c)] Pan, B., Cui, D., He, R., Gao, F., Zhang, Y., *Covalent attachment of quantum dot on carbon nanotubes*, *Chem. Phys. Lett.*, **2006**, *417*, 419.

[29] Lu, F., Gu, L., Meziani, M. J., Wang, X., Luo, P. G., Veca, L. M., Cao, L., Sun, Y.-P., *Advances in Bioapplications of Carbon Nanotubes*, *Adv. Mater.*, **2009**, *21*, 139.

[30] [(a)] Dirian, K., Herranz, M. A., Katsukis, G., Malig, J., Rodriguez-Perez, L., Romero-Nieto, C., Strauss, V., Martín, N., Guldi, D. M., *Low dimensional nanocarbons - chemistry and energy/electron transfer reactions*, *Chemical Science*, **2013**, *4*, 4335; [(b)] Feldman, A. K., Steigerwald, M. L., Guo, X.,

Nuckolls, C., *Molecular Electronic Devices Based on Single-Walled Carbon Nanotube Electrodes*, *Acc. Chem. Res.*, **2008**, *41*, 1731.

[31] Guldi, D. M., Rahman, G. M. A., Zerbetto, F., Prato, M., *Carbon Nanotubes in Electron Donor–Acceptor Nanocomposites*, *Acc. Chem. Res.*, **2005**, *38*, 871.

[32] Herranz, M. Á., Martín, N., Campidelli, S., Prato, M., Brehm, G., Guldi, D. M., *Control over Electron Transfer in Tetrathiafulvalene-Modified Single-Walled Carbon Nanotubes*, *Angew. Chem., Int. Ed.*, **2006**, *45*, 4478.

[33] Baskaran, D., Mays, J. W., Zhang, X. P., Bratcher, M. S., *Carbon Nanotubes with Covalently Linked Porphyrin Antennae: Photoinduced Electron Transfer*, *J. Am. Chem. Soc.*, **2005**, *127*, 6916.

[34] Delgado, J. L., de la Cruz, P., Urbina, A., López Navarrete, J. T., Casado, J., Langa, F., *The first synthesis of a conjugated hybrid of C_{60}–fullerene and a single-wall carbon nanotube*, *Carbon*, **2007**, *45*, 2250.

[35] Rodríguez-Pérez, L., García, R., Herranz, M. Á., Martín, N., *Modified SWCNTs with Amphoteric Redox and Solubilizing Properties*, *Chem. Eur. J.*, **2014**, *20*, 7278.

[36] Yinghuai, Z., Peng, A. T., Carpenter, K., Maguire, J. A., Hosmane, N. S., Takagaki, M., *Substituted Carborane-Appended Water-Soluble Single-Wall Carbon Nanotubes: New Approach to Boron Neutron Capture Therapy Drug Delivery*, *J. Am. Chem. Soc.*, **2005**, *127*, 9875.

[37] Coleman, K. S., Bailey, S. R., Fogden, S., Green, M. L. H., *Functionalization of Single-Walled Carbon Nanotubes via the Bingel Reaction*, *J. Am. Chem. Soc.*, **2003**, *125*, 8722.

[38] Ogrin, D., Chattopadhyay, J., Sadana, A. K., Billups, W. E., Barron, A. R., *Epoxidation and Deoxygenation of Single-Walled Carbon Nanotubes: Quantification of Epoxide Defects*, *J. Am. Chem. Soc.*, **2006**, *128*, 11322.

[39] [(a)] Arai, T., Nobukuni, S., Sandanayaka, A. S. D., Ito, O., *Zinc porphyrins covalently bound to the side walls of single-walled carbon nanotubes via flexible bonds: photoinduced electron transfer in polar solvent*, *J. Phys. Chem. C*, **2009**, *113*, 14493; [(b)] Campidelli, S., Sooambar, C., Lozano Diz, E., Ehli, C., Guldi, D. M., Prato, M., *Dendrimer-Functionalized Single-Wall Carbon Nanotubes: Synthesis, Characterization, and Photoinduced Electron Transfer*, *J. Am. Chem. Soc.*, **2006**, *128*, 12544.

[40] Ballesteros, B., De la Torre, G., Ehli, C., Rahman, G. M. A., Agullo-Rueda, F., Guldi, D. M., Torres, T., *Single-Wall Carbon Nanotubes Bearing Covalently Linked Phthalocyanines - Photoinduced Electron Transfer*, *J. Am. Chem. Soc.*, **2007**, *129*, 5061.

[41] de Freitas, J. N., Maubane, M. S., Bepete, G., van Otterlo, W. A. L., Coville, N. J., Nogueira, A. F., *Synthesis and characterization of single wall carbon nanotube-grafted poly(3-hexylthiophene) and their nanocomposites with gold nanoparticles*, *Synth. Met.*, **2013**, *176*, 55.

[42] [(a)] Pastorin, G., Wu, W., Wieckowski, S., Briand, J. P., Kostarelos, K., Prato, M., Bianco, A., *Double functionalization of carbon nanotubes for multimodal drug delivery*, *Chem. Commun.*, **2006**, 1182; [(b)] Lacerda, L., Bianco, A., Prato, M., Kostarelos, K., *Carbon nanotubes as nanomedicines: from toxicology to pharmacology*, *Adv. Drug Delivery Rev.*, **2006**, *58*, 1460; [(c)] Wu, W., Wieckowski, S., Pastorin, G., Benincasa, M., Klumpp, C., Briand, J. P., Gennaro, R., Prato, M., Bianco, A., *Targeted delivery of amphotericin B to cells by using functionalized carbon nanotubes*, *Angew. Chem., Int. Ed.*, **2005**, *44*, 6358.

[43] Menard-Moyon, C., Dumas, F., Doris, E., Mioskowski, C., *Functionalization of Single-Wall Carbon Nanotubes by Tandem High-Pressure/Cr(CO)$_6$ Activation of Diels-Alder Cycloaddition*, *J. Am. Chem. Soc.*, **2006**, *128*, 14764.

[44] Chang, C.-M., Liu, Y.-L., *Functionalization of multi-walled carbon nanotubes with furan and maleimide compounds through Diels–Alder cycloaddition*, *Carbon*, **2009**, *47*, 3041.

[45] Hudson, J. L., Casavant, M. J., Tour, J. M., *Water-Soluble, Exfoliated, Nonroping Single-Wall Carbon Nanotubes*, *J. Am. Chem. Soc.*, **2004**, *126*, 11158.

[46] Price, B. K., Hudson, J. L., Tour, J. M., *Green Chemical Functionalization of Single-Walled Carbon Nanotubes in Ionic Liquids*, *J. Am. Chem. Soc.*, **2005**, *127*, 14867.

[47] Cheng, F., Adronov, A., *Suzuki coupling reactions for the surface functionalization of single-walled carbon nanotubes*, *Chem. Mater.*, **2006**, *18*, 5389.

[48] Gomez-Escalonilla, M. J., Atienzar, P., Garcia Fierro, J. L., Garcia, H., Langa, F., *Heck reaction on single-walled carbon nanotubes. Synthesis and photochemical properties of a wall functionalized SWNT-anthracene derivative*, *J. Mater. Chem.*, **2008**, *18*, 1592.

[49] Campidelli, S., Ballesteros, B., Filoramo, A., Diaz Diaz, D., de la Torre, G., Torres, T., Rahman, G. M. A., Ehli, C., Kiessling, D., Werner, F., Sgobba, V., Guldi, D. M., Cioffi, C., Prato, M., Bourgoin, J.-P., *Facile Decoration of Functionalized Single-Wall Carbon Nanotubes with Phthalocyanines via "Click Chemistry"*, *J. Am. Chem. Soc.*, **2008**, *130*, 11503.

[50] Yokoi, T., Iwamatsu, S.-i., Komai, S.-i., Hattori, T., Murata, S., *Chemical modification of carbon nanotubes with organic hydrazines*, *Carbon*, **2005**, *43*, 2869.

[51] Wei, L., Zhang, Y., *Covalent sidewall functionalization of single-walled carbon nanotubes via one-electron reduction of benzophenone by potassium*, *Chem. Phys. Lett.*, **2007**, *446*, 142.

[52] Liang, F., Beach, J. M., Rai, P. K., Guo, W., Hauge, R. H., Pasquali, M., Smalley, R. E., Billups, W. E., *Highly Exfoliated Water-Soluble Single-Walled Carbon Nanotubes*, *Chem. Mater.*, **2006**, *18*, 1520.

[53] Engel, P. S., Billups, W. E., Abmayr, D. W., Tsvaygboym, K., Wang, R., *Reaction of Single-Walled Carbon Nanotubes with Organic Peroxides*, *J. Phys. Chem. C*, **2008**, *112*, 695.

[54] Hemraj-Benny, T., Wong, S. S., *Silylation of Single-Walled Carbon Nanotubes*, *Chem. Mater.*, **2006**, *18*, 4827.

[55] Mukherjee, A., Combs, R., Chattopadhyay, J., Abmayr, D. W., Engel, P. S., Billups, W. E., *Attachment of Nitrogen and Oxygen Centered Radicals to Single-Walled Carbon Nanotube Salts*, *Chem. Mater.*, **2008**, *20*, 7339.

[56] Wunderlich, D., Hauke, F., Hirsch, A., *Preferred functionalization of metallic and small-diameter single walled carbon nanotubesvia reductive alkylation*, *J. Mater. Chem.*, **2008**, *18*, 1493.

[57] [(a)] Wunderlich, D., Hauke, F., Hirsch, A., *Preferred Functionalization of Metallic and Small-Diameter Single-Walled Carbon Nanotubes by Nucleophilic Addition of Organolithium and -Magnesium Compounds Followed by Reoxidation*, *Chem. Eur. J.*, **2008**, *14*, 1607; [(b)] Graupner, R., Abraham, J., Wunderlich, D., Vencelová, A., Lauffer, P., Röhrl, J., Hundhausen, M., Ley, L., Hirsch, A., *Nucleophilic–Alkylation–Reoxidation: A Functionalization Sequence for Single-Wall Carbon Nanotubes*, *J. Am. Chem. Soc.*, **2006**, *128*, 6683.

[58] Lee, H.-J., Han, S.-W., Kwon, Y.-D., Tan, L.-S., Baek, J.-B., *Functionalization of multi-walled carbon nanotubes with various 4-substituted benzoic acids in mild polyphosphoric acid/phosphorous pentoxide*, *Carbon*, **2008**, *46*, 1850.

[59] Gebhardt, B., Syrgiannis, Z., Backes, C., Graupner, R., Hauke, F., Hirsch, A., *Carbon Nanotube Sidewall Functionalization with Carbonyl Compounds—Modified Birch Conditions vs the Organometallic Reduction Approach*, *J. Am. Chem. Soc.*, **2011**, *133*, 7985.

[60] Ehli, C., Rahman, G. M. A., Jux, N., Balbinot, D., Guldi, D. M., Paolucci, F., Marcaccio, M., Paolucci, D., Melle-Franco, M., Zerbetto, F., Campidelli, S.,

Prato, M., *Interactions in Single Wall Carbon Nanotubes/Pyrene/Porphyrin Nanohybrids*, *J. Am. Chem. Soc.*, **2006**, *128*, 11222.

[61] Guldi, D. M., Menna, E., Maggini, M., Marcaccio, M., Paolucci, D., Paolucci, F., Campidelli, S., Prato, M., Rahman, G. M., Schergna, S., *Supramolecular hybrids of [60]fullerene and single-wall carbon nanotubes*, *Chem. Eur. J.*, **2006**, *12*, 3975.

[62] Ehli, C., Guldi, D. M., Herranz, M. Á., Martin, N., Campidelli, S., Prato, M., *Pyrene-tetrathiafulvalene supramolecular assembly with different types of carbon nanotubes*, *J. Mater. Chem.*, **2008**, *18*, 1498.

[63] Cheng, F., Zhang, S., Adronov, A., Echegoyen, L., Diederich, F., *Triply Fused ZnII–Porphyrin Oligomers: Synthesis, Properties, and Supramolecular Interactions with Single-Walled Carbon Nanotubes (SWNTs)*, *Chem. Eur. J.*, **2006**, *12*, 6062.

[64] Cheng, F., Adronov, A., *Noncovalent Functionalization and Solubilization of Carbon Nanotubes by Using a Conjugated Zn–Porphyrin Polymer*, *Chem. Eur. J.*, **2006**, *12*, 5053.

[65] Jiang, W., Yu, B., Liu, W., Hao, J., *Carbon Nanotubes Incorporated within Lyotropic Hexagonal Liquid Crystal Formed in Room-Temperature Ionic Liquids*, *Langmuir*, **2007**, *23*, 8549.

[66] Ogoshi, T., Inagaki, A., Yamagishi, T.-a., Nakamoto, Y., *Defection-selective solubilization and chemically-responsive solubility switching of single-walled carbon nanotubes with cucurbit[7]uril*, *Chem. Commun.*, **2008**, 2245.

[67] Yang, W., Thordarson, P., Gooding, J. J., Ringer, S. P., Braet, F., *Carbon nanotubes for biological and biomedical applications*, *Nanotechnol.*, **2007**, *18*, 412001.

[68] Wang, S.-F., Shen, L., Zhang, W.-D., Tong, Y.-J., *Preparation and Mechanical Properties of Chitosan/Carbon Nanotubes Composites*, *Biomacromolecules*, **2005**, *6*, 3067.

[69] Wind, S. J., Penzo, E., Palma, M., Wang, R., Fazio, T., Porath, D., Rotem, D., Livshits, G., Stern, A., *Integrating DNA with functional nanomaterials*, *J. Self-Assem. Mol. Electron.*, **2013**, *1*, 177.

[70] Samanta, S. K., Fritsch, M., Scherf, U., Gomulya, W., Bisri, S. Z., Loi, M. A., *Conjugated Polymer-Assisted Dispersion of Single-Wall Carbon Nanotubes: The Power of Polymer Wrapping*, *Acc. Chem. Res.*, **2014**, *47*, 2446.

[71] Britz, D. A., Khlobystov, A. N., *Noncovalent interactions of molecules with single walled carbon nanotubes*, *Chem. Soc. Rev.*, **2006**, *35*, 637.

[72] [(a)] Lau, C. N., Bao, W., Velasco Jr, J., *Properties of suspended graphene membranes*, *Mater. Today*, **2012**, *15*, 238; [(b)] Castro Neto, A. H., Guinea, F., Peres, N. M. R., Novoselov, K. S., Geim, A. K., *The electronic properties of graphene*, *Rev. Mod. Phys.*, **2009**, *81*, 109.

[73] Bonaccorso, F., Lombardo, A., Hasan, T., Sun, Z., Colombo, L., Ferrari, A. C., *Production and processing of graphene and 2d crystals*, *Mater. Today*, **2012**, *15*, 564.

[74] [(a)] Georgakilas, V., *Functionalization of Graphene*, Wiley-VCH Verlag GmbH & Co. KGaA, **2014**; [(b)] Eigler, S., Hirsch, A., *Chemistry with Graphene and Graphene Oxide—Challenges for Synthetic Chemists*, *Angew. Chem., Int. Ed.*, **2014**, *53*, 7720; [(c)] Rodriguez-Perez, L., Herranz, M. A., Martin, N., *The chemistry of pristine graphene*, *Chem. Commun.*, **2013**, *49*, 3721; [(d)] *Special Issue in Graphene (part I and II), Vol. 46*, Accounts of Chemical Research, American Chemical Society, **2012**.

[75] Luo, G., Liu, L., Zhang, J., Li, G., Wang, B., Zhao, J., *Hole Defects and Nitrogen Doping in Graphene: Implication for Supercapacitor Applications*, *ACS Appl. Mater. Interfaces*, **2013**, *5*, 11184.

[76] Savchenko, A., *Transforming Graphene*, *Science*, **2009**, *323*, 589.

[77] Nair, R. R., Ren, W., Jalil, R., Riaz, I., Kravets, V. G., Britnell, L., Blake, P., Schedin, F., Mayorov, A. S., Yuan, S., Katsnelson, M. I., Cheng, H.-M., Strupinski, W., Bulusheva, L. G., Okotrub, A. V., Grigorieva, I. V., Grigorenko, A. N., Novoselov, K. S., Geim, A. K., *Fluorographene: A Two-Dimensional Counterpart of Teflon*, *Small*, **2010**, *6*, 2877.

[78] Liu, H., Ryu, S., Chen, Z., Steigerwald, M. L., Nuckolls, C., Brus, L. E., *Photochemical Reactivity of Graphene*, *J. Am. Chem. Soc.*, **2009**, *131*, 17099.

[79] Jin, Z., Lomeda, J. R., Price, B. K., Lu, W., Zhu, Y., Tour, J. M., *Mechanically Assisted Exfoliation and Functionalization of Thermally Converted Graphene Sheets*, *Chem. Mater.*, **2009**, *21*, 3045.

[80] Englert, J. M., Dotzer, C., Yang, G., Schmid, M., Papp, C., Gottfried, J. M., Steinrück, H.-P., Spiecker, E., Hauke, F., Hirsch, A., *Covalent bulk functionalization of graphene*, *Nat. Chem.*, **2011**, *3*, 279.

[81] Bao, Q., Zhang, H., Yang, J.-x., Wang, S., Tang, D. Y., Jose, R., Ramakrishna, S., Lim, C. T., Loh, K. P., *Graphene–Polymer Nanofiber Membrane for Ultrafast Photonics*, *Adv. Funct. Mater.*, **2010**, *20*, 782.

[82] Wang, H.-X., Zhou, K.-G., Xie, Y.-L., Zeng, J., Chai, N.-N., Li, J., Zhang, H.-L., *Photoactive graphene sheets prepared by "click" chemistry*, *Chem. Commun.*, **2011**, *47*, 5747.

[83] Ragoussi, M.-E., Malig, J., Katsukis, G., Butz, B., Spiecker, E., de la Torre, G., Torres, T., Guldi, D. M., *Linking Photo- and Redoxactive Phthalocyanines Covalently to Graphene*, *Angew. Chem., Int. Ed.*, **2012**, *51*, 6421.

[84] Choi, E.-K., Jeon, I.-Y., Bae, S.-Y., Lee, H.-J., Shin, H. S., Dai, L., Baek, J.-B., *High-yield exfoliation of three-dimensional graphite into two-dimensional graphene-like sheets*, *Chem. Commun.*, **2010**, *46*, 6320.

[85] Quintana, M., Spyrou, K., Grzelczak, M., Browne, W. R., Rudolf, P., Prato, M., *Functionalization of Graphene via 1,3-Dipolar Cycloaddition*, *ACS Nano*, **2010**, *4*, 3527.

[86] Choi, J., Kim, K.-j., Kim, B., Lee, H., Kim, S., *Covalent Functionalization of Epitaxial Graphene by Azidotrimethylsilane*, *J. Phys. Chem. C*, **2009**, *113*, 9433.

[87] Economopoulos, S. P., Rotas, G., Miyata, Y., Shinohara, H., Tagmatarchis, N., *Exfoliation and Chemical Modification Using Microwave Irradiation Affording Highly Functionalized Graphene*, *ACS Nano*, **2010**, *4*, 7499.

[88] Zhong, X., Jin, J., Li, S., Niu, Z., Hu, W., Li, R., Ma, J., *Aryne cycloaddition: highly efficient chemical modification of graphene*, *Chem. Commun.*, **2010**, *46*, 7340.

[89] Sarkar, S., Bekyarova, E., Haddon, R. C., *Chemistry at the Dirac Point: Diels–Alder Reactivity of Graphene*, *Acc. Chem. Res.*, **2012**, *45*, 673.

[90] Lotya, M., Hernandez, Y., King, P. J., Smith, R. J., Nicolosi, V., Karlsson, L. S., Blighe, F. M., De, S., Wang, Z., McGovern, I. T., Duesberg, G. S., Coleman, J. N., *Liquid Phase Production of Graphene by Exfoliation of Graphite in Surfactant/Water Solutions*, *J. Am. Chem. Soc.*, **2009**, *131*, 3611.

[91] Lin, S., Shih, C.-J., Strano, M. S., Blankschtein, D., *Molecular Insights into the Surface Morphology, Layering Structure, and Aggregation Kinetics of Surfactant-Stabilized Graphene Dispersions*, *J. Am. Chem. Soc.*, **2011**, *133*, 12810.

[92] Liu, N., Luo, F., Wu, H., Liu, Y., Zhang, C., Chen, J., *One-Step Ionic-Liquid-Assisted Electrochemical Synthesis of Ionic-Liquid-Functionalized Graphene Sheets Directly from Graphite*, *Adv. Funct. Mater.*, **2008**, *18*, 1518.

[93] Barun, D., Prasad, K. E., Ramamurty, U., Rao, C. N. R., *Nano-indentation studies on polymer matrix composites reinforced by few-layer graphene*, *Nanotechnol.*, **2009**, *20*, 125705.

[94] Rakesh, V., Barun, D., Chandra Sekhar, R., Rao, C. N. R., *Effects of charge transfer interaction of graphene with electron donor and acceptor molecules examined using Raman spectroscopy and cognate techniques*, *J. Phys.: Condens. Matter*, **2008**, *20*, 472204.

[95] Xu, Y., Bai, H., Lu, G., Li, C., Shi, G., *Flexible Graphene Films via the Filtration of Water-Soluble Noncovalent Functionalized Graphene Sheets*, *J. Am. Chem. Soc.*, **2008**, *130*, 5856.

[96] Mann, J. A., Rodríguez-López, J., Abruña, H. D., Dichtel, W. R., *Multivalent Binding Motifs for the Noncovalent Functionalization of Graphene*, *J. Am. Chem. Soc.*, **2011**, *133*, 17614.

[97] Kozhemyakina, N. V., Englert, J. M., Yang, G., Spiecker, E., Schmidt, C. D., Hauke, F., Hirsch, A., *Non-Covalent Chemistry of Graphene: Electronic Communication with Dendronized Perylene Bisimides*, *Adv. Mater.*, **2010**, *22*, 5483.

[98] Wudl, F., Smith, G. M., Hufnagel, E. J., *Bis-1,3-dithiolium chloride: an unusually stable organic radical cation*, *J. Chem. Soc. D.: Chem, Commun.*, **1970**, 1453.

[99] [(a)] Martin, N., *Tetrathiafulvalene: the advent of organic metals*, *Chem. Commun.*, **2013**, *49*, 7025; [(b)] Fabre, J. M., *Dimensionality and Electrical Properties in Organic Synthetic Metals—Current Results through Selected Recent Examples*, *J. Solid State Chem.*, **2002**, *168*, 367.

[100] Brunetti, F. G., Lopez, J. L., Atienza, C., Martin, N., *π-Extended TTF: a versatile molecule for organic electronics*, *J. Mater. Chem.*, **2012**, *22*, 4188.

[101] [(a)] Wielopolski, M., Molina-Ontoria, A., Schubert, C., Margraf, J. T., Krokos, E., Kirschner, J., Gouloumis, A., Clark, T., Guldi, D. M., Martín, N., *Blending Through-Space and Through-Bond π–π-Coupling in [2,2']-Paracyclophane-oligophenylenevinylene Molecular Wires*, *J. Am. Chem. Soc.*, **2013**, *135*, 10372; [(b)] Molina-Ontoria, A., Wielopolski, M., Gebhardt, J., Gouloumis, A., Clark, T., Guldi, D. M., Martín, N., *[2,2']Paracyclophane-Based π-Conjugated Molecular Wires Reveal Molecular-Junction Behavior*, *J. Am. Chem. Soc.*, **2011**, *133*, 2370; [(c)] Guldi, D. M., Illescas, B. M., Atienza, C. M., Wielopolski, M., Martín, N., *Fullerene for organic electronics*, *Chem. Soc. Rev.*, **2009**, *38*, 1587.

[102] [(a)] Castellanos, S., Vieira, A. A., Illescas, B. M., Sacchetti, V., Schubert, C., Moreno, J., Guldi, D. M., Hecht, S., Martin, N., *Gating Charge Recombination Rates through Dynamic Bridges in Tetrathiafulvalene-Fullerene Architectures*, *Angew. Chem., Int. Ed.*, **2013**, *52*, 13985; [(b)] Martín, N., Sánchez, L., Herranz, M. Á., Illescas, B., Guldi, D. M., *Electronic Communication in Tetrathiafulvalene (TTF)/C60 Systems: Toward Molecular Solar Energy Conversion Materials?*, *Acc. Chem. Res.*, **2007**, *40*, 1015; [(c)] Sánchez, L., Pérez, I., Martín, N., Guldi, D. M., *Controlling Short- and Long-Range Electron Transfer Processes in Molecular Dyads and Triads*, *Chem. Eur. J.*, **2003**, *9*, 2457.

[103] Schubert, C., Rudolf, M., Guldi, D. M., Takano, Y., Mizorogi, N., Herranz, M. Á., Martín, N., Nagase, S., Akasaka, T., *Rates and energetics of intramolecular electron transfer processes in conjugated metallofullerenes*, *Philos. Trans. R. Soc. London, A*, **2013**, *371*.

[104] [(a)] Brunetti, F. G., Romero-Nieto, C., López-Andarias, J., Atienza, C., López, J. L., Guldi, D. M., Martín, N., *Self-Ordering Electron Donor–Acceptor Nanohybrids Based on Single-Walled Carbon Nanotubes Across Different Scales*, *Angew. Chem., Int. Ed.*, **2013**, *52*, 2180; [(b)] Romero-Nieto, C., Garcia, R., Herranz, M. A., Ehli, C., Ruppert, M., Hirsch, A., Guldi, D. M., Martin, N., *Tetrathiafulvalene-Based Nanotweezers-Noncovalent Binding of Carbon Nanotubes in Aqueous Media with Charge Transfer Implications*, *J. Am. Chem. Soc.*, **2012**, *134*, 9183; [(c)] Herranz, M. Á., Ehli, C., Campidelli, S., Gutiérrez, M., Hug, G. L., Ohkubo, K., Fukuzumi, S., Prato, M., Martín, N., Guldi, D. M., *Spectroscopic Characterization of Photolytically Generated Radical Ion Pairs in Single-Wall Carbon Nanotubes Bearing Surface-Immobilized Tetrathiafulvalenes*, *J. Am. Chem. Soc.*, **2007**, *130*, 66.

[105] Brunetti, F. G., Isla, H., Aragó, J., Ortí, E., Pérez, E. M., Martín, N., *Exploiting Multivalent Nanoparticles for the Supramolecular Functionalization of Graphene with a Nonplanar Recognition Motif*, *Chem. Eur. J.*, **2013**, *19*, 9843.

[106] Wenger, S., Bouit, P.-A., Chen, Q., Teuscher, J., Censo, D. D., Humphry-Baker, R., Moser, J.-E., Delgado, J. L., Martín, N., Zakeeruddin, S. M., Grätzel, M., *Efficient Electron Transfer and Sensitizer Regeneration in Stable π-Extended Tetrathiafulvalene-Sensitized Solar Cells*, *J. Am. Chem. Soc.*, **2010**, *132*, 5164.

[107] [(a)] Canevet, D., Pérez, E. M., Martín, N., in *Organic Nanomaterials*, John Wiley & Sons, Inc., **2013**, pp. 147; [(b)] Canevet, D., Pérez, E. M., Martín, N., *Wraparound Hosts for Fullerenes: Tailored Macrocycles and Cages*, *Angew. Chem., Int. Ed.*, **2011**, *50*, 9248; [(c)] Diederich, F., Gomez-Lopez, M., *Supramolecular fullerene chemistry*, *Chem. Soc. Rev.*, **1999**, *28*, 263.

[108] Pérez, E. M., Sánchez, L., Fernández, G., Martín, N., *exTTF as a Building Block for Fullerene Receptors. Unexpected Solvent-Dependent Positive Homotropic Cooperativity*, *J. Am. Chem. Soc.*, **2006**, *128*, 7172.

[109] Isla, H., Gallego, M., Pérez, E. M., Viruela, R., Ortí, E., Martín, N., *A Bis-exTTF Macrocyclic Receptor That Associates C_{60} with Micromolar Affinity*, *J. Am. Chem. Soc.*, **2010**, *132*, 1772.

[110] Canevet, D., Gallego, M., Isla, H., de Juan, A., Pérez, E. M., Martín, N., *Macrocyclic Hosts for Fullerenes: Extreme Changes in Binding Abilities with Small Structural Variations*, *J. Am. Chem. Soc.*, **2011**, *133*, 3184.

[111] Perez, E. M., Capodilupo, A. L., Fernandez, G., Sanchez, L., Viruela, P. M., Viruela, R., Orti, E., Bietti, M., Martin, N., *Weighting non-covalent forces in the molecular recognition of C_{60}. Relevance of concave-convex complementarity*, *Chem. Commun.*, **2008**, 4567.

[112] Iden, H., Fontaine, F. G., Morin, J. F., *Synthesis and complexation study of new ExTTF-based hosts for fullerenes*, *Org. Biomol. Chem.*, **2014**, *12*, 4117.

[113] Yenchalwar, S. G., Reddy Devarapalli, R., Deshmukh, A. B., Shelke, M. V., *Plasmon-Enhanced Photocurrent Generation from Click-Chemically Modified Graphene*, *Chem. Eur. J.*, **2014**, *20*, 7402.

[114] González, S., Martín, N., Guldi, D. M., *Synthesis and Properties of Bingel-type Methanofullerene–π-Extended-TTF Diads and Triads*, *J. Org. Chem.*, **2003**, *68*, 779.

[115] Moore, A. J., Bryce, M. R., *Generation and Trapping of Phosphorus Stabilized 4,5-Ethylenedithio-1,3-dithiol-2-ide Carbanions: Synthesis of Ethylenedithio-1,3-dithiafulvalenes*, *Synthesis*, **1991**, *1991*, 26.

[116] González, S., Martín, N., Swartz, A., Guldi, D. M., *Addition Reaction of Azido-exTTFs to C60: Synthesis of Fullerotriazoline and Azafulleroid Electroactive Dyads*, *Org. Lett.*, **2003**, *5*, 557.

[117] Wu, P., Feldman, A. K., Nugent, A. K., Hawker, C. J., Scheel, A., Voit, B., Pyun, J., Fréchet, J. M. J., Sharpless, K. B., Fokin, V. V., *Efficiency and Fidelity in a Click-Chemistry Route to Triazole Dendrimers by the Copper(I)-Catalyzed Ligation of Azides and Alkynes*, *Angew. Chem., Int. Ed.*, **2004**, *43*, 3928.

[118] Bahr, J. L., Yang, J., Kosynkin, D. V., Bronikowski, M. J., Smalley, R. E., Tour, J. M., *Functionalization of Carbon Nanotubes by Electrochemical Reduction of Aryl Diazonium Salts: A Bucky Paper Electrode*, *J. Am. Chem. Soc.*, **2001**, *123*, 6536.

[119] Corrias, M., Caussat, B., Ayral, A., Durand, J., Kihn, Y., Kalck, P., Serp, P., *Carbon nanotubes produced by fluidized bed catalytic CVD: first approach of the process*, *Chem. Eng. Sci.*, **2003**, *58*, 4475.

[120] Hernandez, Y., Nicolosi, V., Lotya, M., Blighe, F. M., Sun, Z., De, S., McGovern, I. T., Holland, B., Byrne, M., Gun'Ko, Y. K., Boland, J. J., Niraj, P., Duesberg, G., Krishnamurthy, S., Goodhue, R., Hutchison, J., Scardaci, V., Ferrari, A. C., Coleman, J. N., *High-yield production of graphene by liquid-phase exfoliation of graphite*, *Nat. Nanotechnol.*, **2008**, *3*, 563.

[121] Dresselhaus, M. S., Dresselhaus, G., Saito, R., Jorio, A., *Raman spectroscopy of carbon nanotubes*, *Phys. Rep.*, **2005**, *409*, 47.

[122] de Juan, A., Pouillon, Y., Ruiz-Gonzalez, L., Torres-Pardo, A., Casado, S., Martín, N., Rubio, A., Perez, E. M., *Mechanically interlocked single-wall carbon nanotubes*, *Angew. Chem., Int. Ed.*, **2014**, *53*, 5394.

[123] Malard, L. M., Pimenta, M. A., Dresselhaus, G., Dresselhaus, M. S., *Raman spectroscopy in graphene*, *Phys. Rep.*, **2009**, *473*, 51.

[124] Ferrari, A., Meyer, J., Scardaci, V., Casiraghi, C., Lazzeri, M., Mauri, F., Piscanec, S., Jiang, D., Novoselov, K., Roth, S., Geim, A., *Raman Spectrum of Graphene and Graphene Layers*, *Phys. Rev. Lett.*, **2006**, *97*, 187401.

[125] Collman, J. P., Devaraj, N. K., Eberspacher, T. P. A., Chidsey, C. E. D., *Mixed Azide-Terminated Monolayers: A Platform for Modifying Electrode Surfaces*, *Langmuir*, **2006**, *22*, 2457.

[126] Lipińska, M. E., Rebelo, S. L. H., Pereira, M. F. R., Gomes, J. A. N. F., Freire, C., Figueiredo, J. L., *New insights into the functionalization of multi-walled carbon nanotubes with aniline derivatives*, *Carbon*, **2012**, *50*, 3280.

[127] Bachilo, S. M., Strano, M. S., Kittrell, C., Hauge, R. H., Smalley, R. E., Weisman, R. B., *Structure-assigned optical spectra of single-walled carbon nanotubes*, *Science*, **2002**, *298*, 2361.

[128] [(a)] Ortí, E., Viruela, R., Viruela, P. M., *Influence of Benzoannulation on the Molecular and Electronic Structures of Tetracyanoquinodimethanes*, *J. Phys. Chem.*, **1996**, *100*, 6138; [(b)] Martin, N., Behnisch, R., Hanack, M., *Syntheses and electrochemical properties of tetracyano-p-quinodimethane derivatives containing fused aromatic rings*, *J. Org. Chem.*, **1989**, *54*, 2563.

[129] Lehnert, W., *Verbesserte variante der knoevenagel-kondensation mit $TiCl_4$/THF/pyridin(I). Alkyliden- und Arylidenmalonester bei 0–25°C*, *Tetrahedron Lett.*, **1970**, *11*, 4723.

[130] Thordarson, P., in *Supramolecular Chemistry: From Molecules to Nanomaterials*, John Wiley & Sons, Ltd, **2012**.

[131] Marshallsay, G. J., Bryce, M. R., *Synthesis and Multistage Redox Properties of 9,10-Bis(1,3-dithiol-2-ylidene)-9,10-dihydroanthracene Derivatives Functionalized with Ferrocenyl and Tetrathiafulvalenyl Units*, *J. Org. Chem.*, **1994**, *59*, 6847.

[132] Myers, E. L., Raines, R. T., *A Phosphine-Mediated Conversion of Azides into Diazo Compounds*, *Angew. Chem., Int. Ed.*, **2009**, *48*, 2359.

[133] Feng, L., Akasaka, T., Nagase, S., in *Carbon Nanotubes and Related Structures*, Wiley-VCH Verlag GmbH & Co. KGaA, **2010**, pp. 455.

[134] Liu, F., Guan, J., Wei, T., Wang, S., Yang, S., in *Endohedral Fullerenes*, World Scientific Publishing Co., **2014**, pp. 19.

[135] Fatouros, P. P., Corwin, F. D., Chen, Z. J., Broaddus, W. C., Tatum, J. L., Kettenmann, B., Ge, Z., Gibson, H. W., Russ, J. L., Leonard, A. P., Duchamp, J. C., Dorn, H. C., *In vitro and in vivo imaging studies of a new endohedral metallofullerene nanoparticle*, *Radiology*, **2006**, *240*, 756.

[136] [(a)] Garcia-Borràs, M., Osuna, S., Swart, M., Luis, J. M., Solà, M., *Maximum Aromaticity as a Guiding Principle for the Most Suitable Hosting Cages in Endohedral Metallofullerenes*, *Angew. Chem., Int. Ed.*, **2013**, *52*, 9275; [(b)] Rodríguez-Fortea, A., Alegret, N., Balch, A. L., Poblet, J. M., *The maximum pentagon separation rule provides a guideline for the structures of endohedral metallofullerenes*, *Nat. Chem.*, **2010**, *2*, 955.

[137] Heath, J. R., O'Brien, S. C., Zhang, Q., Liu, Y., Curl, R. F., Tittel, F. K., Smalley, R. E., *Lanthanum complexes of spheroidal carbon shells*, *J. Am. Chem. Soc.*, **1985**, *107*, 7779.

[138] Zhang, J., Kiselev, B. M., Ye, Y., Dorn, H. C., in *Endohedral Fullerenes*, World Scientific Publishing Co., **2014**, pp. 401.

[139] [(a)] Lu, X., Bao, L., Akasaka, T., Nagase, S., *Recent progress in the chemistry of endohedral metallofullerenes*, *Chem. Commun.*, **2014**, *50*, 14701; [(b)] Wang, T., Wang, C., *Endohedral metallofullerenes based on spherical I_h-C_{80} cage: molecular structures and paramagnetic properties*, *Acc. Chem. Res.*, **2014**, *47*, 450; [(c)] Popov, A. A., Yang, S., Dunsch, L., *Endohedral Fullerenes*, *Chem. Rev.*, **2013**, *113*, 5989; [(d)] Lu, X., Akasaka, T., Nagase, S., *Chemistry of endohedral metallofullerenes: the role of metals*, *Chem. Commun.*, **2011**, *47*, 5942; [(e)] Chaur, M. N., Melin, F., Ortiz, A. L., Echegoyen, L., *Chemical, Electrochemical, and Structural Properties of Endohedral Metallofullerenes*, *Angew. Chem., Int. Ed.*, **2009**, *48*, 7514.

[140] Lu, X., Slanina, Z., Akasaka, T., Tsuchiya, T., Mizorogi, N., Nagase, S., *Yb@C_{2n} (n = 40, 41, 42): New Fullerene Allotropes with Unexplored Electrochemical Properties*, *J. Am. Chem. Soc.*, **2010**, *132*, 5896.

[141] Inakuma, M., Shinohara, H., *Temperature-Dependent EPR Studies on Isolated Scandium Metallofullerenes: Sc@C_{82}(I, II) and Sc@C_{84}*, *J. Phys. Chem. B*, **2000**, *104*, 7595.

[142] Lu, X., Akasaka, T., Nagase, S., *Carbide Cluster Metallofullerenes: Structure, Properties, and Possible Origin*, *Acc. Chem. Res.*, **2013**, *46*, 1627.

[143] Stevenson, S., Rice, G., Glass, T., Harich, K., Cromer, F., Jordan, M. R., Craft, J., Hadju, E., Bible, R., Olmstead, M. M., Maitra, K., Fisher, A. J., Balch, A. L., Dorn, H. C., *Small-bandgap endohedral metallofullerenes in high yield and purity*, *Nature*, **1999**, *401*, 55.

[144] Wang, T.-S., Feng, L., Wu, J.-Y., Xu, W., Xiang, J.-F., Tan, K., Ma, Y.-H., Zheng, J.-P., Jiang, L., Lu, X., Shu, C.-Y., Wang, C.-R., *Planar Quinary Cluster*

inside a Fullerene Cage: Synthesis and Structural Characterizations of $Sc_3NC@C_{80}$-I_h, *J. Am. Chem. Soc.*, **2010**, *132*, 16362.

[145] [(a)] Zhao, P., Yang, T., Guo, Y. J., Dang, J. S., Zhao, X., Nagase, S., *Dimetallic sulfide endohedral metallofullerene $Sc_2S@C_{76}$: density functional theory characterization*, *J. Comput. Chem.*, **2014**, *35*, 1657; [(b)] Stevenson, S., Mackey, M. A., Stuart, M. A., Phillips, J. P., Easterling, M. L., Chancellor, C. J., Olmstead, M. M., Balch, A. L., *A distorted tetrahedral metal oxide cluster inside an icosahedral carbon cage. Synthesis, isolation, and structural characterization of $Sc_4(\mu_3\text{-}O)_2@I_h\text{-}C_{80}$*, *J. Am. Chem. Soc.*, **2008**, *130*, 11844.

[146] Maeda, Y., Matsunaga, Y., Wakahara, T., Takahashi, S., Tsuchiya, T., Ishitsuka, M. O., Hasegawa, T., Akasaka, T., Liu, M. T. H., Kokura, K., Horn, E., Yoza, K., Kato, T., Okubo, S., Kobayashi, K., Nagase, S., Yamamoto, K., *Isolation and Characterization of a Carbene Derivative of $La@C_{82}$*, *J. Am. Chem. Soc.*, **2004**, *126*, 6858.

[147] Takano, Y., Ishitsuka, M. O., Tsuchiya, T., Akasaka, T., Kato, T., Nagase, S., *Retro-reaction of singly bonded $La@C_{82}$ derivatives*, *Chem. Commun.*, **2010**, *46*, 8035.

[148] [(a)] Akasaka, T., Kono, T., Matsunaga, Y., Wakahara, T., Nakahodo, T., Ishitsuka, M. O., Maeda, Y., Tsuchiya, T., Kato, T., Liu, M. T. H., Mizorogi, N., Slanina, Z., Nagase, S., *Isolation and Characterization of Carbene Derivatives of $La@C_{82}(C_s)$*, *J. Phys. Chem. A*, **2008**, *112*, 1294; [(b)] Tagmatarchis, N., Taninaka, A., Shinohara, H., *Production and EPR characterization of exohedrally perfluoroalkylated paramagnetic lanthanum metallofullerenes: $(La@C_{82})$–$(C_8F_{17})_2$*, *Chem. Phys. Lett.*, **2002**, *355*, 226; [(c)] Akasaka, T., Wakahara, T., Nagase, S., Kobayashi, K., Waelchli, M., Yamamoto, K., Kondo, M., Shirakura, S., Maeda, Y., Kato, T., Kako, M., Nakadaira, Y., Gao, X., Van Caemelbecke, E., Kadish, K. M., *Structural Determination of the $La@C_{82}$ Isomer*, *J. Phys. Chem. B*, **2001**, *105*, 2971.

[149] Cai, T., Xu, L., Anderson, M. R., Ge, Z., Zuo, T., Wang, X., Olmstead, M. M., Balch, A. L., Gibson, H. W., Dorn, H. C., *Structure and Enhanced Reactivity Rates of the D_{5h} $Sc_3N@C_{80}$ and $Lu_3N@C_{80}$ Metallofullerene Isomers: The Importance of the Pyracylene Motif*, *J. Am. Chem. Soc.*, **2006**, *128*, 8581.

[150] Akasaka, T., Kato, T., Kobayashi, K., Nagase, S., Yamamoto, K., Funasaka, H., Takahashi, T., *Exohedral adducts of $La@C_{82}$*, *Nature*, **1995**, *374*, 600.

[151] [(a)] Wakahara, T., Yamada, M., Takahashi, S., Nakahodo, T., Tsuchiya, T., Maeda, Y., Akasaka, T., Kako, M., Yoza, K., Horn, E., Mizorogi, N., Nagase, S., *Two-dimensional hopping motion of encapsulated La atoms in silylated $La_2@C_{80}$*, *Chem. Commun.*, **2007**, 2680; [(b)] Wakahara, T., Iiduka, Y., Ikenaga, O., Nakahodo, T., Sakuraba, A., Tsuchiya, T., Maeda, Y., Kako, M., Akasaka, T.,

Yoza, K., Horn, E., Mizorogi, N., Nagase, S., *Characterization of the Bis-Silylated Endofullerene $Sc_3N@C_{80}$, J. Am. Chem. Soc.*, **2006**, *128*, 9919.

[152] Iezzi, E. B., Duchamp, J. C., Harich, K., Glass, T. E., Lee, H. M., Olmstead, M. M., Balch, A. L., Dorn, H. C., *A Symmetric Derivative of the Trimetallic Nitride Endohedral Metallofullerene, $Sc_3N@C_{80}$, J. Am. Chem. Soc.*, **2001**, *124*, 524.

[153] Maeda, Y., Sato, S., Inada, K., Nikawa, H., Yamada, M., Mizorogi, N., Hasegawa, T., Tsuchiya, T., Akasaka, T., Kato, T., Slanina, Z., Nagase, S., *Regioselective Exohedral Functionalization of $La@C_{82}$ and its 1,2,3,4,5-Pentamethylcyclopentadiene and Adamantylidene Adducts*, *Chem. Eur. J.*, **2010**, *16*, 2193.

[154] Yamada, M., Wakahara, T., Nakahodo, T., Tsuchiya, T., Maeda, Y., Akasaka, T., Yoza, K., Horn, E., Mizorogi, N., Nagase, S., *Synthesis and Structural Characterization of Endohedral Pyrrolidinodimetallofullerene: $La_2@C_{80}(CH_2)_2NTrt$*, *J. Am. Chem. Soc.*, **2006**, *128*, 1402.

[155] Cardona, C. M., Kitaygorodskiy, A., Echegoyen, L., *Trimetallic Nitride Endohedral Metallofullerenes: Reactivity Dictated by the Encapsulated Metal Cluster*, *J. Am. Chem. Soc.*, **2005**, *127*, 10448.

[156] Takano, Y., Aoyagi, M., Yamada, M., Nikawa, H., Slanina, Z., Mizorogi, N., Ishitsuka, M. O., Tsuchiya, T., Maeda, Y., Akasaka, T., Kato, T., Nagase, S., *Anisotropic Magnetic Behavior of Anionic $Ce@C_{82}$ Carbene Adducts*, *J. Am. Chem. Soc.*, **2009**, *131*, 9340.

[157] Cao, B., Nikawa, H., Nakahodo, T., Tsuchiya, T., Maeda, Y., Akasaka, T., Sawa, H., Slanina, Z., Mizorogi, N., Nagase, S., *Addition of Adamantylidene to $La_2@C_{78}$: Isolation and Single-Crystal X-ray Structural Determination of the Monoadducts*, *J. Am. Chem. Soc.*, **2007**, *130*, 983.

[158] Feng, L., Nakahodo, T., Wakahara, T., Tsuchiya, T., Maeda, Y., Akasaka, T., Kato, T., Horn, E., Yoza, K., Mizorogi, N., Nagase, S., *A Singly Bonded Derivative of Endohedral Metallofullerene: $La@C_{82}CBr(COOC_2H_5)_2$, J. Am. Chem. Soc.*, **2005**, *127*, 17136.

[159] Lukoyanova, O., Cardona, C. M., Rivera, J., Lugo-Morales, L. Z., Chancellor, C. J., Olmstead, M. M., Rodríguez-Fortea, A., Poblet, J. M., Balch, A. L., Echegoyen, L., *"Open Rather than Closed" Malonate Methano-Fullerene Derivatives. The Formation of Methanofulleroid Adducts of $Y_3N@C_{80}$, J. Am. Chem. Soc.*, **2007**, *129*, 10423.

[160] Lu, X., Nikawa, H., Tsuchiya, T., Akasaka, T., Toki, M., Sawa, H., Mizorogi, N., Nagase, S., *Nitrated Benzyne Derivatives of $La@C_{82}$: Addition of NO_2 and Its Positional Directing Effect on the Subsequent Addition of Benzynes*, *Angew. Chem., Int. Ed.*, **2010**, *49*, 594.

[161] Li, F.-F., Pinzón, J. R., Mercado, B. Q., Olmstead, M. M., Balch, A. L., Echegoyen, L., *[2 + 2] Cycloaddition Reaction to $Sc_3N@I_h$-C_{80}. The Formation of Very Stable [5,6]- and [6,6]-Adducts*, *J. Am. Chem. Soc.*, **2011**, *133*, 1563.

[162] Kareev, I. E., Lebedkin, S. F., Bubnov, V. P., Yagubskii, E. B., Ioffe, I. N., Khavrel, P. A., Kuvychko, I. V., Strauss, S. H., Boltalina, O. V., *Trifluoromethylated Endohedral Metallofullerenes: Synthesis and Characterization of $Y@C_{82}(CF_3)_5$*, *Angew. Chem., Int. Ed.*, **2005**, *44*, 1846.

[163] Takano, Y., Yomogida, A., Nikawa, H., Yamada, M., Wakahara, T., Tsuchiya, T., Ishitsuka, M. O., Maeda, Y., Akasaka, T., Kato, T., Slanina, Z., Mizorogi, N., Nagase, S., *Radical Coupling Reaction of Paramagnetic Endohedral Metallofullerene $La@C_{82}$*, *J. Am. Chem. Soc.*, **2008**, *130*, 16224.

[164] Popov, A. A., Shustova, N. B., Svitova, A. L., Mackey, M. A., Coumbe, C. E., Phillips, J. P., Stevenson, S., Strauss, S. H., Boltalina, O. V., Dunsch, L., *Redox-Tuning Endohedral Fullerene Spin States: From the Dication to the Trianion Radical of $Sc_3N@C_{80}(CF_3)_2$ in Five Reversible Single-Electron Steps*, *Chem. Eur. J.*, **2010**, *16*, 4721.

[165] Shustova, N. B., Chen, Y.-S., Mackey, M. A., Coumbe, C. E., Phillips, J. P., Stevenson, S., Popov, A. A., Boltalina, O. V., Strauss, S. H., *$Sc_3N@(C_{80}$-$I_h(7))(CF_3)_{14}$ and $Sc_3N@(C_{80}$-$I_h(7))(CF_3)_{16}$. Endohedral Metallofullerene Derivatives with Exohedral Addends on Four and Eight Triple-Hexagon Junctions. Does the Sc_3N Cluster Control the Addition Pattern or Vice Versa?*, *J. Am. Chem. Soc.*, **2009**, *131*, 17630.

[166] Shu, C., Cai, T., Xu, L., Zuo, T., Reid, J., Harich, K., Dorn, H. C., Gibson, H. W., *Manganese(III)-Catalyzed Free Radical Reactions on Trimetallic Nitride Endohedral Metallofullerenes*, *J. Am. Chem. Soc.*, **2007**, *129*, 15710.

[167] Shu, C., Slebodnick, C., Xu, L., Champion, H., Fuhrer, T., Cai, T., Reid, J. E., Fu, W., Harich, K., Dorn, H. C., Gibson, H. W., *Highly Regioselective Derivatization of Trimetallic Nitride Templated Endohedral Metallofullerenes via a Facile Photochemical Reaction*, *J. Am. Chem. Soc.*, **2008**, *130*, 17755.

[168 (a)] Pinzón, J. R., Cardona, C. M., Herranz, M. Á., Plonska-Brzezinska, M. E., Palkar, A., Athans, A. J., Martín, N., Rodríguez-Fortea, A., Poblet, J. M., Bottari, G., Torres, T., Gayathri, S. S., Guldi, D. M., Echegoyen, L., *Metal Nitride Cluster Fullerene $M_3N@C_{80}$ (M=Y, Sc) Based Dyads: Synthesis, and Electrochemical, Theoretical and Photophysical Studies*, *Chem. Eur. J.*, **2009**, *15*, 864; [(b)] Pinzón, J. R., Plonska-Brzezinska, M. E., Cardona, C. M., Athans, A. J., Gayathri, S. S., Guldi, D. M., Herranz, M. Á., Martín, N., Torres, T., Echegoyen, L., *$Sc_3N@C_{80}$-Ferrocene Electron-Donor/Acceptor Conjugates as Promising Materials for Photovoltaic Applications*, *Angew. Chem., Int. Ed.*, **2008**, *47*, 4173.

[169] [(a)] Takano, Y., Obuchi, S., Mizorogi, N., García, R., Herranz, M. Á., Rudolf, M., Wolfrum, S., Guldi, D. M., Martín, N., Nagase, S., Akasaka, T., *Stabilizing Ion and Radical Ion Pair States in a Paramagnetic Endohedral Metallofullerene/π-Extended Tetrathiafulvalene Conjugate*, *J. Am. Chem. Soc.*, **2012**, *134*, 16103; [(b)] Takano, Y., Herranz, M. Á., Martín, N., Radhakrishnan, S. G., Guldi, D. M., Tsuchiya, T., Nagase, S., Akasaka, T., *Donor−Acceptor Conjugates of Lanthanum Endohedral Metallofullerene and π-Extended Tetrathiafulvalene*, *J. Am. Chem. Soc.*, **2010**, *132*, 8048.

[170] Takano, Y., Obuchi, S., Mizorogi, N., García, R., Herranz, M. Á., Rudolf, M., Guldi, D. M., Martín, N., Nagase, S., Akasaka, T., *An Endohedral Metallofullerene as a Pure Electron Donor: Intramolecular Electron Transfer in Donor–Acceptor Conjugates of $La_2@C_{80}$ and 11,11,12,12-Tetracyano-9,10-anthra-p-quinodimethane (TCAQ)*, *J. Am. Chem. Soc.*, **2012**, *134*, 19401.

[171] Ross, R. B., Cardona, C. M., Guldi, D. M., Sankaranarayanan, S. G., Reese, M. O., Kopidakis, N., Peet, J., Walker, B., Bazan, G. C., Van Keuren, E., Holloway, B. C., Drees, M., *Endohedral fullerenes for organic photovoltaic devices*, *Nat. Mater.*, **2009**, *8*, 208.

[172] Schick, G., Jarrosson, T., Rubin, Y., *Formation of an Effective Opening within the Fullerene Core of C_{60} by an Unusual Reaction Sequence*, *Angew. Chem., Int. Ed.*, **1999**, *38*, 2360.

[173] Rubin, Y., Jarrosson, T., Wang, G.-W., Bartberger, M. D., Houk, K. N., Schick, G., Saunders, M., Cross, R. J., *Insertion of Helium and Molecular Hydrogen Through the Orifice of an Open Fullerene*, *Angew. Chem., Int. Ed.*, **2001**, *40*, 1543.

[174] [(a)] Xiao, Z., Yao, J., Yang, D., Wang, F., Huang, S., Gan, L., Jia, Z., Jiang, Z., Yang, X., Zheng, B., Yuan, G., Zhang, S., Wang, Z., *Synthesis of [59]Fullerenones through Peroxide-Mediated Stepwise Cleavage of Fullerene Skeleton Bonds and X-ray Structures of Their Water-Encapsulated Open-Cage Complexes*, *J. Am. Chem. Soc.*, **2007**, *129*, 16149; [(b)] Iwamatsu, S., Uozaki, T., Kobayashi, K., Re, S., Nagase, S., Murata, S., *A Bowl-Shaped Fullerene Encapsulates a Water into the Cage*, *J. Am. Chem. Soc.*, **2004**, *126*, 2668.

[175] Iwamatsu, S.-i., Stanisky, C. M., Cross, R. J., Saunders, M., Mizorogi, N., Nagase, S., Murata, S., *Carbon Monoxide Inside an Open-Cage Fullerene*, *Angew. Chem., Int. Ed.*, **2006**, *45*, 5337.

[176] Whitener, K. E., Frunzi, M., Iwamatsu, S., Murata, S., Cross, R. J., Saunders, M., *Putting Ammonia into a Chemically Opened Fullerene*, *J. Am. Chem. Soc.*, **2008**, *130*, 13996.

[177] [(a)] Murata, Y., Kato, N., Komatsu, K., *The Reaction of Fullerene C_{60} with Phthalazine: The Mechanochemical Solid-State Reaction Yielding a New C_{60}*

Dimer versus the Liquid-Phase Reaction Affording an Open-Cage Fullerene, *J. Org. Chem.*, **2001**, *66*, 7235; [(b)] Murata, Y., Murata, M., Komatsu, K., *The Reaction of Fullerene C_{60} with 4,6-Dimethyl-1,2,3-triazine: Formation of an Open-Cage Fullerene Derivative*, *J. Org. Chem.*, **2001**, *66*, 8187.

[178] [(a)] Murata, Y., Murata, M., Komatsu, K., *Synthesis, Structure, and Properties of Novel Open-Cage Fullerenes Having Heteroatom(s) on the Rim of the Orifice*, *Chem. Eur. J.*, **2003**, *9*, 1600; [(b)] Murata, Y., Komatsu, K., *Photochemical Reaction of the Open-Cage Fullerene Derivative with Singlet Oxygen*, *Chem. Lett.*, **2001**, *30*, 896.

[179] Chuang, S.-C., Murata, Y., Murata, M., Komatsu, K., *The outside knows the difference inside: trapping helium by immediate reduction of the orifice size of an open-cage fullerene and the effect of encapsulated helium and hydrogen upon the NMR of a proton directly attached to the outside*, *Chem. Commun.*, **2007**, 1751.

[180] Komatsu, K., Murata, M., Murata, Y., *Encapsulation of Molecular Hydrogen in Fullerene C_{60} by Organic Synthesis*, *Science*, **2005**, *307*, 238.

[181] Maroto, E. E., Izquierdo, M., Murata, M., Filippone, S., Komatsu, K., Murata, Y., Martín, N., *Catalytic stereodivergent functionalization of $H_2@C_{60}$*, *Chem. Commun.*, **2014**, *50*, 740.

[182] Murata, M., Murata, Y., Komatsu, K., *Synthesis and Properties of Endohedral C_{60} Encapsulating Molecular Hydrogen*, *J. Am. Chem. Soc.*, **2006**, *128*, 8024.

[183] Murata, M., Maeda, S., Morinaka, Y., Murata, Y., Komatsu, K., *Synthesis and Reaction of Fullerene C_{70} Encapsulating Two Molecules of H_2*, *J. Am. Chem. Soc.*, **2008**, *130*, 15800.

[184] Kurotobi, K., Murata, Y., *A Single Molecule of Water Encapsulated in Fullerene C_{60}*, *Science*, **2011**, *333*, 613.

[185] Chai, Y., Guo, T., Jin, C., Haufler, R. E., Chibante, L. P. F., Fure, J., Wang, L., Alford, J. M., Smalley, R. E., *Fullerenes with metals inside*, *J. Phys. Chem.*, **1991**, *95*, 7564.

[186] Maroto, E. E., de Cózar, A., Filippone, S., Martín-Domenech, Á., Suarez, M., Cossío, F. P., Martín, N., *Hierarchical Selectivity in Fullerenes: Site-, Regio-, Diastereo-, and Enantiocontrol of the 1,3-Dipolar Cycloaddition to C_{70}*, *Angew. Chem., Int. Ed.*, **2011**, *50*, 6060.

[187] Zhao, Y., Truhlar, D., *The M06 suite of density functionals for main group thermochemistry, thermochemical kinetics, noncovalent interactions, excited states, and transition elements: two new functionals and systematic testing*

of four M06-class functionals and 12 other functionals, *Theor. Chem. Acc.*, **2008**, *120*, 215.

[188] Coldham, I., Hufton, R., *Intramolecular Dipolar Cycloaddition Reactions of Azomethine Ylides*, *Chem. Rev.*, **2005**, *105*, 2765.

[189] Haddon, R. C., *Chemistry of the fullerenes: the manifestation of strain in a class of continuous aromatic molecules*, *Science*, **1993**, *261*, 1545.

[190 (a)] Tsuchiya, T., Rudolf, M., Wolfrum, S., Radhakrishnan, S. G., Aoyama, R., Yokosawa, Y., Oshima, A., Akasaka, T., Nagase, S., Guldi, D. M., *Coordinative Interactions between Porphyrins and C_{60}, La@C_{82}, and La_2@C_{80}*, *Chem. Eur. J.*, **2013**, *19*, 558; [(b)] Braida, B., Walter, C., Engels, B., Hiberty, P. C., *A clear correlation between the diradical character of 1,3-dipoles and their reactivity toward ethylene or acetylene*, *J. Am. Chem. Soc.*, **2010**, *132*, 7631.

[191] Kikuchi, K., Nakao, Y., Suzuki, S., Achiba, Y., Suzuki, T., Maruyama, Y., *Characterization of the Isolated Y@C_{82}*, *J. Am. Chem. Soc.*, **1994**, *116*, 9367.

[192] Filippone, S., Maroto, E. E., Martin-Domenech, A., Suarez, M., Martin, N., *An efficient approach to chiral fullerene derivatives by catalytic enantioselective 1,3-dipolar cycloadditions*, *Nat Chem*, **2009**, *1*, 578.

[193] Maroto, E. E., Filippone, S., Suárez, M., Martínez-Álvarez, R., de Cózar, A., Cossío, F. P., Martín, N., *Stereodivergent Synthesis of Chiral Fullerenes by [3 + 2] Cycloadditions to C_{60}*, *J. Am. Chem. Soc.*, **2013**, *136*, 705.

[194] Sawai, K., Takano, Y., Izquierdo, M., Filippone, S., Martín, N., Slanina, Z., Mizorogi, N., Waelchli, M., Tsuchiya, T., Akasaka, T., Nagase, S., *Enantioselective Synthesis of Endohedral Metallofullerenes*, *J. Am. Chem. Soc.*, **2011**, *133*, 17746.

[195] Marco-Martínez, J., Marcos, V., Reboredo, S., Filippone, S., Martín, N., *Asymmetric Organocatalysis in Fullerenes Chemistry: Enantioselective Phosphine-catalyzed Cycloaddition of Allenoates onto C_{60}*, *Angew. Chem., Int. Ed.*, **2013**, *52*, 5115.

[196] Marco-Martínez, J., Reboredo, S., Izquierdo, M., Marcos, V., López, J. L., Filippone, S., Martín, N., *Enantioselective Cycloaddition of Münchnones onto [60]Fullerene: Organocatalysis versus Metal Catalysis*, *J. Am. Chem. Soc.*, **2014**, *136*, 2897.

[197] Maroto, E. E., Filippone, S., Martín-Domenech, A., Suarez, M., Martín, N., *Switching the Stereoselectivity: (Fullero)Pyrrolidines "a la Carte"*, *J. Am. Chem. Soc.*, **2012**, *134*, 12936.

[198] Aroua, S., Garcia-Borràs, M., Osuna, S., Yamakoshi, Y., *Essential Factors for Control of the Equilibrium in the Reversible Rearrangement of M_3N@I_h-C_{80}*

Fulleropyrrolidines: Exohedral Functional Groups versus Endohedral Metal Clusters, *Chem. Eur. J.*, **2014**, *20*, 14032.

[199] Yamamoto, K., Funasaka, H., Takahasi, T., Akasaka, T., Suzuki, T., Maruyama, Y., *Isolation and Characterization of an ESR-Active La@C_{82} Isomer*, *J. Phys. Chem.*, **1994**, *98*, 12831.

[200 (a)] López-Pérez, A., Adrio, J., Carretero, J. C., *The Phenylsulfonyl Group as a Temporal Regiochemical Controller in the Catalytic Asymmetric 1,3-Dipolar Cycloaddition of Azomethine Ylides*, *Angew. Chem., Int. Ed.*, **2009**, *48*, 340; [(b)] Wang, C.-J., Liang, G., Xue, Z.-Y., Gao, F., *Highly Enantioselective 1,3-Dipolar Cycloaddition of Azomethine Ylides Catalyzed by Copper(I)/TF-BiphamPhos Complexes*, *J. Am. Chem. Soc.*, **2008**, *130*, 17250.

[201] Filippone, S., Maroto, E. E., Martín-Domenech, Á., Martín, N., in *Advances in Organometallic Chemistry and Catalysis*, John Wiley & Sons, Inc., **2013**, pp. 459.